# Mechanisms of anaphase B spindle elongation & scaling in Schizosaccharomyzes pombe

Lara Krüger

PSL
UNIVERSITÉ PARIS

THÈSE DE DOCTORAT
DE L'UNIVERSITÉ PSL

Préparée à l'institut Curie

# Mechanisms of anaphase B spindle elongation & scaling in *Schizosaccharomyzes pombe*

---

## *Mécanismes de l'élongation du fuseau mitotique en anaphase B et de l'adaptation à la taille des cellules chez S. pombe*


Soutenue par

**Lara K. KRÜGER**

Le 15 octobre 2021


Ecole doctorale n° 577

**Structure et dynamique des systèmes vivants**

Spécialité

**Sciences de la vie et de la santé**

Composition du jury :

| | |
|---|---|
| Buzz BAUM<br>Professeur,<br>LMB-MRC, University College London | *Président*<br>*Rapporteur* |
| Marileen DOGTEROM<br>Professeur<br>TU Delft | *Rapporteur* |
| Nicolas MINC<br>Directeur de Recherche,<br>Institut Jacques Monod | *Examinateur* |
| Anna AKHMANOVA<br>Professeur<br>Universiteit Utrecht | *Examinateur* |
| Marie-Hélène VERLHAC<br>Directeur de Recherche,<br>Collège de France | *Examinateur* |
| Phong TRAN<br>Directeur de recherche,<br>Institut Curie | *Directeur de thèse* |

institutCurie | PSL

# Mechanisms of anaphase B spindle elongation & scaling in *Schizosaccharomyces pombe*

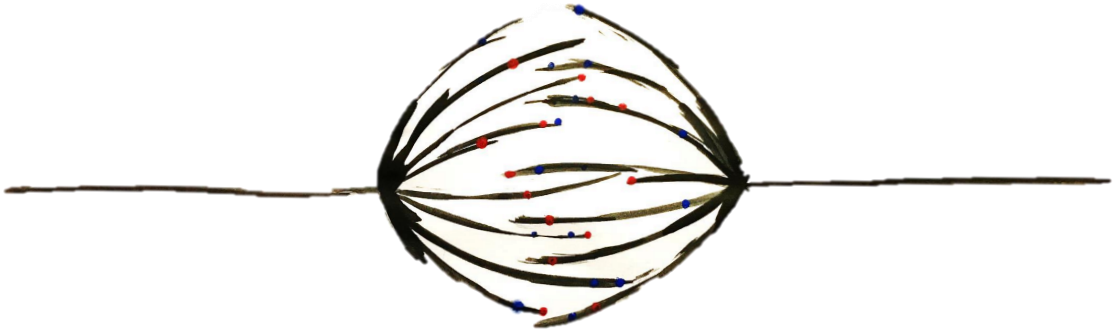

DISSERTATION

submitted for the degree of

***Doctor of Philosophy***

by

**Lara Katharina Krüger**

Paris, the 17.08.2021

***To my mother***

*i carry your heart with me (i carry it in*
*my heart) i am never without it*

*(E. E. Cummings)*

ACKNOWLEDGEMENTS

I am uncertain if the words on this page can convey how thankful I am, for having had the support of so many people, for the friendly faces that welcomed me in France, that I met throughout these years, for the people by my side.

To Phong, for giving me the opportunity to take this path, for giving me the freedom to find out what I am capable of. I had the most useful lessons, because you allowed me to do mistakes, to find them, and solve them by myself. I also want to thank you for never putting pressure on me and, most importantly, for being a very very kind person.

To Anne Paoletti, for being an incredible person, which even though she is loaded with work, always has an open ear and is eager to help.

To my thesis committee, Renata Basto, Patricia Bassereau, and Manuel Théry for all the fruitful discussions, your support, and guidance throughout these years.

To the thesis jury, Anna Akhmanova, Marileen Dogterom, Nicolas Minc, Marie-Hélène Verlhac and Buzz Baum for kindly accepting to evaluate my thesis.

To Matthieu Gélin for patiently and very kindly introducing me to the world of *in vitro* reconstitution assays, to Laurent Blanchoin for extremely helpful Zoom calls, and always knowing what to test, when I did not know what to try anymore, and Carlos Kikuti for showing me the world of Äkta and giving me the ability to purify my very first proteins.

To the whole lab, present and past members, Sergio - the one and only yeast connoisseur, Federica - the italian gourmet, Frederique, Lucien, Chloe, and Chahrazed for a very pleasant atmosphere, and to Sabine Bardin, the lab mate from another lab, for being on top of things and always (and literally always) being ready to help.

To my stars of these years, Ana Loncar and Manuel (L'Erephant) Lera Ramirez. I have the feeling that I would have had quite a lame time without you. With you, it was pretty neat. I am really happy that you were my companions for all these years, inside and outside the office. I thank you for all your support, your open ears, the chouquette Manu left on my desk when it was again time for one of those devouring 'purification days', not because of the immense dose of sugar, but because of the gentle gesture.
Ana, I am telling you via typed words on a paper, since you and me can not bear overly sentimental moments. Even though you are trying to hide it behind your 'croatian rudeness' (certainly, this means 'being direct'), you are one exceptionally sensitive person. When barely anyone knew what to say, you allowed me to escape rainy hours without even mentioning the clouds. From the bottom of my heart, I thank you, I thank the coincidence that brought us together.

To my family. My father, even though your least preferred tool is words, I know that I can lean on you, always, that you will bring me and my few things wherever I am going, and that I can always come home. To my brother, without whom I would have never studied biochemistry in the first place, and who, I now know, will always be by my side (and I will be by yours). To my grandmothers, two incredible ladies. I am not sure if I always deserve how proud you are, but I am very grateful you are and even more to have you.
To my mother, to my unconditional supporter, to the bond that held me together, to an exceptional woman. I thank you for always being there, for preventing me from feeling alone, ever. For your support, for being proud and supportive, even when I was not performing that great. You have been there, by my side, no matter what. I thank you for not always looking at me like your kid, but as someone who's opinion matters equally. I would be nowhere, I would be no one without you.

To Marcel. I thank you for being with me, being by my side for all these years, for giving me strength, and bringing me back on track. For having me showed so many things, so many places, for broadening my horizons. Most importantly, for being my home. *Für dich würd' ich auf die gangster schießen.*

During cell division, a highly dynamic molecular machine, the mitotic spindle, separates the previously duplicated DNA into two identical sets. This is achieved by movement of sister chromatids to opposite spindle poles (anaphase A) and separation of the spindle poles driven by an elongation of the spindle (anaphase B). In most organisms, anaphase B spindle elongation is primarily driven by microtubule sliding forces generated by kinesin motors at the spindle midzone, the region of antiparallelly overlapping microtubules at the spindle center. At the same time, spindle microtubules have to grow in order to allow the spindle to elongate. In fact, microtubule sliding and microtubule growth have to be coordinated to ensure flawless spindle elongation.

This work demonstrates that, in the model organism *Schizosaccharomyces pombe*, the homotetrameric kinesin-6 Klp9 is a crucial regulator of anaphase B spindle elongation. A combination of *in vivo* and *in vitro* experiments indicate that the motor holds a dual function: it can slide microtubules apart and regulate their growth velocity. Thus, the motor may inherently coordinate microtubule sliding and growth during anaphase.
Accordingly, altering the number of motors present at the spindle midzone was sufficient to alter the speed of anaphase B spindle elongation. In fact, this is utilized by cells of different sizes to adjust the speed of spindle elongation to cell size. Increasing the Klp9 levels allows bigger cells, which form longer spindles, to elongate the spindle with higher speeds, as compared to smaller cells, which form shorter spindles. Scaling of the spindle elongation velocity eventually allows cells of different sizes with different spindle length to keep the process of sister chromatid separation in a constant time frame, a potential advantage for cell viability.

# Contents

# List of Figures

# Abbreviations

| | |
|---|---|
| **ATP** | **A**denosine **T**ri **P**hosphate |
| **aa** | **a**mino **a**cid |
| **BASS** | Central **B**ipolar **Ass**embly domain |
| **CPC** | **C**hromsome **P**assenger **C**omplex |
| **DNA** | **D**esoxyribo **N**ucleic **A**cid |
| **EM** | **E**lectron **M**icroscopy |
| **GAP** | **G**TPase **A**ctivating **P**rotein |
| **γ-TuRC** | γ-**Tu**bulin **R**ing **C**omplex |
| **γ-TuSC** | γ-**Tu**bulin **S**mall **C**omplex |
| **GDP** | **G**uanosine **D**i **P**hosphate |
| **GTP** | **G**uanosine **T**ri **P**hosphate |
| **K-fiber** | **K**inetochore-fiber |
| **MAP** | **M**icrotubule **A**ssociated **P**rotein |
| **MT** | **M**icro**t**ubule |
| **MTOC** | **M**icro**t**ubule **O**rganizing **C**enter |
| **µM** | **M**icro **M**olar |
| **NE** | **N**uclear **E**nvelope |
| **NEBD** | **N**uclear **E**nvelope **B**reak **D**own |
| **PCM** | **P**eri**C**entriolar **M**aterial |
| **SAC** | **S**pindle **A**ssembly **C**heckpoint |
| **SPB** | **S**pindle **P**ole **B**ody |
| **TIRF** | **T**otal **I**nternal **R**eflection **F**luorescence |
| **UV** | **U**ltra **V**iolet |

# Introduction

## 1 The cell, cell division & methods of observation

In 1667, Robert Hooke observed cork through a microscope and identified structures he found to resemble a *cellula*, a small room monks used to live in, thus terming them **cells**, and opening the field of cell biology [1]. Indeed, cells could be described as 'rooms'. The cell membrane encloses the cytosol, and forms a distinct unit, containing numerous cell organelles and the cell cytoskeleton. Yet, today we know that the cell is highly dynamic, can rapidly alter its shape, and steadily exchanges with its environment. In part, this dynamicity is conveyed by the cell cytoskeleton. Microtubules, actin, and intermediate filaments continously assemble and reassemble, and thereby shape the cell, form routes for vesicle transport, or build very dynamic and complex structures, such as the mitotic spindle.

Almost 200 years after Hooke's description of cells, Virchow, in his 'Zelltheorie' (the theory of cells), postulated: *Omnis cellula e cellula* - all cells come from cells [2]. This represented an opposition to theories claiming that cells could form spontaneously, and strongly impacted the understanding of what we call today 'the basic unit of life': a cell that can divide and develop into multicellular organisms. Accordingly, in 1878, Walther Flemming first described **mitosis**, the process of cell division (Figure 1) by means of the movement of **chromosomes**, which encompass the genetic material in the form of deoxyribonucleic acid (DNA), from their alignment at the cell center to their separation to opposite sides of the cell [3].
Today we know that cells repeatedly go through a cycle, the **cell cycle**, to prepare for and ultimately undergo cell division. During **interphase**, the cell grows and produces proteins (G1-phase), duplicates the DNA (S-phase), grows further and corrects errors in the newly synthesized DNA (G2-phase). Eventually, the cell can enter mitosis to separate the duplicated DNA into two daughter cells.

As was the case for Flemming [3], the early studies of mitosis solely observed chromosomes, while the presence of 'mitotic fibers' that attach to and move chromosomes, was proposed much later. In particular, polarized light microscopy visualized fibrous material in mitotic cells (Figure 1) [4, 5]. **Electron microscopy (EM)** studies then revealed that those spindle fibers were bundles of multiple, much thinner tubular fibers, which mostly originate from two **spindle poles** and attach to specific regions on chromosomes, the **kinetochores** (Figure 1) [6, 7]. These fibers are today known as **microtubules**, the main building block of mitotic spindles. Subsequently, 3D-reconstructions of EM sections from human cells (Figure 1) revealed another spindle microtubule population, not attached to kinetochores, that emanates from opposite spindle poles and overlaps at the spindle center to form the central spindle or **spindle midzone**. These so-called interpolar microtubule bundles span the distance between the two spindle poles and keep them separated [8]. Therefore, interpolar microtubules are fundamental for spindle stability.

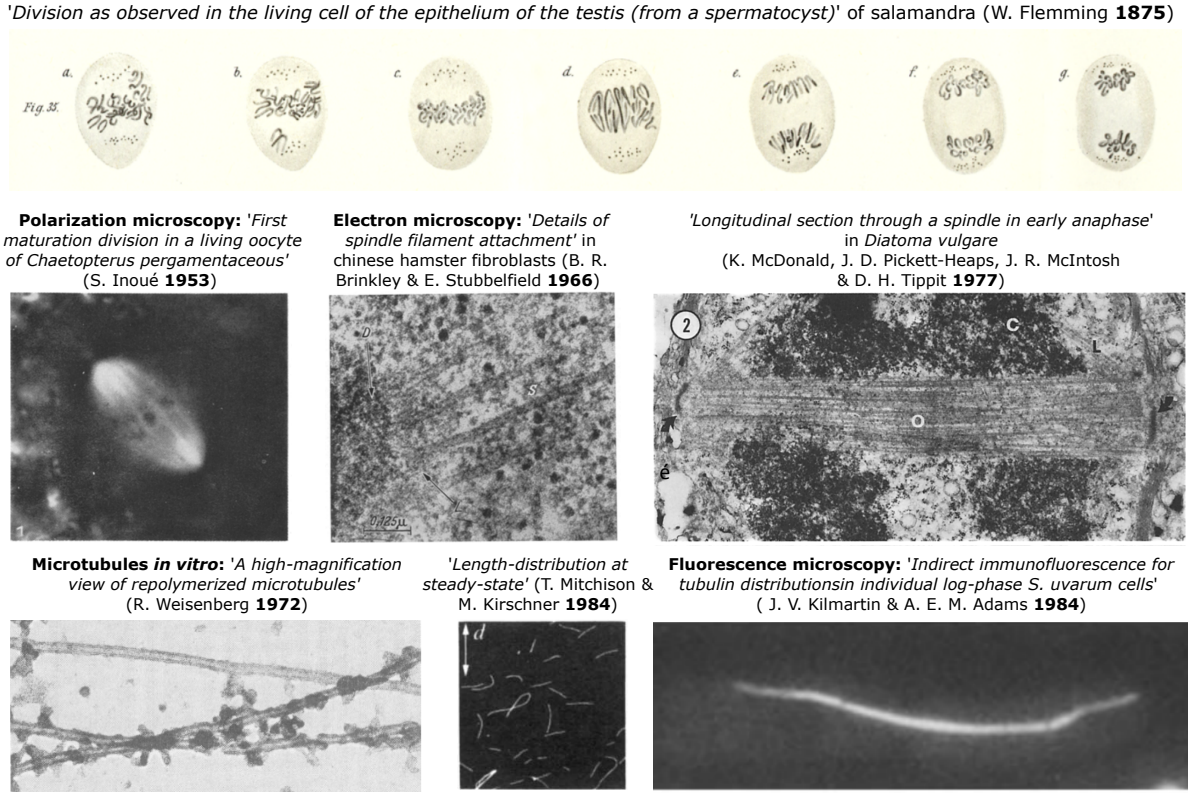


FIGURE 1: **History of mitotic spindle research** - Images taken different from studies that greatly contributed to today's knowledge and illustrate milestones in mitotic spindle research. From the first description of mitotic events by means of chromosome movements by W. Flemming in 1875 [3], the observation of mitotic fibers by polarization microscopy by S. Inoué in 1953 [5], electron microscopy studies of mammalian and yeast spindles [6, 9], *in vitro* reconstitution of dynamic microtubules from purified tubulin dimers [10], to the observation of mitotic spindles *in vivo* using fluorescence microscopy [11]. Images were taken and adapted from [3, 5, 6, 9–12].

Similar EM-studies on smaller yeast spindles revealed the architectural development of the mitotic spindle with mitosis progression [9, 13]. First, concomitant to the appearance of numerous microtubules, emanating from two spindle poles, these poles are separated to form a bipolar structure (**prophase**). Subsequently, microtubules, emanating from both spindle poles, attach to sister kinetochores to align them at the cell equator (**metaphase**), followed by, movement of chromosomes to spindle poles (**anaphase A**) and the an elongation of the mitotic spindle (**anaphase B**), which further separates the two chromosome sets.
These dramatic rearrangements of the spindle indicate the presence of forces that drive the dynamic spindle behavior. Indeed, anaphase B spindle elongation was inhibited upon the destruction of the spindle midzone in diatoms by a UV microbeam. This was not observed not when microtubules near spindle poles were destroyed, and suggested that the forces that shape the spindle during this mitotic stage stem from the structure itself. In this case, the region of interdigitating microtubules is a source of force generation for spindle elongation [14]. This was later confirmed in fission yeast cells by laser microsurgery [15, 16].

The dynamics of the mitotic spindle, from assembly to final elongation, suggested by EM studies were corroborated by immunofluorescence images of fixed fission yeast cells (Figure 1) when labelled antibodies and **fluorescence microscopy** were introduced into the field of cell biology [11]. The introduction of this method represents a milestone in cell biology and especially mitosis research. Determination of the localization and abundance of various proteins within the mitotic spindle has provided notable insights into their functional contribution to the process of chromosome separation. Later on, the availability of protein dyes for living cells enabled the study of the dynamic protein behavior during mitosis by fluorescence **live-cell imaging**, a technique that appears indispensable today.

Another breakthrough was the introduction of methods that allowed to **genetically modify** an organism's DNA - to mutate, to inactivate, or to add fluorescent tags to genes of interest. Work on yeast has paved the way for these tools into cell biology, given the simplicity of DNA cloning in these organisms [17–19]. In budding and fission yeast, random mutagenesis screens for temperature-sensitive mutants, denoting mutations that render a gene inactive at the restrictive temperature, have identified numerous mitosis-associated genes. For instance, Hirano et *al.* identified a plethora of mutants that lead to the cut of chromosomes by the cytokinetic ring, due to defects in chromosome separation during mitosis. Among others the screen revealed Cut7, a **molecular motor**, later classified as a kinesin-5 and microtubule sliding motor, that is essential during mitosis from yeast to human [19–22]. Together, these and similar screens in

different organisms, have allowed assembling a list of mitotic spindle components that appears almost complete to date.

While genetic modifications and fluorescence microscopy simplified the observation and manipulation of mitotic processes in the cell, *in vivo*, this is not always sufficient to gain a comprehensive understanding of underlying mechanisms. The complexity of the mitotic spindle makes it difficult to determine the contribution of individual components. To overcome this, proteins can be extracted from cells and studied in 'a tube', *in vitro*.

**Tubulin**, the subunit of microtubules, was first extracted from cells via binding to colchicine from the mammalian brain [23] and could assemble into microtubules *in vitro* (Figure 1) [10]. This allowed Mitchison and Kirschner in 1984 to discover that microtubules transition between states of growth and shrinkage, a characteristic termed **dynamic instability** (Figure 1) [12].

The purification of tubulin and a myriad of other spindle components enabled the determination of their protein structure by **cryo-EM**, which allows structural preservation of proteins due to an ultra-fast freezing process [24, 25]. Studies using this and similar techniques vigorously contributed to today's understanding of how microtubules assemble and grow, and how motor proteins and other **microtubule-associated proteins (MAPs)** affect these processes [26].

Another powerful tool to gain functional insight into those interactions is represented by ***in vitro* reconstitution assays** encompassing microtubules assembled from fluorescently labelled purified tubulin dimers, motors, and/or MAPs of interest [27]. Fluorescence microscopy subsequently allows the analysis of microtubule and motor movement and microtubule dynamic parameters. Together, these and various other assays have provided important contributions to the understanding of the operating mechanism of spindle components and their role in spindle function.

# 2 The mitotic spindle component parts

The mitotic spindle is build of typically two spindle poles, most prominently microtubules, chromosomes, as well as molecular motors and non-motor microtubule associated proteins.

## 2.1 Spindle poles

In most organisms and cell types, a substantial amount of spindle microtubules originates from **microtubule organizing centers (MTOCs)**, where microtubule nucleation is initiated and they

are anchored with their minus-ends. Typically, two MTOCs in the cell promote assembly of a bipolar spindle structure as they are located at opposite spindle ends and form the spindle poles. A bipolar structure is essential for faithful chromosome separation, since the position of spindle poles defines the position of sister chromatids after their separation (see chapter 3.3). Accordingly, multipolar spindles, a common result of an impaired spindle pole structure, often separate chromosomes unequally, leading to aneuploidy, DNA fragmentation, and proliferative defects [28–32].

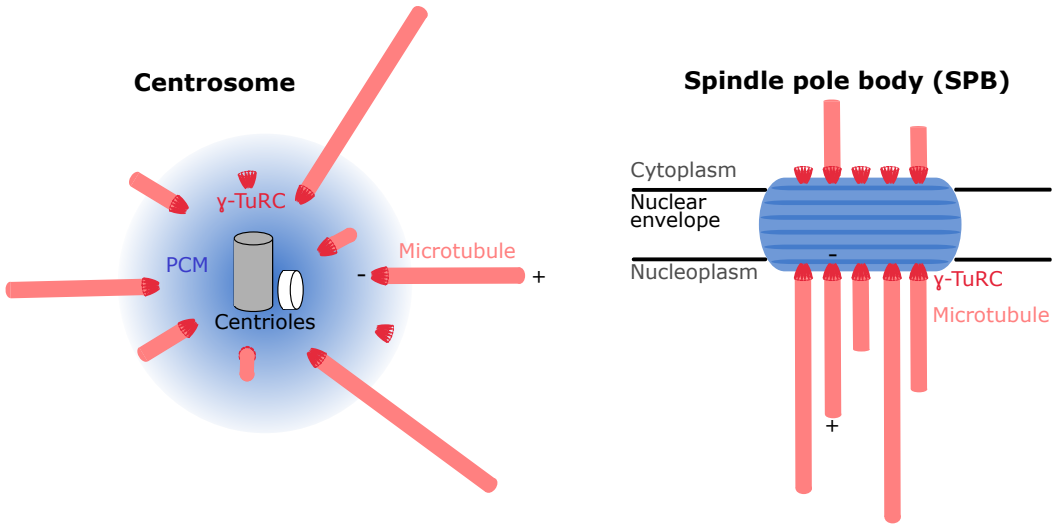


FIGURE 2: **Centrosomes & spindle pole bodies** - Scheme illustrating the composition of vertebrate centrosomes and yeast spindle pole bodies. Centrosomes contain two centrioles (gray, white) at the core, surrounded by the pericentriolar material (PCM, blue), which includes the γ-TuRC (red) to promote microtubule (pink) nucleation. The spindle pole body (blue) exhibits an ellipsoid shape and becomes stably inserted into the nuclear envelope during mitosis. γ-TuSCs (in *S. cerevisae*) or γ-TuRCs (in *S. pombe*) are recruited to the cytoplasmic and nucleoplasmic side of SPBs.

In the majority of animal cells, spindle poles are formed by centrosomes (Figure 2, left panel). **Centrosomes** can be described as self-assembling membrane-less organelles with two centrioles at the core, surrounded by the pericentriolar material [33]. The two **centrioles** encompass a mother and a daughter centriole, each representing a short nine-fold cylindrical microtubule structure. The **pericentriolar material (PCM)** is a dense matrix containing a variety of different proteins [33]. As MTOCs, centrosomes are a crucial source for microtubule nucleation and anchoring, in particular during mitosis. Before mitosis, centrosomes, therefore, undergo a maturation process, during which the PCM expands [34–36] due to increased incorporation of PCM components [37], that elevates the microtubule nucleation capacity. Centrosome maturation is promoted by the mitotic kinase PLK1 (Polo in *Drosophila*, PLK-1 in *C. elegans*),

which phosphorylates various PCM components and promotes anchoring of MOZART1 and NEDD1 to the PCM lattice [38–43]. MOZART1 and NEDD1 (or GCP-WD5) both recruit the **γ-tubulin ring complex (γ-TuRC)**, a template for microtubule nucleation (see chapter 2.2.1) [44–48]. Also, other PCM components, such as pericentrin and CDK5RAP2, associate with γ-TuRC and thus anchor microtubules at centrosomes [49, 50].
Despite the importance of centrosomes as mitotic MTOCs, cell division in animal cells can occur in their absence [51, 52]. In that case, cells utilize other mechanisms to form a bipolar spindle. For instance, in mouse oocytes, numerous small acentriolar MTOCs are clustered to form a bipolar array [53]. Nevertheless, centrosomes generally ensure robust and error-free chromosome separation, as acentriolar cells often undergo prolonged spindle assembly, and display chromosome segregation errors, DNA damage, and diminished cell viability [52, 54–56].

The yeast equivalent to the centrosome is the **spindle pole body (SPB)** (Figure 2, right panel). In *Saccharomyces cerevisiae* and *Schizosaccharomyces pombe*, budding and fission yeast, SPBs inherit an ellipsoid, layered structure composed of strata of different SPB-proteins [57]. An important difference between fungi and mammalian cells is that they undergo so-called **closed mitosis**, meaning that the nuclear envelope (NE) does not break down at mitosis onset and the mitotic spindle is assembled within the nucleus [58, 59]. This requires the SPBs, which are located in the cytoplasm during interphase, to be inserted into the NE to promote microtubule nucleation and mitotic spindle formation in the nucleoplasm [57, 60]. Upon entry into mitosis, the NE invaginates next to each SPB and locally disassembles to form a fenestra into which the SPB can settle [60]. Recruitment of the γ-TuRC to the nuclear side of the SPB subsequently allows spindle microtubule nucleation inside the nucleus [61].

## 2.2 Microtubules

Microtubules are polymers assembled from heterodimers, consisting of **α-tubulin** and **β-tubulin** (Figure 3), which can bind **guanosine triphosphate (GTP)** and catalyze hydrolysis into **guanosine diphosphate (GDP)** and a phosphate group ($P_i$) [62, 63]. The longitudinal association of αβ-tubulin heterodimers results in the formation of linear **protofilaments** (Figure 3). In cells, typically thirteen protofilaments interact laterally and form a hollow tubular structure, the **microtubule** [64, 65]. Lateral contacts between protofilaments are formed between homologous α- and α-tubulin and β- and β-tubulin, but since association occurs slightly

offset, two protofilaments in the polymer are linked by heterologous α- β-tubulin interaction, thus forming the '**seam**' (Figure 3) [66, 67].

Assembly of a microtubule occurs by initial nucleation and subsequent elongation, which will be discussed in the following chapters 2.2.1 and 2.2.2.

Importantly, due to the lateral head-to-tail association of αβ-tubulin heterodimers, microtubules are **polarized** [68], with the α-tubulin being exposed at the **minus-end** and the β-tubulin at the **plus-end** (Figure 3). This polar nature of microtubules is crucial for mitotic spindle function as it conveys different dynamic behavior [69]. Moreover, it defines spindle architecture, as minus-ends are typically anchored through interaction with the γ-TuRC (see chapter 2.2.1), while plus-ends are free within the cytoplasm, and their dynamic parameters are regulated by interaction with various plus-tip proteins (see chapter 2.4 and 2.5.2). Plus-ends also interact with other spindle or cellular components, such as kinetochores or the cell cortex. Furthermore, microtubule polarity dictates the moving direction of microtubule motors, which can be plus- and minus-end-directed.

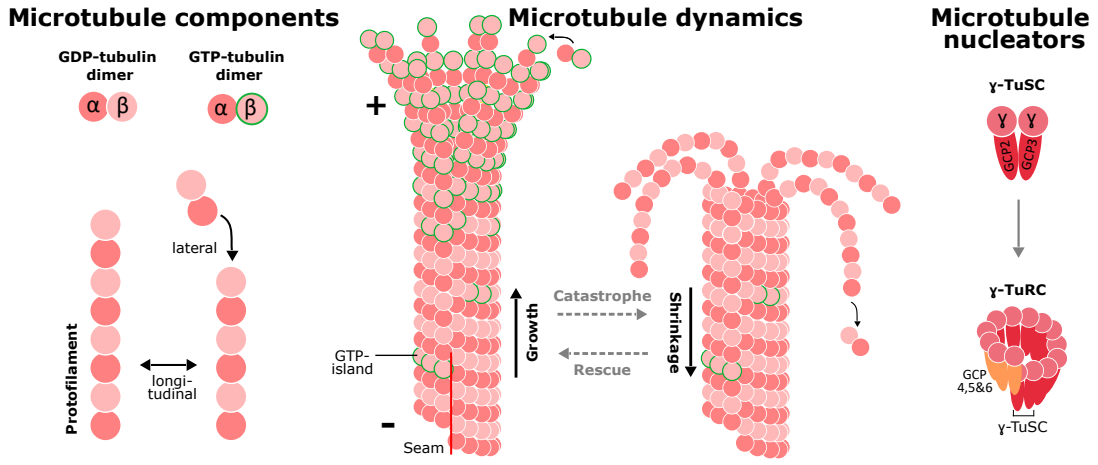


FIGURE 3: **Microtubule dynamics and nucleation** - Scheme depicting microtubule structure and dynamics, and the composition of microtubule nucleation factors γ-TuSC and γ-TuRC. (i) Tubulin heterodimers (pink), consisting of α- (dark pink) and β-tubulin (light pink) can exist in a GDP- or GTP-bound form (encircled in green). (ii) Longitudinal interaction of tubulin dimers leads to assembly of protofilaments. (iii) Lateral interaction of protofilaments allows assembly of a microtubule with a minus-, a plus-end and a seam. (iv) The growing plus-end is characterized by a GTP-cap, containing GTP-tubulin dimers, while the microtubule shaft primarily contains GDP-tubulin. (v) Within the microtubule shaft, GTP-tubulin dimers can be present in the form of GTP-islands. (vi) Growing microtubule plus-ends exhibit a tapered structure, while the plus-ends of shrinking microtubules are characterized by the presence of strongly curved protofilaments. (vii) Microtubule nucleation is promoted by the small γ-TuSC, encompassing two γ-tubulin molecules, GCP2, and GCP3, in *S. cerevisiae*, while in presence of GCP4, GCP5, and GCP6, several γ-TuSCs assemble into the γ-TuRC in *S. pombe* and animal cells.

### 2.2.1 Microtubule nucleation

Spontaneous nucleation of microtubules *in vitro* can occur only in the presence of purified tubulin dimers, GTP, and $Mg^{2+}$ ions [70]. However, the required concentration of free tubulin for efficient nucleation *in vitro* is very high, around 20 µM, which greatly exceeds the tubulin concentration in cells [70–72]. Thus, factors that lower the energy barrier are required for microtubule nucleation *in vivo*. Also, microtubule geometry has to be controlled. *In vitro* microtubules consisting of 11 to 16 protofilaments can be assembled [73], but, *in vivo* microtubules are generally composed of 13 protofilaments [64, 65, 74].

Microtubule nucleation is induced by **γ-tubulin** (Gtb1 in *S. pombe*), a member of the tubulin family, in all organisms [47, 75–77]. Two γ-tubulin molecules interact with the conserved γ-tubulin complex protein 2 (**GCP2**; Alp4 in *S. pombe*) and **GCP3** (Alp6 in *S. pombe*) to form the **γ-tubulin small complex (γ-TuSC)** (Figure 3, right panel) [76, 78–81]. The γ-TuSC is the functional microtubule nucleation complex in budding yeast. Seven of these v-shaped γ-TuSC complexes assemble into a conus-like structure when recruited to the SPB through interaction with Spc110 [82]. Assembly into a conical structure ensures overlap of half of the first and last γ-TuSCs in the spiral, exposing only 13 γ-tubulin molecules for interaction with αβ-tubulin (Figure 3, right panel) [82]. With this configuration, the complex can serve as a template for the formation of a 13 protofilament microtubule, through longitudinal interactions of γ-tubulin with the α-tubulin of an αβ-tubulin heterodimer, thus capping only microtubule minus-ends [37, 83–87]. This **'template model'** also accounts for microtubule nucleation in *S. pombe* and higher organisms which form the **γ-tubulin ring complex (γ-TuRC)** (Figure 3, right panel) [79, 87, 88]. The γ-TuRC is composed of multiple γ-TuSCs, **GCP4** (Gfh1 in *S. pombe*), **GCP5** (Mod21), and **GCP6** (Alp16), and is also organized in a ring-like structure [84, 87–92]. While it was initially hypothesized that GCP4, 5, and 6 bind GCP2 and 3 of γ-TuSCs and form the distal tip of the γ-TuRC [37], recent evidence suggests that they are part of the ring structure. Some GCP2 and GCP3s appear to be replaced by GCP4, 5, and 6 (Figure 3, right panel) [93–95].

*In vitro* data suggests that γ-TuRCs can exist in an open, less nucleation-efficient conformation [93, 96]. Transformation into a closed, nucleation-competent conformation can be promoted by different factors, such as MOZART1 and MOZART2 [37, 46, 48, 93], CDK5RAP [49, 76, 97], NEDD1 [98], and the microtubule growth-promoting proteins XMAP215/ch-TOG and TPX2 [98–101]. Recently, actin in the lumen of the ring complex has also been implicated in stabilizing the closed γ-TuRC conformation [93].

Within the mitotic spindle, a substantial amount of γ-TuRCs is recruited to spindle poles (see chapter 2.1). However, in animal cells, microtubule nucleation does not only occur from centrosomes. γ-TuRCs are also targeted to spindle microtubules to generate branched microtubule networks and denser spindle structures in plants, animal, and human cells, but not in yeast [102–105]. An important regulator of γ-TuRC localization to spindle microtubules is the eight subunit-sized **augmin** complex, depletion of which leads to loss of γ-TuRC from spindle microtubules but not centrosomes, and reduced spindle microtubule density [106–110]. Branched microtubule nucleation in vertebrates is also regulated by **TPX2** in an augmin-dependent manner [111, 112]. TPX2 is activated by the **Ran-GTP gradient**, which originates from chromosomes, as Ran-GTP releases TPX2 from inhibitory binding to importins [113–115]. Next to the Ran-GTP pathway, the **chromosomal passenger complex (CPC)**, including aurora B, which inhibits microtubule-destabilizing agents, promotes microtubule assembly from chromosomes [116, 117]. Hence, in animal cells, microtubule nucleation can occur from centrosomes, microtubules, and chromosomes.

Even though γ-tubulin is crucial for microtubule nucleation, especially within the spindle, its depletion does not necessarily prevent the formation of all microtubules, suggesting that other nucleation mechanisms exist [118–122]. Effectively, the microtubule dynamics regulating proteins **XMAP215** [100, 123, 124], **TPX2** [124, 125], **CLASP** [126, 127] and **CAMSAP/Patronin** [128, 129] have been reported to contribute to microtubule formation.

### 2.2.2 Microtubule elongation & dynamic instability

Upon initial nucleation of a short template, microtubules can elongate. When a GTP-bound αβ-tubulin heterodimer, the predominant form of tubulin heterodimers in solution, comes in contact with the end of a protofilament, it will be incorporated into the microtubule lattice via a head-to-tail arrangement of tubulin dimers. Therefore, *in vitro*, microtubules grow faster in presence of a higher tubulin concentration: an increased frequency of a free tubulin dimer meeting the tip of a microtubule protofilament increases the microtubule growth velocity [130]. Upon formation of this bond, the α-tubulin of the newly added tubulin dimer contributes residues to complete the GTP pocket, the site of GTP hydrolysis, of the β-tubulin of the last tubulin dimer in the protofilament [131, 132]. This triggers the GTPase activity, resulting in GTP hydrolysis and phosphate release, which transforms the GTP-tubulin dimer into a GDP-tubulin dimer [63]. Since GTP hydrolysis upon dimer incorporation is delayed, a region enriched in GTP-tubulin at

microtubule ends named **'GTP-cap'** is formed, which stabilizes the microtubule [12, 63, 133]. Consequently, the GTP-cap size presumably depends on the rate of GTP hydrolysis. Indeed, slowing down GTP hydrolysis by introducing a mutation in recombinant human tubulin extends the size of the GTP-cap and stabilizes microtubules *in vitro* [134].
Besides the presence of a GTP-cap, growing microtubule tips also differ structurally from the microtubule shaft. The precise structural conformation remains to be determined, but generally, microtubule ends are tapered, due to some protofilaments being longer than others (Figure 3). Furthermore, distal protofilaments display an outward curved configuration. This curved shape is intrinsic to the curved conformation of tubulin dimers [135–137]. Thus, when protofilaments interact laterally and the growing tip matures into the microtubule shaft by complete lattice incorporation, tubulin dimers are straightened and experience unfavourable conformational changes, leading to the generation of a lattice strain [138, 139]. As a result, protofilaments appear to peel off and curl outward, as microtubules depolymerize or shrink (Figure 3), and the lattice strain is released [140].

Generally, microtubules can exist in two states of persistent growth or shrinkage. They undergo alternating periods of growth and shrinkage in a stochastic manner, a behavior termed **dynamic instability** [12]. The transition from a phase of growth to a phase of shrinkage is called catastrophe. The transition from a phase of shrinkage to a phase of growth is called rescue (Figure 3).

Microtubule **catastrophe** occurs when the stabilizing GTP-cap is lost. Accordingly, cutting of microtubules at the shaft with a UV microbeam results in immediate catastrophe of the newly generated plus-end [141]. Interestingly, the newly generated minus-end does not undergo rapid shortening, emphasizing the differential behavior of plus- and minus-ends [141]. In addition, microtubules polymerized in presence of the non-hydrolyzable GTP analog, GMPCPP, do not undergo catastrophe, further supporting a model in which microtubule depolymerization is triggered by the loss of the GTP-cap [142].
The mechanism of microtubule catastrophe remains rather elusive. The catastrophe frequency is largely independent of the tubulin concentration and the probability of a microtubule to undergo catastrophe increases with time, indicating that 'older' microtubules are more likely to shrink [143]. This could be a result of an accumulation of lattice defects during growth [144] or of increased tapering at the tips [145].

How microtubule **rescue** is induced is scarcely understood. An insight was given by observation of a link between rescue events and the presence of GTP-tubulin dimers within the microtubule lattice, which form so-called **'GTP-islands'** [146, 147]. These GTP-islands are believed to be formed because tubulin-dimer exchange does not only occur at the microtubule tips but also along the microtubule shaft [148]. In fact, microtubule **lattice defects**, in the form of missing dimers, dislocations, or a change in lattice periodicity [148], can occur spontaneously during polymerization, due to mechanical stress or microtubule severing enzymes [149–152]. These defects can be repaired by incorporation of free GTP-tubulin dimers, which may subsequently stabilize the microtubule by promoting microtubule rescues [146, 147, 149, 151, 152].

Importantly, while *in vitro* microtubules rapidly switch between phases of growth and shrinkage in a stochastic manner, microtubules in the cell, and in particular within the spindle can undergo net polymerization or depolymerization, depending on the mitotic phase or/and the spindle microtubule class. This precise temporal and spatial regulation of microtubules requires a plethora of microtubule motors and non-motor microtubule-associated proteins, which will be introduced in chapters 2.4 and 2.5.

### 2.2.3 Mitotic spindle microtubules

Depending on the localization and the connections made, spindle microtubules can be classified into three classes: kinetochore microtubules, interpolar microtubules, and astral microtubules.

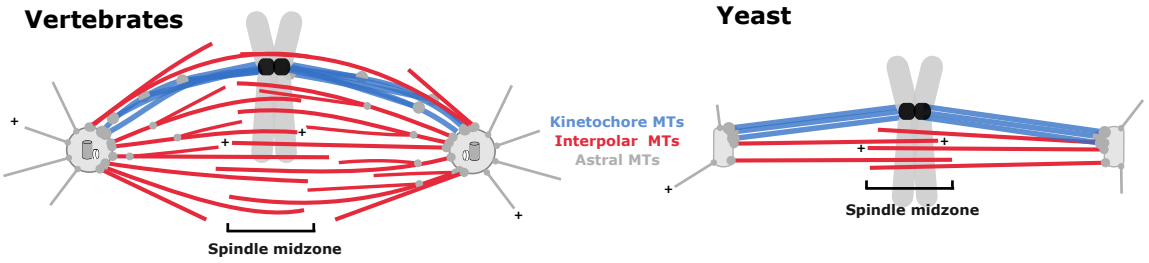


FIGURE 4: **Mitotic spindle microtubules in vertebrates & yeast** - Scheme illustrating spindle architecture in vertebrate and yeast cells. Kinetochore microtubules (MTs) are shown in blue, interpolar microtubules in red, astral microtubules in gray, and microtubule minus-ends are highlighted by gray circles. Chromosomes are depicted in gray and kinetochores in black. The spindle midzone is formed by antiparallely overlapping microtubules at the spindle center.

**Kinetochore microtubules** attach with their plus-ends to kinetochores, the microtubule attachment sites on chromosomes (see chapter 2.3.1), and typically span the distance to spindle poles, where the minus-ends are anchored (Figure 4, blue lines) [153, 154]. The main function of these spindle microtubules lies in connecting chromosomes to spindle poles and in promoting chromosome motion: they align chromosomes at the cell center during metaphase and separate sister chromatids towards opposite spindle poles during anaphase A. While in mammalian cells 10-30 microtubules are attached to one kinetochore and form a kinetochore-fiber (**k-fiber**) [154, 155], 2-4 microtubules attach to a fission yeast kinetochore [156], and only one microtubule to a budding yeast kinetochore [13]. Kinetochore microtubules are stabilised at both ends, so their lifetimes are considerably longer than that of interpolar or astral microtubules [157, 158]. Moreover, kinetochore microtubules are detyrosinated to a strong degree, which contributes to their stability [159]. Thus, kinetochore microtubules differ from other spindle microtubules in their 'tubulin code', which classifies microtubules assembled from different $\alpha\beta$-tubulin isotypes, and/or with different posttranslational modifications [159, 160].

**Interpolar microtubules** span the regions between the two spindle poles and form antiparallel overlaps at the spindle center (Figure 4, red lines) [153, 161]. These microtubules provide structural integrity for the spindle by keeping spindle poles apart. In PtK1 and HeLa cells, minus-ends of interpolar microtubules were found throughout the spindle [161, 162], as microtubule nucleation occurs at centrosomes, microtubules, and chromosomes (see chapter 2.2.1). Contrarily, in yeast, microtubules originate only from SPBs [105, 156].
The antiparallel microtubule overlap at the spindle center is formed by microtubules originating from one spindle pole, or one side of the spindle, overlapping with microtubules from the other spindle pole. This region is called the **spindle midzone** or central spindle.
Recently, a new class of interpolar microtubules has been introduced, the **bridging fibers**. These describe interpolar microtubule bundles, which form a bridge between sister k-fibers, by being tightly crosslinked with this class of spindle microtubules [163]. Bridging fibers are proposed to balance the forces acting on sister kinetochores [163].

**Astral microtubules** are anchored at spindle poles with their minus-end and extend toward the cell cortex with their plus-ends (Figure 4, gray lines). They are important for spindle positioning, as cortical dynein can exert forces on spindle poles [164, 165] and very prominent in *C. elegans* embryos [166].

## 2.3 Chromosomes

The duplicated DNA is organized into individual entities, the **chromosomes**. While human cells inherit 46 chromosomes, fission yeast contains only three [167].

### 2.3.1 Cohesin & kinetochores

After DNA duplication each chromosome consists of two identical **sister chromatids**, which are connected by the multimeric **cohesin** complex from S-phase to mitotic anaphase A, the moment of their separation (see chapter 3.3). The cohesin complex is composed of the conserved components Smc1$\alpha$, Smc3, Rad21, and SA1/2, which form a ring-like structure that is proposed to entrap sister chromatids and keep them together [168, 169].
In order to move chromosomes and separate sister chromatids, a physical link between sister chromatids and spindle microtubules has to be established. Therefore, **kinetochores**, the microtubule attachment sites, consisting of numerous proteins, are present on each sister chromatid, facing opposite sides of the chromatid pair [170]. Kinetochores are assembled on specific chromatin regions named **centromeres**, that can vary largely in size, from 125 base pairs (bp) in *S. cerevisiae* [171], 40-100 kbp in *S. pombe* [172] to 0.2-4 Mbps on human chromosomes [173]. Centromere sequence length correlates with kinetochore size and the number of microtubules that can attach (see chapter 2.2.3).

Very briefly, kinetochores form thin disk-like plates with an inner and an outer layer, referring to the inner kinetochore, localized on the centromere, and the outer kinetochore, which associates with spindle microtubules [170]. A crucial regulator of the kinetochore-microtubule attachment is the conserved **Ndc80 complex** [174, 175], which is composed of a kinetochore-targeting domain at the N-terminus and a microtubule-binding domain at the C-terminus [176–178]. Moreover, the Ndc80 complex interacts with the human **Ska** complex or the yeast **Dam1**/**DASH** complex, which are both able to track dynamic microtubules [179–182]. These complexes remain attached to microtubule ends when they shrink, so when kinetochore fibers depolymerize back to spindle poles, kinetochores and the sister chromatids stay associated [179–182].

### 2.3.2 Chromosomes as active spindle components

While chromosomes have long been described as passengers within the mitotic spindle, evidence exists that identifies them as active spindle components. As mentioned in chapter 2.2.1, chromosomes can initiate microtubule nucleation via the small GTPase Ran and thereby contribute to spindle assembly in vertebrates [52, 183].
In contrast, microtubule nucleation from chromosomes was not found in fission yeast [156, 184]. However, even in this situation, chromosomes actively regulate spindle function by contributing to a force balance, important for the assembly of a bipolar spindle. Loosening the connection between sister chromatids prevented bipolar spindle assembly under certain conditions, suggesting that they contribute to or oppose the forces acting in the spindle [185]. Moreover, errors in spindle microtubule-kinetochore attachments often lead to spindle length fluctuations during metaphase [186–188].

## 2.4 Microtubule motors

Microtubule motors represent the force generating machines of the mitotic spindle. During mitosis, they promote the generation of **microtubule sliding forces**, **crosslink microtubules** and **regulate microtubule dynamics**.
Members of the kinesin or dynein family are molecular motors that use microtubules as tracks and walk along them, typically with a given direction (towards the microtubule plus- or minus-end). These molecular machines use chemical energy provided by adenosine triphosphate (ATP)-hydrolysis, catalyzed by their P-loop ATPase, to exhibit conformational changes to move along the lattice [189, 190]. This so-called mechanochemical coupling is granted by the fact that binding of the motor domain to microtubules strongly increases its ATPase activity [191–196].
Most of the members of the kinesin super-family, which consists of at least 14 subfamilies [197], preferentially walk towards the microtubule plus-end, except for kinesin-14 which, like dynein, moves towards the minus-end. Kinesins contain a structurally conserved, approximately 300 amino acid long motor domain with a site for nucleotide-binding and a microtubule-interacting domain (Figure 5) [198]. The following neck-linker, which is highly conserved within one kinesin family, connects the motor domain with the stalk region, and is important for the coordination of two motor heads in a dimer. The stalk contains an $\alpha$-helical coiled-coil, which promotes dimerization or tetramerization of individual motor molecules [199]. The following

globular tail domain promotes interaction with co-proteins, other regulatory kinases or cargo molecules [200]. The position of the neck and stalk domains, C- or N-terminally to the motor domain, has been shown to dictate the walking direction of kinesins [201, 202]. Accordingly, kinesin-14 members, the only minus-end-directed kinesins, possess the motor domain at the C-terminus, while all other kinesin families have an N-terminal motor domain [198]. However, in yeast kinesin-5 members move bidirectionally along the microtubule lattice under certain conditions *in vitro* [203–205], reopening the question of what determines kinesin's directionality.

Importantly, for proper spindle function, several motors have to move **processively** along microtubules: they walk several steps before detaching from the microtubule. This typically requires dimerization of motor proteins and coordination between motor heads [198].

In the following chapter, I will introduce the structure and features of mitotic motors that are crucial spindle components from yeast to human, while chapter 3 will focus on their function within the spindle, and how these motors promote assembly of the spindle into a force-generating machine.

### 2.4.1 Plus-end-directed motors

Plus-end-directed kinesins constitute the largest group of mitotic motors. Members of this group have been shown to generate microtubule sliding forces or regulate microtubule dynamics. Several have also been shown to be able to perform both tasks, such as kinesin-4, -5, and -8. Of the crucial mitotic spindle motors, in particular, the ones required for the mitotic phase of anaphase B, fission yeast does not contain members of the kinesin-4 and kinesin-13 families. However, given their key role in other organisms, they will be introduced in this chapter.

**Kinesin-4** (**Kif4A**, Kif4B, Kif7, Kif21A, Kif21B and Kif27 in mammals, **KLP3A**, KLP31E in *Drosophila*, **XKLP1** in *X. laevis*, **KLP-12** & KLP-19 in *C. elegans*) has been found to **suppress microtubule plus-end dynamics** *in vitro* and *in vivo* (Figure 5, orange) [206–210]. Plus-end-directed KIF4A displays weak processivity *in vitro*, which can be enhanced upon interaction with the microtubule bundler PRC1 [211]. Binding to PRC1 also promotes localization of kinesin-4 to antiparallel microtubules at the spindle midzone, where the motor reduces

microtubule plus-end growth [206, 207, 212]. Besides the prominent role in regulating microtubule dynamics, KIF4A has recently been shown to slide antiparallelly oriented microtubules *in vitro* and *in vivo* [213–215]. Lastly, several kinesin-4 members interact with chromosomes, thus belonging to the family of chromokinesins, which actively move chromosomes along spindle microtubules [216, 217].

**Kinesin-5** (**Kif11** in mammals, **Eg5** in *X. laevis*, **Klp61F** in *Drosophila*, **Cin8 & Kip1** in *S. cerevisiae*, **Cut7** in *S. pombe*) is crucial for mitotic spindle assembly from yeast to human. Members of the kinesin-5 family form antiparallel homotetramers with two motor heads being located at each end of the structure (Figure 5, light blue) [22, 218–222]. Tetramerization is promoted by the family-specific **central bipolar assembly domain (BASS)**, a four-helix bundle, located in the motor's stalk domain [218, 220]. The bipolar configuration allows kinesin-5 tetramers to **crosslink antiparallelly oriented microtubules** and slide them apart [22, 218, 221, 223–227]. As the two motor heads, on each crosslinked microtubule, walk towards the plus-ends, the motor moves these microtubules relative to each other [22]. *In vitro* experiments using recombinant Eg5, demonstrated that in microtubule overlaps, the forces generated by kinesin-5 molecules increase with increasing overlap length and motor number [228]. This work also demonstrated that the motor can act as a brake and slow down microtubule sliding if the microtubule sliding velocity exceeds the Eg5-mediated sliding velocity under zero load [228].

Plus-end-directed movement has been observed *in vitro* for monomeric, dimeric, or full-length kinesin-5 constructs in almost all model organisms [22, 203, 204, 223, 229–232]. However, in yeast, Cin8, Kip1, and Cut7 **switch to minus-end-directed motion** *in vitro* at high ionic strength or at low motor densities [203, 204, 231, 233–235]. The ability to switch directionality depending on the motor concentration may regulate kinesin-5 localization within the mitotic spindle, allowing motors located on parallel microtubules in presumably less dense regions to move towards the minus-end, ensuring spindle pole localization, and motors to localize to antiparallel overlapping microtubules, where a high motor density favors plus-end-directed movement and consequently keeps the motors at the midzone [236]. In higher eukaryotes, where it is unclear if kinesin-5 motors also exhibit bidirectional movement, spindle pole localization of kinesin-5 is ensured by additional spindle components, such as the minus-end-directed dynein [237] or TPX2 [238].

Lastly, besides the kinesin-5's crucial function in promoting microtubule crosslinking and sliding, the motor has been recently implicated in the regulation of microtubule dynamics (Figure

5, right panel). A dimeric Eg5 construct enhances microtubule polymerization *in vitro* [239] by inducing a curved-to-straight conformational change of tubulin dimers at microtubule plus-ends [240]. Thus, the motor stabilizes newly added tubulin dimers at protofilament tips and consequently promotes microtubule growth. Contrarily, *in vivo* Klp61F or Cin8 deletion results in the formation of longer and more stable microtubules, indicative of a destabilizing effect on microtubules [241–243].

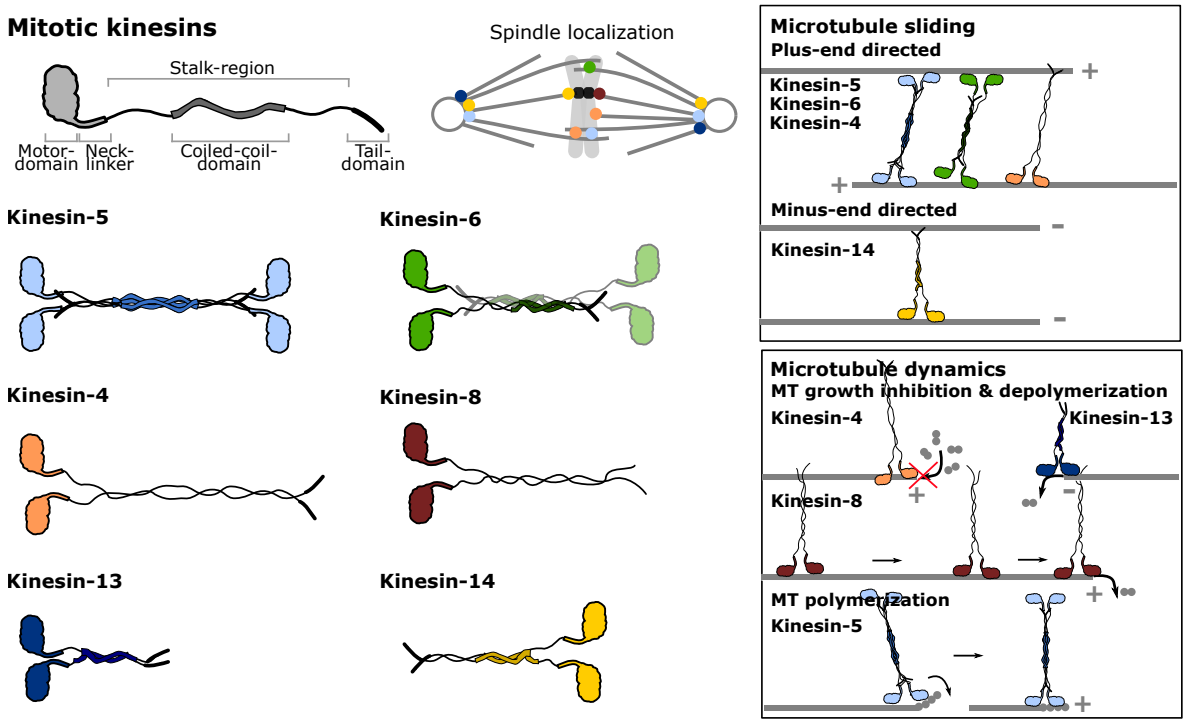


FIGURE 5: **Mitotic kinesins** - Scheme depicting the composition, proposed structure, function, and spindle localization of kinesin-4 (orange),-5 (light blue),-6 (green),-8 (dark red),-13 (dark blue), and -14 (yellow). Kinesins consist of a motor-domain, located N- or C-terminally, a stalk region, encompassing a coiled-coil domain and a tail domain. While kinesin-5 proteins and the fission yeast kinesin-6 Klp9 form homotetramers, the other mitotic kinesins exist as dimers. Spindle localization of each depicted kinesin is illustrated by the circles with the corresponding color. The right panel illustrates the function of the listed mitotic kinesins in regulating microtubule sliding and/or microtubule dynamics.

**Kinesin-6** (**Kif23**/**MKLP1, Kif20A**/**MKLP2** & Kif20B/MPP1 in mammals, **Subito**/**Pavarotti** in *Drosophila*, **ZEN-4** in *C. elegans*, **Klp9** in *S. pombe*) family members in mammals typically form dimers (Figure 5, green) [244, 245]. The motor domain of kinesin-6 proteins contains several unique loop insertions, most prominently a very long aminoacid (aa) insertion in loop 6. In MKLP2 this insertion is 99 aa long and forms a distinct subdomain that protrudes from the motor core and away from the bound microtubule [246]. Insertions in loops 2, 8, and 12 form additional contacts between the motor domain and the microtubule and have been

demonstrated to convey an atypical behavior to the MKLP2 motor domain [246]. MKLP2 binds differently to microtubules than, for instance kinesin-1, with a bias towards the adjacent protofilament, leading to a shifted binding of the motor domain on the microtubule lattice [246]. This may result in kinesin-6 motors moving along microtubules with a left-handed helical trajectory along the microtubule axis, as has been observed for MKLP1 [247].

The coiled-coil region in the stalk domain mediates interactions with numerous binding partners. MKLP1 and ZEN-4 form a complex with a Rho family GTPase activating protein (GAP) CYK-4/MgcTACGAP, termed **centralspindlin, which crosslinks antiparallel microtubules** at the central spindle [245, 248]. Alone, CYK-4 or MKLP1 are not capable of efficiently bundling microtubules *in vitro* [249], even though the kinesin-6 KIF20A contains an additional microtubule-interaction site in the C-terminal region, which could enable the motor to crosslink microtubules [250]. The centralspindlin complex is also crucial for the regulation of cytokinesis [251], as is the ability of MKLP2 to interact with and transport the chromosome passenger complex (CPC) along microtubules [244, 252]. MKLP2 also interacts with other mitotic kinases, such as Cdk1/cyclin B [253, 254], suggesting that kinesin-6 in mammals acts as a **signaling hub** at the central spindle for late mitotic events.

In fission yeast, kinesin-6 Klp9 is also required for the translocation of CPC components from the kinetochore to the spindle midzone at anaphse onset [255]. Additionally, Klp9 is an active force generator for anaphase B spindle elongation. **Klp9**, like kinesin-5 members, forms a homotetramer (Figure 5) [256] and it appears to contain a tetramerization domain that resembles the kinesin-5 specific BASS domain [257]. Since Klp9 is a **processive plus-end-directed motor** [258], the fission yeast kinesin-6 can **crosslink and slide antiparallelly oriented microtubules** apart (Figure 5, right panel) [256, 257, 259–261].

MKLP2 has also been shown to move processively towards microtubule plus-ends *in vitro*, and its processivity is enhanced by CPC binding, even though structural studies suggested that the motor might not show processive movements due to an unusually extended neck-linker [246]. However, it appears that unlike the mammalian kinesin-6 members, which form dimers and are not essential for microtubule sliding during anaphase B [214], Klp9 has retained several features of kinesin-5, namely tetramerization, which allows crosslinking and sliding of antiparallel microtubules without the support of binding partners.

**Kinesin-8** (**KIF18A**, KIF18B, KIF19 in mammals, **KLP67A** in *Drosophila*, **KLP-13** in *C. elegans*, **Kip3** in *S. cerevisiae*, **Klp5 & Klp6** in *S. pombe*) members form dimers and are generally implicated in the **regulation of microtubule depolymerization** (Figure 5, dark red)

[262–266]. An extensively studied example is the budding yeast Kip3 which is highly processive, allowing the motor to strongly accumulate at microtubule plus-ends [265, 266], where it promotes microtubule depolymerization [262, 265]. Kip3 regulates microtubule dynamics in a **length-dependent manner** due to its high processivity (Figure 5, right panel): on longer microtubules more motors land along the lattice and accumulate at the plus-end, resulting in longer microtubules displaying more Kip3 molecules arriving at the tip, which was proposed to lead to the removal of tubulin dimers when the motor dissociates from the tip [265, 266]. Thus, Kip3 contributes to microtubule length regulation. An active depolymerase activity has also been attributed to mammalian KIF18A [263], which is under debate since monomeric KIF18A constructs also promote microtubule depolymerization at plus- and minus-ends *in vitro* [267]. A mechanism that could explain this observation has been proposed for Kip3 [268]. Kip3 binds with a higher affinity to curved tubulin dimers at microtubule tips, which in turn inhibits the motor's ATPase activity and, by stabilizing the protofilament curvature, triggers microtubule depolymerization [268]. The two fission yeast kinesin-8 members form heterotetramers and do not constitute active depolymerases, but destabilize microtubules by increasing the catastrophe frequency in a microtubule-length dependent manner [264, 269–271]. Moreover, Kip3 has been implicated in the regulation of microtubule crosslinking and sliding at the central spindle [272, 273]. Yet, most kinesin-8 members have only been shown to control plus-end dynamics of kinetochore microtubules [263, 274–276].

**Kinesin-13** (**KIF2A, KIF2B, KIF2C**/**MCAK**, KIF24 in mammals, **XKCM1** in *X. laevis*, **KLP10A**, KLP59C, KLP59D in *D. melanogaster*, **KLP7** in *C. elegans*) proteins have been shown to **promote microtubule depolymerization at the minus-end** and contribute to the regulation of microtubule flux (Figure 5, dark blue) [277–280].

### 2.4.2 Minus-end-directed motors

**Kinesin-14** (**HSET** in mammals, **XCTK2** in *X. laevis*, **Ncd** in *Drosophila*, **Kar3** in *S.cerevisae*, **Klp2 & Pkl1** in *S. pombe*) members constitute a class of minus-end-directed kinesins [202, 281]. Kinesin-14 members typically form homodimers (Figure 5, yellow). Most family members contain an additional microtubule-binding site in the tail region that can diffuse along microtubules [282, 283], enabling the motor to **crosslink and slide microtubules** (Figure 5, right panel) [284, 285]. HSET, XCTK2, Ncd, and Klp2 can sort microtubules by sliding antiparallel microtubules and crosslinking parallelly oriented microtubules [284–287]. Moreover, due

to the presence of a diffusive tail, kinesin-14 can produce passive sliding of microtubules in absence of ATP. This sliding is driven by entropic forces that tend to maximize the microtubule overlap, similarly to the diffusive crosslinker Ase1 *in vitro* [286, 288]. Furthermore, Ncd, Kar3, and Pkl1 have been implicated in the regulation of microtubule dynamics [289–291].
Given the minus-end-directed motility, kinesin-14 motors localize to mitotic spindle poles and also to spindle microtubules [292, 293]. In fission yeast, which possesses two kinesin-14 members, Pkl1 is preferentially localized to spindle poles [294, 295], while Klp2 is present on spindle microtubules [261, 296].

**Cytoplasmic dynein-1**, the dynein family that functions within the mitotic spindle, is, like all dyneins, structurally rather different from kinesins [297, 298]. Dynein heavy chains (DHC) contain a C-terminal motor domain, and form a dimer together with a dimer of dynein intermediate chains, a dimer of light intermediate chains, and three light chain dimers [299, 300]. Dynein interacts with numerous adaptor proteins, which are responsible for targeting the motor to distinct locations within the cell and the spindle [298]. Dynactin targets dynein to kinetochores, the cell cortex, microtubule plus-ends, and the nuclear envelope [301–303]. NuMA promotes dynein recruitment to the cortex [304, 305] and Spindly regulates dynein localization at kinetochores [306, 307]. Importantly, dynein can be stably attached to these cellular structures, while the two motor domains associate with microtubules and exert forces by processively walking towards their minus-ends [308]. For instance, dynein anchored to the cell cortex generates **pulling forces on spindle poles** while walking towards the minus-end of astral microtubules [165].

## 2.5 Non-motor microtubule-associated proteins (MAPs)

In addition to motor proteins, several non-motor microtubule-associated proteins are important for spindle architecture and function. This mainly includes MAPs that can crosslink microtubules or control microtubule dynamics.

### 2.5.1 Microtubule crosslinker

Members of the conserved **Ase1**/**PRC1**/**MAP65** family (PRC1 in mammals, MAP65 in plants, Feo in *Drosophila*, SPD-1 in *C. elegans*, Ase1 in yeast) are crucial regulators of microtubule bundling at the spindle midzone. They are composed of an N-terminal coiled-coil domain that

regulates dimerization, a globular microtubule-binding domain containing a spectrin motif, and a C-terminal regulatory region [207, 223, 309–312]. As antiparallel dimers, all members of this family **preferentially crosslink antiparallelly oriented microtubules** (Figure 6, left panel) [207, 223, 310, 311], while they can also diffuse along parallel bundles or single microtubules [223, 311]. Cryo-EM analysis suggested that the rather flexible dimerization domain of PRC1 becomes ordered when PRC1 crosslinks antiparallel microtubules, possibly explaining the preference for this microtubule configuration [311]. Due to its crosslinking activity, Ase1 can resist microtubule sliding forces generated by kinesin-14 members Ncd or Klp2 *in vitro*. Since crosslinkers remain bound to and accumulate in the shrinking microtubule overlap, they can oppose motor sliding and prevent microtubules from completely sliding apart [288, 310, 313]. However, sliding generated by the kinesin-5 Eg5, which is a stronger motor than kinesin-14, is not opposed by PRC1 [311].

Ase1 and its homologs are targets of multiple mitotic kinases, namely Cdk1, Aurora B, and Plk1, and the phosphorylation state can regulate microtubule-binding affinity, as it is the case for Ase1, oligomerization of PRC1, or the interaction with other spindle components [256, 314–317]. The latter allows Ase1 to serve as a **regulatory hub** for localization of various spindle components to antiparallel microtubule overlaps, which emphasizes its role as a major scaffold protein of the spindle midzone [318].

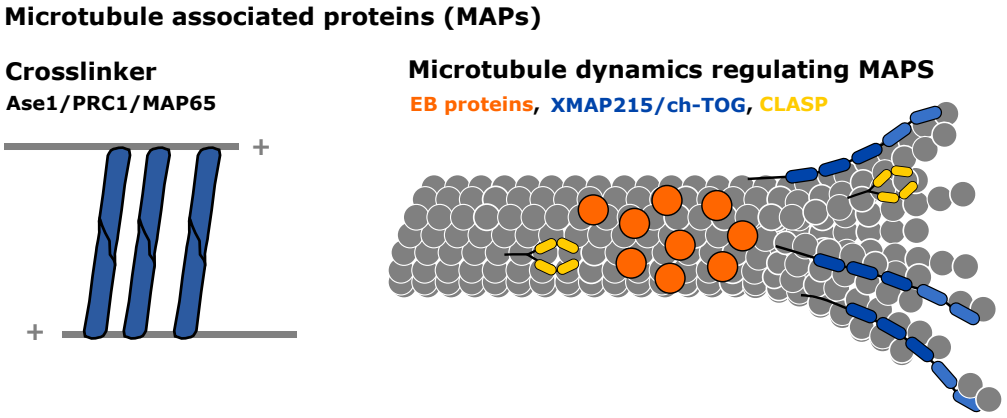


FIGURE 6: **Non-motor microtubule associated proteins** - Scheme depicting MAPs present in yeast and higher organisms that associate with spindle microtubules. (i) The dimeric microtubule crosslinker Ase1/PRC1 (blue) preferentially binds antiparallely oriented microtubules. (ii) MAPs that regulate microtubule dynamics encompass members of the XMAP215 family (blue) localized to the outermost plus-tip, EB proteins (orange) localize posterior to the XMAP215 signal. CLASP (yellow) has been found along the microtubule lattice and at the microtubule tip.

### 2.5.2 Microtubule dynamics regulating MAPs

**End-binding proteins** (**EB1**, EB2 & EB3 in metazoans, **Bim1** in *S. cerevisiae*, and **Mal3** in *S. pombe*) localize to growing microtubule ends and are crucial regulators of microtubule plus-tip dynamics (Figure 6, right panel). Family members are composed of a calponin-homology (CH) domain at the N-terminus, a subsequent neck-linker region, and a coiled-coil domain, important for dimerization of EB proteins and interaction with numerous partner proteins, mediated by the end-binding homology domain (EBH domain) [319–322]. EB proteins in mammals and yeast **track growing microtubule plus-tips**, due to a high affinity for the growing GTP-tubulin-containing tip and a much lower affinity for the GDP-tubulin-containing microtubule lattice [134, 321, 323–326]. In cells and *in vitro* fluorescently labeled EB proteins appear as comet-like structures at growing microtubule tips, and have thus been suggested to mark the microtubules GTP-cap [134, 326–328].

However, interpretation of *in vitro* data on the binding of EB proteins to microtubules polymerized in presence of different GTP-analogs [324, 325, 329], together with the observation that the outermost region of the microtubule tip appears free of EB proteins (Figure 6, right panel) [330], has led to contradicting models of EB protein binding to microtubules. It was not clear if EB proteins do preferntially bind to GTP-tubulin dimers. However, a recent *in vitro* study demonstrated that microtubules polymerized from tubulin bearing a mutation that renders it incapable of hydrolyzing GTP were covered by EB over their entire length, suggesting that EB1 indeed binds GTP-tubulin [134]. Consistent with this, microtubules assembled from tubulin mutants with a slower GTP hydrolysis rate increased the EB comet length [134].

Binding of EBs to the outermost microtubule end may be prevented by means of a different structure. EBs might not be able to bind tapered microtubule tips with curved protofilaments [331], but only bind straightened GTP-tubulin dimers (Figure 6).

At microtubule tips, EB proteins **increase the velocity of microtubule growth and increase the frequency of catastrophe** [321, 327, 330, 332, 333]. Interestingly, while the effect on the microtubule growth velocity is comparatively small, it can be greatly enhanced upon addition of XMAP215 in a synergistic manner to levels comparable to those in cells [333]. This was surprising because their binding sites at the microtubule tip are spatially different. In contrast to EB1, XMAP215 binds to the outermost microtubule tip [330], and EB1 and XMAP215 do not interact physically in mammals [333]. In fission yeast, however, Mal3 and the XMAP215 homolog Dis1 interact directly [332]. Moreover, in mammals and yeast, EB proteins target a variety of proteins to microtubule tips [331, 334, 335]. For instance, besides Dis1, the fission

yeast Mal3 interacts with the microtubule rescue factor CLASP [336], the CLIP170 protein Tip1 [336, 337], the plus-end-directed motor Tea2 [337], and the kinesin-14 Klp2 [338].

**Dis1/XMAP215/ch-TOG** family members (ch-TOG in human, XMAP215 in *X. laevis*, MiniSpindles/MSPS in *Drosophila*, Zyg9 in *C. elegans*, Stu2 in *S. cerevisae*, Dis1 & Alp14 in *S. pombe*) are classified as **microtubule polymerases**, which promote and accelerate microtubule growth [332, 339–343]. Crucial for their polymerase activity are the so-called **TOG domains**, which specifically **bind free tubulin dimers in the curved conformation**, rather than lattice incorporated tubulin (Figure 6, right panel) [340, 341, 344–346]. Vertebrate family members, acting as monomers, contain five individual TOG domains [341], while yeast proteins encompass only two TOG domains, but exist as homodimers [340]. While the TOG domains are responsible for the binding of free tubulin dimers and concentrating them at microtubule plus-ends to increase the local tubulin concentration and promote polymerization, binding of XMAP215 proteins to the microtubule lattice is promoted by a disordered basic region at the C-terminus [341, 347]. Microtubule lattice-binding occurs with low affinity, which allows XMAP215 proteins to undergo several cycles of binding and unbinding and thus diffuse along the microtubule to eventually concentrate at microtubule ends [341, 347].
XMAP215 binding to the outermost protofilament tip [330, 348] may arise from the preferential binding of TOGs to curved tubulin dimers [344, 345, 345]. However, the coordination between microtubule tip tracking (XMAP215 remains at the tip for the addition of approximately 25 tubulin dimers [341]) and polymerization is less well understood. *In vitro* data on Stu2 proposes a ratcheting model [349]. When TOG domains are bound to free tubulin dimers, Stu2 binds weakly to the microtubule lattice, but binding is enhanced when TOG domains are empty. Thus, upon tubulin dimer release from Stu2, as the tubulin becomes incorporated at the growing tip, binding to the lattice via the basic region is triggered, which subsequently keeps the polymerase at the tip for a new round of tubulin dimer incorporation [349].
Uniquely, fission yeast possesses two family members: **Dis1 and Alp14** [350, 351], which both act as microtubule polymerases *in vitro* [332, 339]. Yet, while Alp14 is clearly implicated in the regulation of interphase microtubule dynamics [339], deletion of *dis1* only leads to a slight reduction of the interphase microtubule shrinkage speed [352]. In accordance, Dis1 does not track growing microtubule tips, but was found to be present in microtubule overlaps, where the MAP bundles interphase microtubules with preference for parallel oriented microtubules [352]. Additionally, Alp14 and Dis1 differ in their interaction partners and localization. While Dis1 interacts directly with Mal3 [332], and with kinetochore proteins [353–355], Alp14,

next to binding to kinetochores [356], also interacts with Alp7 (TACC homolog), which targets Alp14 to SPBs [260, 357]. Alp14, like XMAP215, is also implicated in promoting microtubule nucleation [100, 101, 123, 124, 358].

**CLASP** (CLASP1 & CLASP2 in human, MAST/orbit in *Drosophila*, Cls2 in *C. elegans*, Stu1 in *S. cerevsiae*, Cls1 or Peg1 in *S. pombe*) proteins have been reported to stabilize microtubules by **suppressing microtubule catastrophe and promoting rescue events** in yeast, *Drosophila* and human [359–363]. CLASP proteins also contain TOG domains, homologous to that of XMAP215 proteins [360, 364]. Yet, the human CLASP-specific TOG2 domain exhibits a different arrangement of the conserved tubulin-binding residues, which suggests that the CLASP TOG2 binds to tubulin dimers of a different conformation as XMAP215 TOGs [365–367]. CLASP and Cls1 can bind free tubulin dimers [364], indicating that they promote tubulin dimer incorporation into the microtubule lattice. Indeed, CLASP2$\alpha$, an isoform of CLASP2, has recently been shown to repair microtubule lattice defects by promoting tubulin dimer incorporation *in vitro* [368]. This requires solely the TOG2 domain with a microtubule-tethering region, contrarily to XMAP215 proteins whose polymerase activity relies on two linked TOG-domains [346, 347, 349]. In human cells CLASP can localize to microtubule plus-ends via interaction with EB1 [364, 369], or, like the fission yeast Cls1 and the Drosophila MAST/orbit, to antiparallel microtubule overlaps via Ase1/PRC1, and, hence, to the microtubule shaft (Figure 6, right panel) [370–372]. In fission yeast, **Cls1** does not localize to microtubule plus-ends [370], and does not track growing plus-ends *in vitro* [360]. In contrast, CLASP is restricted to microtubule overlaps by interaction with Ase1 where it resides with a very low turnover rate [360]. *In vitro* Cls1 accumulated as discrete spots along single microtubules and induced rescue, when the microtubule depolymerized back to the position of Cls1 accumulation [360]. Therefore, when a depolymerizing spindle microtubule enters the Cls1-enriched spindle midzone, microtubule rescue is induced [360, 370].

# 3 Assembly into a dynamic force-generating machine

Dynamic microtubules, centrosomes or SPBs, and chromosomes, together with numerous molecular motors and MAPs, self-assemble into a highly dynamic yet stable structure that can exert forces in the pN to nN range to segregate the entangled DNA into two identical sets. This requires continuous and extensive rearrangement of the spindle from its assembly in prophase, to the separation of sister chromatids in anaphase.

## 3.1 Prophase & prometaphase - Spindle assembly & kinetochore capture

During prophase and prometaphase, the mitotic spindle is assembled while microtubules are nucleated from MTOCs (centrosomes or SPBs) and spindle poles are separated. Furthermore, chromosomes are attached via microtubule-kinetochore attachments, and eventually aligned at the equatorial plate to achieve chromosome biorientation (each sister kinetochore is attached to microtubules from the opposite spindle pole).

Mitosis onset is initiated by association of the conserved **cyclin-dependent kinase 1** (**Cdc2** in *S. pombe*) with cyclin B [373–375], which promotes phosphorylation of an array of mitotic spindle components. This leads to increased microtubule nucleation from centrosomes or SPBs [376, 377]. Subsequently, **spindle poles become separated** in order to establish a **bipolar spindle array** (Figure 7). The master regulator of this process, from yeast to human, is **kinesin-5** (Figure 5, blue) [20, 22, 224]. Deletion or inactivation of the homotetrameric bipolar kinesin-5 leads to spindle collapse and the generation of **monopolar spindles**, ultimately resulting in erroneous chromosome segregation [20, 378–380]. Based on the motors ability to crosslink and slide apart antiparallelly oriented microtubules (see chapter 2.4.1), kinesin-5 motors localize to contact sites of microtubules originating from opposite spindle poles, crosslink them in an antiparallel configuration, and exert pushing forces by sliding them apart. As a result, spindle poles become separated and moved away from each other until they are located at opposite ends of the spindle (Figure 5) [22, 223, 381]. Accordingly, it has been demonstrated in *X. laevis* extracts that the rate of spindle assembly, referring to the velocity of spindle elongation until reaching a steady-state spindle length, matches the rate of KIF11-driven microtubule sliding [382].
Given the recent observation that purified Eg5 promotes microtubule polymerization [239], the hypothesis arises that the crucial contribution of kinesin-5 also depends on its ability to directly promote the growth of the microtubules that it crosslinks and slides, which remains to be tested *in vivo*.
In human cells, the plus-end-directed kinesin-12 KIF15 contributes to the generation of outward-directed microtubule sliding forces. KIF15 knockdown increases the fraction of monopolar spindles upon kinesin-5 inhibition, suggesting that these two kinesins contribute to spindle pole separation [383, 384].

These outward-directed forces appear to be antagonized by minus-end-directed motors of the **kinesin-14** and **dynein** families, which led to the proposition of a **force balance** within the

spindle [385] (Figure 7, yellow & dark red). Deletion or inactivation of kinesin-14 and/or dynein members could rescue bipolar spindle formation in absence of kinesin-5 activity in yeast, *X. laevis*, *Drosophila*, and human cells [224, 294, 384, 386–391]. In addition to its role in the generation of inward forces, kinesin-14 and dynein also focus microtubules close to the spindle poles [302, 392, 393].

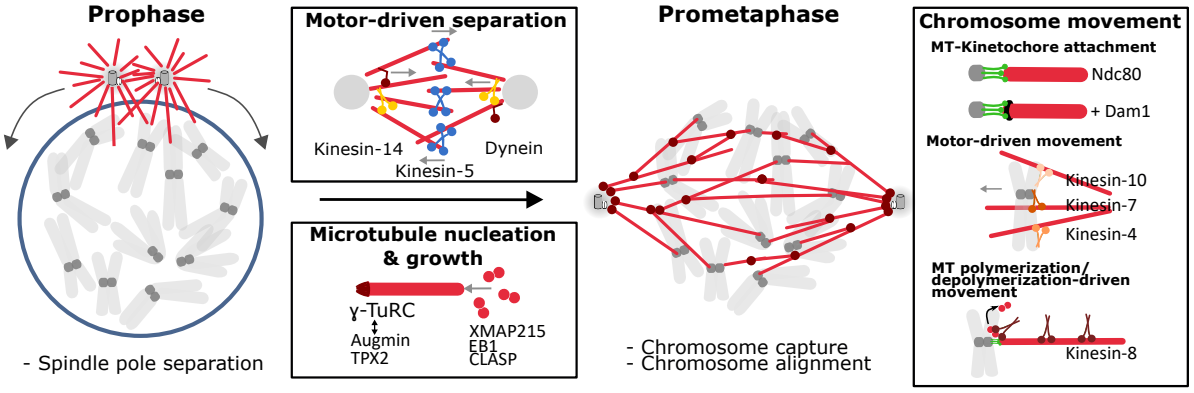


FIGURE 7: **Prophase & Prometaphase** - Scheme depicting the mechanisms of spindle pole separation and chromosome attachment and alignment. Spindle pole separation, promoted by microtubule motors that slide apart antiparallely oriented microtubules, most prominently kinesin-5 (blue) and opposing force generators, namely kinesin-14 (yellow) and dynein (dark red), occurs during prophase. A precise control of microtubule dynamics, by spindle components such as XMAP215, EB1 and CLASP is crucial for the process. While in yeasts, which undergoes closed mitosis, kinetochore capture occurs during prophase, the nuclear envelope (blue) breaks down in animal cells, marking the beginning of prometaphase. At that stage, spindle microtubules can explore the nuclear space and attach to chromosomes via the Ndc80 complex and the Dam1/DASH complex in yeast or the Ska complex in mammalian cells. Furthermore, microtubule nucleation from chromosomes and preexisting microtubules, mediated by Augmin and TPX2, assists the process of spindle assembly and speeds up the process of kinetochore capture. Upon establishment of microtubule-kinetochore attachments, chromosomes are moved toward the cell equator by motors in animal cells, namely members of the kinesin-4, -7 and -10 families and by microtubule polymerization, which is limited by kinesin-8 proteins in yeast and human.

Since fission yeast cells deleted for *cut7* (kinesin-5) and *pkl1* (kinesin-14) divide normally despite a decreased metaphase spindle length and a prolonged metaphase duration [259, 389], these mutant cells were used to identify the minimal requirements for spindle pole separation. In fact, in fission yeast, bipolar spindles can form in absence of all mitotic kinesins [259]. However, the presence of **Ase1**, the conserved microtubule crosslinker (see chapter 2.5.1), and **Cls1** (CLASP), the microtubule rescue factor (see chapter 2.5.2), becomes essential in the *cut7*Δ*pkl1*Δ mutant [259]. Hence, in yeast, passive microtubule crosslinking and microtubule stabilisation driven by Ase1 and Cls1 is sufficient to promote spindle bipolarity in the absence of sliding forces [394].

Importantly strong evidence exists, suggesting that a **precise balance between the microtubule sliding/crosslinking activity of kinesin-5 and the control of microtubule dynamics** is crucial for bipolar spindle assembly. Deletion of microtubule dynamics regulating MAPS, such as Csi1, Csi2, Alp7 (TACC), Alp14 & Dis1 (ch-TOG/XMAP215), and Mal3 (EB1) rendered the *cut7*Δ*pkl1*Δ mutant lethal by preventing bipolar spindle formation [395]. Further, it has been shown that *cut7*-deleted cells, which are otherwise lethal, were viable when grown in presence of low doses of microtubule-destabilizing drugs [395].

Upon successful spindle pole separation, the nuclear envelope breaks down (NEBD) in animal cells, allowing spindle microtubules to invade the former nuclear space and attach to kinetochores on chromosomes. This initiates **prometaphase**, encompassing the events from NEBD to the alignment of chromosomes at the equatorial plate at metaphase onset. Since yeast undergoes closed mitosis, there is no distinct prometaphase, and microtubule-kinetochore attachments are established during prophase simultaneously with spindle pole separation [275].

**Kinetochore capture** by microtubules has been explained by the prominent **'search-and-capture'** model, established by Mitchison & Kirschner, after observing the dynamic behavior of microtubules [12]. By undergoing stochastic transitions between phases of growth and shrinkage, microtubules explore the cytoplasm until they find and capture kinetochores [396]. However, mathematical modeling demonstrated that the time required to capture all kinetochores by this mechanism alone would greatly exceed mitosis duration [397].
Consequently, other mechanisms have been shown to assist in the process. These include **centrosome-independent microtubule nucleation** (Figure 7) from spindle microtubules and chromosomes (see chapter 2.2.1). In particular, the Ran-GTP gradient and the CPC generate an environment that favors microtubule nucleation and growth around chromosomes, and these microtubules can subsequently be incorporated into the spindle [109, 114, 115, 117, 183, 398]. In fission yeast, where microtubules are nucleated only from SPBs [399, 400], microtubules pivot around the SPB, which further allows exploration of the intranuclear space and potentially speeds up kinetochore capture [400, 401]. Moreover, the likelihood of a microtubule finding a kinetochore is increased in fission yeast cells, due to the fact that kinetochores are localized in very close proximity to SPBs at mitosis onset [167]. Hence, the area that has to be scanned for kinetochores is smaller as compared to the area in mammalian cells, and consequently the time required for kinetochore capture by microtubules emanating from spindle poles is shorter.

Formation of **kinetochore-microtubule attachments** relies on kinetochore components (Figure 7, right panel), such as the conserved Ndc80 complex [174, 175], the human Ska complex, and the yeast Dam1/DASH complex [180–182, 402] (see chapter 2.3.1). In *S. pombe*, the two members of the XMAP215 family, Dis1 and Alp14, and the kinesin-8 motors Klp5 and Klp6 are components of mitotic kinetochores as they physically interact with the Ndc80 complex [274, 350, 351, 354, 356, 403]. This establishes a direct link between kinetochore capture and kinetochore microtubule dynamics.

Upon kinetochore-microtubule attachment, **chromosomes are aligned at the equatorial plate**, which favors biorientation of chromosomes. In animal cells, kinetochores often form an initial contact with the lateral microtubule lattice. Chromosomes are subsequently moved along the microtubule lattice towards the cell equator. This requires active transport by **dynein** and members of the **kinesin-7** family (KIF10, CENP-E) attached to kinetochores, as well as **chromokinesins**, including kinesin-10 and -4 (Kid/NOD and KIF4A/Xklp1), which generate pushing forces acting on chromosome arms, so-called 'polar ejection forces' (Figure 7, right panel) [404–410].
In contrast to animal cells and budding yeast [411–413], in fission yeast kinetochores rarely attach to the lateral microtubule surface, but rather connect directly by end-on attachment of the microtubule plus-end to the kinetochore [180, 399]. This could, again, be a consequence of kinetochores being localized adjacently to SPBs, out of which the microtubule plus-ends originate [167]. The primary formation of end-on attachments may explain why the homologous motors acting on kinetochore movements along microtubules in animal cells are either not involved in the process or not present in *S. pombe* [399, 414]. On the contrary, kinetochore movement during pro- and metaphase is mostly driven by **microtubule polymerization/depolymerization**. Deletion of MAPs that regulate microtubule dynamics and associate with mitotic kinetochores such as Alp14 & Dis1 [187, 354, 356], Mal3 [188, 415], and the kinesin-8 motors Klp5/Klp6 [186, 270, 274, 275, 403] strongly impairs kinetochore movement and attachment. Members of the **kinesin-8** family also regulate k-fiber dynamics in higher organisms (Figure 7, right panel). Mammalian Kif18a accumulates at the plus-end of kinetochore microtubules and, due to its ability to regulate microtubule dynamics in a length-dependent manner (see chapter 2.4.1), the motor favors depolymerization of longer k-fibers and contributes to chromosome alignment at the metaphase plate [416]. Accordingly, deletion of the fission yeast *klp6* results in an off-centered distribution of kinetochores along the spindle [270, 275]. By the end of prophase in yeast or prometaphase in animal cells, the mitotic

spindle is assembled and chromosomes are aligned at the equatorial plate.

Yet during the process of kinetochore capture, **erroneous kinetochore-microtubule attachments** commonly occur. Only one sister kinetochore can be attached to microtubules from the same pole (monotelic), both sister kinetochores can be attached to microtubules from the same pole (syntelic) or one kinetochore can be attached to microtubules emanating from both spindle poles (merotelic) [115]. To achieve segregation of sister chromatids towards opposite spindle poles, one sister kinetochore must be attached to microtubules emanating from one spindle pole and the other sister kinetochore to microtubules from the opposite spindle pole (amphitelic). Attachment errors must, therfore, be corrected before sister chromatids are separated at anaphase onset, during prometaphase and metaphase. Briefly, correction occurs via recognition of unattached kinetochores or a reduced tension between sister kinetochores [372, 417] via components of the **spindle assembly checkpoint (SAC)** that eventually destabilize erroneous kinetochore-microtubule attachments [418]. A key regulator of the correction process is the Aurora B kinase [417, 419–421]. Low tension at kinetochores results in increased Aurora B-dependent phosphorylation of kinetochore components, such as the Ndc80, the Dam1, or Ska1 complexes, leading to destabilization of the erroneous microtubule-kinetochore attachment and allowing for correction of the attachment [422].

## 3.2 Metaphase - Spindle length regulation

While metaphase provides more time for the correction of erroneous kinetochore-microtubule attachments, a **steady-state spindle length** is maintained over considerable time scales. This is quite remarkable, because, as in all other mitotic phases, the mitotic spindle remains highly dynamic: microtubules grow and shrink while microtubule motors continue to generate forces. Hence, these processes must be accurately balanced to keep the metaphase spindle at a constant length. Importantly, this is crucial for proper chromosome segregation [353, 423]. In fission yeast cells, chromosome segregation defects directly correlate with altered metaphase spindle length [259, 424].

Metaphase spindle length can be altered by perturbing the following processes (Figure 8): (i) microtubule sliding, (ii) microtubule dynamics, (iii) microtubule flux, (iv) pulling forces acting on astral microtubules, and (v) microtubule nucleation. The contribution of each process to spindle length regulation strongly depends on spindle architecture and dynamics.

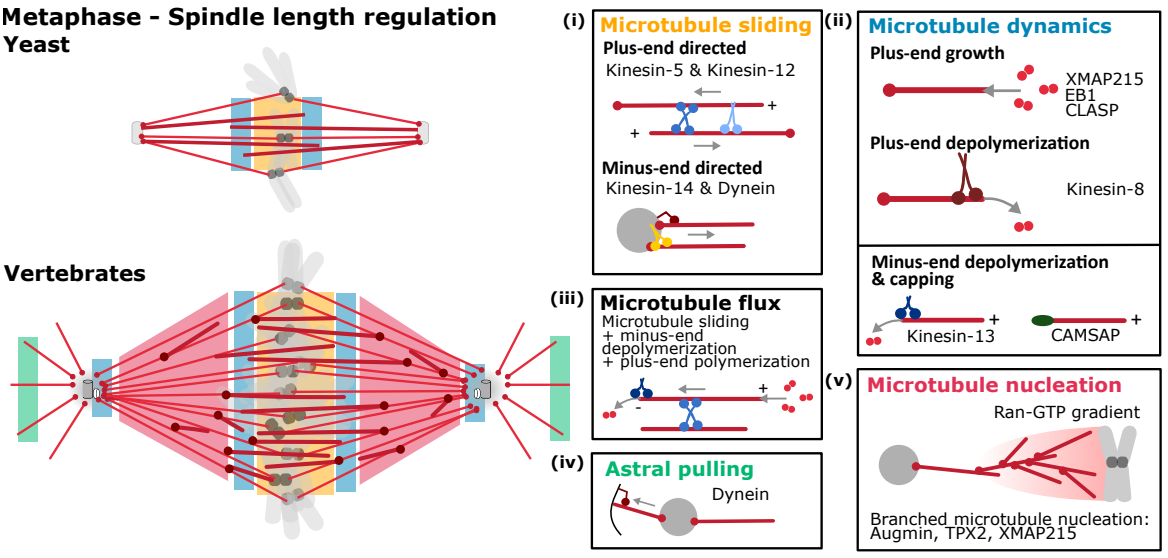


FIGURE 8: **Metaphase spindle length regulation** - Scheme depicting the structure of metaphase spindles in yeast and vertebrates, and the modules that regulate spindle length are illustrated by the color-coded areas within the spindle and the underlying mechanism of each module in the boxes. In yeast spindles, mitotic spindle length is mainly controlled by (i) microtubule sliding forces (yellow), generated by kinesin-5 (blue) and its opposing motor kinesin-14 (yellow), and (ii) microtubule dynamics (blue) regulating MAPs such as the XMAP215 members, CLASP and kinesin-8 (dark red). In animal cells these mechanisms are also active, whereby additional spindle components are involved, such as kinesin-12 (light blue) and dynein (dark red) as microtubule motors, EB1 as a microtubule growth promoting factor, and kinesin-13 (dark blue) and CAMSAPs (green) as regulators of microtubule minus-end dynamics. In *Drosophila* (iii) microtubule flux, generated by a combination of microtubule sliding, microtubule plus-end polymerization and minus-end depolymerization, contributes to spindle length regulation. In *C. elegans* (iv) astral pulling forces (green) generated by cortical dynein are involved in the regulation of spindle length. Moreover, in animal cells, the (v) microtubule nucleation profile (red), prominently regulated by the Ran-GTP gradient originating from chromosomes, has been shown to determine spindle length.

In fission yeast, microtubules originate only from spindle poles, microtubules do not undergo flux, and pulling forces on astral microtubules from the cell cortex are not active. Thus, spindle length is only regulated by a balance of microtubule sliding motors, and precise control of microtubule dynamics (Figure 8) [105, 156, 400].

**(i) microtubule sliding forces** (Figure 8, i) generated by plus- and minus-end-directed motors are fine-tuned to achieve a force balance that maintains a constant spindle length [385]. Accordingly, *S. pombe* cells deleted for *cut7* (**kinesin-5**) and *pkl1* (**kinesin-14**) exhibit reduced metaphase spindle length, indicative of a perturbed force balance in absence of the plus-end-directed sliding motor Cut7 [259, 261, 424]. While *pkl1* deletion alone does not affect spindle length, additional deletion of the second fission yeast kinesin-14 *klp2* in *cut7*Δ*pkl1*Δ mutant cells increases metaphase length, suggesting that kinesin-14 motors do oppose kinesin-5 [261]. A similar kinesin-5/kinesin-14 mediated force balance is proposed to maintain spindle

length in *Drosophila* early embryos [388, 425]. In human cells, metaphase spindle length is reduced upon kinesin-5 inactivation and depletion of the other plus-end-directed sliding motor KIF15 (**kinesin-12**) [384, 426].
Interestingly, in absence of kinesin-14 activity, spindle length is often reduced, which appears to contradict the hypothesis that the minus-end-directed motor generates inward forces, which oppose kinesin-5. This could stem from the motor's function in aligning spindle midzone microtubules, and in that way facilitating the binding of kinesin-5, as suggested in *S. cerevisiae* [427]. Alternatively, the function in regulating microtubule nucleation and dynamics proposed for the *S. pombe* Pkl1 [428, 429] could play a role.
In human cells, the kinesin-5 and kinesin-12 mediated outward forces are additionally opposed by **dynein** [302, 430, 431], with the depletion of dynein, but not dynactin subunits, leading to increased metaphase spindle length [302].

Control of **(ii) microtubule dynamics** (Figure 8, ii) is also directly linked to the regulation of spindle length in yeast cells. In absence of the microtubule-depolymerizing motors of the **kinesin-8** family, Klp5 and Klp6, metaphase spindle length is increased [403, 432]. Kinesin-8 proteins also regulate spindle length in *S. cerevisiae*, *Drosophila*, and human cells [263, 272, 433, 434]. Moreover, inactivation of the **XMAP215** homolog Alp14, a microtubule polymerase, reduces metaphase spindle length [339]. This effect is enhanced in absence of its paralog Dis1, which has also been shown to promote microtubule growth *in vitro* [332, 395]. In *X. laevis*, XMAP215 depletion reduces spindle length as well [435] and in egg extracts and *in vivo* the XMAP215 levels set spindle length in a dose-dependent manner [436, 437]. Other microtubule dynamics regulating spindle components have also been implicated in the regulation of spindle length. **CLASP** controls microtubule and spindle length from yeast to human [369, 438–442]. **CAMSAP1**/**Patronin** protects microtubule minus-ends from depolymerization by the *kinesin-13* Klp10A in *Drosophila* [443]. Kinesin-13 members promote minus-end depolymerization, in *Drosophila*, *Xenopus*, and human, with their depletion resulting in increased spindle length [278, 280, 293, 443, 444]. Lastly, the microtubule severing enzyme **katanin** regulates spindle length in *C. elegans* and frogs [445–447].

In animal cells, a coordination of microtubule sliding forces, microtubule plus-end polymerization, and microtubule minus-end depolymerization generates a so-called **(iii) microtubule flux** (Figure 8, iii), which is implicated in the maintenance of a steady-state spindle length [280, 426, 448, 449]. The poleward movement of lattice incorporated tubulin dimers was already observed in the early days of spindle research by polarization microscopy when a UV

microbeam was used to create an area of lower birefringence as compared to the birefringence of unaffected spindle fibers [450]. This reduced birefringence area moved towards spindle poles before disappearing [450]. Tim Mitchison confirmed this observation, using photoactivatable fluorescent tubulin in mammalian cells, demonstrating that, within kinetochore fibers, the photoactivated area moved toward spindle poles [449]. The poleward flux is generated by sliding of microtubules coupled to plus-end growth, mediated for instance by CLASP [451, 452], and kinesin-13 mediated depolymerization at microtubule minus-ends [278, 280, 426, 453]. Accordingly, an up- or down-regulation of either of these components leads to a change in spindle length.

Next to the poleward microtubule flux, the regulation of pulling forces from the cortex and of microtubule nucleation contributes to spindle length regulation in animal cells, but not in fission yeast (Figure 8).
In *C. elegans embryos*, which are remarkable with regards to the extensive amount of astral microtubules growing from centrosomes, **(iv) pulling forces acting on astral microtubules** can regulate spindle length (Figure 8, iv) [165, 454]. Moreover, these forces are crucial for mitotic spindle positioning [165]. **Dynein** at the cell cortex binds to astral microtubules and actively pulls on them by walking towards the minus-end, moving spindle poles towards the cell cortex [165]. Consequently, impairment of cortical force generation results in decreased spindle length [165].

In vertebrates, as opposed to yeast and *C.elegans* [156, 455], the spatial regulation and the extent of **(v) microtubule nucleation** (Figure 8, v) contribute to the determination of spindle length. In fact, in *X. laevis* egg extract spindles, the length distribution of individual microtubules is exponential, with the majority of microtubules being rather short and the average length of spindle microtubules is shorter than half-spindle length [102, 456]. This suggested microtubule nucleation initiated on spindle microtubules, that emanate from centrosomes, is required to reach wild-type metaphase spindle length. Indeed, using *Xenopus* egg extract monopolar spindles and U2OS cells it has been elegantly shown that spindle length does not only depend on the length of individual spindle microtubules, but also on the nucleation profile of microtubules within the spindle [457, 458]. In particular, in the *Xenopus* egg extract spindles, it has been demonstrated that microtubule nucleation from centrosomes and chromosomes alone can not account for the regulation of spindle length, and microtubule nucleation from pre-existing microtubules is necessary for spindles to reach a sufficient length [457]. Accordingly, spindle length is sensitive to TPX2 levels in human cells [458, 459].

While the spindle maintains a steady-state spindle length, metaphase provides additional time for the correction of erroneous kinetochore-microtubule attachments. By the end of metaphase, when all chromosomes are bioriented and the SAC is satisfied, progression to anaphase is enabled, which promotes separation of sister chromatids into two identical sets [460]. Before sister chromatids can be separated, the protease separase cleaves the cohesin complex between sister chromatids [461–464].

At the **metaphase-anaphase** transition, SAC satisfaction leads to activation of the anaphase promoting complex (APC), promoting Cyclin B degradation and **downregulation of CDK1 activity** (**Cdc2** in *S. pombe*) [318, 465–467]. The concomitant activity increase of phosphatases of the **Cdc14** (**Clp1** in *S. pombe*) or PP1/PP2A families enables dephosphorylation of CDK1-target proteins [466–470]. This leads to a **phosphorylation-dephosphorylation switch** of multiple spindle components, a prominent example being the microtubule crosslinker and crucial anaphase B spindle component Ase1/PRC1/MAP65, and a stark shift in localization and activity of numerous other proteins that eventually alters spindle architecture and behavior from metaphase to anaphase [184, 318, 471–473].

## 3.3 Anaphase A - Chromosome separation

The process of sister chromatid separation can be mechanistically divided into anaphase A, the movement of chromatids to spindle poles (chapter 3.3), and anaphase B, the separation of spindle poles driven by the elongation of the mitotic spindle (chapter 3.4). In many cell types, both processes occur simultaneously, while, in *S. pombe* anaphase A and B occur sequentially [184, 187].

Early EM studies indicated that kinetochore-associated microtubules shorten and disappear concomitantly to chromosome movement toward spindle poles [13, 156, 161]. Also, fission and budding yeast cells still promote poleward movement of kinetochores in absence of all minus-end-directed motors [399, 474], which could in principle account for poleward chromosome motion. In higher organisms, the contribution of, for instance, kinetochore-associated dynein to the process can vary dramatically from a prominent impact in *Drosophila* to little contribution in mammalian Ptk1 cells [410, 475, 476]. Thus, motor-driven transport of chromosomes does not represent the major mechanism of anaphase A.

Instead, **microtubule depolymerization** appears to be the driving force from yeast to human (Figure 9). In most organisms, the kinetochore-attached microtubule plus-end undergoes loss

of tubulin dimers [15, 184, 279, 472, 477], while in organisms where microtubules undergo flux, depolymerization at microtubule minus-ends can contribute to the process (Figure 9, left panel) [279, 280].

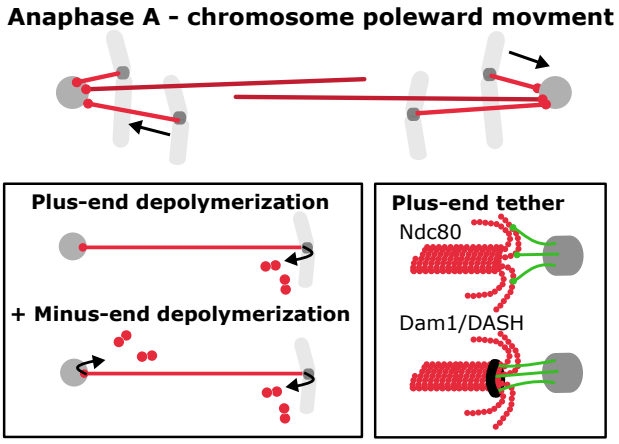


FIGURE 9: **Anaphase A - sister chromatid separation** - Scheme depicting the mechanism of sister chromatid poleward movement during anaphase A. Microtubule depolymerization is the driving force in almost all organisms. Microtubules depolymerize only at the plus-end, such as in yeast, or concomitantly at the minus-end, as it is the case in *Drosophila*. To allow movement of kinetochores by depolymerizing microtubule plus-tips they must be connected by a dynamic tether. A prominent example is the yeast Dam1/DASH complex (black), which forms a ring-like structure around the microtubule and is suggested to be pushed towards the microtubule minus-ends by the protofilaments that 'peel off' as the microtubule depolymerizes. Interaction of the Dam1/DASH complex with the kinetochore Ndc80 (green) complex subsequently allows kinetochores (gray) to track depolymerizing microtubule tips.

To couple microtubule plus-end depolymerization and kinetochore movement, a tether that remains associated with the disassembling microtubule tip is necessary (Figure 9, right panel). Such a function can be fulfilled by the yeast Dam1 complex (see chapter 2.3.1) [478, 479], which assembles into a ring around the microtubule (Figure 9, right panel) [480, 481]. As protofilaments bend and curl away from the microtubule axis upon depolymerization [140], they translocate the Dam1-complex along the microtubule lattice towards spindle poles [179, 482]. In animal cells, this task is performed by the Ska complex, which does not form a ring but lateral bridges between the Ndc80 complex and the disassembling microtubule tip, serving as a dynamic tether [182, 483, 484].

Kinetochore microtubule depolymerization at the plus-end may be promoted by kinesin-8 proteins [432, 485] or kinetochore-localized kinesin-13 [280, 486].

## 3.4 Anaphase B - Spindle elongation

While *Xenopus* extract spindles separate their chromosomes almost exclusively by anaphase A [487], **spindle elongation** during anaphase B contributes equally to chromosome separation in human cells [488], is the main driver of the process in yeast [184, 226], and is the sole source of chromosome separation in *C. elegans* [79].

### 3.4.1 The anaphase B spindle structure & composition

Even though the microtubule number varies greatly, from approximately 6 microtubules in fission yeast [105] to hundreds in mammalian cells [8, 161], anaphase B spindles in all organisms form a highly ordered structure where interpolar microtubules overlap in an antiparallel manner, the **spindle midzone** (Figure 10) [13, 105, 156, 161].
The emergence of this highly ordered spindle architecture is concomitant with and promoted by a change in the spindle composition at anaphase onset, initiated by the phosphorylation-dephosphorylation switch at the metaphase-anaphase transition [318]. Dephosphorylation of **Ase1/PRC1** (Figure 8, dark blue) at Cdk1-phosphosites reduces crosslinker turnover at the antiparallelly oriented microtubules at the spindle center and, hence, promotes the formation of a stable spindle midzone [256, 489, 490]. PRC1 family members subsequently recruits a myriad of proteins (see chapter 2.5.1). Ase1/PRC1 regulates midzone localization of the kinesin-6 proteins MKLP1 and MKLP2 in mammalian cells and Klp9 in *S. pombe* [256, 491], the microtubule dynamics regulating kinesin-4 KIF4 [207, 212, 490], and the microtubule rescue factor CLASP [212, 315, 370, 491].

### 3.4.2 Microtubule sliding forces to promote spindle elongation

The numerous modifications of spindle midzone composition at the metaphase-anaphase transition already stress the importance of this region for anaphase B. Effectively, laser-mediated destruction of interpolar microtubules at the midzone in diatoms, fission yeast, and human cells prevents spindle elongation, which can proceed when astral microtubules are cut [14–16, 162, 488]. Therefore, the spindle midzone represents a major source of force generation for anaphase B spindle elongation. It was proposed early on that spindle elongation is driven by **sliding apart of antiparallel spindle microtubules at the midzone**: microtubule motors that crosslink microtubules and walk towards their plus-ends slide apart adjacent microtubules

and increase spindle length [492]. This was assumed to be a plausible mechanism for elongation of spindles where interpolar microtubule minus-ends reach spindle poles, as in yeast or diatom spindles [9, 13, 105, 156]. In this situation, midzone-generated forces can be directly transmitted to spindle poles. However, in spindles of higher organisms, where microtubule minus-ends are present along the entire length of the spindle and are not directly anchored at centrosomes [161], midzone-mediated microtubule sliding also drives spindle elongation [493]. This may be ensured, since midzone microtubules are crosslinked to other spindle microtubules, which in turn originate from spindle poles [161]. In particular, bridging fibers, are crosslinked to a high degree with the associated k-fibers [163, 488, 494]. Thus, in both cases, the force generated at the midzone can be transferred to spindle poles and push them apart.

**Kinesin-5** family members are crucial midzone-associated force generators that drive spindle elongation. Since these motor proteins typically form homotetramers, they can crosslink and slide apart antiparallel microtubules without the help of other binding partners, and drive anaphase B spindle elongation (Figure 10, light blue; see chapter 2.4.1). Depletion or inactivation of kinesin-5 proteins reduces the speed of spindle elongation in *S. cerevisiae*, *S. pombe*, *Drosophila*, and human cells [214, 226, 278, 425, 476, 495, 496].

Besides kineisn-5, also other central spindle components contribute to the generation of microtubule sliding forces in human cells and *S. pombe* [214, 256, 259]. In human cells, perturbation of the activity of Eg5 and PRC1 completely prevents spindle elongation, and the same phenotype was observed upon Eg5 inhibition in cells depleted for the plus-end-directed **kinesin-4** KIF4A [214]. Since PRC1 promotes KIF4A recruitment to antiparallel overlaps [206, 207, 212], and KIF4A has been shown to promote microtubule sliding *in vitro* when bound to PRC1 [211, 213, 215], the observed effect upon PRC1 depletion is thought to stem from the abolished recruitment of KIF4A [214]. Hence, Eg5 and KIF4A promote microtubule sliding at the spindle midzone and drive spindle elongation during anaphase B in human cells [214]. Even though to a smaller extent, also other motors contributed to spindle elongation, namely the **kinesin-6** motors MKLP1 and MKLP2 and the kinesin-8 KIF18A [214]. The authors of this study proposed that the role of kinesin-6 motors during spindle elongation in human cells rather originates from a signalling function, as kinesin-6 recruits Aurora B [244, 252], and Aurora B phosphorylates KIF4A [206].

Contrarily, in fission yeast, the **kinesin-6 Klp9** represents the main driver of antiparallel microtubule sliding during anaphase B (Figure 10, green) [256, 259, 261]. The kinesin-5 Cut7

also promotes spindle elongation, as in absence of the activity of Klp9 and Cut7, spindle elongation is completely abolished, while the presence of either Klp9 or Cut7 alone still allows the spindle to elongate, although with reduced velocity [259].

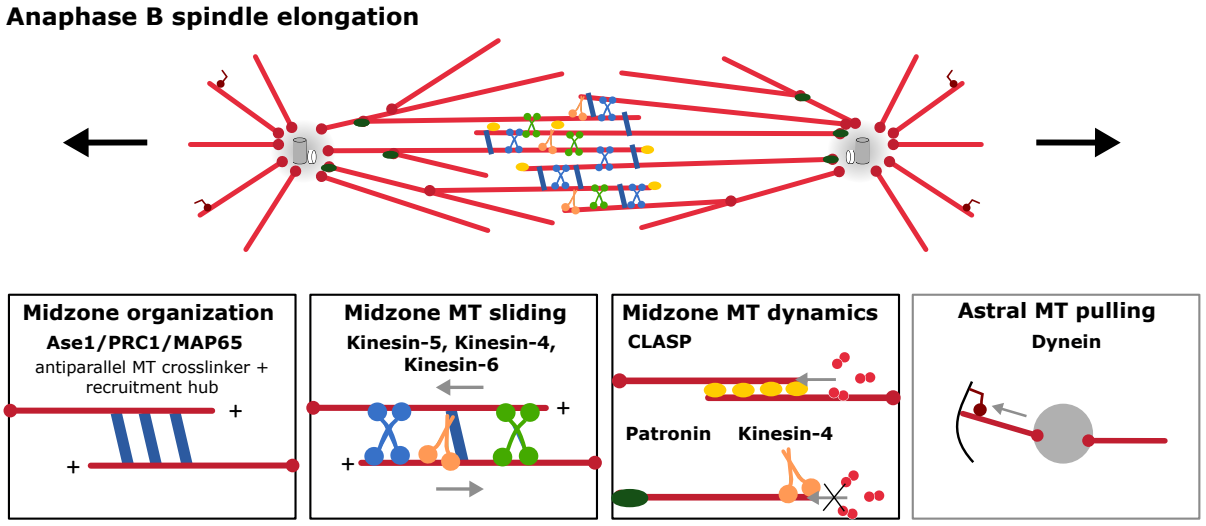


FIGURE 10: **Anaphase B - spindle elongation** - Scheme illustrating the anaphase B spindle structure and the modules that promote spindle elongation. The spindle midzone is organized by microtubule crosslinkers of the Ase1/PRC1 (dark blue) family from yeast to human. Given its microtubule crosslinking function and the additional role in recruiting many midzone components, Ase1/PRC1 is a crucial midzone organizer. In many organisms, spindle elongation is driven by microtubule sliding forces generated at the midzone, promoted by kinesin-5 (blue) and kinesin-4 (orange) in human cells and by kinesin-5 and kinesin-6 (green) in fission yeast. Moreover, microtubule dynamics have to be precisely controlled to allow net polymerization and enable spindle elongation and sustained microtubule sliding. CLASP (yellow) as a growth promoting and rescue factor, Patronin (dark green) as a minus-end stabilizer and Kinesin-4 as a factor that inhibits microtubule growth have been implicated in the regulation of microtubule dynamics during anaphase B. In a few systems, such as Ptk1 cells, astral pulling forces mediated by dynein (dark red) contribute to spindle elongation.

### 3.4.3 Astral pulling forces to promote spindle elongation

While microtubule sliding is the dominant mechanism of spindle elongation during anaphase B in most organisms [15, 16, 162, 225, 455, 493, 497], cortical pulling forces acting on astral microtubules have been shown to promote spindle elongation in the fungus *Ustilago maydis* and Ptk1 cells [498, 499]. Cortical pulling forces can be generated by **dynein** anchored at the cell cortex (Figure 10, dark red), which walks towards the microtubule minus-end and pulls on spindle poles [500], or by polymerization of the cortex-linked microtubule plus-ends [501]. In presence of this mechanism, kinesin-5 can act as a brake against spindle elongation [502]. This matches the *in vitro* observation that recombinant Eg5 slows down microtubule sliding

when it occurs with velocities that exceed the motor's inherent sliding velocity [228].
Cortical pulling forces have also been implicated in the regulation of spindle elongation in *C. elegans* [165, 454, 503]. Perturbation of cortical dynein activity reduces the extent of spindle elongation, measured by the centrosome-centrosome distance [162, 165, 454]. Yet, it has recently been shown that the movement of chromosomes during anaphase B is primarily promoted by microtubule sliding [162]. While spindle pole movement was impaired upon disruption of cortical pulling forces, chromosome movement during anaphase B was rather inhibited by laser ablation of midzone microtubules [162]. Importantly, the speed by which chromosomes were moved was equal to the speed of microtubule sliding, indicating that chromosomes are strongly coupled to midzone microtubules [162]. Microtubule sliding is, therefore, proposed to be the dominant mechanism of chromosome separation during anaphase A and B [162].
Arguing against a prominent contribution of cortical pulling forces in fission yeast or human cells, dynein deletion or inactivation of dynein did not significantly impact spindle elongation [256, 431, 490].

### 3.4.4 Microtubule growth to allow spindle elongation

Motor-mediated force generation without interpolar microtubule polymerization does not seem sufficient to allow the fission yeast spindle to elongate from approximately 2 to 12 µm [105, 187]. Also in human cells an elongation extent of 6 to 9 µm can not be realized without microtubule growth, since the average midzone length accounts to approximately 5 µm [504, 505]. Theoretically, if microtubule sliding would be the only mechanism of spindle elongation, the extent of elongation can not exceed the microtubule overlap length, as otherwise the spindle would be unstable and separate into two half spindles.
Hence, **interpolar microtubule polymerization** is required for anaphase B spindle elongation. Indeed, early photobleaching experiments in Ptk1 cells showed that tubulin subunits are added to microtubule plus-ends, while the interpolar microtubules are slid apart [506]. Consistent with the requirement of interpolar microtubules to grow in order to sustain sliding, isolated diatom spindles stop elongating in absence of soluble tubulin and resume elongation when soluble tubulin is added [507–509].
The regulation of plus-end growth during anaphase B (Figure 10) has been proposed to be regulated by the microtubule rescue factor **CLASP** in *C. elegans* zygotes and mammalian cells [442, 510], which is also required to maintain a stable anaphase spindle in fission yeast [370].

On the other hand, the **kinesin-4** KIF4A suppresses microtubule dynamics and restricts the overlap length, which is required to terminate anaphase B spindle elongation [511].
Interpolar microtubule net polymerization can be enhanced by suppression of kinesin-13 mediated minus-end depolymerization, in organisms where spindle microtubules undergo flux, such as *Drosophila* embryos [278, 425, 453]. Kinesin-13 inhibition is regulated by the minus-end stabilizer **Patronin** upon cyclin B degradation at anaphase onset [280, 453]. This induces a switch from the steady-state spindle length during metaphase, where microtubule plus-end polymerization and minus-end depolymerization match, to microtubule elongation during anaphase, where microtubule minus-end depolymerization is turned off. In these cells, a spatial gradient of microtubule plus-end catastrophes, that declines towards the spindle midzone, is also supposed to facilitate spindle elongation [471]. An increased catastrophe frequency of microtubules close to the spindle midzone, elevates the microtubule density at this location and supports the formation of robust antiparallel interpolar microtubule bundles, which may allow the binding of more sliding motors [471].

Besides, allowing motor-generated microtubule sliding, the growth of interpolar microtubules at the plus-ends itself could generate the forces necessary for spindle elongation by means of active pushing [512], for instance against crosslinked microtubules from the opposite spindle pole. However, evidence for such a mechanism is missing *in vivo*.

### 3.4.5 Coordination of microtubule sliding and growth

Regarding the requirement of both microtubule sliding and microtubule plus-end growth during spindle elongation in several organisms, the question arises of how both processes are coordinated. Is microtubule growth limiting for microtubule sliding and, consequently spindle elongation, or is microtubule sliding limited by microtubule growth. Alternatively, the two processes could be regulated independently. However, to achieve robust spindle elongation, we assume that coordination of growth and sliding is necessary. Supporting this hypothesis, the spindle midzone is kept at a constant length throughout anaphase B spindle elongation in fission yeast and human cells [105, 511, 513], which indicates that microtubule growth and sliding have to occur at similar speeds.
Two models have been proposed to explain the coordination of microtubule sliding and growth.

*In vitro* experiments including recombinant Xklp1, the *Xenopus* kinesin-4, and PRC1, suggest a model in which **microtubule growth is induced by microtubule sliding** (Figure 11)

[207]. PRC1 forms the overlap, with the overlap length correlating with the number of bound PRC1 molecules, and recruits Xklp1, which inhibits microtubule polymerization. Accordingly, the number of kinesin-4 molecules is set by the overlap length. When microtubules are slid apart, the overlap shrinks, and subsequently the number of kinesin-4 molecules decreases, therefore allowing the associated microtubules to grow [207, 213].

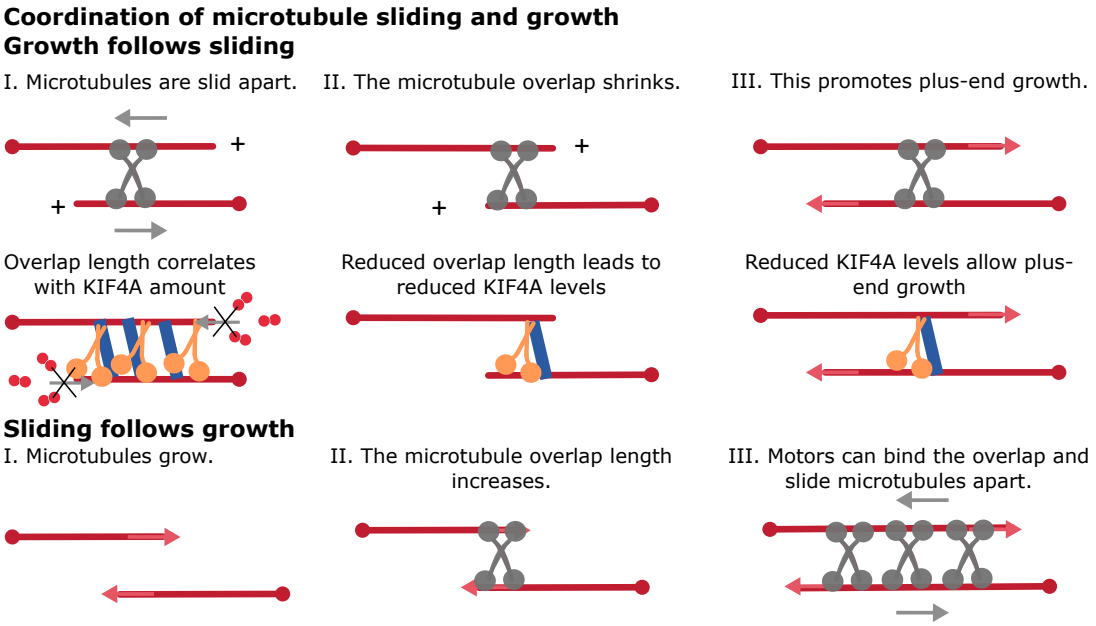


FIGURE 11: **Coordination of microtubule sliding and growth** - Scheme depicting the two models that have been proposed for the coordination of microtubule sliding and growth. (i) Microtubule sliding limits growth: When a microtubule is slid apart by a motor (gray), the overlap length decreases, which promotes microtubule growth. This has been demonstrated *in vitro*, where a reduction in the overlap length causes a reduction in PRC1-recruited (blue) KIF4A (orange), which consequently allows microtubules to grow. (ii) Microtubule growth limits sliding: growth of interpolar microtubules results in an increase of the overlap length, which allows binding of sliding motors (gray) and subsequently spindle elongation.

On the other hand, in *S. pombe*, treatment with low doses of microtubule destabilizing drugs, resulted in a reduction of the anaphase B spindle elongation [257], indicating that the **growth velocity may limit the speed of microtubule sliding** (Figure 11). Also in other systems, a perturbation of microtubule dynamics and reduced microtubule growth rates resulted in a decreased spindle elongation velocity [514, 515], while increased microtubule growth rates were linked to faster spindle elongation [272]. However, the precise mechanism that coordinates both processes and determines the speed of spindle elongation *in vivo* is unknown.

### 3.4.6 Relevance of anaphase B spindle elongation

By significantly contributing to the separation of sister chromatids into two identical sets with a sufficient distance between them and the cytokinetic ring, which is formed at the position of the spindle midzone, anaphase B is a crucial phase of mitosis. Accordingly, completely abolishing spindle elongation in fission yeast (in absence of Klp9 and Cut7 activity) or in human cells (in absence of Eg5 and PRC1 or KIF4 activity) leads to major defects in chromosome segregation and the generation of aneuploid cells [214, 259]. Furthermore, anaphase B spindle elongation is implicated in the correction of chromosome attachment errors [516–518]. Finally, with anaphase onset, cytokinetic ring assembly and constriction is initiated, in part, by the spindle midzone component PRC1 and its downstream effectors MKLP1 and MKLP2 [318].
In conclusion, anaphase B promotes the sufficient spatial separation of sister chromatids, and is involved in the regulation of cytokinesis, which eventually separates the mother cell into two daughter cells with identical chromosome sets.

# 4 Adjustment to the cellular environment - Mitotic spindle scaling

Besides the regulation of the previously described interplay of microtubules, molecular motors, and MAPs that allows chromosome segregation, the mitotic spindle must additionally adjust to its cellular environment. One such parameter the spindle adjusts to is **cell size**.
For instance spindle length scaling with cell size was already evident from early EM studies in fission yeast and Ptk1 cells, where the small yeast cells assembled much shorter spindles as compared to Ptk1 cells [13, 156, 161]. Though, attention to the phenomenon of **spindle length scaling** was paid only later when studied within the same organism. The early embryonic development of various model organisms is an ideal system to study scaling of cell structures, since cell size gradually decreases by, sometimes, several orders of magnitude while the embryo undergoes successive rounds of cell division.

## 4.1 Spindle length scaling with cell size

During early embryogenesis of *X. laevis*, *C. elegans*, the sea urchin *P. lividus*, mouse, and other metazoans, spindle length at metaphase, defined by the pole-to-pole distance, linearly

increases with cell size until an upper-limit [440, 454, 519–524]. Below an approximate maximum spindle length of 50 µm, spindle length decreases with cell size as embryonic development progresses (Figure 12) [520]. The scaling of spindle length with cell size also happens in single cell organisms that do not undergo embryogensis, like *S. cerevisiae* [272], where anaphase B spindle length has been examined, and in different cancer cell lines [525]. Scaling of spindle length with cell size can also be observed when comparing closely related organisms, such as the frogs *Xenopus tropicalis* and *X. laevis* [526]. Evidently, spindle length scaling with cell size is conserved among various organisms.

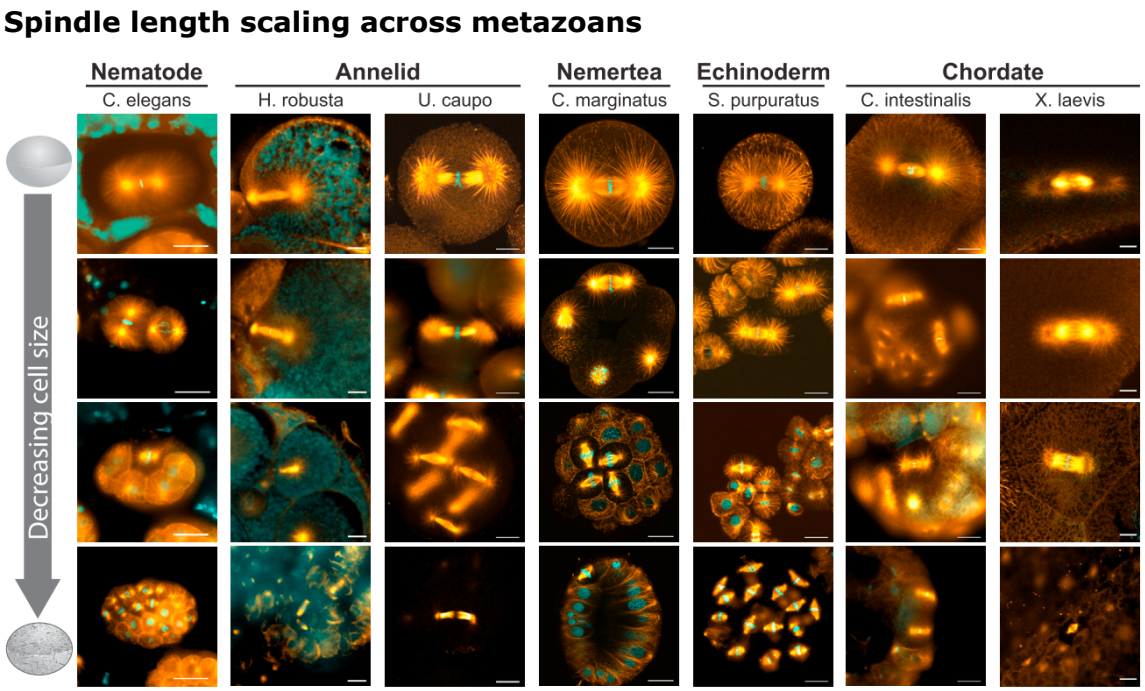


FIGURE 12: **Spindle length scaling across metazoan embryos** - Fluoresecence images of fixed mitotic embryos at different stages of embryonic development stained for tubulin (orange) and DNA (cyan). Scale bars represent 20 micrometer. Reproduced with permission from [520] under the CCC terms.

The mechanisms of spindle length control during metaphase and anaphase are described in chapters 3.2 and 3.4. Spindle length is regulated in a cell size-dependent manner by fine-tuning these pathways through different mechanisms: (i) a specific spindle length regulator is limiting and its amount scales with cell size, (ii) spindle length regulators can be sequestered in a cell size dependent manner, or (iii) the cytoplasmic composition is altered.

### 4.1.1 Limiting component mechanism

Elegant experiments using encapsulated *X. laevis* egg extracts in liposomes of different diameter demonstrated that increasing the cytoplasmic volume is sufficient to achieve spindle length scaling [527, 528]. Until an upper limit, comparable to the maximum spindle length observed *in vivo*, spindle length scales linearly with the droplet diameter. Spindle length could not be altered by droplet compression, indicating that spindle length regulation depends on the **cytoplasmic volume** rather than cell boundaries [527, 528]. Evidence for the role of the cytoplasmic volume has also been obtained *in vivo*, where removal of cytoplasm or an increased volume by fusion of mouse oocytes results in a corresponding reduction or increase in spindle length [529, 530].

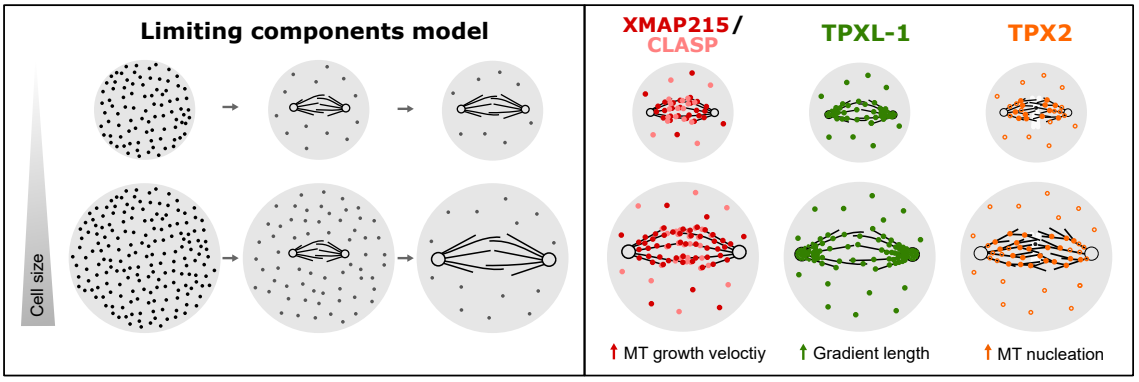


FIGURE 13: **Limiting components model** - Scheme depicting the limiting components model for the regulation of cell size-dependent spindle length (left panel) and the potential limiting components (right panel). These include the microtubule dynamics regulating MAPs XMAP215 (red) and CLASP (pink), TPXL-1 (green), the *C. elegans* homolog of TPX2, which forms a gradient from the centrosomes towards the spindle center, and the microtubule nucleation-promoting factor TPX2 (orange). The figure has been taken and adapted from [531].

The underlying mechanism may be described by a **limiting components model** (Figure 13): one or several crucial **spindle length regulators are limiting** [532, 533]. Typically during early embryogenesis, the cytoplasmic composition, and thus the protein concentration, is assumed to be constant [533]. Accordingly, increasing cell size with increasing cytoplasmic volume leads to an increase in the absolute amount of proteins. As a spindle assembles, the limiting component is incorporated into the structure, which results in its depletion from the cytoplasm. While the mitotic spindle assembles, the concentration of the free component is reduced in the cytoplasm, subsequently reducing the spindle assembly rate. Since the limiting

component is less abundant in smaller cells, the growth rate will be reduced faster as the spindle assembles, in comparison to bigger cells. As a result, the size of the spindle is adjusted to cell size (Figure 13, left panel) [533].

A limiting component could be tubulin, as the main building block of the mitotic spindle. However, this is unlikely the case, since the addition of free tubulin into encapsulated *X. laevis* extracts does not alter spindle length [527].

In contrast, factors that regulate **microtubule dynamics** and can determine microtubule length and spindle length (see chapter 3.2) have been implicated in the regulation of spindle length scaling (Figure 13, right panel). In fact, in *C. elegans* and *P. lividus* embryos, the growth velocity of spindle microtubules correlates with spindle length [440].
Accordingly, the conserved microtubule polymerase **XMAP215**/ch-TOG (see chapter 2.5.2) is critical for spindle length regulation in *X. laevis* egg extracts. Spindle length scaled with XMAP215 levels *in vivo* and *in vitro* [436, 437], suggesting XMAP215 as a limiting component in the regulation of spindle length. In *C. elegans*, CLS-2/**CLASP** depletion reduces spindle length in a dose-dependent manner [440]. Furthermore, the amount of **TPXL-1** present at centrosomes as well as the length of the gradient that the protein forms towards the spindle center, scales with spindle length [522]. Consequently, deletion of TPXL-1, homolog of TPX2, reduces spindle length [522]. How TPXL-1 performs this task is not clear, since in *C. elegans* microtubule nucleation on pre-existing microtubules, a pathway TPX2 is a crucial part of in mammalian cells (see chapter 2.2.1), has not been observed [455]. However, in HeLa cells, TPX2 also interacts with CLASP and the kinesin-13 KIF2A, which are both involved in spindle length regulation during metaphase [534] (see chapter 2.5.2). In *S. cerevisiae*, anaphase B spindle length scaling with cell size is regulated by the microtubule depolymerase of the **kinesin-8** family Kip3, which prevents over-proportional spindle elongation [272].

Besides the control of microtubule dynamics, spindle length is also regulated by **microtubule nucleation** (see chapter 3.2). As previously described, the length of individual spindle microtubules does not reach half spindle length in *X. laevis* egg extracts and can correspondingly not account for spindle length regulation [102]. Therefore, spindle length is determined by the spatial profile of microtubule nucleation [457].
In fact, in U2OS cells, spindle length is sensitive to the levels of **TPX2** (Figure 13, right panel) [458, 459]. With regards to scaling of spindle length, it has been shown that microtubule-stimulated nucleation sets the upper limit of spindle length in *Xenopus* egg extracts [457], and

it has been suggested that the microtubule nucleation profile may rather be critical in large cells [535]. However, microtubule nucleation has recently also been found responsible for the scaling of smaller spindles in zebrafish embryos [536].

Interestingly, motor proteins that are involved in the regulation metaphase spindle length, such as kinesin-5 or kinesin-14 (see chapter 3.2), have not been found to act as limiting components for the cell size-dependent regulation of spindle length so far.

### 4.1.2 Sequestration to limit cytoplasmic components & alteration of cytoplasmic composition

Besides a simple increase of the amount of a limiting component with cell size, the activity of crucial spindle length regulators have been proposed to be controlled by different mechanisms (Figure 14). Encapsulation of *Xenopus laevis* extracts obtained from early (stage 3 and 4) and late stages (stage 8) of embryonic development in the same volume lead to the formation of spindles with different lengths [527, 537], implicating additional mechanisms for spindle length regulation. Here, **sequestration** of the microtubule destabilizing motor **kinesin-13** Kif2a [537] controls spindle length (Figure 14, i).

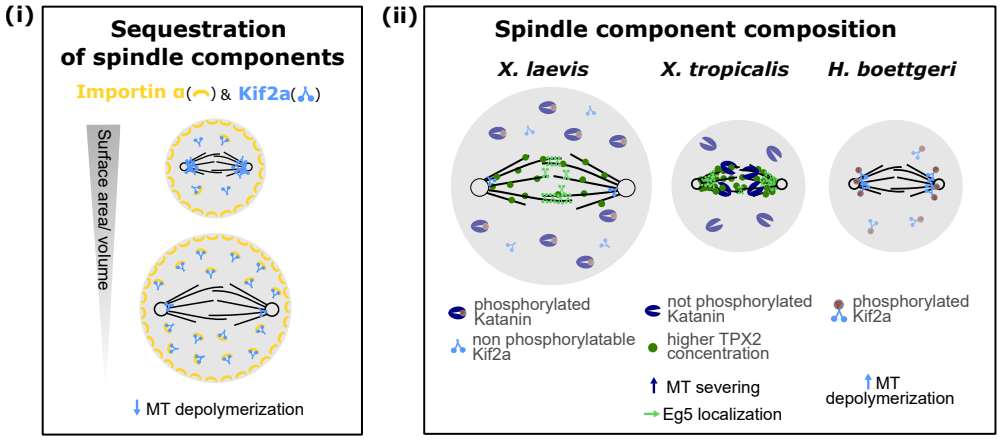


FIGURE 14: **Sequestration & cytoplasmic composition** - (i) Scheme depicting the mechanism of spindle component sequestration to regulate spindle length in a cell size-dependent manner. With increasing cell size the surface area/volume ratio decreases. Consequently, in bigger cells a smaller proportion of cell membrane-bound importin α (yellow) is sequestered by the cell membrane and more importin α is freely available in the cytoplasm. Free importin α binds Kif2a (light blue) and prevents the microtubule destabilizer from binding spindle microtubules, which subsequently allows the formation of bigger spindles. (ii) Scheme depicting the mechanism of altered cytoplasmic composition for the cell size-dependent regulation of spindle length. Differential posttranslational modifications of katanin (dark blue) and Kif2a (light blue) in the different size frogs *X. laevis*, *X. tropicalis*, and *H. boettgeri* control spindle length. The figure has been taken and adapted from [531].

Cytoplasmic importin α binds Kif2a and inhibits its activity. Moreover, importin α binds to the cell membrane, which consequently suppresses its sequestration activity. Smaller cells are characterized by a **higher surface area to volume ratio than bigger cells**, and consequently, proportionally more importin α is bound to the membrane, preventing Kif2a sequestration. This results in increased recruitment of the kinesin-13 to the spindle, increased microtubule catastrophe frequency, and consequently smaller spindles in smaller cells [537, 538]. Additionally, importin α partitioning to the plasma membrane is regulated by palmitoylation [538], which may explain the different spindle length observed in extracts of earily and late stage embryos [527, 537].

An **altered cytoplasmic composition** with regards to protein concentration and post-translational modifications also promotes spindle length scaling between closely related organisms (Figure 14, ii). For instance, in the bigger frog *Xenopus laevis*, **katanin**, a microtubule severing enzyme, is phosphorylated by Aurora B, which inhibits its activity and allows the formation of longer spindles. Contrarily, in the smaller frog *Xenopus tropicalis*, katanin lacks this inhibitory phosphorylation, enabling the protein to sever microtubules, consequently promoting the formation of smaller spindles [445]. Moreover, the concentration of **TPX2** is around three-fold higher in *X. tropicalis*, which leads to increased recruitment of the **kinesin-5** motor Eg5 [539]. This results in an increased crosslinking of microtubules close to spindle poles and a decreased microtubule overlap at the spindle midzone, which was proposed to reduce spindle length [539]. In addition, the even smaller frog *Hymenochirus boettgeri* contains kinesin-13 Kif21, phosphorylated at Ser252, which activates the depolymerase and results in shorter spindles [540]. *X. laevis* Kif21 cannot be phosphorylated as it contains isoleucine at the same position [540]. Recently, differences in the dynamic properties of tubulin have also been proposed to account for different spindle lengthts in *X. laevis* and *X. tropicalis* [541]. Microtubules assembled from purified *X. laevis* tubulin *in vitro* display faster growth rates and lower catastrophe frequencies than microtubules grown from *X. tropicalis* tubulin [541].

## 4.2 Spindle velocity scaling with cell size

While the main focus with regards to mitotic spindle length scaling has been laid on the cell size-dependent regulation of spindle length, a few studies have shed light on the phenomenon of **cell size-dependent spindle elongation velocity** (Figure 15).

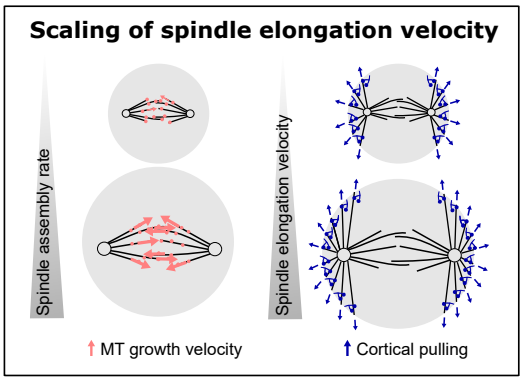


FIGURE 15: **Spindle elongation velocity scaling** - Scheme depicting the proposed mechanism for the scaling of the spindle assembly velocity and the anaphase B spindle elongation velocity in *C. elegans* embryos. The velocity of spindle assembly is determined by the growth velocity of spindle microtubules [440], but the precise mechanism remains elusive. The velocity of anaphase B spindle elongation during anaphase B was shown to depend on the increasing levels of cortical force generators (blue) with cell size [454]. The figure has been taken and adapted from [531].

Based on an increased microtubule growth velocity with increasing cell size in *C. elegans* embryos, the **speed of spindle assembly scales** accordingly (Figure 15, left panel) [440]. In *C. elegans* embryos, also the **velocity of anaphase B spindle elongation scales with cell size** [454]. Longer spindles within bigger cells are elongated with proportionally higher speeds. Combining experimental data with computer simulations has revealed that this is regulated by dynein-dependent cortical pulling forces. With a constant density of force generators at the cell cortex, the number of cortical dynein increases with cell size and thus the pulling forces exerted on spindle poles are elevated in bigger cells, resulting in faster spindle elongation (Figure 15, right panel) [454].

In addition, a study including numerous *C. elegans* isolates and other nematodes from around the world demonstrated that the rate of spindle elongation from mitosis onset to the attainment of final spindle length at the end of anaphase B, correlated with cell size [521, 523].

# 5 Fission yeast as a model system to study the mitotic spindle

The fission yeast *Schizosaccharomyces pombe* is a rod-shaped single cell eukaryote, which generally lives as a haploid under nutrient-rich conditions, and undergoes mitosis to proliferate. The easily genetically modifiable fission yeast represents a suitable model system to study the mitotic spindle due to its simple composition and dynamics when compared to animal cells, as well as the presence of various conserved spindle components and mechanisms. In contrast to the spindles of higher organisms, fission yeast spindles are built from only approximately

30 microtubules during metaphase [105, 156], contain only three chromosomes, and undergo easily distinguishable and highly consistent phases of spindle dynamics [187].

## 5.1 Spindle dynamics

Due to the consistent rates of spindle elongation and the duration of each mitotic phase, spindle dynamics, e.g. the development of spindle length over time, can typically be categorized into three stereotypical phases (Figure 16) [184, 187].

### 5.1.1 Phase I - Spindle assembly

The first phase of spindle dynamics encompasses the process of spindle assembly during prophase. After **SPB insertion** into the nuclear envelope [59, 60, 156], γ-TuRC, encompassing γ-tubulin Gtb1, Alp4 (GCP), Alp6 (GCP3), Gfh1 (GCP4), Mod21 (GCP5) and Alp16 (GCP6) [80, 88, 90, 92, 542], is recruited to the nucleoplasmic side of the SPB to initiate microtubule nucleation. Recruitment of γ-TuRC is, in part, regulated by Mzt1 (MOZART1) [543] and the Pericentrin-homolog Pcp1 [61].
Microtubule anchorage to the SPB by the γ-TuRC is not sufficient in yeast and requires additional proteins, such as the Msd1-Wdr8 complex and the kinesin-14 Pkl1 [295, 389, 544]. In absence of these proteins, spindle microtubules often protrude beyond the SPBs with their minus-ends, parallel to the long spindle axis [295, 389].

Subsequently, the two SPBs, located adjacent to each other, become discernible, while remaining connected through spindle microtubules [545], and spindle bipolarity is established. **SPB separation** is primarily regulated by the kinesin-5 Cut7, as its inactivation leads to the formation of monopolar spindles [20, 21]. In addition, the microtubule crosslinker Ase1 and particularly the microtubule rescue factor CLASP are important for the establishment of spindle bipolarity [259, 260, 394, 546]. In absence of the activity of all mitotic motors, Ase1 and CLASP ensure assembly of a bipolar spindle [259, 394]. Corroborating the importance of CLASP activity for spindle assembly, Cls1 inactivation often results in the formation of monopolar spindles [370].

While spindle poles are separated spindle length, described by the pole-to-pole distance, increases throughout phase I (Figure 16) [187].

Furthermore, during prophase, spindle microtubules attach to kinetochores, which are located in close proximity to SPBs [187]. Next to several proteins that localize to kinetochores throughout the cell cycle [547], a number of mitosis-specific kinetochore components assist establishment and maintenance of microtubule-kinetochore attachments. These include the XMAP215 proteins Alp14 and Dis1 [350, 353, 356, 548], which directly interact with the Ndc80-complex [354, 356], the kinesin-8 motors Klp5 and Klp6 [186, 188, 270, 274, 403], and the Dam1/DASH-complex [180, 188]. Consequently, deletion or inactivation of these proteins often leads to defects in chromosome attachment and sister chromatid separation [180, 186, 188, 350, 354, 403, 548].

In wild-type cells the attached kinetochores already move to the spindle center during prophase, where they remain during the following metaphase [275].

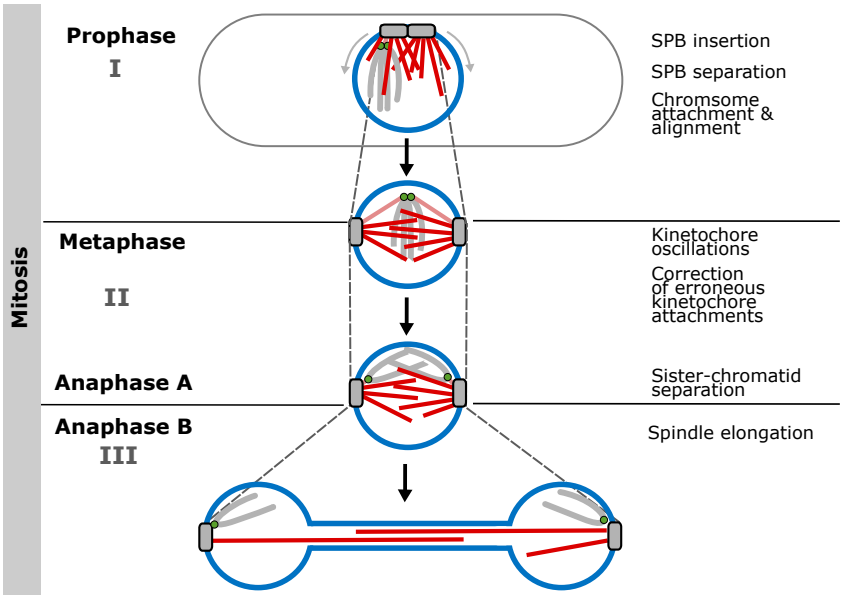


FIGURE 16: **Spindle dynamics in fission yeast** - Scheme depicting the fission yeast spindle and the stereotypical phases of spindle dynamics (I-III). Spindle poles are shown in gray, the nuclear envelope in blue, microtubules in red, kinetochores in green and chromosomes in light gray. The dashed line highlights the pole-to-pole distance and its development during each phase of spindle dynamics.

### 5.1.2 Phase II - Metaphase & anaphase A

Phase II is characterized by a **steady-state spindle length** and encompasses metaphase and anaphase A (Figure 16) [187]. The metaphase wild-type spindle consists of approximately 30 microtubules [105], and all their minus-ends are anchored to spindle poles [156, 184]. During metaphase, kinetochores, which are attached to 2-4 microtubules, are bi-oriented and display

oscillatory movements along the spindle center [156, 167, 187, 275]. Chromosome positioning at the spindle equator is, thereby, most prominently regulated by the kinesin-8 proteins Klp5 and Klp6 [270, 275]. The oscillatory movement depends primarily on the stochastic alteration between phases of microtubule growth and shrinkage [270].

The steady-state metaphase spindle length is regulated by the microtubule motors Cut7/Kinesin-5, Pkl1/Kinesin-14 and Klp2/Kinesin-14 and the microtubule dynamics regulating proteins Klp5 & Klp6/Kinesin-8 and Alp14 & Dis1/XMAP215 (see chapter 3.2). Also, inactivation of Ase1 leads to the formation of shorter metaphase spindles, which may be linked to the microtubule crosslinker's function in recruiting the microtubule rescue factor CLASP [370, 424].

Additionally, kinetochore-microtubule attachments are hypothesized to be involved in spindle length regulation, since mutations in *mis12*, *mis6* and *mis4*, encoding kinetochore proteins, lead to the formation of longer metaphase spindles [353]. Generally, defective kinetochore-spindle microtubule attachments lead to fluctuations in spindle length [186–188]. In fact, sister chromatids connected by cohesin, which acts as an elastic linker, can oppose forces acting on kinetochores through the attached microtubules [517]. In addition, forces acting on kinetochores can affect kinetochore microtubule dynamics, since the Ndc80 complex directly interacts with Dis1, Alp14, Klp5 and Klp6 [186, 270, 354, 356, 403]. *In vitro* experiments that attached the Dam1-complex, itself associated with a microtubule plus-tip, to an optically trapped bead, demonstrated that kinetochore microtubule dynamics are regulated in a force-dependent manner [549]. When a microtubule depolymerized, the microtubule shrinkage velocity was reduced and microtubule rescue promoted when Dam1 was attached. Moreover, when Dam1 was pulled away from the attached microtubule tip this effect was enhanced, suggesting that tension applied on kinetochores induces growth of kinetochore microtubules [549].

When chromosomes are properly attached, cohesin is cleaved [464] and kinetochore microtubules disassemble [105, 156], resulting in the movement of sister chromatids towards opposite spindle poles in anaphase A [167, 187]. **Kinetochore microtubule depolymerization** leads to a strong decrease in the total number of spindle microtubules and is concomitant to the emergence of a more organized spindle architecture at anaphase B onset [105, 156].

### 5.1.3 Phase III - Anaphase B spindle elongation

Phase III is characterized by a dramatic elongation of the spindle from approximately 2 to 2 µm and, therefore, refers to anaphase B. The anaphase B spindle is primarily build of interpolar microtubules originating from the two opposite spindle poles, which form the spindle midzone, where antiparallelly oriented microtubules are closely packed and form square arrays [105, 156]. This crystalline microtubule architecture is optimal for microtubule sliding and persists throughout anaphase B (Figure 16) [105, 184, 187]. At this mitotic stage, not only the spindle midzone but also the flanking regions become more tightly packed with the microtubules being arranged in a triangular motif, indicative of parallel microtubule bundles [105]. This architecture confers resistance to buckling to the long bar-shaped spindle, which loses microtubules as it elongates [105, 156, 477]. While a wild-type spindle is composed of approximately 10 microtubules at anaphase onset, the spindle contains only 6 microtubules when it reaches its maximum length [105]. Anaphase B spindle elongation promotes spatial separation of the two chromosome sets, located at each spindle pole, and results in the deformation of the NE, arranged in a dumbbell shape with a bridge along the anaphase spindle (Figure 16) [59, 167, 184]. Eventually, all spindle microtubules depolymerize and the spindle disassembles, while the NE remodels to enclose the two DNA sets and form two daughter nuclei at the end of mitosis [59, 156, 477].

The mechanisms of anaphase B spindle elongation have been described in chapter 3.4. Here, I will briefly summarize the current knowledge about the process in *S. pombe* (Figure 17).
Like in most organisms, spindle stability is promoted by the conserved crosslinker **Ase1** [550, 551]. Upon dephosphorylation at Cdc2-phosphosites by the phosphatase Clp1 [256], Ase1 localizes to the spindle midzone from anaphase B onset onwards (Figure 17, dark blue). In absence of the crosslinker, anaphase spindles often break into two unconnected spindle halves [310, 550, 551], since midzone formation is disrupted. The tubulin signal does not display increased intensity at the spindle center, typical for the presence of a spindle midzone, in *ase1* deleted cells [550]. However, not all spindles break, and in some cases separated spindle halves can even reconnect [550], suggesting that other crosslinking proteins compensate for the absence of Ase1.

Candidates for this function are the homotetrameric crosslinking and sliding motors **Cut7 (kinesin-5)** and **Klp9 (kinesin-6)** (Figure 17, blue and green) [256, 258, 259]. Accordingly, the double deletion of *ase1* and *klp9*, as well as Cut7 inactivation and *ase1* deletion are lethal

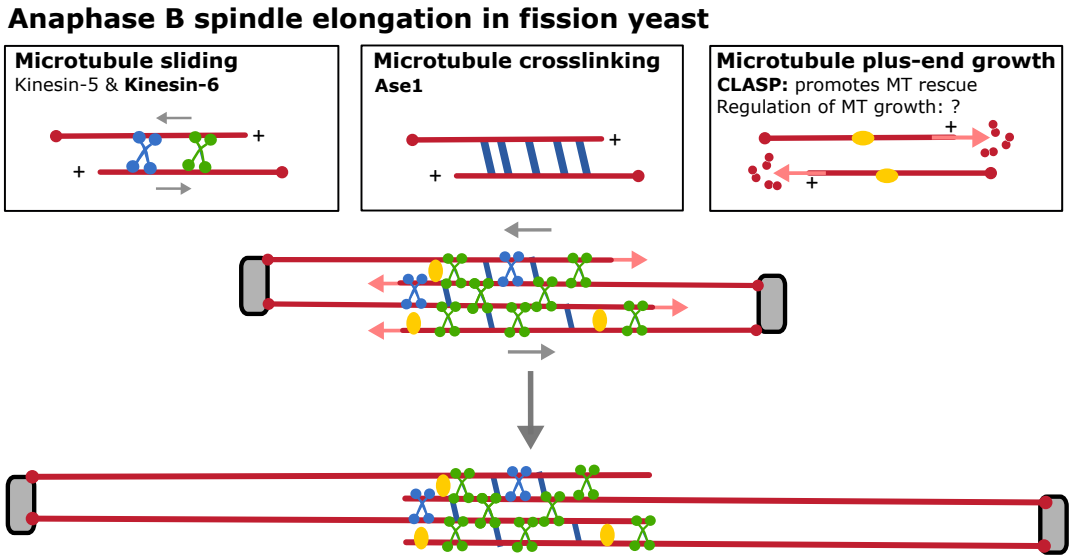


FIGURE 17: **Anaphase B in fission yeast** - Scheme depicting the fission yeast anaphase B spindle and the modules that drive spindle elongation. In *S. pombe* crucial anaphase B spindle components are the microtubule crosslinker Ase1 (dark blue) and the homotetrameric microtubule sliding motors kinesin-5 Cut7 (blue) and Kinesin-6 Klp9 (green), where Klp9 represents the major force generator for spindle elongation. CLASP, which is recruited to the overlap by Ase1, has been shown to stabilize the spindle midzone by inducing microtubule rescue events. However, how microtubule growth, which is crucial to allow spindle elongation, is precisely regulated remains elusive. While the spindle elongates, the midzone length remains constant, suggesting that microtubule sliding and growth occur at similar speeds.

[258, 259]. Moreover, cells deleted for *ase1* expressing a rigor (ATPase dead) mutant of Klp9 are viable [258], highlighting the importance of a motor-independent function of Klp9 that may depend on its crosslinking activity. Given their capability of microtubule sliding, both Klp9 and Cut7 are crucial force generators of anaphase B spindle elongation. Consequently, in absence of Cut7 and Klp9 activity, spindles do not elongate, which often results in the 'cut' of chromosomes by the cytokinetic ring, due to insufficient spatial separation between the two chromosome sets [259].

Deletion of all other mitotic motors, including several kinesins and dynein, which do not crosslink microtubules, does not significantly alter the velocity of spindle elongation [256], providing further evidence that Cut7 and Klp9 are the crucial force generators of anaphase B. Importantly, deletion of *klp9* reduces the elongation velocity to a greater extent than inactivation of Cut7 using the temperature-sensitive mutant *cut7-24* [256, 259]. This suggests that Klp9 generates the majority of the required microtubule sliding forces.

In contrast to Cut7, Klp9 localizes to the spindle only during anaphase B, and its recruitment to the spindle midzone depends on dephosphorylation by the Cdc14-homolog **Clp1** at Cdc2-(Cdk1)-phosphosites [256]. In more detail, Klp9 dephosphorylation was proposed to promote

physical interaction with Ase1, which is also dephosphorylated by Clp1, and subsequently, the microtubule crosslinker is thought to recruit Klp9 to the microtubule overlap [256].
Besides, Klp9 has also been implicated in the regulation of the metaphase-anaphase transition by promoting activation of the anaphase-promoting complex (APC) by regulating the midzone localization of crucial APC components such as Aurora B (Ark1 in *S. pombe*) [255].

Emphasizing the importance of microtubule dynamics regulation during anaphase B, inactivation of **Cls1**, also called Peg1 (CLASP) (Figure 17, yellow), often leads to anaphase spindle breakage, comparable to the phenotype of *ase1* deletion [370]. Cls1 is recruited via interaction with Ase1 to antiparallel microtubule overlaps [310], where it promotes microtubule rescue, preventing microtubules from shrinking back to spindle poles [370]. Thus Cls1 maintains a stable microtubule overlap [370, 552]. In contrast to CLASP, the EB1 homolog Mal3 does not display a strong phenotype during anaphase B [553]. The role of the XMAP215 homologs Dis1 and Alp14 in anaphase B spindle elongation is unclear.

How microtubule growth is precisely regulated remains an open question in fission yeast, as in most other organisms. As described in chapter 3.4.5, the fact that, in fission yeast, the length of the microtubule overlap at the spindle midzone is maintained constant (Figure 17) while the spindle continuously elongates, suggests that microtubule sliding and growth occur with equal speeds and have to be precisely coordinated, but how this coordination is achieved remains unknown.

## 5.2 Fission yeast to study scaling with cell size

In addition to being a useful tool to study mitotic spindle function, the unicellular fission yeast also allows the study of scaling mechanisms. While wild-type fission yeast cells consistently enter mitosis at a cell length of typically around 14 µm, cell cycle mutants that divide at abnormal cell sizes are available. Mutation of the cell cycle regulator Wee1 accelerates the transition from G2 to mitosis, and as a result, *wee1-50* cells divide at a shorter length compared to wild-type cells. Conversely, *cdc25-22* cells divide at an abnormally long length [18]. These mutants have been previously utilized to study the scaling of nuclear size with cell size [554]. Since rod-shaped fission yeast cells grow only at the cell tips, while the cell diameter does not change [555], cell size can be easily quantified by measurement of the cell length from tip-to-tip. Importantly, changes in cell size lead to a proportional down- or up-regulation of the global protein transcription levels [556]. This ensures that protein concentrations are not

altered in these mutants that exhibit different cell sizes and that the cytoplasmic composition is kept constant.

# 6 *In vitro* assays to functionally characterize mitotic spindle components

Despite the comparatively simple architecture and composition of the fission yeast spindle, the system is still too complex to gain a comprehensive understanding of the contribution of every component. Functional characterization of mitotic spindle components often requires *in vitro* reconstitution assays with pure proteins. To determine a spindle component's function, the analysis of its interaction with static microtubules or its effect on dynamic microtubules is of crucial importance [27, 557]. These *in vitro* reconstitution studies have contributed substantially to the state-of-the-art understanding of the mitotic spindle. Accordingly, most of the existing knowledge about microtubule-based motors and MAPs, described in chapters 2.4 and 2.5, finds its origin in *in vitro* assays.

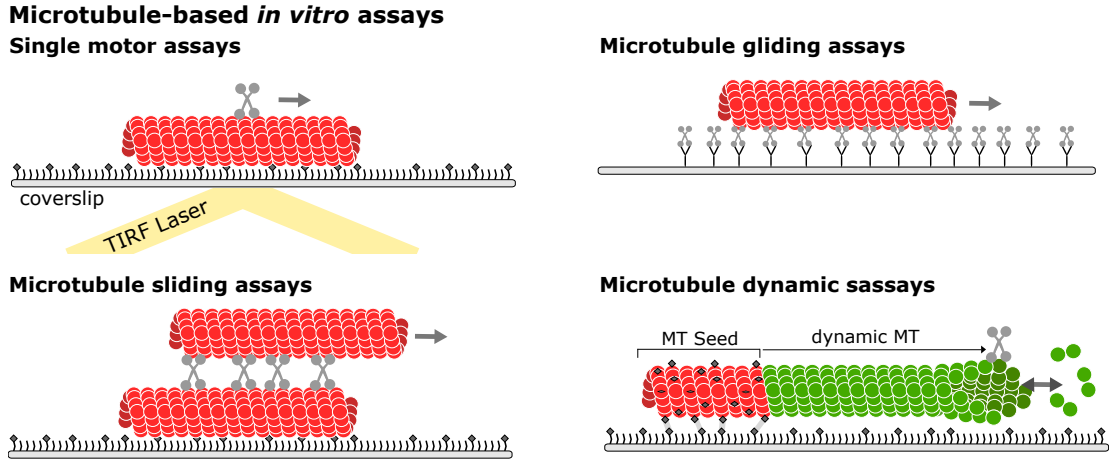


FIGURE 18: **Microtubule-based *in vitro* set ups** Schemes depicting the set-ups of conventional *in vitro* reconstitution assays used to study the function of microtubule-associated motors or non-motor proteins. The glass coverslip of flow chambers is shown in gray: they can either be passivated as is the case for single motor assays, microtubule sliding assays and microtubule dynamic assays, or coated with antibodies (black) that bind the motor of interest, or, alternatively, the motor sticks directly to the coverslip. Stabilized microtubules or seeds are depicted in red and dynamic microtubules assembled from free tubulin dimers in green. Microtubule motors are shown in gray.

Mostly four different set-ups have been used: (i) single motor experiments, (ii) microtubule gliding assays, (iii) microtubule sliding assays, and (iv) microtubule dynamics assays (Figure

18) which are generally imaged with a **Total Internal Reflection (TIRF)-microscope**.
TIRF microscopy allows the selective excitation of fluorophores located in very close proximity to a solid surface, such as a glass coverslip, while avoiding the excitation of fluorophores approximately more than 100 nm away from the surface [558, 559]. This allows a substantial reduction of background fluorescence as compared to other light microscopy set-ups, and eventually the detection of single molecules with attached fluorophores (Axelrod, 2016). Briefly, this is achieved by the light beam that reaches the sample surface at a very high angle, allowing the beam not to refract through the sample, but to totally internally reflect (TIR) (Figure 18) [558, 559]. Therefore, conventionally used *in vitro* set-ups require the microtubules or motor proteins to be attached to the glass surface of a flow chamber.

In (i) **single motor experiments** (Figure 18, upper left panel), fluorescent microtubules are attached to passivated glass surfaces and the movement of a labeled motor protein can be followed. Additionally, optical traps, where a bead linked to a single motor protein or a microtubule is trapped by a focused laser beam can be used. Bead displacement scales linearly with the forces exerted by the motor and allows measurement of their individual force production [560, 561].

In (ii) **microtubule gliding assays** (Figure 18, upper right panel), the motor protein is typically immobilized on the surface, either directly or via antibodies, and microtubules free in solution are added to the flow chamber. These microtubules can then be bound by the motors and moved either plus-end- or minus-end-leading. Using polarity-marked microtubules thereby allows determining the motor's walking direction.

In (iii) **microtubule sliding assays** (Figure 18, lower left panel), stabilized microtubules are bound to the surface and motor proteins or MAPs and stabilized free microtubules are added in solution. If the tested motor protein possesses sufficient microtubule crosslinking activity it will bundle an immobilized microtubule and a free microtubule and slide them apart. Alternatively, a microtubule crosslinker, such as MAP65, can additionally be added to the flow chamber [562].

Lastly, instead of stabilized microtubules, dynamic microtubules can be used in (iv) **microtubule dynamics assays** (Figure 18, lower right panel) to determine a motors or MAPs effect on microtubule polymerization, catastrophe, rescue, and depolymerization. To do so, stabilized microtubule seeds are immobilized on the surface. From the seeds dynamic microtubules can be assembled from free tubulin dimers in presence of the protein of interest [327].

# Results

## 7 Scaling of anaphase B spindle elongation in fission yeast

### 7.1 Summary I

The scaling of metaphase spindle length with cell size has been extensively studied during embryogenesis of various organisms (see chapter 4.1). A few studies have suggested that this relationship holds true apart from embryogenesis [272, 525].
Interested by this phenomenon, I validated that also fission yeast cells, which divide at different sizes, adjust spindle length to cell size throughout mitosis, from spindle assembly until the attainment of maximum spindle length. Concomitantly, I observed that even though the size of the spindle was altered, **the mitotic time frame was constant**. Although bigger cells assembled longer spindles, final spindle length and chromosome separation were achieved within approximately 30 minutes, similar to mitosis duration in smaller cells with shorter spindles. This was ensured by a **cell size-dependent dynamics** of mitotic processes, such as spindle assembly and anaphase B spindle elongation, which has previously been observed in *C. elegans* embryos [440, 454].
While these studies have focused on the duration of individual mitotic phases, my observation provided evidence that cell size-dependent velocities of mitotic processes allow cells to maintain a constant mitotic time frame from the beginning of spindle assembly to the maximum separation of chromosomes. In fact, prolongation of mitosis has often been shown to negatively impact cell viability [32, 563–567]. Hence, cell size-dependent mitotic spindle dynamics may ensure cell fitness.

Moreover, even though the phenomenon has been observed in *C. elegans*, the precise underlying mechanism remained unclear [440, 454]. During anaphase B spindle elongation in *C. elegans* embryos, the level of cortical force generators has been proposed to determine the

speed of spindle elongation [454]. However, cortical pulling does not appear to be the major driving force in most organisms (see chapter 3.4.3). In fission yeast, human cells [493], and several other organisms (see chapter 3.4.2) the forces that drive anaphase B spindle elongation are generated at the spindle midzone. I, therefore, decided to unravel the underlying mechanism of cell size-dependent spindle dynamics in fission yeast by focusing on anaphase B spindle elongation.

Deleting a plethora of spindle components by genetic manipulation and conducting spindle dynamics and intensity measurements revealed the microtubule-sliding motor kinesin-6 Klp9 as the crucial motor that adjusts the spindle elongation velocity to cell size. In fact, the amount of Klp9 motors dictates the speed of spindle elongation: coupled to cell size, the **spindle elongates faster as the amount of motors at the spindle midzone increases**. Additionally, due to an increase of midzone length and the number of associated microtubules, the number of binding sites for Klp9 increases over-proportionally in relation to the motor amount. This suggests that **molecular crowding inversely correlates to cell size** and may assist the regulation of the cell size-dependent spindle elongation velocity.

## 7.2 Article I: Kinesin-6 regulates cell-size-dependent spindle elongation velocity to keep mitosis duration constant in fission yeast

**Authors**: Lara K. Krüger[1], Jérémie Luc-Sanchez[1], Anne Paoletti[1] & Phong T. Tran[1 & 2]

**Affiliations**: 1. Institut Curie, PSL Research University, CNRS, UMR 144, Paris, France; 2. Department of Cell and Developmental Biology, University of Pennsylvania, Philadelphia, United States

**Journal**: eLife

**Volume**: 8:e42182

**Year**: 2019

**DOI**: https://doi.org/10.7554/eLife.42182

eLIFE elifesciences.org

RESEARCH ARTICLE

# Kinesin-6 regulates cell-size-dependent spindle elongation velocity to keep mitosis duration constant in fission yeast

**Lara Katharina Krüger[1]*, Jérémie-Luc Sanchez[1], Anne Paoletti[1], Phong Thanh Tran[1,2]***

[1]Institut Curie, PSL Research University, CNRS, UMR 144, Paris, France; [2]Department of Cell and Developmental Biology, University of Pennsylvania, Philadelphia, United States

**Abstract** The length of the mitotic spindle scales with cell size in a wide range of organisms during embryonic development. Interestingly, in *C. elegans* embryos, this goes along with temporal regulation: larger cells speed up spindle assembly and elongation. We demonstrate that, similarly in fission yeast, spindle length and spindle dynamics adjust to cell size, which allows to keep mitosis duration constant. Since prolongation of mitosis was shown to affect cell viability, this may resemble a mechanism to regulate mitosis duration. We further reveal how the velocity of spindle elongation is regulated: coupled to cell size, the amount of kinesin-6 Klp9 molecules increases, resulting in an acceleration of spindle elongation in anaphase B. In addition, the number of Klp9 binding sites to microtubules increases overproportionally to Klp9 molecules, suggesting that molecular crowding inversely correlates to cell size and might have an impact on spindle elongation velocity control.

DOI: https://doi.org/10.7554/eLife.42182.001

***For correspondence:** lara-katharina.kruger@curie.fr (LKK); phong.tran@curie.fr (PTT)

**Competing interests:** The authors declare that no competing interests exist.

**Funding:** See page 19

**Received:** 19 September 2018
**Accepted:** 13 February 2019
**Published:** 26 February 2019

**Reviewing editor:** Thomas Surrey, The Francis Crick Institute, United Kingdom



## Introduction

The size of the mitotic spindle robustly scales with cell size in various organisms. During early embryogenesis in *C. elegans*, *X. laevis* and various metazoans where cell size gradually decreases while the embryo undergoes successive rounds of cell division, spindle length can be reduced from 60 to a few micrometers (***Crowder et al., 2015***; ***Hara and Kimura, 2009***; ***Wühr et al., 2008***). Also apart from embryogenesis, spindle length has been shown to adjust to cell size in *S. cerevisiae* and human cells (***Rizk et al., 2014***; ***Yang et al., 2016***). This relationship is regulated by the cytoplasmic volume through limiting cytoplasmic components, such as tubulin (***Good et al., 2013***; ***Hazel et al., 2013***), as well as by molecules modulating microtubule dynamics (***Hara and Kimura, 2013***; ***Lacroix et al., 2018***; ***Reber and Goehring, 2015***; ***Wilbur and Heald, 2013***). In general, the regulation of the size of subcellular structures is considered crucial for many cellular processes, and especially for mitosis. For instance, mitotic spindle length can ensure proper chromosome segregation. In *Drosophila* neuroblast mutant cells exhibiting abnormally long chromosome arms, cells elongate and form slightly longer spindles to exclude chromatid from the cleavage plane (***Kotadia et al., 2012***). Thus, in cells of different sizes the adjustment of spindle length might be critical to separate the two chromosome sets by an appropriate distance, avoiding that chromosomes intrude into the site of cell cleavage, which would result in chromosome cut (***Syrovatkina and Tran, 2015***).

Interestingly, evidence exists that such a scaling relationship is not restricted to size but also applies to the speed of mitotic processes. In *C. elegans* embryos, the velocity of spindle assembly in prophase and the velocity of spindle elongation in anaphase B adjust to cell size, such that longer spindles assemble and elongate with proportionally higher speeds (***Hara and Kimura, 2009***;

*Lacroix et al., 2018*). This may prevent extension of mitosis duration in larger cells. In fact, prolongation of mitosis has often been shown to result in cell death or arrest in subsequent cell cycle phases (*Araujo et al., 2016*; *Lanni and Jacks, 1998*; *Orth et al., 2012*; *Quignon et al., 2007*; *Rieder and Palazzo, 1992*; *Uetake and Sluder, 2010*). Thus, the time frame needed for chromosome segregation has to be regulated to ensure flawless cell division.

Still, it is not known how the scaling of spindle dynamics and cell size is established. Computer simulations suggest that the cell-size-dependent spindle elongation velocity in *C. elegans* embryos depends on the number of cortical force-generators pulling on spindle poles (*Hara and Kimura, 2009*). In contrast to this mechanism of anaphase B, many other organisms push spindle poles apart via microtubule sliding forces generated between antiparallel overlapping microtubules (MTs) at the spindle center (spindle midzone) (*Brust-Mascher et al., 2004*; *Brust-Mascher and Scholey, 2011*; *Hayashi et al., 2007*; *Khodjakov et al., 2004*; *Tolić-Nørrelykke et al., 2004*). In most organisms, these forces are generated by kinesin-5 (*Avunie-Masala et al., 2011*; *Brust-Mascher et al., 2009*; *Kapitein et al., 2008*; *Kapitein et al., 2005*; *Saunders et al., 1995*; *Sharp et al., 2000*) but also kinesin-6, as in fission yeast, can accomplish this task (*Fu et al., 2009*; *Rincon et al., 2017*). In vitro it has been shown that the forces generated by several kinesin-5 molecules, that crosslink and slide apart antiparallel overlapping microtubules add up (*Shimamoto et al., 2015*). However, regarding the complex structure of the mitotic spindle and the variety of forces potentially opposing outward sliding of microtubules, it is unclear if the production of a higher force by a bigger motor ensemble at the midzone would directly result in an increasing speed of spindle elongation.

By using the easily-genetically modifiable fission yeast *S. pombe*, we show that even though cells of various sizes adjust mitotic spindle length to cell size, the process of chromosome segregation is accomplished within a constant time frame. Independent of cell and spindle size, chromosomes are separated within approximately 30 min. To keep mitosis duration constant, larger cells speed up spindle elongation of their longer spindles. Focusing on anaphase B, we reveal that the kinesin-6 Klp9 (human CHO1/MKLP1) (*Nislow et al., 1992*; *Nislow et al., 1990*), which is a key regulator for anaphase B spindle elongation in fission yeast (*Fu et al., 2009*; *Rincon et al., 2017*), regulates spindle elongation velocity in a cell-size-dependent manner and consequently controls mitosis duration. We demonstrate that the velocity of spindle elongation is determined by the number of Klp9 molecules. With increasing cell size the motor amounts increase, leading to the recruitment of more motors to the spindle and an acceleration of spindle elongation. In addition, longer spindles form longer regions of antiparallel overlapping microtubules, within which more microtubules are assembled. Thereby, the number of Klp9 binding sites to microtubules increases to a greater extent than the number of Klp9 molecules on the spindle. The lower relative concentration of Klp9 motors at the midzone of longer spindles might additionally impact the regulation of spindle elongation velocity, based on the effects of molecular crowding. We propose a simple limited components model, where the amount of available Klp9 molecules and the amount of binding sites for the motor to the mitotic spindle regulates the velocity of spindle elongation and gives rise to a constant mitosis duration in cells of various sizes.

## Results

### Mitosis duration is constant in *S. pombe* cells, irrespective of spindle length or cell size

In the rod-shaped fission yeast, cell growth only occurs at cell tips and the diameter does not change (*Kelly and Nurse, 2011*). Final cell size can therefore be easily quantified by measuring cell length from tip-to-tip at mitosis, when cells stop growing. To investigate the impact of cell size on mitotic spindle length and mitosis duration, we used cell-cycle mutants, dividing at an abnormally short (*wee1-50*: 10.50 µm ± 1 µm) and abnormally long cell length (*cdc25-22*: 24.7 µm ± 2.6 µm) compared to wild-type cells (13.3 µm ± 0.7 µm) (*Figure 1A* and *Figure 1—source data 1*). Live cell imaging was performed in cells expressing α-tubulin (Atb2) linked to mCherry, to monitor the mitotic spindle, and the kinetochore component Mis12 tagged with GFP, to follow the position of chromosomes within the spindle (*Figure 1B*).

First, we determined if spindle length scales with cell size also in *S. pombe*. Maximum spindle length was measured just before spindle breakdown at the end of anaphase B by the length of the

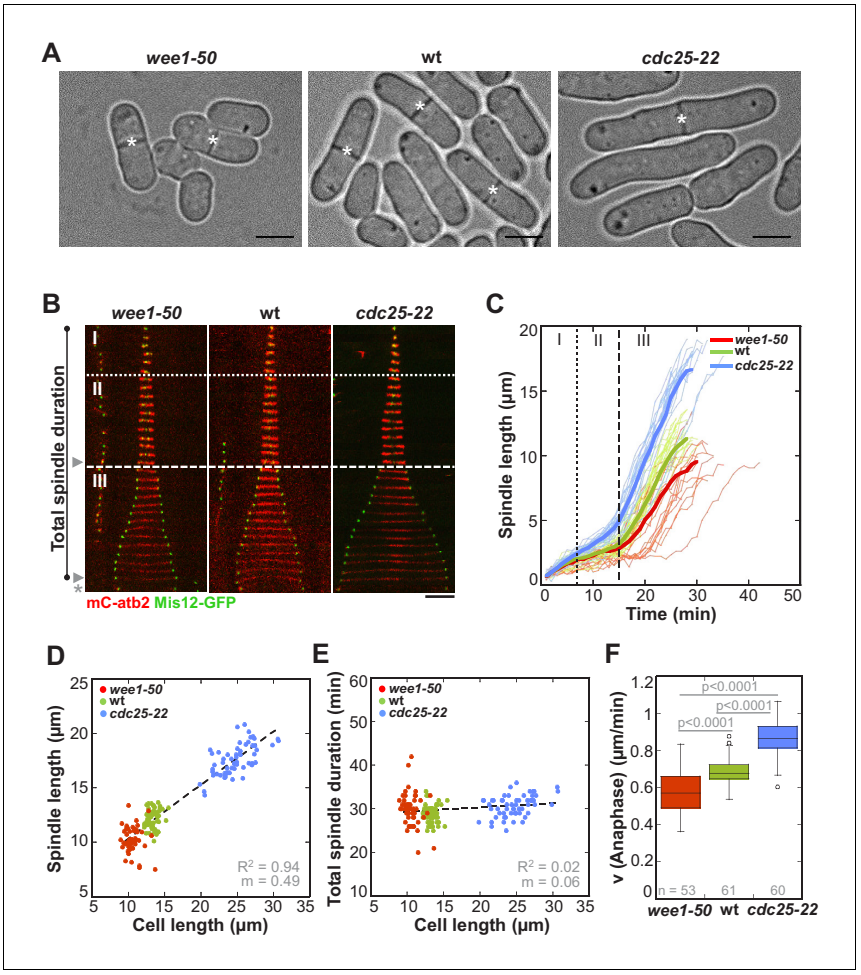


**Figure 1.** In *S. pombe* spindle length scales with cell size but total spindle duration is kept constant. (**A**) Brightfield images of *S. pombe* wild-type cells (central panel) and cell cycle mutants *wee1-50* (left panel) and *cdc25-22* (right panel). Cells reach their maximum cell length at mitosis/cell division, represented by the septum (asterisk). Scale bar, 5 µm. (**B**) Time-lapse images of *wee1-50*, wild-type (wt) and *cdc25-22* cells expressing mCherry-Atb2 (tubulin) and Mis12-GFP from spindle assembly to spindle breakdown (asterisk). Dotted line corresponds to transition from phase I to II (prophase to metaphase). Dashed line corresponds to transition from phase II to III (metaphase to anaphase). Arrowheads indicate the last time point of phase II or III, corresponding to spindle length plotted in (D) and ***Figure 1—figure supplement 1***. Each frame corresponds to 1 min interval. Scale bar, 5 µm. (**C**) Comparative plot of spindle length dynamics of *wee1-50* (red curves, n = 20), wild-type (green curves, n = 20) and *cdc25-22* cells (blue curves, n = 20). Bold curves correspond to mean spindle dynamics. As in (**B**) dotted and dashed lines display phase transitions. (**D**) Final spindle length plotted against cell length (*wee1-50*: n = 53, wt: n = 61, *cdc25-22*: n = 60). (**E**) Total spindle duration plotted against cell length (*wee1-50*: n = 53, wt: n = 61, *cdc25-22*: n = 60). Data in (**D–E**) was fitted by linear regression (dashed lines), showing the regression coefficient $R^2$ and the slope m. (**F**) Boxplot comparison of anaphase B spindle elongation velocities (**v**) in *wee1-50*, wild-type and *cdc25-22* cells. Data from n cells was collected from three independent experiments. P values were calculated by Mann-Whitney U test.

DOI: https://doi.org/10.7554/eLife.42182.002

The following source data and figure supplements are available for figure 1:

**Source data 1.** Mean values of spindle length and dynamics.

DOI: https://doi.org/10.7554/eLife.42182.005

**Figure supplement 1.** Metaphase spindle length plotted against maximum cell length.

DOI: https://doi.org/10.7554/eLife.42182.003

*Figure 1 continued on next page*

*Figure 1 continued*

**Figure supplement 2.** Boxplot comparison of spindle elongation velocity in prophase (I), metaphase (II) and anaphase B (III).

DOI: https://doi.org/10.7554/eLife.42182.004

mCherry-Atb2 signal (***Figure 1B***: phase III-arrowhead). Short *wee1-50* cells assembled spindles with a maximum length of 10.14 ± 1.2 µm, wild-type cells of 11.93 ± 0.9 µm and long *cdc25-22* cells of 17.34 ± 1.4 µm on average (***Figure 1C and D***). This shows that maximum spindle length increased in proportion to cell size (***Figure 1D***: $R^2$ = 0.94, m = 0.49). Metaphase spindle length, measured at the end of metaphase (***Figure 1B***: phase II-arrowhead), also scaled with cell size, although to a slightly lower extent (***Figure 1—figure supplement 1***: $R^2$ = 0.6, m = 0.07). Hence, as observed in various other organisms, a strong correlation of spindle length and cell size exists in *S. pombe*.

We next analyzed spindle dynamics, that is the development of spindle length over time, in relation to cell size. Similar to wild-type, *wee1-50* and *cdc25-22* cells exhibited three easily distinguishable phases (***Figure 1B and C***): phase I with low spindle elongation velocity (prophase), phase II with no or little spindle elongation (metaphase and anaphase A) and phase III characterized by dramatic and comparatively fast spindle elongation (anaphase B). Strikingly, even though spindle length adjusted to cell length, duration of each phase did not correlate with cell size (***Figure 1B,C*** and ***Figure 1—source data 1***). Consequently, total spindle duration, that is the time from the appearance of the spindle until its breakdown (***Figure 1B***), was constant among cells of different sizes, taking place within approximately 30 min (***Figure 1E***). Total spindle duration, which we define as mitosis duration, was thus independent of cell size (***Figure 1E***: $R^2$ = 0.02, m = 0.06). This is achieved by an increase of the spindle elongation velocity with cell size. The scaling relationship of spindle dynamics and cell size was observed in all mitotic phases (***Figure 1—figure supplement 2***): the rate of spindle assembly in prophase, the velocity of very modest spindle elongation in metaphase and, most strikingly, the velocity of extensive spindle elongation in anaphase B increased with cell size (***Figure 1F***).

To test if these results indeed originate from changes in cell size and not from mutations of the cell cycle regulators wee1 and cdc25, we additionally used other methods to alter cell size without changing the basic levels of wee1 or cdc25 (***Figure 2***). Abnormally short cells were obtained by growing wild-type cells under conditions of starvation, which then divide at an average cell length of 10.91 ± 0.95 µm (***Figure 2A***: starved wt). Abnormally long cells were created by, first, treatment of wild-type cells with hydroxyurea (HU), which allows to arrest them in early S-Phase by disturbing DNA replication. After a few hours of incubation the drug can be washed out, allowing the cells to resume the cell cycle and enter mitosis at an average length of 15.73 ± 0.95 µm (***Figure 2A***: wt +HU). Second, we used an analogue-sensitive (as) mutant of cdc2, homolog of the cyclin-dependent kinase Cdk1 (***Figure 2A***: *cdc2-asM17*). Treatment of this mutant with ATP-analogue inhibitors blocks cells at the G1/S and G2/M transition due to inactivation of cdc2. After washout of the inhibitor, full function of cdc2 can be restored and cells enter mitosis (***Aoi et al., 2014***). Depending on the duration of incubation with the ATP-analogue inhibitor NM-PP1, *cdc2-asM17* cells divided at cell lengths ranging from 12.24 to 27.09 µm (***Figure 2A***: *cdc2-asM17* + NMPP1). Using these methods, we could confirm the previously observed scaling relationship of spindle length and cell length (***Figure 2B***), the constant mitosis duration in cells of varying sizes (***Figure 2C***), as well as the increase of spindle elongation velocity with increasing cell size (***Figure 2D***). Thus, these cells behave similarly compared to the *wee1-50* and *cdc25-22* mutants, indicating that the observed changes of spindle dynamics stem from differences in cell size, not different levels of cell cycle regulators.

Taken together, in fission yeast spindle length scales with cell size, however mitosis can still be realized within a constant time frame, through a cell-size-dependent spindle elongation velocity.

## Kinesin-6 Klp9 controls spindle elongation velocity and mitosis duration

We set out to understand how spindle dynamics adjust to cell size. The most significant cell-size-dependent acceleration of spindle elongation occurred in anaphase B (***Figure 1—figure supplement 2***), which takes approximately half of the total mitosis time in fission yeast (***Figure 1B and C***). Therefore, we focused on this mitotic phase to examine how mitosis duration is maintained constant, irrespective of cell size.

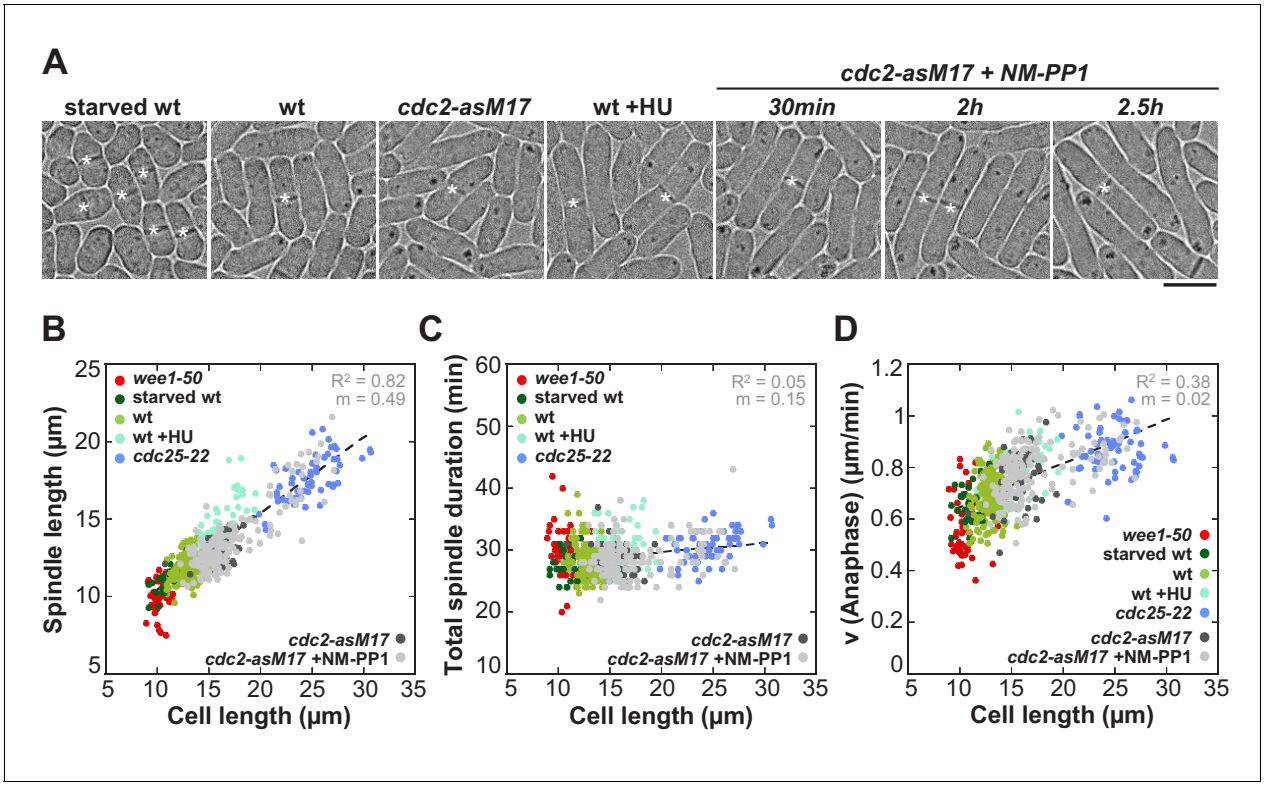


**Figure 2.** Spindle length and spindle elongation velocity scales with cell length in multiple conditions. (**A**) Brightfield images of *S. pombe* wild-type cells in starvation (starved wt), wild-type cells in exponential growth phase (wt), *cdc2-asM17* cells, wild-type cells treated with hydroxyurea (wt+HU), *cdc2-asM17* cells treated with NM-PP1 for 30 min, 2 hr or 2.5 hr. Cells reach their maximum cell length at mitosis/cell division, represented by the septum (asterisk). Scale bar, 5 µm. (**B**) Final spindle length plotted against cell length. (**C**) Total spindle duration plotted against cell length. (**D**) Anaphase spindle elongation velocity plotted against cell length. Data in (**B–D**) was fitted by linear regression (dashed lines), showing the regression coefficient $R^2$ and the slope m. Data was obtained from n cells (starved wt: n = 27, wt: n = 133, wt +HU: n = 52, *cdc2-asM17*: n = 49, *cdc2-asM17* + NM-PP1: n = 163) was collected from three independent experiments.

DOI: https://doi.org/10.7554/eLife.42182.006

In *S. pombe*, outward sliding of antiparallel microtubules is predominantly executed by the kinesin-6 Klp9 (***Figure 3C***) (***Fu et al., 2009***). At anaphase onset the highly conserved MT-crosslinker Ase1 (PRC1/MAP65) bundles antiparallel microtubules, organizing a structure of overlapping microtubules that is called spindle midzone (***Bieling et al., 2010***; ***Gaillard et al., 2008***; ***Glotzer, 2009***; ***Janson et al., 2007***; ***Loïodice et al., 2005***; ***Mollinari et al., 2002***; ***Pellman et al., 1995***; ***Schuyler et al., 2003***; ***Yamashita et al., 2005***). In this position, Ase1 is thought to recruit Klp9, which is localized to the nucleus, in a dephosphorylation-dependent manner to the midzone (***Figure 3B and C***) (***Fu et al., 2009***). As a plus-end directed homotetrameric motor, Klp9 can slide apart the antiparallel microtubules and elongate the mitotic spindle (***Fu et al., 2009***; ***Rincon et al., 2017***).

Deletion of Klp9 decreased the speed of anaphase B spindle elongation velocity in *wee1-50*, wild-type and *cdc25-22* cells (***Figure 3A***). Strikingly, anaphase spindle elongation velocities decreased to very similar values in all three cell types (***Figure 3D and E***), as well as in the *cdc2-asM17* mutant (***Figure 3—figure supplement 1***), ranging between 0.3–0.5 µm/min. Thus, the correlation between spindle elongation velocity and cell size is abolished in absence of Klp9. Despite this, the scaling relationship of spindle length and cell size was still effective (***Figure 3F*** and ***Figure 3—figure supplement 2***). As a result of similar spindle elongation velocities in the absence of Klp9, longer cells needed proportionally more time to complete chromosome segregation compared to

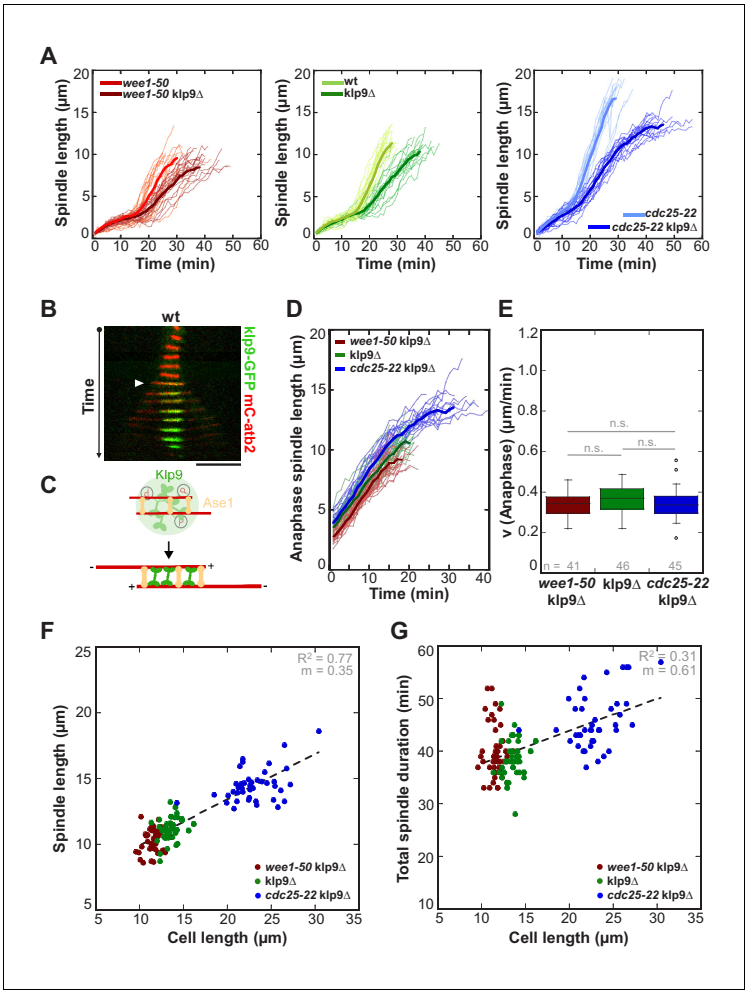


**Figure 3.** Kinesin-6 Klp9 deletion abolishes cell-size-dependent spindle elongation velocity and constant mitosis duration. (**A**) Comparative plots of spindle length dynamics of *wee1-50* (light-red, n = 20) and *wee1-50*klp9Δ (dark-red, n = 20) [left panel], wild-type (light-green, n = 20) and klp9Δ (dark-green, n = 20) [central panel], *cdc25-22* (light-blue n = 20) and *cdc25-22*klp9Δ (dark-blue, n = 20) [right panel]. Bold curves correspond to mean spindle dynamics of each cell type. (**B**) Time-lapse image from mitosis onset until spindle breakdown of a wild-type (wt) cell expressing mCherry-Atb2 (tubulin) and Klp9-GFP. Each frame corresponds to 2 min interval. Arrowhead marks the start of anaphase B. Scale bar, 5 µm. (**C**) Model for anaphase spindle elongation by Klp9, based on ***Fu et al., 2009***. Microtubules are shown in red, Klp9 in green and Ase1 in orange. (**D**) Comparative plot of anaphase spindle dynamics of *wee1-50*klp9Δ (dark-red, n = 20), klp9Δ (dark-green, n = 20) and *cdc25-22*klp9Δ (dark-blue, n = 20). Bold curves correspond to mean spindle dynamics. (**E**) Box plot comparison of anaphase B spindle elongation velocities (**v**) in *wee1-50*klp9Δ, klp9Δ and *cdc25-22*klp9Δ. P values were calculated by Mann-Whitney U test; data sets are defined as not significantly different (n.s.) if p>0.05. (**F**) Final spindle length in the klp9Δ background plotted against maximum cell length (*wee1-50*klp9Δ: n = 41, klp9Δ: n = 46, *cdc25-22*klp9Δ: n = 45). (**G**) Total spindle duration in the klp9Δ background plotted against cell length (*wee1-50*klp9Δ: n = 41, klp9Δ: n = 46, *cdc25-22*klp9Δ: n = 45). Data in (**F–G**) was fitted by linear regression (dashed lines), showing the regression coefficient $R^2$ and the slope m. Data obtained from n cells was collected from three independent experiments.

DOI: https://doi.org/10.7554/eLife.42182.007

The following figure supplements are available for figure 3:

**Figure supplement 1.** Anaphase spindle elongation velocity plotted against cell length of *cdc2-asM17*klp9Δ and *cdc2-asM17*klp9Δ + NM-PP1.

*Figure 3 continued on next page*

*Figure 3 continued*

DOI: https://doi.org/10.7554/eLife.42182.008

**Figure supplement 2.** Final spindle length plotted against cell length of *cdc2-asM17*klp9Δ and *cdc2-asM17*klp9Δ + NM-PP1.

DOI: https://doi.org/10.7554/eLife.42182.009

**Figure supplement 3.** Total spindle duration plotted against cell length of *cdc2-asM17*klp9Δ and *cdc2-asM17*klp9Δ + NM-PP1.

DOI: https://doi.org/10.7554/eLife.42182.010

shorter cells (***Figure 3G*** and ***Figure 3—figure supplement 3***). Thus, the phenomenon of constant mitosis duration irrespective of cell size is abolished in absence of Klp9. Together, these results suggest that the kinesin-6 Klp9 is a key component of the mechanism that adjusts spindle elongation velocity to cell size.

## The number of Klp9 molecules determines spindle elongation velocity

It was previously suggested by computer simulations that the number of force generators acting on the spindle could regulate the speed of spindle elongation (***Hara and Kimura, 2009***). To test this hypothesis, we performed intensity measurements of Klp9-GFP expressed in *wee1-50*, wild-type and *cdc25-22* cells. Following the Klp9-GFP signal intensity throughout anaphase B (***Figure 4A and B***), revealed that, despite fluctuations, the intensity was largely unaffected from shortly after anaphase onset (***Figure 4A and B***: arrowhead) to the end of anaphase B spindle elongation, before the signal intensity dropped down when the spindle disassembled (***Figure 4A and B***: asterisk). In general, the Klp9-GFP intensity increased from *wee1-50* to wild-type to *cdc25-22* cells at every given time point (***Figure 4B***). Moreover, in addition to the Klp9-GFP intensity at the midzone of anaphase spindles (***Figure 4C***: unfilled dots) also the total Klp9-GFP intensity in cells (***Figure 4C***: filled dots), measured shortly before mitosis onset within the nucleus, increased with cell size (***Figure 4C*** and ***Figure 4—source data 1***). This was similarly observed in the *cdc2as-M17* mutant (***Figure 4—figure supplement 1***), showing that the increased recruitment of Klp9 to the spindle occurs due to an increase in cell size, and is not a result of mutations of *wee1* and *cdc25*.

It is tempting to think that total numbers of Klp9 molecules could directly determine the extent of Klp9 recruitment to the spindle. Klp9 could thus represent a limited component within the regulation of spindle elongation velocity, such as tubulin does within the regulation of spindle length (***Good et al., 2013***; ***Hazel et al., 2013***). In this classical model for scaling relationships, the concentration of a limited component, is constant and thus total amounts increase proportional to cell size. Consequently, in larger cells more of this limited component is available, for example leading to the assembly of longer mitotic spindles due to the presence of more tubulin (***Reber and Goehring, 2015***) or potentially an acceleration of spindle elongation due to the presence of more Klp9 motors, allowing the recruitment of more motors to the spindle.

The latter is supported by the fact that the ratio of Klp9-GFP intensity at anaphase spindles over its total intensity in the cell, referred to as Klp9 spindle fraction, did not correlate with cell size (***Figure 4D***: $R^2 = 0.08$, m = 0.0015; and ***Figure 4—figure supplement 2***). More precisely, approximately 40% of the total cellular Klp9 pool was recruited to anaphase spindles in all cell types (***Figure 4D*** and ***Figure 4—figure supplement 2***). This indicates that the number of motors recruited to the spindle directly correlates with the total number of available motors. Moreover, if the extent of Klp9 recruitment is similar in cells of different sizes, we expect the Klp9 concentration in the cell to be constant as well. The concentration of Klp9 was estimated by the ratio of total intensity over cell volume, with the cell volume being calculated by treating the rod-shaped cell as a cylinder (***Figure 4—figure supplement 3***). Indeed, we found the Klp9 concentration in the cell to be largely independent of cell size (***Figure 4E***: $R^2 = 0.09$, m = −0.02 and ***Figure 4—source data 1***).

Similarly to the quantities of Klp9, we observed, that the amount of tubulin, either the total amount of tubulin within the cell (***Figure 4—figure supplement 4***: filled dots) or the amount of tubulin incorporated within the late anaphase spindle (***Figure 4—figure supplement 4***: unfilled dots) increased proportional to cell size. Furthermore the concentration of tubulin in the cell, estimated by the ratio of total mCherry-Atb2 intensity and cell volume, remained constant in cells of different sizes (***Figure 4—figure supplement 5***).

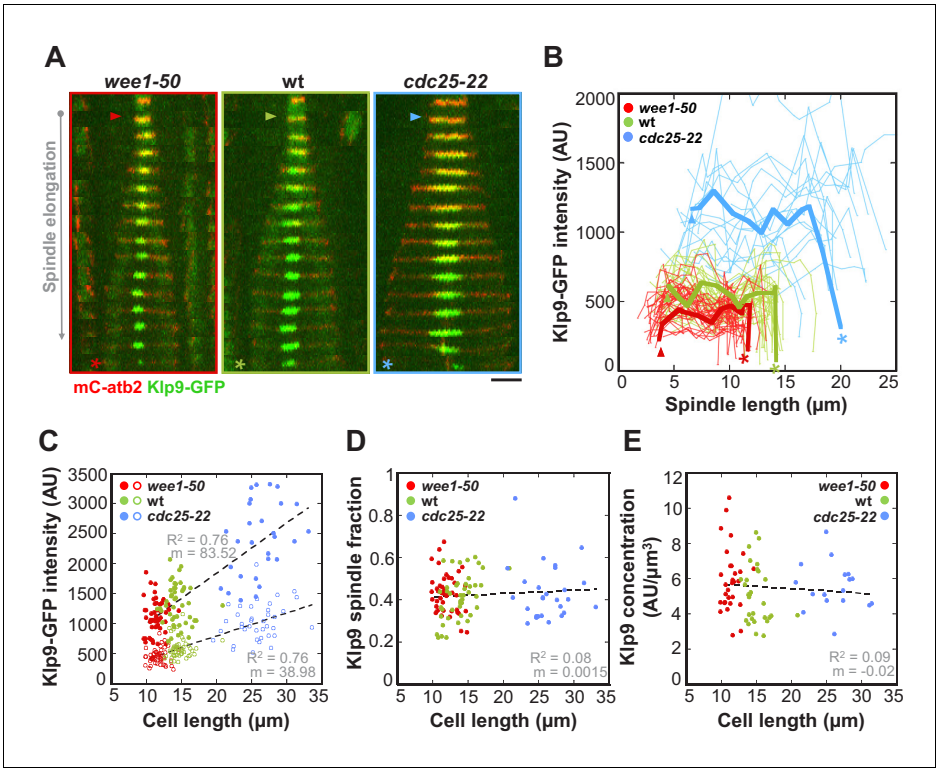


**Figure 4.** The total number of Klp9 molecules and the number of motors on anaphase spindles increase with cell size. (**A**) Time-lapse images of *wee1-50*, wild-type (wt) and *cdc25-22* cells expressing mCherry-Atb2 (tubulin) and Klp9-GFP from anaphase onset (arrowhead) to spindle breakdown (asterisk). Each frame corresponds to 1 min interval. Scale bar, 5 µm. (**B**) Comparative plot of Klp9-GFP intensity over spindle length. Each line corresponds to the Klp9-GFP intensity values of one cell throughout progressing spindle elongation in anaphase. Bold curves correspond to a representative cell of each cell type. (**C**) Total Klp9-GFP intensity (•, filled dots) and Klp9-GFP intensity at anaphase spindles (○, unfilled dots) plotted against cell length (*wee1-50*: n = 48, wt: n = 46, *cdc25-22*: n = 30). Shown values of Klp9-GFP intensity of anaphase spindles correspond to the mean intensity values of late anaphase. (**D**) Ratio between Klp9-GFP intensity at the anaphase spindle and the total Klp9-GFP intensity, referred to as Klp9 spindle fraction, plotted against cell length (*wee1-50*: n = 48, wt: n = 46, *cdc25-22*: n = 30). (**E**) Ratio of total Klp9-GFP intensity and cell volume plotted against cell length (*wee1-50*: n = 30, wt: n = 29, *cdc25-22*: n = 17). Data in (**C–E**) was fitted by linear regression (dashed lines), showing the regression coefficient $R^2$ and the slope m. Data obtained from n cells was collected from three independent experiments.

DOI: https://doi.org/10.7554/eLife.42182.011

The following source data and figure supplements are available for figure 4:

**Source data 1.** Mean values of Klp9-GFP intensity and concentration.

DOI: https://doi.org/10.7554/eLife.42182.017

**Figure supplement 1.** Total Klp9-GFP intensity and Klp9-GFP intensity at anaphase spindles plotted against cell length of *cdc2-asM17* and *cdc2-asM17* + NM-PP1.

DOI: https://doi.org/10.7554/eLife.42182.012

**Figure supplement 2.** Ratio between Klp9-GFP intensity at anaphase spindles and in the nucleus plotted against cell length of *cdc2-asM17* and *cdc2-asM17* + NM-PP1.

DOI: https://doi.org/10.7554/eLife.42182.013

**Figure supplement 3.** Estimation of cell volume of *S. pombe* cells.

DOI: https://doi.org/10.7554/eLife.42182.014

**Figure supplement 4.** Total mCherry-Atb2 intensity and mCherry-Atb2 intensity of anaphase spindles in *wee1-50*, wild-type and *cdc25-22* cells.

DOI: https://doi.org/10.7554/eLife.42182.015

*Figure 4 continued on next page*

*Figure 4 continued*

**Figure supplement 5.** Ratio of total mCherry-Atb2 intensity and cell volume plotted against cell length.
DOI: https://doi.org/10.7554/eLife.42182.016

To further probe the impact of the amount of Klp9 molecules on spindle elongation velocity, we modified expression levels of *klp9* by inserting the thiamine repressible *nmt* promoters *pnmt1, pnmt41 or pnmt81* upstream of the endogenous *klp9* open reading frame. Expression of *klp9* under the control of *pnmt81* led to low, *pnmt41* to mild and *pnmt1* to very strong overexpression (***Figure 5A***). Spindle dynamics were measured in cells overexpressing untagged *klp9* and intensity measurements were performed in cells expressing *GFP-klp9*. Anaphase B spindle elongation velocity was altered in a dose-dependent manner relative to the expression level of *klp9* (***Figure 5B***). Generally, the stronger *klp9* was overexpressed, the faster anaphase spindles elongated (***Figure 5C***). We further tested if the acceleration of spindle elongation was due to an increase in Klp9 recruitment to the spindle. Intensity measurements in cells expressing *GFP-klp9* under the control of the different *nmt* promoters revealed an increase of GFP-klp9 intensities, measured in anaphase spindles, in proportion to expression levels (***Figure 5E*** and ***Figure 5—source data 1***). An increase of GFP-klp9 signal on the spindle correlates with an increase of spindle elongation velocity until a certain upper-limit (***Figure 5D***). At a velocity of approximately 1.1–1.2 µm/min no strong acceleration occurred even though GFP-klp9 intensities increased further (***Figure 5D***). This upper-limit could stem from either the maximum velocity a Klp9 motor can walk, the saturation of binding sites for Klp9 or the velocity of microtubule growth.

However, we observed a difference in the slope of the velocity versus intensity correlation between the control condition (*wee1-50*, wt and *cdc25-22*) and cells in which *klp9* was overexpressed. Linear regression of mean values of control cells gives a greater slope ($m = 5.2\times10^{-3}$) than cells in which *klp9* was overexpressed ($m = 0.3\times10^{-3}$; values used for GFP-klp9 <500 AU) (***Figure 5—figure supplement 1***). This indicates that other factors might contribute to ensure such an efficient adjustment of spindle elongation to cell size, as accomplished in the control condition. Nevertheless, modifying the number of Klp9 molecules is sufficient to regulate spindle elongation velocity.

## Ase1, Cut7 and Klp2 do not regulate cell-size-dependent spindle elongation velocity

How is the cell-size-dependent spindle elongation velocity regulated besides the available number of kinesin-6 molecules? Many other midzone components assist or oppose microtubule sliding (***Scholey et al., 2016***) and could thus regulate spindle elongation velocity as well. However, since the scaling relationship with cell size was completely abolished in absence of Klp9, we argue that, this additional level of regulation has to occur through modifying the action of Klp9.

Interaction of Klp9 with the MT crosslinker Ase1 (***Figure 6G***) has been proposed to bring Klp9 into a tetrameric conformation at the spindle midzone, in which it preferentially binds antiparallel microtubules, thus enhancing the efficiency of spindle elongation (***Fu et al., 2009***). Therefore, we decided to examine the role of Ase1 within the underlying mechanism. Ase1 localizes to the midzone shortly before anaphase onset (***Figure 6A***: arrowhead) and stays at the midzone as well as at spindle poles throughout anaphase B, as previously reported (***Loïodice et al., 2005***; ***Yamashita et al., 2005***). Intensity measurements in wild-type, *wee1-50* and *cdc25-22* cells expressing Ase1-GFP revealed an increase at the spindle midzone proportional to cell size (***Figure 6B,C*** and ***Figure 6—source data 1***). To probe the role of the MT bundler, we overexpressed *ase1* by using *nmt* promoters. Expression of *ase1* under the control of *pnmt81* and *pnmt41* decreased anaphase B spindle elongation velocity in a dose-dependent manner (***Figure 6D and E***). Cells, which expressed *ase1* under the control of the strongest *nmt* promoter (*pnmt1*) appeared very sick and spindles did not seem to elongate at all after metaphase (data not shown). Thus, if present in excess, Ase1 resists spindle elongation. This is consistent with previous in vitro studies where Ase1 has been shown to act as a brake, opposing the action of kinesins, which slide apart antiparallel microtubules (***Braun et al., 2011***; ***Lansky et al., 2015***). We thus wondered if Ase1 instead of promoting spindle elongation, opposes the action of Klp9. To test this, we reduced the amount of Ase1 by using an Ase1 shut-off strain ($ase1^{Off}$). In contrast to the full deletion of *ase1*, the presence of a reduced

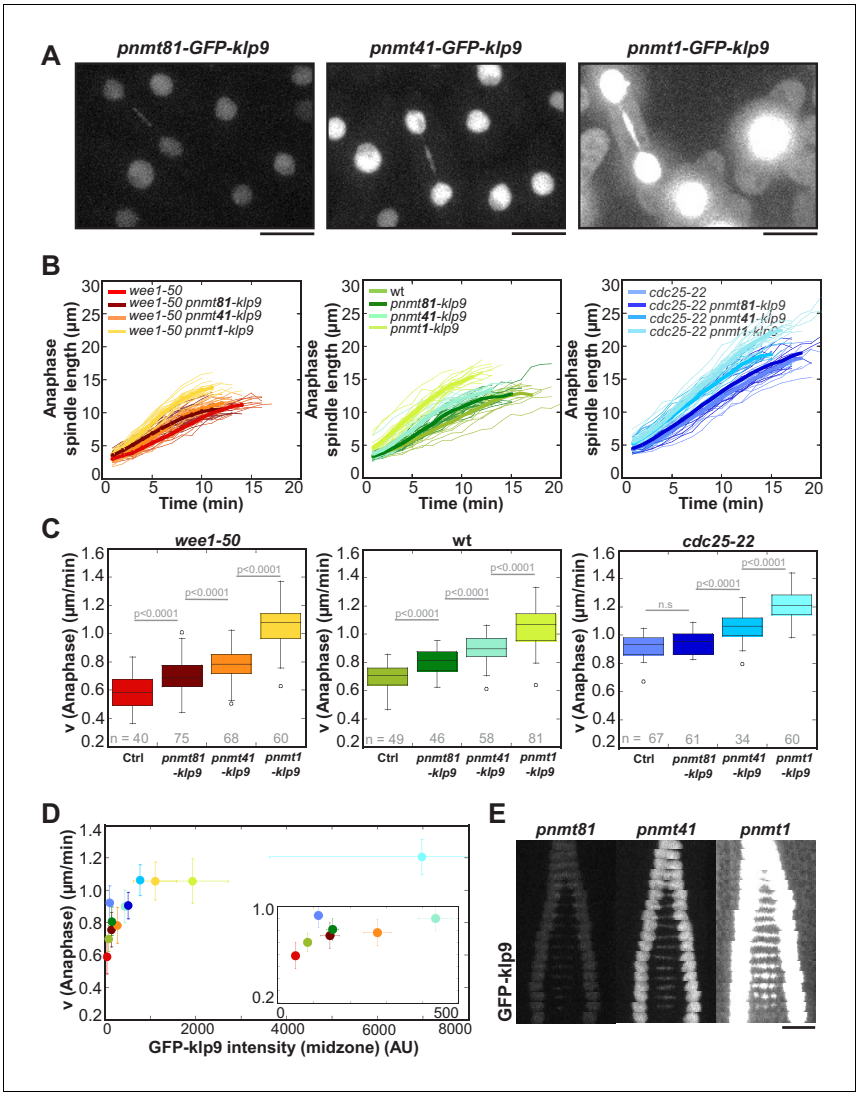


**Figure 5.** Overexpression of Klp9 accelerates anaphase B spindle elongation in a dose-dependent manner. (**A**) Images of cells expressing *GFP-klp9* under the control of thiamine repressible *nmt* promoters. Scale bar, 5 µm. (**B**) Comparative plot of spindle length dynamics of *wee1-50* (left panel), wild-type (middle panel) and *cdc25-22* cells (right panel) with endogenous *klp9* expression, *pnmt81-klp9*, *pnmt41-klp9* and *pnmt1-klp9* (each strain: n = 20). (**C**) Box plot comparison of anaphase B spindle elongation velocities (**v**) in cells with endogenous *klp9* expression (Ctrl), *pnmt81-klp9*, *pnmt41-klp9* and *pnmt1-klp9*. P values were calculated by Mann-Whitney U test. (**D**) Mean values and corresponding standard deviations of anaphase B velocity plotted against mean values of GFP-klp9 intensity at anaphase spindles. The inset shows the same data on a 0 to 500 AU x-axis and a 0.2 to 1.0 µm/min y-axis. The color code is equal to the one used in (**B**) and (**C**). (**E**) Time-lapse images from metaphase to spindle breakdown in cells expressing GFP-klp9 under the control of *nmt* promoters. Each frame corresponds to 1 min interval. Scale bar, 5 µm. Data obtained from n cells was collected from three independent experiments.

DOI: https://doi.org/10.7554/eLife.42182.018

The following source data and figure supplement are available for figure 5:

**Source data 1.** Mean values of spindle elongation velocity and the Klp9-GFP intensity at anaphase spindles in pnmt-klp9 strains.

DOI: https://doi.org/10.7554/eLife.42182.020

*Figure 5 continued on next page*

*Figure 5 continued*

**Figure supplement 1.** Linear regression of the function of spindle elongation velocity and Klp9-GFP intensity.
DOI: https://doi.org/10.7554/eLife.42182.019

amount of the MT-bundler still allows the formation of relatively stable spindles, since they do not break early in anaphase B (***Figure 6—figure supplement 1***). We reasoned that if Ase1 acts as a brake for MT sliding, this strong reduction of the Ase1 pool would result in an acceleration of spindle elongation. However, we could not observe a significant difference in anaphase B spindle elongation between wild-type and *ase1$^{off}$* cells (***Figure 6F and H***), even though Ase1-GFP intensities at the midzone were strongly diminished (***Figure 6—figure supplement 2***). Accordingly, analysis of Klp9-GFP signals in both conditions did not reveal significant differences in intensity of Klp9-GFP or signal length at the midzone (***Figure 6—figure supplements 3*** and ***4***). In some cells the distribution of Klp9 over the spindle was expanded, as previously observed upon *ase1* deletion (***Fu et al., 2009***). Nevertheless, even though only a few Ase1 molecules organize the midzone, Klp9 can be normally recruited and slide apart antiparallel spindle MTs at wild-type speed. Together, with regards to velocity, Ase1 does not promote or oppose spindle elongation in anaphase when expressed at endogenous levels, even though it has been shown to be essential for spindle stability (***Janson et al., 2007***; ***Loïodice et al., 2005***; ***Yamashita et al., 2005***). The deceleration of spindle elongation upon Ase1 overexpression might only occur when Ase1 is strongly accumulated but not under physiological conditions. Accordingly, in vitro microtubule sliding is stalled only upon a Ase1:Ncd (*Drosophila* kinesin-14) ratio of 4:1 (***Braun et al., 2011***), or a ratio of 25:1 using PRC1 and Eg5 (***Subramanian et al., 2010***).

Besides Ase1, Kinesin-5 (***Figure 6G***) could oppose the action of Klp9 and thus modify spindle elongation velocity. For instance, in absence of the *C. elegans* kinesin-5 BMK-1 spindle elongation during anaphase is abnormally fast (***Saunders et al., 2007***). In fission yeast, as in most other organisms, deletion of the kinesin-5 Cut7 is lethal, due to the formation of monopolar spindles. However, upon deletion of the kinesin-14 Pkl1, Cut7 deletion is viable and cells are able to form bipolar spindles (***Olmsted et al., 2014***; ***Rincon et al., 2017***; ***Syrovatkina and Tran, 2015***; ***Yukawa et al., 2018***). We therefore examined spindle dynamics in a double pkl1Δcut7Δ deletion strain. Comparing anaphase velocity with wild-type cells showed a slight but significant decrease (***Figure 6H***). Since the absence of Pkl1 alone does not affect elongation velocity (***Figure 6H***), this decrease may result from the absence of Cut7. Therefore, Cut7 does not act as a brake in fission yeast and might in the opposite be required to promote spindle elongation in Anaphase B, to a small extent, as previously suggested (***Rincon et al., 2017***). However, even with its role in promoting spindle elongation, Cut7 is not sufficient to regulate a cell-size-dependent spindle elongation velocity, since the velocity of spindle elongation is similar in cells of different size in absence of Klp9 but presence of Cut7 (klp9Δ strains, ***Figure 3***).

Another candidate was the kinesin-14 Klp2, a minus-end directed motor present at the midzone (***Figure 6G***) which was recently shown to generate inward forces against Cut7 in fission yeast (***Yukawa et al., 2018***). However, its deletion did not significantly alter anaphase B elongation velocity either (***Figure 6H***).

Together, even though Ase1 interacts with Klp9 (***Fu et al., 2009***), Cut7 contributes to microtubule sliding in anaphase in absence of Klp9 (***Rincon et al., 2017***), and Klp2 opposes outward sliding of microtubules by Cut7 (***Yukawa et al., 2018***), these spindle components do not seem to have a substantial impact on the regulation of the cell-size-dependent spindle elongation velocity.

## Microtubule density and overlap length increase with spindle length

The spindle midzone is a key structure for anaphase B spindle elongation (***Khodjakov et al., 2004***; ***Scholey et al., 2016***; ***Tolić-Nørrelykke et al., 2004***) and the site of action for Klp9 (***Fu et al., 2009***). We hypothesized that differences in its structure could therefore affect spindle elongation velocity in addition to the number of Klp9 molecules.

Line scan-analysis of Klp9-GFP signals at anaphase spindles in *wee1-50*, wild-type and *cdc25-22* cells revealed an increase in signal length in *cdc25-22* cells compared to wild-type and *wee1-50* cells (***Figure 7A***). This indicates, that the length of microtubule overlap increases in longer spindles.

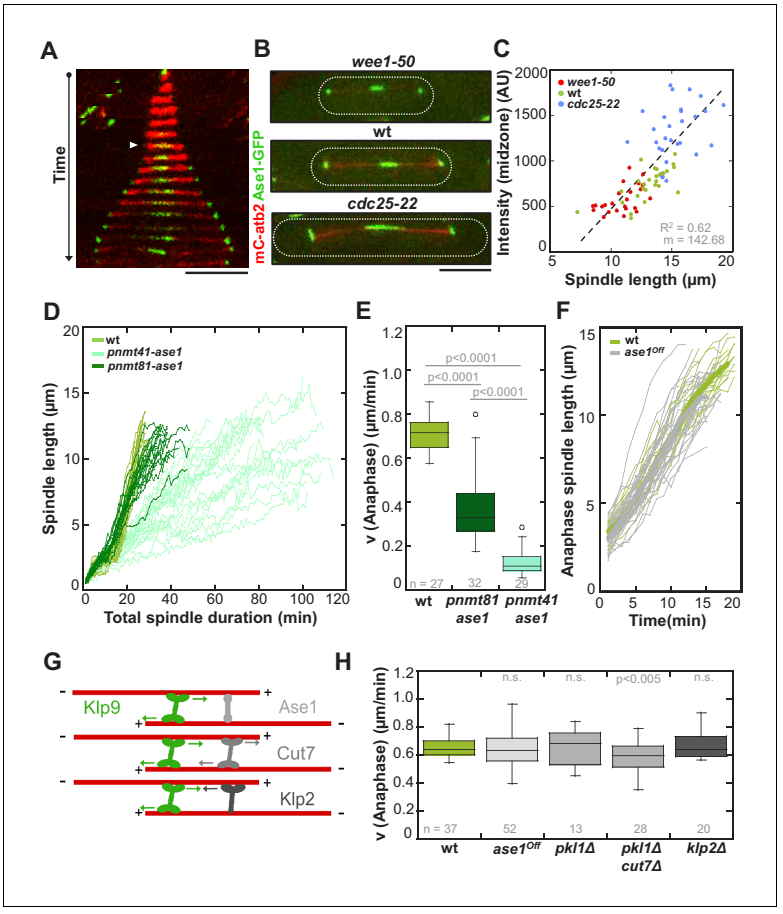


**Figure 6.** Ase1, Cut7 and Klp2 do not contribute to the regulation of cell-size-dependent spindle elongation velocity. (**A**) Time-lapse image from mitosis onset until spindle breakdown of a wild-type cell expressing mCherry-Atb2 (tubulin) and Ase1-GFP. Arrowhead corresponds to anaphase B onset. Each frame corresponds to 2 min interval. (**B**) Images of *wee1-50*, wild-type (wt) and *cdc25-22* cells expressing mCherry-Atb2 (tubulin) and Ase1-GFP in late anaphase. Scale bar, 5 µm. (**C**) Ase1-GFP intensity at anaphase spindles plotted against final spindle length (*wee1-50*: n = 24, wt: n = 28, *cdc25-22*: n = 30). Data was fitted by linear regression (dashed lines), showing the regression coefficient $R^2$ and the slope m. (**D**) Comparative plot of spindle length dynamics of wild-type (n = 27) cells, *pnmt81-ase1* (n = 32) and *pnmt41-ase1* (n = 29). (**E**) Box plot comparison of anaphase B spindle elongation velocities (**v**) in wild-type, *pnmt81-ase1* and *pnmt41-ase1* cells. (**F**) Comparative plot of anaphase spindle dynamics of wild-type (n = 28) and $ase1^{Off}$ cells (n = 52). Bold curves correspond to mean spindle dynamics. (**G**) Model of the role of tested midzone components. (**H**) Box plot comparison of anaphase B spindle elongation velocities (**v**) in wild-type cells, ase1-Shut-Off ($ase1^{Off}$), *pkl1*Δ, the double-deletion *pkl1*Δ*cut7*Δ and *klp2*Δ cells. P values were calculated by Mann-Whitney U test; data sets are defined as not significantly different (n.s.) if p>0.05. Data obtained from n cells was collected from three independent experiments.

DOI: https://doi.org/10.7554/eLife.42182.021

The following source data and figure supplements are available for figure 6:

**Source data 1.** Mean values of Ase1-GFP intensity and signal length.

DOI: https://doi.org/10.7554/eLife.42182.026

**Figure supplement 1.** Upon reduction of the Ase1 level spindles remain stable until late anaphase.

DOI: https://doi.org/10.7554/eLife.42182.022

**Figure supplement 2.** GFP-Ase1 intensity at anapahse spindles in $ase1^{Off}$ and wild-type cells.

DOI: https://doi.org/10.7554/eLife.42182.023

**Figure supplement 3.** Klp9-GFP intensity at anaphase spindles in $ase1^{Off}$ and wild-type cells.

*Figure 6 continued on next page*

*Figure 6 continued*

DOI: https://doi.org/10.7554/eLife.42182.024

**Figure supplement 4.** Klp9-GFP signal length at anaphase spindles in *ase1*$^{Off}$ and wild-type cells.

DOI: https://doi.org/10.7554/eLife.42182.025

Indeed, midzone length, measured by the length of increased mCherry-Atb2 fluorescence at the center of the spindle in a kymograph (***Figure 7—figure supplement 1***), correlated strongly with spindle length (***Figure 7B***: $R^2$ = 0.82, m = 0.26). In *wee1-50* cells the mean midzone length was 2.6 ± 0.4 µm, while it measured 3.2 ± 0.5 µm in wild-type and 5.0 ± 0.6 µm in *cdc25-22* cells. Furthermore, the midzone length, while fluctuating, was kept rather constant throughout the progression of spindle elongation (***Figure 7—figure supplement 2***). This indicates, that the microtubule growth rate is largely correlated to anaphase B spindle elongation.

Furthermore, the number of binding sites for Klp9 on the spindle is not only determined by the overlap length but also by the amount of MTs associated with the midzone. Microtubule density, examined by the mCherry-Atb2 intensity value of a fixed area at the midzone region, slightly increased with spindle length (***Figure 7C***: $R^2$ = 0.53, m = 18.36) whereas values are significantly different between *wee1-50*, wild-type and *cdc25-22* cells (***Figure 7C***). The increased microtubule density of longer spindles is moreover suggested by the fact, that the ratio of tubulin intensity of the anaphase spindle and spindle length, giving the tubulin intensity per unit length of the spindle, scaled with cell size (***Figure 7—figure supplement 3***). Taking both parameters, overlap length and density, into account by measuring the total mCherry-Atb2 intensity of the whole length of the midzone, we observed a strong increase proportional to spindle length (***Figure 7D***: $R^2$ = 0.82, m = 92.22). Thus, longer spindles provide much more binding sites for Klp9 by forming longer regions of antiparallel overlapping microtubules and by bundling more microtubules within this region (***Figure 7E***). Similar to spindle length, the density of the spindle could be regulated by the cytoplasmic volume through limiting the amount of tubulin. This is supported by the fact, that the extent by which the amount of tubulin increases with cell size is greater than the extent by which the spindle length scales with cell size: the ratio of total mCherry-Atb2 intensity and spindle length increases with cell size (***Figure 7—figure supplement 4***). In other words, per unit length of the spindle more tubulin is available in longer cells, potentially resulting in the assembly of more microtubules within the structure.

Interestingly, the ratio of Klp9-GFP intensity and total mCherry-Atb2 intensity of the midzone, which we use as an estimate for the occupancy of the midzone with motors, decreased with spindle length (***Figure 7F***). Hence, within larger cells the midzone of longer spindles might be less occupied with Klp9 molecules in relation to shorter spindles in smaller cells. The inverse correlation of molecular crowding at the spindle midzone might additionally impact the control of spindle elongation velocity. This would explain the difference in the slope of the correlation of spindle elongation velocity and Klp9-GFP intensity between control cells and cells in which Klp9 was overexpressed (***Figure 5—figure supplement 1***). Increasing motor amounts are sufficient to accelerate spindle elongation, but when motors additionally work in a less crowded environment, this might further increase the speed of spindle elongation.

## Discussion

### Mechanism of cell-size-dependent spindle elongation velocity

Our results show that spindle length scales with cell size in fission yeast, and that mitosis duration, defined from spindle assembly to disassembly, is constant irrespective of cell and spindle size (***Figures 1***, ***2*** and ***8***). We reveal that the kinesin-6 Klp9 is an essential player in fixing a constant duration of mitosis in cells of different sizes through adjusting the velocity of spindle elongation in Anaphase B (***Figures 3*** and ***8***). Central to this conclusion is the observation that deletion of Klp9 eliminates the scaling relationship between spindle elongation velocity and cell size (***Figure 3***). In this background, the mitotic spindle can still elongate, due to the presence of the kinesin-5 Cut7 (***Rincon et al., 2017***), but Cut7 alone does not promote the establishment of a cell-size dependent spindle elongation velocity. Consequently, in absence of Klp9 a correlation between mitosis duration and cell size

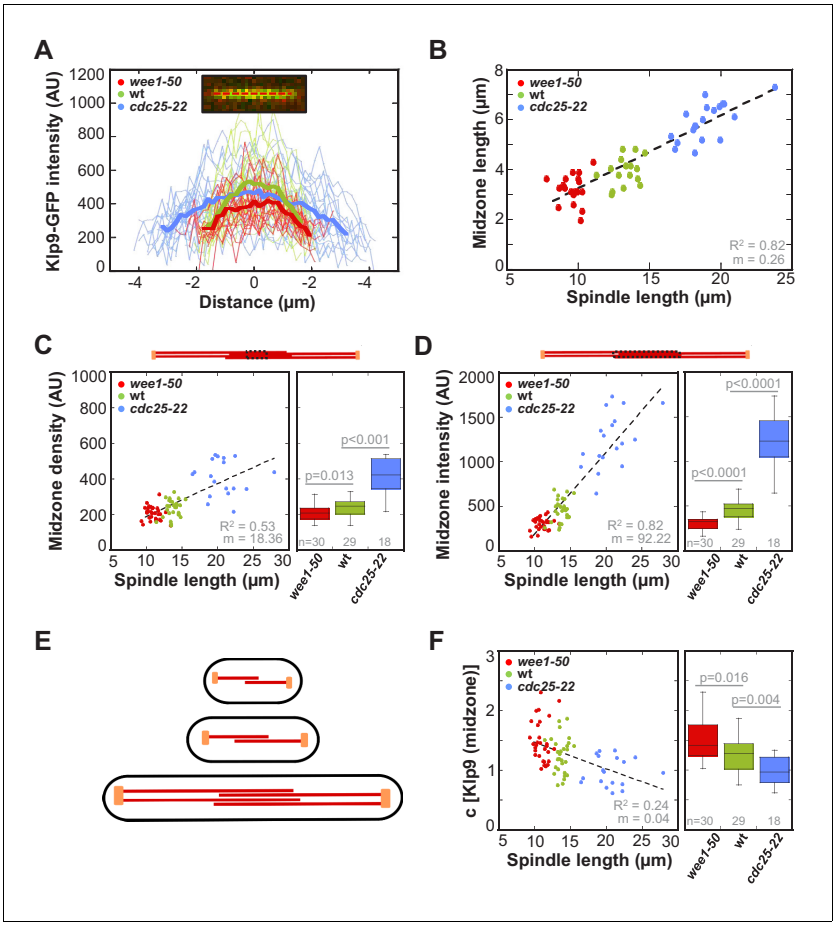


**Figure 7.** Longer spindles provide overproportionally more binding sites for Klp9. (**A**) Intensities obtained by line scan analysis of Klp9-GFP signals at anaphase spindles of *wee1-50* (n = 20), wild-type (n = 20) and *cdc25-22* (n = 20) cells. A line was placed over the whole length of the Klp9-GFP signal (red dashed line, inset) and the resulting intensity spectrum is shown. Bold curves correspond to the mean intensity distribution for each cell type. (**B**) Mean midzone length plotted against spindle length (*wee1-50*: n = 19, wt: n = 16, *cdc25-22*: n = 19). (**C**) mCherry-Atb2 density of the midzone, measured as illustrated by the dashed box within the scheme illustrating the mitotic spindle, plotted against final spindle length (left panel) and box plot comparison of the mCherry-Atb2 density of the midzone (right panel). (**D**) Total mCherry-Atb2 intensity of the midzone, measured as illustrated by the dashed box within the scheme illustrating the mitotic spindle, plotted against final spindle length (left panel) and box plot comparison of the total mCherry-Atb2 intensity of the midzone (right panel). (**E**) Model for mitotic spindle structure in fission yeast cells of different sizes. MTs are shown in red and spindle poles in orange. (**F**) Effective concentration of Klp9 at the midzone plotted against spindle length (left panel) and box plot comparison of the effective concentration of Klp9 at the midzone (right panel). Data in (**B–D**) and (**F**) was fitted by linear regression (dashed lines), showing the regression coefficient $R^2$ and the slope m. P values were calculated by Mann-Whitney U test. Data obtained from n analyzed cells was collected from three independent experiments.

DOI: https://doi.org/10.7554/eLife.42182.027

The following figure supplements are available for figure 7:

**Figure supplement 1.** Measurement of midzone length.

DOI: https://doi.org/10.7554/eLife.42182.028

**Figure supplement 2.** Midzone length throughout progressing spindle elongation in anaphase plotted against time.

DOI: https://doi.org/10.7554/eLife.42182.029

*Figure 7 continued on next page*

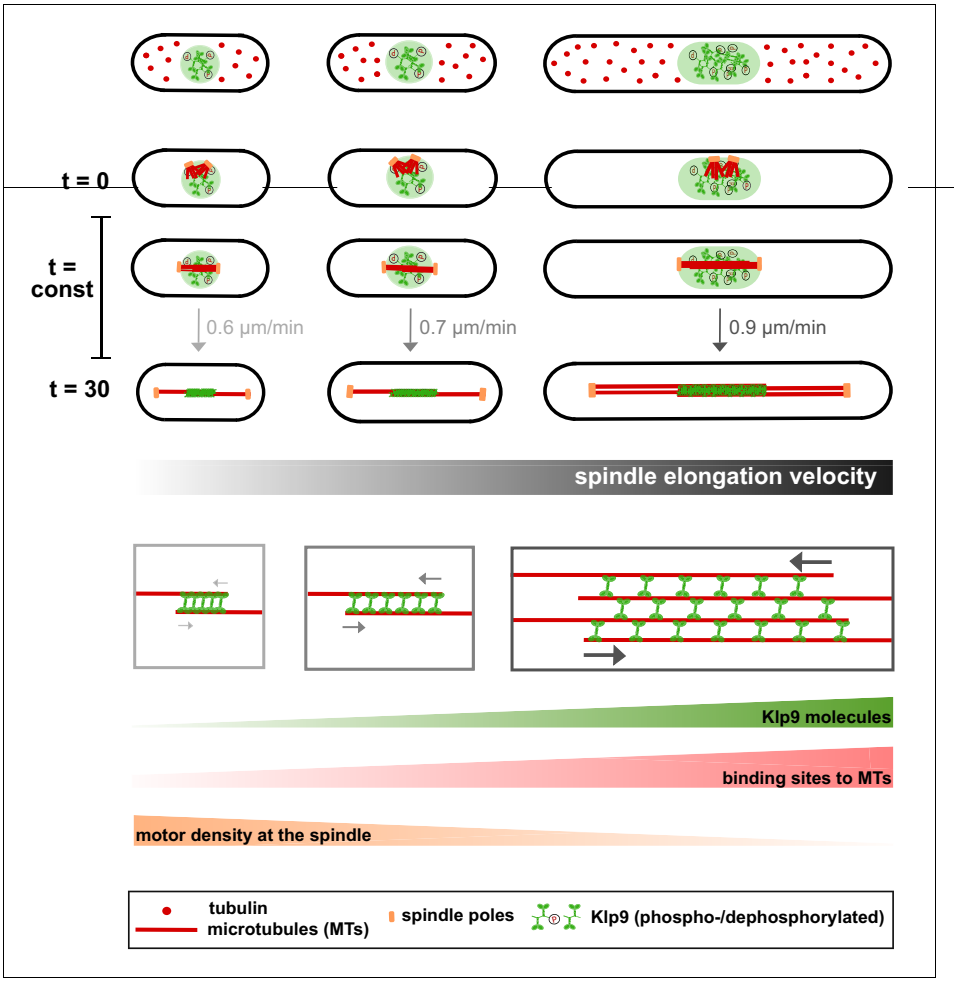


**Figure 8.** Limited components model for the regulation of cell-size-dependent spindle elongation and a constant mitosis duration. Upper panel: The concentration of essential components such as tubulin (red) and Klp9 (green) is constant in cells of different sizes. Thus, total amounts increase proportional to cell size. Due to the presence of more tubulin molecules, longer and more dense spindles can be assembled in larger cells (from t = 0 to t = 30). Likewise, the presence of more Klp9 molecules allows the recruitment of more motors to the anaphase spindle (from t = 0 to t = 30). Lower panel: Since, both the length of antiparallel overlap and the number of microtubules within the midzone increase with cell size, the number of binding sites for Klp9 to the spindle scales overproportionally with spindle and cell length. Thereby, the motor density of Klp9 at the midzone is reduced. With more motors acting in a less crowded environment, spindle elongation can be accelerated and the overall duration of chromosome segregation is kept constant: with increasing cell size, longer spindles are elongated with increasing velocity.

DOI: https://doi.org/10.7554/eLife.42182.032

is established and therefore the constant mitosis duration is abolished. Intensity measurements and overexpression of Klp9 demonstrated that the more Klp9 is available, the more it is recruited to the spindle and the faster the spindle is elongated (***Figures 4***, ***5*** and ***8***).

Klp9 could achieve this role by different mechanisms. First, the forces generated by many individual Klp9 motors might add up and concomitantly elongate the spindle faster than fewer motors. Similarly, the force produced by several full-length *Xenopus* kinesin-5, that crosslink and slide apart two antiparallel microtubules, has been shown to depend linearly on the motor number in vitro

(*Shimamoto et al., 2015*). Why a cell-size-dependent spindle elongation would be established by the kinesin-6 Klp9 but not by the kinesin-5 Cut7 in fission yeast remains an open question. One possibility is that these motors show different behaviors when acting in teams: the forces of several Klp9 motors could add up, but not the forces generated by several Cut7 molecules. Similarly, in contrast to *Xenopus* kinesin-5 (*Shimamoto et al., 2015*), forces generated by kinesin-1 molecules do not scale with motor number in vitro (*Furuta et al., 2013*; *Jamison et al., 2012*). Another possibility is that the force outcome or velocity of Cut7 is regulated by other midzone components such as Klp2 (*Yukawa et al., 2018*) or Ase1, but this may not be the case for Klp9. Such a differential regulation has been reported for the MAP TPX2 and the kinesin-5 Eg5. In vitro TPX2 slowed down MT-sliding of Eg5 but not of kinesin-1 (*Ma et al., 2011*).

Second, the amount of available binding sites for Klp9 to the spindle midzone could be part of the regulation of spindle elongation velocity. Accordingly, the force generated by ensembles of full-length *Xenopus* kinesin-5 scales with the number of motors bound and the overlap length in vitro (*Shimamoto et al., 2015*). Moreover, in vitro studies using the Ase1 homolog PRC1 and the plus-end directed motor Kif4A showed that the sliding velocity of antiparallel oriented microtubules scales with the initial overlap length (*Wijeratne and Subramanian, 2018*). In agreement with this hypothesis we demonstrate, that midzone length scales with cell and spindle length. In addition, we observed that within longer spindles, more microtubules are organized within the midzone (*Figures 7* and *8*). This is consistent with EM-based electron tomographic reconstructions of wild-type *S. pombe* spindles (*Ward et al., 2014*) and serial-section reconstructions of *cdc25-22* spindles (*Ding et al., 1993*). At the metaphase-to-anaphase transition, spindles in wild-type cells consist of about nine microtubules and *cdc25-22* spindles contain approximately sixteen microtubules (*Ding et al., 1993*; *Ward et al., 2014*). With both overlap length and density correlating with cell size, the number of Klp9 binding sites to microtubules increases to a greater extent than the number of Klp9 molecules at the midzone. This results in a lower effective concentration of the motor at the midzone of longer spindles (*Figures 7F* and *8*). We speculate that this local concentration could assist the regulation of a cell-size-dependent elongation speed. Indeed, increasing motor densities, for instance of kinesin-8, have been reported to reduce motor velocity (*Leduc et al., 2012*). As motors entered a region of high motor density, their velocity was slowed down, potentially due to steric interference. This phenomenon might result from the fact that the motor cannot step forward if the next binding-site is already occupied by another motor (*Leduc et al., 2012*). Similarly, increasing densities of Cut7, immobilized on a coverslip, decreased the sliding velocity of attached microtubules (*Britto et al., 2016*).

Third, the velocity of growth of antiparallel microtubules organized in the spindle midzone could impact the speed of spindle elongation. The fact that the overlap length did not shrink during spindle elongation, suggests that the associated microtubules grow constantly, as reported for Ptk1 cells and diatom spindles (*Cande, 1986*; *Cande and McDonald, 1985*; *Masuda and Cande, 1987*; *Saxton and McIntosh, 1987*). One could thus think that, instead of the velocity of microtubule sliding, the velocity of microtubule growth could determine the velocity of spindle elongation. Accordingly, in *Drosophila* embryos depletion of the kinesin-8 KLP67A, which is thought to trigger microtubule plus-end depolymerization (*Varga et al., 2009*; *Varga et al., 2006*), increased the velocity of microtubule sliding and thus of anaphase B spindle elongation (*Wang et al., 2010*). If this would similarly be the case in fission yeast, we think, that Klp9 would be part of the regulation of microtubule growth, since the scaling relationship of spindle elongation velocity and cell size was completely abolished in absence of Klp9. Moreover, increasing the number of Klp9 motors increased the velocity of spindle elongation, which would not occur if the speed of microtubule growth determines the speed of microtubule sliding independent of Klp9. The kinesin-6 could achieve this role by either acting as a MT polymerase itself, as it has been suggested for the other MT sliding motor kinesin-5 (*Chen and Hancock, 2015*) or by recruiting other spindle components that regulate microtubule polymerization. In contrast to this model, the velocity of microtubule sliding could impact the velocity of microtubule growth. In this case, the velocity of microtubule sliding determines the velocity of spindle elongation, while the rate of microtubule growth is adjusted accordingly, preventing the overlap region to shrink throughout spindle elongation. An example for this model, proposing microtubule growth to follow microtubule sliding, was established by in vitro studies using PRC1 and the kinesin-4 Xklp1, which is recruited to overlap regions by PRC1 and inhibits microtubule growth (*Bieling et al., 2010*). The number of kinesin-4 molecules is determined by the overlap length. Thus,

upon decreasing overlap length due to microtubule sliding, the number of kinesin-4 molecules may decrease, enabling the overlap to grow. Consequently, microtubule polymerization follows the rate of microtubule sliding. In general, it is not clear which parameter eventually determines the dynamics of spindle elongation and this could be different from one organism to another. In fission yeast, reducing the microtubule growth rate by disrupting the interaction between Mal3, an EB1 protein, and Dis1, a member of the XMAP215/TOG family, resulted in a slightly faster spindle elongation (***Matsuo et al., 2016***). This result is hard to interpret and one would expect the following two outcomes. Either, in case the microtubule growth rate is limiting, spindle elongation velocity would decrease; or, if the microtubule sliding velocity is limiting for the speed of spindle elongation, spindle elongation velocity would be unaltered. However, decreasing the speed of microtubule growth does not seem to directly result in a decreased velocity of spindle elongation and thus might not be limiting in fission yeast.

To conclude, we propose a model in which larger cells provide more Klp9 molecules resulting in the recruitment of more motors to the spindle midzone (***Figure 8***). An increased amount of motors at the midzone accelerates the velocity of spindle elongation, either by increasing the velocity of microtubule sliding or by increasing the rate of microtubule growth. In addition, this effect may be enhanced by a lower rate of molecular crowding on longer spindles (***Figure 8***: lower panel).

Cumulatively, this study suggests that cell-size-dependent spindle elongation velocity, which ultimately ensures a constant mitotic time frame in cells of various sizes, may be a consequence of scaling of essential spindle components or parameters with cell size: the number of Klp9 molecules, microtubule density and midzone length (***Figure 8***). We thus wonder if, like spindle length (***Good et al., 2013***; ***Hazel et al., 2013***), the constant mitotic time frame could be regulated by the cytoplasmic volume. Consistent with this model we found the concentration of tubulin and Klp9 to be constant in fission yeast cells of different sizes. With an unaltered concentration, total amounts increase proportionally to cell size: larger cells provide more tubulin and Klp9 molecules (***Figure 8***). This eventually leads to the assembly of longer and more dense mitotic spindles, the recruitment of more motors to these spindles, and consequently an acceleration of spindle elongation.

### Constant mitosis duration

With this study we describe one mechanism that allows diverse cells to accomplish chromosome segregation in a constant time frame. It was previously reported that in various human cell lines the duration of G1-, S- and G2-phase varied widely while mitosis duration was remarkably constant (***Araujo et al., 2016***). Together, this sheds light on the importance of the regulation of mitosis duration and provides evidence that chromosome segregation has to be finished within a certain time frame. This time frame might even be similar in different organisms. The time needed to accomplish chromosome segregation in mammalian cells and in yeast is strikingly similar. Mammalian cells spend 20–60 min in mitosis (***Yang et al., 2008***) with an average of 45 min in various human cell lines (***Araujo et al., 2016***). Fission yeast spends approximately 30 min in mitosis. In contrast, interphase duration accounts for 12–30 hr in mammalian cells (***Ganem and Pellman, 2012***; ***Yang et al., 2008***), but only for around 3 hr in *S. pombe* cells.

## Materials and methods

### Production of *S. pombe* mutant strains

All used strains are isogenic to wild-type 972 and were obtained from genetic crosses, selected by random spore germination and replica on plates with according drugs or supplements. All strains are listed in the ***Supplementary file 1***. Gene deletion and tagging was performed as described previously (***Bähler et al., 1998***).

### Fission yeast culture

All *S. pombe* strains were maintained at 25°C and cultured in standard media. Strains were either maintained on YE5S plates or EMM plates additionnally containing adenine, leucine and uracil in case of the Ase1-Shut-Off strain, at 25°C and refreshed every third day. Generally, one day before imaging cells were transferred into liquid YE5S and imaged the following day at exponential growth.

Cells in starvation phase were grown until an optical density at a wavelength of 600nm ($OD_{600}$) of 1.2–1.5 and then imaged. To generate abnormally long cells by treatment of wild-type cells with Hydroxyurea (HU, sigma aldrich), 110 mM HU was added to the cell culture (in liquid YE5S) at exponential growth. After incubation of 3 to 4 hr at 25˚C, cells were washed three times with $H_2O$ and resuspended in YE5S. Following one hour at 25 ˚C cells were imaged.

The *cdc2-asM17* mutants were arrested by adding 1 µM NM-PP1 (Calbiochem, CA) to the culture at exponential growth. After 30 min, 2 hr or 2.5 hr of incubation at 25˚C, cells were washed three times with $H_2O$ and resuspended in YE5S. Following one hour at 25 ˚C cells were imaged.

For overexpression experiments, strains (pnmt-klp9, pnmt-GFP-klp9 and pnmt-ase1) were cultured two days before imaging in liquid EMM with adenine, leucine, uracil and thiamine. The next day cells were centrifuged at 3000 rpm for 5 min, washed three times with $H_2O$ and resuspended in EMM with adenine, leucine and uracil. After 18 to 20 hr at 25 ˚C cells were imaged.

For shut-off experiments, strains (pnmt81-ase1) were cultured in EMM with adenine, leucine and uracil two days before imaging. Approximately 20 hr before imaging, cells were transferred into YE5S.

## Live microscopy

For live-cell imaging cells were mounted on YE5S agarose pads, containing 2% agarose (***Tran et al., 2004***). Imaging was performed at 25˚C.

Images were acquired on a motorized inverted Nikon Eclipse Ti-E microscope, equipped with a spinning-disk CSUX1 confocal head (Yokogawa Electric Corporation), a Plan Apochromat 100x/1.45 N.A. oil immersion objective lens (Nikon), a PIFOC objective stepper, a Mad City Lab piezo stage, a CCD CoolSNAP HQ2 camera (Photometrics) and a laser bench (Erol) with 491 and 561 nm diode lasers, 100 mW each (Cobolt). Stacks of 7 planes spaced by 1 µm were acquired for each channel with 400 msec exposure time, binning two and an electronic gain of 3 for both wavelengths.

For each time-lapse movie, an image was taken every minute for a duration of 90–120 min.

## Image analysis

Using Metamorph 7.2, maximum projections of each stack were performed for analysis of spindle dynamics and for presentation and sum projections for intensity measurements.

Spindle dynamics were examined by the length of the mCherry-Atb2 signal over time. Metaphase and anaphase spindle length refers to the maximum spindle length of each phase.

Intensity measurements were performed by drawing a region around the area of interest, reading out the average intensity per pixel, subtracting the background and multiplying this value with the size of the area.

Kymographs for the determination of midzone length were constructed with Metamorph.

## Quantification and statistical tests

All graphs and box plots were generated using Kaleidagraph 4.5 (Synergy). Analysis of statistical significance was performed by using Mann-Whitney U test, which unlike the Student T-test does not assume a normal distribution of values. Obtained p values are shown within box plots and data sets were defined as significantly different if $p>0.05$. N values, representing the number of cells, are displayed either in the figure legend or inside the box plot. Data was fitted by linear regression analysis and the obtained coefficient of determination ($R^2$) and the slope (m) of the corresponding regression line is displayed inside the graph. Within boxplots, the box encloses 50% of each data set with the median value displayed as a line. Top or bottom of the box correspond to the value halfway between median and the largest or smallest data value. Lines extending from top and bottom of a box illustrate the maximum or minimum values of the data set, which fall within an acceptable range. Values outside this range are displayed as individual points.

# Acknowledgements

We thank Sergio Rincon and Marcel Hennes for fruitful discussions and critical reading of the manuscript. We appreciate the maintenance of microscopes by Vincent Fraisier and Ludovic Leconte from PICT- IBiSA Imaging facility (Institut Curie), a member of the France-BioImaging national research infrastructure, where imaging was performed. LKK is supported by a PhD fellowship from the French

Ministry of Science and Education. This work was supported in part by grants from La Ligue, Fondation ARC, and INCa to PTT. We thank the lab of Masamitsu Sato (Waseda University) for generously providing strains.

## Additional information

### Funding

| Funder | Grant reference number | Author |
|---|---|---|
| Fondation ARC pour la Recherche sur le Cancer | | Phong Thanh Tran |
| Institut National Du Cancer | | Phong Thanh Tran |
| Ligue Contre le Cancer | Ile de France | Phong Thanh Tran |

The funders had no role in study design, data collection and interpretation, or the decision to submit the work for publication.

### Author contributions

Lara Katharina Krüger, Conceptualization, Formal analysis, Investigation, Visualization, Methodology, Writing—original draft, Writing—review and editing; Jérémie-Luc Sanchez, Data curation, Investigation; Anne Paoletti, Phong Thanh Tran, Supervision, Funding acquisition, Writing—review and editing

### Author ORCIDs

Lara Katharina Krüger https://orcid.org/0000-0002-0439-951X
Phong Thanh Tran http://orcid.org/0000-0002-2410-2277

### Decision letter and Author response

Decision letter https://doi.org/10.7554/eLife.42182.036
Author response https://doi.org/10.7554/eLife.42182.037

## Additional files

### Supplementary files

- Supplementary file 1. *S. pombe* strain list.

DOI: https://doi.org/10.7554/eLife.42182.033

- Transparent reporting form

DOI: https://doi.org/10.7554/eLife.42182.034

### Data availability

All data are included in the manuscript.

## References

**Aoi Y**, Kawashima SA, Simanis V, Yamamoto M, Sato M. 2014. Optimization of the analogue-sensitive Cdc2/Cdk1 mutant by in vivo selection eliminates physiological limitations to its use in cell cycle analysis. *Open Biology* **4**: 140063. DOI: https://doi.org/10.1098/rsob.140063, PMID: 24990387

**Araujo AR**, Gelens L, Sheriff RS, Santos SD. 2016. Positive feedback keeps duration of mitosis temporally insulated from upstream Cell-Cycle events. *Molecular Cell* **64**:362–375. DOI: https://doi.org/10.1016/j.molcel.2016.09.018, PMID: 27768873

**Avunie-Masala R**, Movshovich N, Nissenkorn Y, Gerson-Gurwitz A, Fridman V, Kõivomägi M, Loog M, Hoyt MA, Zaritsky A, Gheber L. 2011. Phospho-regulation of kinesin-5 during anaphase spindle elongation. *Journal of Cell Science* **124**:873–878. DOI: https://doi.org/10.1242/jcs.077396, PMID: 21378308

**Bähler J**, Wu JQ, Longtine MS, Shah NG, McKenzie A, Steever AB, Wach A, Philippsen P, Pringle JR. 1998. Heterologous modules for efficient and versatile PCR-based gene targeting in schizosaccharomyces pombe. *Yeast* **14**:943–951. DOI: https://doi.org/10.1002/(SICI)1097-0061(199807)14:10<943::AID-YEA292>3.0.CO;2-Y, PMID: 9717240

**Bieling P**, Telley IA, Surrey T. 2010. A minimal midzone protein module controls formation and length of antiparallel microtubule overlaps. *Cell* **142**:420–432. DOI: https://doi.org/10.1016/j.cell.2010.06.033, PMID: 20691901

**Braun M**, Lansky Z, Fink G, Ruhnow F, Diez S, Janson ME. 2011. Adaptive braking by Ase1 prevents overlapping microtubules from sliding completely apart. *Nature Cell Biology* **13**:1259–1264. DOI: https://doi.org/10.1038/ncb2323, PMID: 21892183

**Britto M**, Goulet A, Rizvi S, von Loeffelholz O, Moores CA, Cross RA. 2016. *Schizosaccharomyces pombe* kinesin-5 switches direction using a steric blocking mechanism. *PNAS* **113**:E7483–E7489. DOI: https://doi.org/10.1073/pnas.1611581113, PMID: 27834216

**Brust-Mascher I**, Civelekoglu-Scholey G, Kwon M, Mogilner A, Scholey JM. 2004. Model for anaphase B: role of three mitotic motors in a switch from poleward flux to spindle elongation. *PNAS* **101**:15938–15943. DOI: https://doi.org/10.1073/pnas.0407044101, PMID: 15522967

**Brust-Mascher I**, Sommi P, Cheerambathur DK, Scholey JM. 2009. Kinesin-5-dependent poleward flux and spindle length control in Drosophila embryo mitosis. *Molecular Biology of the Cell* **20**:1749–1762. DOI: https://doi.org/10.1091/mbc.e08-10-1033, PMID: 19158379

**Brust-Mascher I**, Scholey JM. 2011. Mitotic motors and chromosome segregation: the mechanism of anaphase B. *Biochemical Society Transactions* **39**:1149–1153. DOI: https://doi.org/10.1042/BST0391149, PMID: 21936780

**Cande WZ**, McDonald KL. 1985. In vitro reactivation of anaphase spindle elongation using isolated diatom spindles. *Nature* **316**:168–170. DOI: https://doi.org/10.1038/316168a0, PMID: 4010787

**Cande WZ**. 1986. Physiological and ultrastructural analysis of elongating mitotic spindles reactivated in vitro. *The Journal of Cell Biology* **103**:593–604. DOI: https://doi.org/10.1083/jcb.103.2.593

**Chen Y**, Hancock WO. 2015. Kinesin-5 is a microtubule polymerase. *Nature Communications* **6**:1–10. DOI: https://doi.org/10.1038/ncomms9160

**Crowder ME**, Strzelecka M, Wilbur JD, Good MC, von Dassow G, Heald R. 2015. A comparative analysis of spindle morphometrics across metazoans. *Current Biology* **25**:1542–1550. DOI: https://doi.org/10.1016/j.cub.2015.04.036, PMID: 26004761

**Ding R**, McDonald KL, McIntosh JR. 1993. Three-dimensional reconstruction and analysis of mitotic spindles from the yeast, schizosaccharomyces pombe. *The Journal of Cell Biology* **120**:141–151. DOI: https://doi.org/10.1083/jcb.120.1.141, PMID: 8416984

**Fu C**, Ward JJ, Loiodice I, Velve-Casquillas G, Nedelec FJ, Tran PT. 2009. Phospho-regulated interaction between kinesin-6 Klp9p and microtubule bundler Ase1p promotes spindle elongation. *Developmental Cell* **17**:257–267. DOI: https://doi.org/10.1016/j.devcel.2009.06.012, PMID: 19686686

**Furuta K**, Furuta A, Toyoshima YY, Amino M, Oiwa K, Kojima H. 2013. Measuring collective transport by defined numbers of processive and nonprocessive kinesin motors. *PNAS* **110**:501–506. DOI: https://doi.org/10.1073/pnas.1201390110, PMID: 23267076

**Gaillard J**, Neumann E, Van Damme D, Stoppin-Mellet V, Ebel C, Barbier E, Geelen D, Vantard M. 2008. Two microtubule-associated proteins of arabidopsis MAP65s promote antiparallel microtubule bundling. *Molecular Biology of the Cell* **19**:4534–4544. DOI: https://doi.org/10.1091/mbc.e08-04-0341, PMID: 18667529

**Ganem NJ**, Pellman D. 2012. Linking abnormal mitosis to the acquisition of DNA damage. *The Journal of Cell Biology* **199**:871–881. DOI: https://doi.org/10.1083/jcb.201210040, PMID: 23229895

**Glotzer M**. 2009. The 3ms of central spindle assembly: microtubules, motors and MAPs. *Nature Reviews Molecular Cell Biology* **10**:9–20. DOI: https://doi.org/10.1038/nrm2609, PMID: 19197328

**Good MC**, Vahey MD, Skandarajah A, Fletcher DA, Heald R. 2013. Cytoplasmic volume modulates spindle size during embryogenesis. *Science* **342**:856–860. DOI: https://doi.org/10.1126/science.1243147, PMID: 24233724

**Hara Y**, Kimura A. 2009. Cell-size-dependent spindle elongation in the Caenorhabditis Elegans early embryo. *Current Biology* **19**:1549–1554. DOI: https://doi.org/10.1016/j.cub.2009.07.050, PMID: 19682904

**Hara Y**, Kimura A. 2013. An allometric relationship between mitotic spindle width, spindle length, and ploidy in Caenorhabditis Elegans embryos. *Molecular Biology of the Cell* **24**:1411–1419. DOI: https://doi.org/10.1091/mbc.e12-07-0528, PMID: 23468523

**Hayashi T**, Sano T, Kutsuna N, Kumagai-Sano F, Hasezawa S. 2007. Contribution of anaphase B to chromosome separation in higher plant cells estimated by image processing. *Plant and Cell Physiology* **48**:1509–1513. DOI: https://doi.org/10.1093/pcp/pcm117, PMID: 17855443

**Hazel J**, Krutkramelis K, Mooney P, Tomschik M, Gerow K, Oakey J, Gatlin JC. 2013. Changes in cytoplasmic volume are sufficient to drive spindle scaling. *Science* **342**:853–856. DOI: https://doi.org/10.1126/science.1243110, PMID: 24233723

**Jamison DK**, Driver JW, Diehl MR. 2012. Cooperative responses of multiple kinesins to variable and constant loads. *Journal of Biological Chemistry* **287**:3357–3365. DOI: https://doi.org/10.1074/jbc.M111.296582, PMID: 22158622

**Janson ME**, Loughlin R, Loïodice I, Fu C, Brunner D, Nédélec FJ, Tran PT. 2007. Crosslinkers and motors organize dynamic microtubules to form stable bipolar arrays in fission yeast. *Cell* **128**:357–368. DOI: https://doi.org/10.1016/j.cell.2006.12.030, PMID: 17254972

**Kapitein LC**, Peterman EJ, Kwok BH, Kim JH, Kapoor TM, Schmidt CF. 2005. The bipolar mitotic kinesin Eg5 moves on both microtubules that it crosslinks. *Nature* **435**:114–118. DOI: https://doi.org/10.1038/nature03503, PMID: 15875026

**Kapitein LC**, Kwok BH, Weinger JS, Schmidt CF, Kapoor TM, Peterman EJ. 2008. Microtubule cross-linking triggers the directional motility of kinesin-5. *The Journal of Cell Biology* **182**:421–428. DOI: https://doi.org/10.1083/jcb.200801145, PMID: 18678707

**Kelly FD**, Nurse P. 2011. Spatial control of Cdc42 activation determines cell width in fission yeast. *Molecular Biology of the Cell* **22**:3801–3811. DOI: https://doi.org/10.1091/mbc.e11-01-0057, PMID: 21849474

**Khodjakov A**, La Terra S, Chang F. 2004. Laser microsurgery in fission yeast; role of the mitotic spindle midzone in anaphase B. *Current Biology : CB* **14**:1330–1340. DOI: https://doi.org/10.1016/j.cub.2004.07.028, PMID: 15296749

**Kotadia S**, Montembault E, Sullivan W, Royou A. 2012. Cell elongation is an adaptive response for clearing long chromatid arms from the cleavage plane. *The Journal of Cell Biology* **199**:745–753. DOI: https://doi.org/10.1083/jcb.201208041, PMID: 23185030

**Lacroix B**, Letort G, Pitayu L, Sallé J, Stefanutti M, Maton G, Ladouceur AM, Canman JC, Maddox PS, Maddox AS, Minc N, Nédélec F, Dumont J. 2018. Microtubule dynamics scale with cell size to set spindle length and assembly timing. *Developmental Cell* **45**:496–511. DOI: https://doi.org/10.1016/j.devcel.2018.04.022, PMID: 29787710

**Lanni JS**, Jacks T. 1998. Characterization of the p53-dependent postmitotic checkpoint following spindle disruption. *Molecular and Cellular Biology* **18**:1055–1064. DOI: https://doi.org/10.1128/MCB.18.2.1055, PMID: 9448003

**Lansky Z**, Braun M, Lüdecke A, Schlierf M, ten Wolde PR, Janson ME, Diez S. 2015. Diffusible crosslinkers generate directed forces in microtubule networks. *Cell* **160**:1159–1168. DOI: https://doi.org/10.1016/j.cell.2015.01.051, PMID: 25748652

**Leduc C**, Padberg-Gehle K, Varga V, Helbing D, Diez S, Howard J. 2012. Molecular crowding creates traffic jams of kinesin motors on microtubules. *PNAS* **109**:6100–6105. DOI: https://doi.org/10.1073/pnas.1107281109, PMID: 22431622

**Loïodice I**, Staub J, Setty TG, Nguyen NP, Paoletti A, Tran PT. 2005. Ase1p organizes antiparallel microtubule arrays during interphase and mitosis in fission yeast. *Molecular Biology of the Cell* **16**:1756–1768. DOI: https://doi.org/10.1091/mbc.e04-10-0899, PMID: 15689489

**Ma N**, Titus J, Gable A, Ross JL, Wadsworth P. 2011. TPX2 regulates the localization and activity of Eg5 in the mammalian mitotic spindle. *The Journal of Cell Biology* **195**:87–98. DOI: https://doi.org/10.1083/jcb.201106149, PMID: 21969468

**Masuda H**, Cande WZ. 1987. The role of tubulin polymerization during spindle elongation in vitro. *Cell* **49**:193–202. DOI: https://doi.org/10.1016/0092-8674(87)90560-5, PMID: 2882855

**Matsuo Y**, Maurer SP, Yukawa M, Zakian S, Singleton MR, Surrey T, Toda T. 2016. An unconventional interaction between Dis1/TOG and Mal3/EB1 in fission yeast promotes the fidelity of chromosome segregation. *Journal of Cell Science* **129**:4592–4606. DOI: https://doi.org/10.1242/jcs.197533, PMID: 27872152

**Mollinari C**, Kleman JP, Jiang W, Schoehn G, Hunter T, Margolis RL. 2002. PRC1 is a microtubule binding and bundling protein essential to maintain the mitotic spindle midzone. *The Journal of Cell Biology* **157**:1175–1186. DOI: https://doi.org/10.1083/jcb.200111052, PMID: 12082078

**Nislow C**, Sellitto C, Kuriyama R, McIntosh JR. 1990. A monoclonal antibody to a mitotic microtubule-associated protein blocks mitotic progression. *The Journal of Cell Biology* **111**:511–522. DOI: https://doi.org/10.1083/jcb.111.2.511, PMID: 2199459

**Nislow C**, Lombillo VA, Kuriyama R, McIntosh JR. 1992. A plus-end-directed motor enzyme that moves antiparallel microtubules in vitro localizes to the interzone of mitotic spindles. *Nature* **359**:543–547. DOI: https://doi.org/10.1038/359543a0, PMID: 1406973

**Olmsted ZT**, Colliver AG, Riehlman TD, Paluh JL. 2014. Kinesin-14 and kinesin-5 antagonistically regulate microtubule nucleation by γ-TuRC in yeast and human cells. *Nature Communications* **5**:1–15. DOI: https://doi.org/10.1038/ncomms6339

**Orth JD**, Loewer A, Lahav G, Mitchison TJ. 2012. Prolonged mitotic arrest triggers partial activation of apoptosis, resulting in DNA damage and p53 induction. *Molecular Biology of the Cell* **23**:567–576. DOI: https://doi.org/10.1091/mbc.e11-09-0781, PMID: 22171325

**Pellman D**, Bagget M, Tu H, Fink GR. 1995. Two microtubule-associated proteins required for anaphase spindle movement in saccharomyces cerevisiae. *J Cell Bio* **130**:1373–1385.

**Quignon F**, Rozier L, Lachages AM, Bieth A, Simili M, Debatisse M. 2007. Sustained mitotic block elicits DNA breaks: one-step alteration of ploidy and chromosome integrity in mammalian cells. *Oncogene* **26**:165–172. DOI: https://doi.org/10.1038/sj.onc.1209787, PMID: 16832348

**Reber S**, Goehring NW. 2015. Intracellular scaling mechanisms. *Cold Spring Harbor Perspectives in Biology* **7**:a019067. DOI: https://doi.org/10.1101/cshperspect.a019067, PMID: 26254310

**Rieder CL**, Palazzo RE. 1992. Colcemid and the mitotic cycle. *Journal of Cell Science* **102**:387–392. PMID: 1506421

**Rincon SA**, Lamson A, Blackwell R, Syrovatkina V, Fraisier V, Paoletti A, Betterton MD, Tran PT. 2017. Kinesin-5-independent mitotic spindle assembly requires the antiparallel microtubule crosslinker Ase1 in fission yeast. *Nature Communications* **8**:15286. DOI: https://doi.org/10.1038/ncomms15286, PMID: 28513584

**Rizk RS**, Discipio KA, Proudfoot KG, Gupta ML. 2014. The kinesin-8 Kip3 scales anaphase spindle length by suppression of midzone microtubule polymerization. *The Journal of Cell Biology* **204**:965–975. DOI: https://doi.org/10.1083/jcb.201312039, PMID: 24616221

**Saunders WS**, Koshland D, Eshel D, Gibbons IR, Hoyt MA. 1995. Saccharomyces cerevisiae kinesin- and dynein-related proteins required for anaphase chromosome segregation. *The Journal of Cell Biology* **128**:617–624. DOI: https://doi.org/10.1083/jcb.128.4.617, PMID: 7860634

**Saunders AM**, Powers J, Strome S, Saxton WM. 2007. Kinesin-5 acts as a Brake in anaphase spindle elongation. *Current Biology* **17**:R453–R454. DOI: https://doi.org/10.1016/j.cub.2007.05.001, PMID: 17580072

**Saxton WM**, McIntosh JR. 1987. Interzone microtubule behavior in late anaphase and telophase spindles. *The Journal of Cell Biology* **105**:875–886. DOI: https://doi.org/10.1083/jcb.105.2.875, PMID: 3305523

**Scholey J**, Civelekoglu-Scholey G, Brust-Mascher I. 2016. Anaphase B. *Biology* **5**:51. DOI: https://doi.org/10.3390/biology5040051

**Schuyler SC**, Liu JY, Pellman D. 2003. The molecular function of Ase1p: evidence for a MAP-dependent midzone-specific spindle matrix. *The Journal of Cell Biology* **160**:517–528.

**Sharp DJ**, Rogers GC, Scholey JM. 2000. Microtubule motors in mitosis. *Nature* **407**:41–47. DOI: https://doi.org/10.1038/35024000, PMID: 10993066

**Shimamoto Y**, Forth S, Kapoor TM. 2015. Measuring pushing and braking forces generated by ensembles of Kinesin-5 crosslinking two microtubules. *Developmental Cell* **34**:669–681. DOI: https://doi.org/10.1016/j.devcel.2015.08.017, PMID: 26418296

**Subramanian R**, Wilson-Kubalek EM, Arthur CP, Bick MJ, Campbell EA, Darst SA, Milligan RA, Kapoor TM. 2010. Insights into antiparallel microtubule crosslinking by PRC1, a conserved nonmotor microtubule binding protein. *Cell* **142**:433–443. DOI: https://doi.org/10.1016/j.cell.2010.07.012, PMID: 20691902

**Syrovatkina V**, Tran PT. 2015. Loss of kinesin-14 results in aneuploidy via kinesin-5-dependent microtubule protrusions leading to chromosome cut. *Nature Communications* **6**:1–8. DOI: https://doi.org/10.1038/ncomms8322, PMID: 26031557

**Tolić-Nørrelykke IM**, Sacconi L, Thon G, Pavone FS. 2004. Positioning and elongation of the fission yeast spindle by microtubule-based pushing. *Current Biology* **14**:1181–1186. DOI: https://doi.org/10.1016/j.cub.2004.06.029, PMID: 15242615

**Tran PT**, Paoletti A, Chang F. 2004. Imaging green fluorescent protein fusions in living fission yeast cells. *Methods* **33**:220–225. DOI: https://doi.org/10.1016/j.ymeth.2003.11.017, PMID: 15157889

**Uetake Y**, Sluder G. 2010. Prolonged prometaphase blocks daughter cell proliferation despite normal completion of mitosis. *Current Biology* **20**:1666–1671. DOI: https://doi.org/10.1016/j.cub.2010.08.018, PMID: 20832310

**Varga V**, Helenius J, Tanaka K, Hyman AA, Tanaka TU, Howard J. 2006. Yeast kinesin-8 depolymerizes microtubules in a length-dependent manner. *Nature Cell Biology* **8**:957–962. DOI: https://doi.org/10.1038/ncb1462, PMID: 16906145

**Varga V**, Leduc C, Bormuth V, Diez S, Howard J. 2009. Kinesin-8 motors act cooperatively to mediate length-dependent microtubule depolymerization. *Cell* **138**:1174–1183. DOI: https://doi.org/10.1016/j.cell.2009.07.032, PMID: 19766569

**Wang H**, Brust-Mascher I, Cheerambathur D, Scholey JM. 2010. Coupling between microtubule sliding, plus-end growth and spindle length revealed by kinesin-8 depletion. *Cytoskeleton* **67**:715–728. DOI: https://doi.org/10.1002/cm.20482, PMID: 20814910

**Ward JJ**, Roque H, Antony C, Nédélec F. 2014. Mechanical design principles of a mitotic spindle. *eLife* **3**:e03398. DOI: https://doi.org/10.7554/eLife.03398, PMID: 25521247

**Wijeratne S**, Subramanian R. 2018. Geometry of antiparallel microtubule bundles regulates relative sliding and stalling by PRC1 and Kif4A. *eLife* **7**:e32595. DOI: https://doi.org/10.7554/eLife.32595, PMID: 30353849

**Wilbur JD**, Heald R. 2013. Mitotic spindle scaling during xenopus development by kif2a and importin α. *eLife* **2**:e00290. DOI: https://doi.org/10.7554/eLife.00290, PMID: 23425906

**Wühr M**, Chen Y, Dumont S, Groen AC, Needleman DJ, Salic A, Mitchison TJ. 2008. Evidence for an upper limit to mitotic spindle length. *Current Biology* **18**:1256–1261. DOI: https://doi.org/10.1016/j.cub.2008.07.092, PMID: 18718761

**Yamashita A**, Sato M, Fujita A, Yamamoto M, Toda T. 2005. The roles of fission yeast ase1 in mitotic cell division, meiotic nuclear oscillation, and cytokinesis checkpoint signaling. *Molecular Biology of the Cell* **16**:1378–1395. DOI: https://doi.org/10.1091/mbc.e04-10-0859, PMID: 15647375

**Yang Z**, Loncarek J, Khodjakov A, Rieder CL. 2008. Extra centrosomes and/or chromosomes prolong mitosis in human cells. *Nature Cell Biology* **10**:748–751. DOI: https://doi.org/10.1038/ncb1738, PMID: 18469805

**Yang C-F**, Tsai W-Y, Chen W-A, Liang K-W, Pan C-J, Lai P-L, Yang P-C, Huang H-C. 2016. Kinesin-5 contributes to Spindle-length scaling in the evolution of cancer toward metastasis. *Scientific Reports* **6**:1–9. DOI: https://doi.org/10.1038/srep35767

**Yukawa M**, Yamada Y, Yamauchi T, Toda T. 2018. Two spatially distinct kinesin-14 proteins, Pkl1 and Klp2, generate collaborative inward forces against kinesin-5 Cut7 in *S. pombe*. *Journal of Cell Science* **131**:jcs210740. DOI: https://doi.org/10.1242/jcs.210740, PMID: 29167352

# 8 Mechanism of anaphase B spindle elongation in fission yeast

## 8.1 Summary II

The previous study has identified the homotetrameric **kinesin-6 Klp9 as a crucial regulator of anaphase B spindle elongation velocity** in fission yeast. Since Klp9 was identified as a microtubule sliding motor [258, 259], it was tempting to speculate that control of the microtubule sliding velocity is sufficient to regulate the velocity of spindle elongation.
However, the observation that the microtubule overlap length at the spindle midzone remained constant throughout spindle elongation, suggested that **microtubule sliding and growth occur with equal speeds** and have to be **precisely coordinated**. Furthermore, a reduction of microtubule growth has been shown to slow down spindle elongation in various contexts and organisms [257, 514, 515]. Yet, our understanding of the regulation of microtubule dynamics during anaphase B is limited. In particular, how microtubule growth can allow sustained microtubule sliding and spindle elongation and how in general microtubule dynamics and sliding can be balanced remained elusive.

As a result, I set out to determine how microtubule growth is regulated during anaphase B and how it is coordinated with microtubule sliding. Given the prominent role of Klp9 during spindle elongation, I hypothesized that the motor itself may simultaneously regulate and set equal microtubule sliding and growth velocities and thus coordinate both processes.

However, the determination of the dynamics parameters of individual microtubules within the densely packed anaphase B spindle is challenging. So far, in fission yeast, this has only been achieved under non-physiological conditions, upon ectopic overexpression of tubulin [477]. Moreover, the signal of Mal3, the EB1 homolog, tagged with GFP is spread all along the anaphase B spindle, when imaged with a conventional spinning disk microscope. This is in contrast to fluorescently labeled EB1 proteins in other systems, which appear as comet-like structures at growing microtubule tips, and are commonly used for the analysis of microtubule growth events [324].

To test the role of Klp9 on microtubule dynamics during anaphase B *in vivo*, I established monopolar spindles as a suitable tool. Despite unseparated spindle poles, monopolar spindles proceed to anaphase B and behave as wild type-like half-spindles. This *in vivo* set-up in combination with *in vitro* reconstitution assays using recombinant Klp9 allowed to determine

the motor's effect on microtubule dynamics. The **kinesin-6, indeed, controls microtubule growth *in vivo* and *in vitro***, suggesting the motor as a promising candidate for the coordination of microtubule sliding and growth. The obtained *in vitro* data, moreover, suggest an unconventional mechanism for the regulation of microtubule growth: Klp9 can enhance and dampen the growth velocity depending on the tubulin concentration. This eventually allows the motor to set a well-defined microtubule growth velocity, ideal for orchestrating the coordination of microtubule growth and sliding.

In addition, I observed that **Klp9 recruitment to spindle microtubules upon anaphase onset is promoted by its dephosphorylation, regulated by the microtubule polymerase Dis1/XMAP215**. Finally, since Dis1 is responsible for the regulation of spindle length scaling and Klp9 for the regulation of spindle elongation velocity, this recruitment mechanism links both processes, and ensures that longer spindles elongate with higher speeds as demonstrated in the previous study [513].

## 8.2 Article II: Kinesin-6 Klp9 orchestrates spindle elongation by regulating microtubule sliding and growth

**Authors**: Lara K. Krüger[1], Matthieu Gélin[2], Carlos Kikuti[1], Anne Houdusse[1], Manuel Théry[2,3], Laurent Blanchoin[2,3] & Phong T. Tran[1 & 4]

**Affiliations**: 1. Institut Curie, PSL Research University, CNRS, UMR 144, Paris, France; 2. Institut de Recherche Saint Louis, U976 Human Immunology Pathophysiology Immunotherapy (HIPI), CytoMorpho Lab, University of Paris, INSERM, CEA, Paris, France; 3. Interdisciplinary Research Institute of Grenoble, Laboratoire de Physiologie Cellulaire & Végétale, CytoMorpho Lab, University of Grenoble-Alpes, CEA, CNRS, INRA, Grenoble, Paris, France; 4. Department of Cell and Developmental Biology, University of Pennsylvania, Philadelphia, United States

**Journal**: eLife

**Volume**: 10:e67489

**Year**: 2021

**DOI**: https://doi.org/10.7554/eLife.67489

RESEARCH ARTICLE

# Kinesin-6 Klp9 orchestrates spindle elongation by regulating microtubule sliding and growth

**Lara Katharina Krüger[1]*, Matthieu Gélin[2], Liang Ji[1], Carlos Kikuti[1], Anne Houdusse[1], Manuel Théry[2,3], Laurent Blanchoin[2,3], Phong T Tran[1,4]***

[1]Institut Curie, PSL Research University, Sorbonne Université CNRS, UMR 144, Paris, France; [2]Institut de Recherche Saint Louis,U976 Human Immunology Pathophysiology Immunotherapy (HIPI), CytoMorpho Lab, University of Paris, INSERM, CEA, Paris, France; [3]Interdisciplinary Research Institute of Grenoble, Laboratoire de Physiologie Cellulaire & Végétale, CytoMorpho Lab, University of Grenoble-Alpes, CEA, CNRS, INRA, Grenoble, Paris, France; [4]Department of Cell and Developmental Biology, University of Pennsylvania, Philadelphia, United States

**Abstract** Mitotic spindle function depends on the precise regulation of microtubule dynamics and microtubule sliding. Throughout mitosis, both processes have to be orchestrated to establish and maintain spindle stability. We show that during anaphase B spindle elongation in *Schizosaccharomyces pombe*, the sliding motor Klp9 (kinesin-6) also promotes microtubule growth in vivo. In vitro, Klp9 can enhance and dampen microtubule growth, depending on the tubulin concentration. This indicates that the motor is able to promote and block tubulin subunit incorporation into the microtubule lattice in order to set a well-defined microtubule growth velocity. Moreover, Klp9 recruitment to spindle microtubules is dependent on its dephosphorylation mediated by XMAP215/Dis1, a microtubule polymerase, creating a link between the regulation of spindle length and spindle elongation velocity. Collectively, we unravel the mechanism of anaphase B, from Klp9 recruitment to the motors dual-function in regulating microtubule sliding and microtubule growth, allowing an inherent coordination of both processes.

***For correspondence:**
lara-katharina.kruger@curie.fr (LKK);
phong.tran@curie.fr (PTT)

**Competing interests:** The authors declare that no competing interests exist.

**Funding:** See page 21

**Received:** 12 February 2021
**Accepted:** 02 June 2021
**Published:** 03 June 2021

**Reviewing editor:** Thomas Surrey, Centre for Genomic Regulation (CRG), Spain



## Introduction

Mitotic spindle assembly and function requires microtubules to undergo alternating periods of growth and shrinkage, together with the action of molecular motors, that can crosslink and slide apart spindle microtubules. A fine balance of microtubule dynamics and microtubule sliding is essential in all mitotic processes to achieve faithful chromosome separation (***Cande and McDonald, 1986***; ***Cande and McDonald, 1985***; ***Cheerambathur et al., 2007***; ***Yukawa et al., 2019b***). Yet, while work has mainly been focused on each process independently, it is unclear how they are coordinated.

During anaphase B, the spindle elongates to push apart the spindle poles and separate the two chromosome sets (***Mallavarapu et al., 1999***; ***Oegema et al., 2001***; ***Roostalu et al., 2010***; ***Scholey et al., 2016***; ***Straight et al., 1998***; ***Vukušić et al., 2017***). While in the fungus *Ustilago maydis* and Ptk1 cells, spindle elongation is mainly achieved through cortical pulling forces acting on astral microtubules (***Aist et al., 1993***; ***Fink et al., 2006***; ***Grill et al., 2001***), these forces are not present or dispensable in a plethora of other species. In yeast, *Caenorhabditis elegans*, *Drosophila melanogaster*, plants, and human, spindle elongation is realized by the generation of microtubule sliding forces at the spindle midzone (***Euteneuer et al., 1982***; ***Khodjakov et al., 2004***; ***Kiyomitsu and Cheeseman, 2013***; ***Redemann et al., 2017***; ***Sharp et al., 1999***; ***Tolić-Nørrelykke et al., 2004***; ***Vukušić et al., 2019***; ***Yu et al., 2019***). The spindle midzone refers to the microtubule overlap at the

spindle center, formed by antiparallel-oriented microtubules (interpolar microtubules), which originate from the two opposite spindle poles (**Ding et al., 1993**; **Euteneuer et al., 1982**; **Mastronarde et al., 1993**; **McDonald et al., 1977**; **McIntosh and Landis, 1971**; **Ward et al., 2014**; **Winey et al., 1995**).

Microtubule sliding is promoted by members of the kinesin-5 family in most organisms (**Avunie-Masala et al., 2011**; **Brust-Mascher et al., 2009**; **Saunders et al., 1995**; **Sharp et al., 2000**; **Straight et al., 1998**). The tetrameric kinesin crosslinks antiparallel microtubules and slides them apart (**Avunie-Masala et al., 2011**; **Brust-Mascher et al., 2009**; **Kapitein et al., 2005**; **Saunders et al., 1995**; **Shimamoto et al., 2015**; **Straight et al., 1998**). By walking toward the microtubule plus-ends of each of the two microtubules, that it crosslinks, kinesin-5 can move the microtubules relative to each other (**Kapitein et al., 2005**). In fission yeast, this task is mainly performed by the kinesin-6 Klp9, which localizes to the spindle midzone upon anaphase B onset (**Fu et al., 2009**; **Krüger et al., 2019**; **Rincon et al., 2017**; **Yukawa et al., 2019a**). The kinesin-5 Cut7 also generates microtubule sliding forces, but to a lower extent than Klp9 (**Rincon et al., 2017**). In the absence of both sliding motors, spindle elongation is abolished, leading to 'cut' of chromosomes by the cytokinetic ring and mis-segregated chromosomes (**Rincon et al., 2017**).

Concomitantly with microtubule sliding, the interpolar microtubules have to grow at a rate that allows the spindle to elongate while maintaining the spindle midzone (**Cande and McDonald, 1986**; **Cande and McDonald, 1985**; **Cheerambathur et al., 2007**; **Masuda, 1995**; **Masuda and Cande, 1987**; **Saxton and McIntosh, 1987**). Microtubule growth has to occur with at least the velocity the spindle microtubules slide apart to keep the microtubule overlap, necessary for spindle stability. Microtubule dynamics during anaphase B have been shown to be regulated by CLASP, which promotes microtubule polymerization or increases the frequency of microtubule rescues (**Bratman and Chang, 2007**; **Maton et al., 2015**; **Pereira et al., 2006**). Moreover, silencing of the transforming acid coiled-coil (TACC) protein TACC3, which stabilizes microtubules together with XMAP215 (**Gergely et al., 2003**; **Kinoshita et al., 2005**; **Peset et al., 2005**), reduces the rate of spindle elongation by destabilizing midzone microtubules (**Lioutas and Vernos, 2013**). This strongly suggests that precise regulation of microtubule stability is necessary for proper spindle elongation. Accordingly, in animal cells, the kinesin-4 member Kif4a terminates anaphase B spindle elongation by promoting the inhibition of microtubule polymerization and thus restricting spindle midzone length (**Hu et al., 2011**). However, how the required velocity of microtubule growth is set precisely and how microtubule dynamics are coordinated with microtubule sliding to allow seamless spindle elongation remains enigmatic.

A straightforward way of coupling microtubule growth and sliding could involve a motor that sets equal sliding and polymerization speeds. Supporting this possibility, *Xenopus* kinesin-5 promotes microtubule polymerization in vitro (**Chen and Hancock, 2015**). The motor has been proposed to induce a curved-to-straight conformational transition of tubulin at microtubule plus-ends, thus promoting microtubule growth by virtue of a stabilizing effect (**Chen et al., 2019**). This may allow the motor to directly regulate the dynamic behavior of the microtubule tracks which it simultaneously slides. However, the biological significance of the polymerization function of kinesin-5 still has to be investigated in vivo.

Like kinesin-5 in most organisms, the kinesin-6 Klp9 promotes anaphase B spindle elongation in fission yeast (**Fu et al., 2009**; **Rincon et al., 2017**; **Yukawa et al., 2017**). Both motors form homotetramers and both slide apart microtubules. Moreover, Klp9 sets the velocity of spindle elongation in a dose-dependent manner (**Krüger et al., 2019**). Spindles elongate faster as the amount of motors increases at the spindle midzone. Thus, Klp9 is able to set the speed of spindle elongation. We, therefore, wondered if this is solely an effect of the microtubule sliding function or if Klp9 simultaneously regulates microtubule dynamics.

In the present study, we provide insight into the mechanism of anaphase B spindle elongation, from the regulation of Klp9 localization to the anaphase spindle, to the Klp9-mediated coordination of microtubule sliding and growth. Klp9 recruitment to spindle microtubules is regulated in a dephosphorylation-dependent manner by the microtubule polymerase Dis1, homolog of XMAP215 and ch-TOG (**Matsuo et al., 2016**). Furthermore, we provide evidence that, at the spindle, Klp9 performs two functions: the generation of microtubule sliding forces, as shown previously, and the regulation of microtubule dynamics. By using monopolar spindles in vivo and in vitro reconstitution assays with recombinant Klp9, we could show that the kinesin-6 is a crucial regulator of microtubule

growth. In fact, Klp9 increases or decreases the microtubule growth speed depending on the condition. Whereas, at low tubulin concentration, where microtubule growth is comparatively slow, Klp9 increases the microtubule growth speed, at high tubulin concentration, where microtubule growth is fast, Klp9 decreases microtubule growth speed in a dose-dependent manner. This suggests an unconventional mechanism by which Klp9 can promote and block tubulin dimer addition to the microtubule lattice. Eventually, Klp9 is able to set a well-defined microtubule growth velocity. With the dual-function of Klp9 in regulating the microtubule sliding and growth velocity, both processes are inherently coordinated to allow flawless spindle elongation.

## Results

### Monopolar spindles to study microtubule dynamics in anaphase B

We found monopolar spindles to be a useful tool to examine microtubule dynamics not only during early mitotic phases (***Costa et al., 2013***), but also during anaphase B. Monopolar spindles can be generated by the temperature-sensitive mutant *cut7-24* (***Hagan and Yanagida, 1992***; ***Hagan and Yanagida, 1990***). Since the kinesin-5 Cut7 is essential to establish spindle bipolarity during spindle assembly by separating the two spindle poles (***Hagan and Yanagida, 1992***), inactivation of Cut7 at its restrictive temperature results in the formation of monopolar spindles (***Figure 1A***).

Live-cell imaging of fission yeast cells expressing α-tubulin (Atb2) linked to mCherry to visualize microtubules and Sid4 linked to GFP to mark spindle pole bodies (SPBs) showed the typical three phases of spindle dynamics in wild-type cells: prophase, metaphase and anaphase A, and anaphase B, during which the spindle dramatically elongates until it disassembles (***Figure 1A***; ***Nabeshima et al., 1998***). In contrast, the *cut7-24* monopolar spindle underwent only two distinguishable phases (***Figure 1A***). First, short and rather dynamic microtubules emanated from the two unseparated spindle poles for approximately 2 hr. Following this phase, one or up to three long microtubule bundles grew from the spindle poles until they disassembled, just before the cell divided (***Figure 1A***, ***Figure 1—figure supplement 1***). This extensive growth of microtubule bundles was reminiscent of the microtubule polymerization that is necessary to allow spindle elongation during anaphase B in bipolar spindles. The bundles grew up to an average length of 6.1 ± 1.0 µm, which is slightly longer than half of the average wild-type spindle length (11.6 ± 1.3 µm) (***Figure 1B***) with an average speed of 0.7 ± 0.2 µm/min, slightly faster than half of the velocity at which the bipolar wild-type spindle elongated (1.2 ± 0.2 µm/min) (***Figure 1B***, ***Figure 1—source data 1***), while cell size is slightly decreased in the *cut7-24* mutant (***Figure 1—figure supplement 2***, ***Figure 1—figure supplement 2—source data 1***). Thus, monopolar spindles appear to behave like half-spindles. Moreover, the growth velocity of individual bundles increased with final bundle length (***Figure 1C***, ***Figure 1—source data 1***), a correlation we have previously observed for bipolar anaphase B spindles: longer spindles elongate with respectively higher velocities (***Krüger et al., 2019***). Together, the second phase of *cut7-24* spindle dynamics resembled anaphase B with the bundle growth velocity matching the speed of spindle elongation in bipolar spindles, and its final length being similar to half the final length of a bipolar anaphase spindle.

To further test whether monopolar spindles indeed proceed to anaphase B, we used the cyclin B Cdc13 linked to GFP as a marker. Cdc13 disappears from spindle microtubules just before anaphase B onset (***Decottignies et al., 2001***). Accordingly, we observed fading of the signal on wild-type spindle microtubules and *cut7-24* monopolar spindle microtubules just before the spindle or bundle was elongated (***Figure 1D***).

Next, we investigated the localization of crucial anaphase B spindle components in monopolar spindles. In bipolar spindles, the sliding motor Klp9 (kinesin-6) localizes to the spindle midzone from anaphase B onset (***Fu et al., 2009***; ***Figure 1E***, left panel). In the *cut7-24* monopolar spindle, Klp9-GFP localized to the tip of the microtubule bundle once it started to elongate (***Figure 1E***, right panel, asterisk). The Klp9-GFP intensity profile obtained at three different time points of anphase B revealed that Klp9-GFP preferentially localized to the tip of the bundle from the first time point of bundle elongation (***Figure 1F***) and the intensity increased with anaphase B progression (***Figure 1F, G***, ***Figure 1—source data 1***). Hence, while the bundle was growing Klp9 accumulated at its tip. In general, we observed a strong correlation of the Klp9-GFP intensity at the bundle tip and the bundle length (***Figure 1H***, ***Figure 1—source data 1***).

eLife Research article Cell Biology

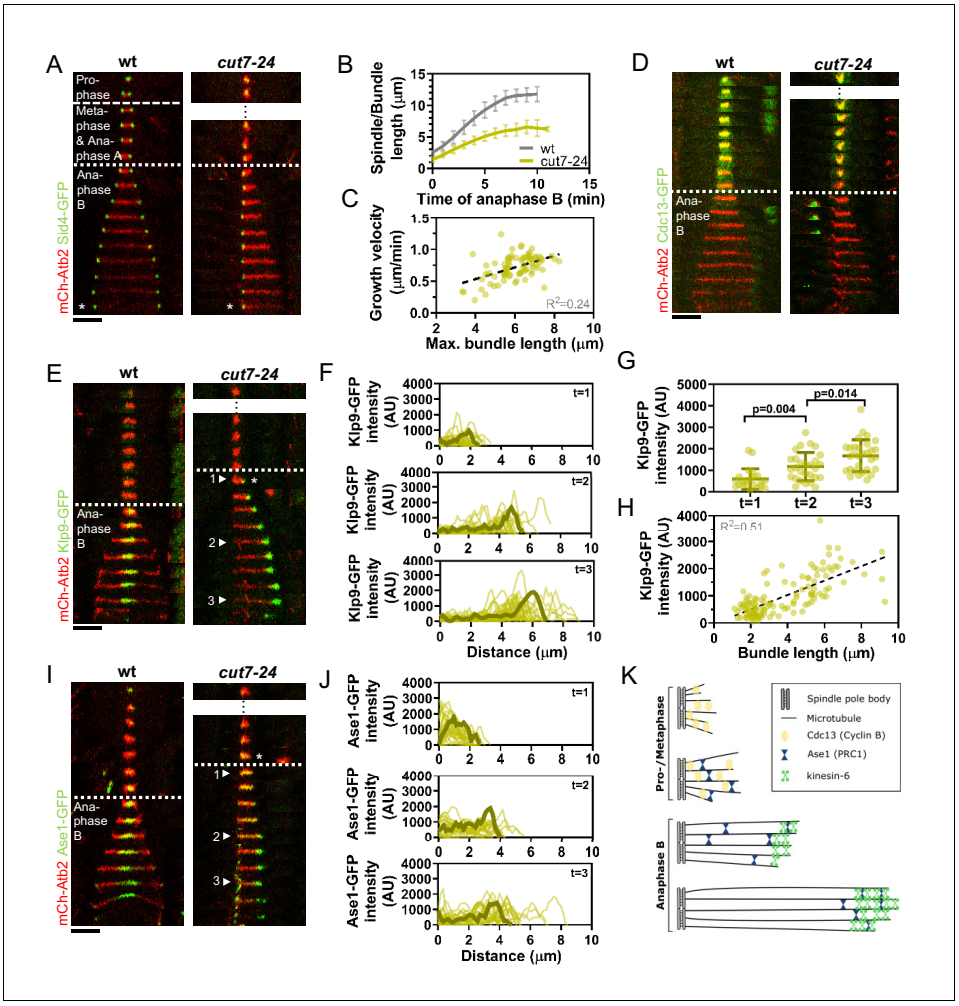


**Figure 1.** *Cut7-24* monopolar spindle as a tool to study microtubule dynamics during anaphase B. (**A**) Time-lapse images of wild-type and *cut7-24* cells expressing mCherry-Atb2 (tubulin) and Sid4-GFP (SPBs) at 37˚C. The dashed line denotes the transition from prophase to metaphase. Dotted line denotes the transition to anaphase B. Asterisk marks spindle disassembly. (**B**) Comparative plot of anaphase B spindle dynamics of wild-type (n = 40) and bundle dynamics of *cut7-24* cells (n = 40) at 37˚C. Bold curves correspond to the mean and error bars to the standard deviation. (**C**) Microtubule bundle growth velocity in *cut7-24* cells plotted against final bundle length. n = 79 microtubule bundles (**D**) Time-lapse images of wild-type and *cut7-24* cells expressing mCherry-Atb2 (tubulin) and Cdc13-GFP (cyclin B) at 37˚C. (**E**) Time-lapse images of wild-type and *cut7-24* cells expressing mCherry-Atb2 (tubulin) and Klp9-GFP (kinesin-6) at 37˚C. Asterisk marks the appearance of the Klp9-GFP signal on the microtubule bundle. Arrowheads 1, 2, and 3 correspond to the time points used for linescan analyses at t = 1 (first time point of anaphase B), t = 2 (5 min after anaphase onset), and t = 3 (last time point of anaphase B). (**F**) Intensity spectra obtained by linescan analysis of Klp9-GFP signals along the microtubule bundles of *cut7-24* cells at time points 1, 2, and 3. 0 µm on the x-axis marks the origin of the microtubule bundle at spindle pole bodies. Dark green lines display an exemplary spectrum. (**G**) Dot plot comparison of the Klp9-GFP intensity on microtubule bundles of *cut7-24* cells at time points 1 (n = 22), 2 (n = 28), and 3 (n = 30). Dark green lines display the mean and standard deviation. p-values were calculated using Mann–Whitney U test. (**H**) Klp9-GFP intensities along microtubule bundles of *cut7-24* cells plotted against bundle length. n = 122 (**I**) Time-lapse images of wild-type and *cut7-24* cells expressing mCherry-Atb2 (tubulin) and Ase1-GFP at 37˚C. Asterisk marks the appearance of the Ase1-GFP signal on the microtubule bundle. Arrowheads 1, 2, and 3 correspond to the time points used for linescan analysis at t = 1 (first time point of anaphase B), t = 2 (5 min after anaphase onset), and t = 3 (last time point of anaphase B). Scale bar, 5 µm. (**J**) Intensity spectra obtained by linescan analysis of Ase1-GFP signals along microtubule bundles at time points 1, 2, and 3. 0 µm on the x-axis marks the origin of the microtubule bundle at spindle pole bodies. Dark green lines display an exemplary spectrum. (**K**) Model of *cut7-24* monopolar spindles displaying phase I, termed pro-metaphase, and phase II corresponding to anaphase B as judged by the absence of the Cdc13-GFP signal and the presence of Klp9-GFP and Ase1-GFP in the long microtubule bundles. In (**A**, **D**, **E**) and (**I**), each frame corresponds

*Figure 1 continued on next page*

*Figure 1 continued*

to 1 min interval. Dotted lines denote the transition to anaphase B. Scale bar, 5 µm. In (**C**) and (**H**), data was fitted by linear regression (dashed line), showing the regression coefficient ($R^2$) and the slope m. Data from n cells was collected from at least three independent experiments.
The online version of this article includes the following source data and figure supplement(s) for figure 1:

**Source data 1.** Numerical data used for ***Figure 1B, C, F, G, H, and J***.
**Figure supplement 1.** *Cut7-24* cells expressing mCherry-Atb2 (tubulin) and Sid4-GFP (SPBs) at 37˚C.
**Figure supplement 2.** Dot plot comparison of cell length (µm) of wild-type and *cut7-24* cells at mitosis onset.
**Figure supplement 2—source data 1.** Numerical data used for ***Figure 1—figure supplement 2***.

Last, we analyzed the localization of the conserved microtubule bundler Ase1/PRC1. Ase1 cross-links the antiparallel-overlapping microtubules at the spindle center and stabilizes the spindle structure (***Janson et al., 2007***; ***Loïodice et al., 2005***; ***Yamashita et al., 2005***). In the wild-type spindle, Ase1-GFP localized to the spindle midzone just before anaphase B onset and onward, as previously reported (***Loïodice et al., 2005***; ***Figure 1I***, left panel). In the monopolar spindle, Ase1-GFP similarly localized to the spindle just before the microtubule bundle started to grow (***Figure 1I***, right panel, asterisk). The signal was spread all along the bundle at early time points of bundle elongation (***Figure 1I,J***; timepoint 1), and accumulated at the bundle tip at later time points (***Figure 1I,J***; timepoint 2 and 3, ***Figure 1—source data 1***). This could result from Ase1 binding all along the parallel microtubule lattice initially, then being carried to the bundle tip by a plus-end directed motor. Klp9 may transport Ase1, as the motor has previously been shown to physically interact with the cross-linker (***Fu et al., 2009***).

Taken together, besides unseparated spindle poles, *cut7-24* monopolar spindles proceed to anaphase B, as judged by the absence of the Cdc13-GFP signal, and the presence of Klp9-GFP and Ase1-GFP on growing microtubule bundles (***Figure 1K***). Initiation of anaphase B, despite unsegregated DNA in this mutant (***Hagan and Yanagida, 1990***), appears to be the result of a leaky checkpoint at the metaphase-to-anaphase transition. After 1–2 hr, *cut7-24* cells will proceed to anaphase B irrespectively of unseparated spindle poles or DNA. During this phase long microtubule bundles are polymerized with a bundle growth velocity that equals half of the spindle elongation velocity of bipolar spindles, suggesting that microtubule dynamics are not altered in the mutant and regulated independently of microtubule sliding forces. Therefore, monopolar spindles constitute a suitable tool to study microtubule dynamics during anaphase B.

## The kinesin-6 Klp9 affects microtubule growth during anaphase B

Using monopolar spindles, we could now analyze the effect of Klp9 on microtubule dynamics. As reported earlier (***Fu et al., 2009***), deletion of *klp9* strongly decreased the speed of bipolar spindle elongation in anaphase B (***Figure 2A***). Deletion of *klp9* in the *cut7-24* background prevented the formation of long microtubule bundles (***Figure 2B***). While anaphase B microtubule bundles reached a maximum length of 6.1 ± 1.0 µm in the presence of Klp9, the bundles only grew up to 2.7 ± 0.5 µm upon *klp9* deletion (***Figure 2C***, ***Figure 2—source data 1***). Moreover, the growth velocity of the bundles was strongly reduced in *klp9* deleted cells (*cut7-24*: 0.7 ± 0.2 µm/min; *cut7-24 klp9*Δ: 0.1 ± 0.1 µm/min) (***Figure 2C***, ***Figure 2—source data 1***). To test whether this effect is dose dependent, we used a shut-off strain, in which the expression of *klp9* is strongly reduced, but some Klp9 molecules are still present. Indeed, the phenotype was slightly less dramatic as compared to the deletion of *klp9* (***Figure 1C***). The bundles reached a maximum length of 3.2 ± 0.8 µm and grew with an average velocity of 0.2 ± 0.2 µm/min. Together, this suggests that Klp9 is involved in the regulation of microtubule growth during anaphase B.

However, Klp9 has been previously implicated in the regulation of the metaphase-to-anaphase B transition (***Meadows et al., 2017***). We thus had to rule out that the observed reduction of microtubule growth is not a consequence of an impaired anaphase B transition in monopolar spindles upon *klp9* deletion. To do so, we analyzed the localization of Cdc13-GFP. In a bipolar *klp9*Δ spindle, Cdc13-GFP disappeared from the spindle just before initiation of anaphase B spindle elongation (***Figure 2D***). In the *cut7-24 klp9*Δ mutant, Cdc13-GFP also disappeared from the spindle microtubules, but still no long microtubule bundle was formed (***Figure 2D***). Hence, the observed phenotype can be attributed to the Klp9 function in microtubule growth regulation during anaphase B.

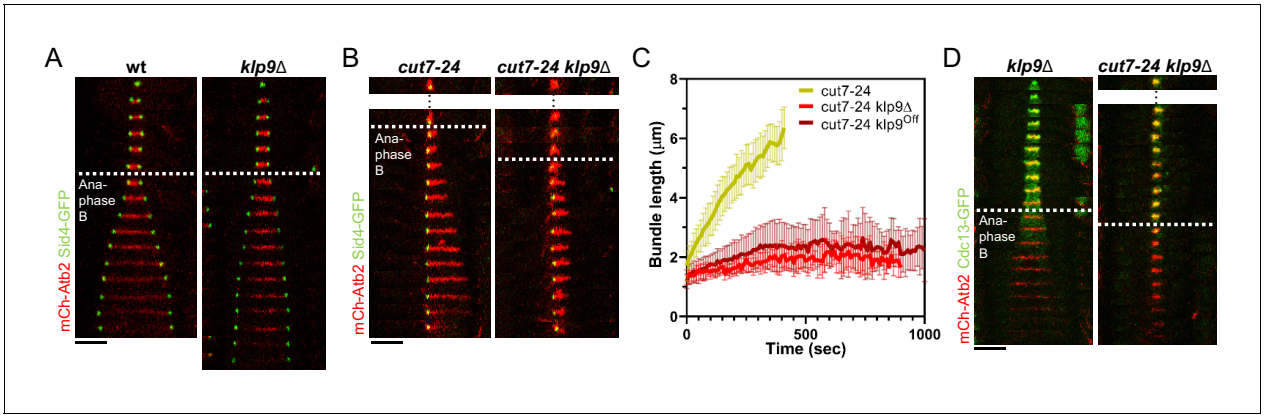


**Figure 2.** Klp9 promotes microtubule growth during anaphase B in monopolar spindles. (**A**) Time-lapse images of wild-type and *klp9*Δ cells expressing mCherry-Atb2 (tubulin) and Sid4-GFP (SPBs) at 37˚C. (**B**) Time-lapse images of *cut7-24* and *cut7-24 klp9*Δ cells expressing mCherry-Atb2 (tubulin) and Sid4-GFP (SPBs) at 37˚C. (**C**) Comparative plot of microtubule bundle dynamics in *cut7-24* (n = 40), *cut7-24 klp9*Δ (n = 40), and *cut7-24 klp9*$^{Off}$ (n = 40) at 37˚C. Bold curves correspond to the mean and error bars to the standard deviation. (**D**) Time-lapse images of *klp9*Δ and *cut7-24 klp9*Δ cells expressing mCherry-Atb2 (tubulin) and Cdc13-GFP (cyclin B) at 37˚C. In (**A–B**) and (**D**), each frame corresponds to 1 min interval. Dotted lines denote the transition to anaphase B. Scale bar, 5 μm. Data from n cells was collected from at least three independent experiments.
The online version of this article includes the following source data for figure 2:

**Source data 1.** Numerical data used for ***Figure 2C***.

## The XMAP215 family member Dis1 displays a similar effect on microtubule bundle growth as Klp9

Klp9 could either regulate microtubule dynamics by itself or indirectly through another microtubule-associated protein (MAP). To probe the involvement of other proteins, we analyzed the impact of the deletion of several candidates on microtubule bundle growth. Namely, the conserved microtubule bundler Ase1, which has been proposed to recruit Klp9 and other spindle components, such as CLASP to the mitotic spindle (***Bratman and Chang, 2007***; ***Fu et al., 2009***); the EB1 homolog Mal3, which impacts microtubule dynamics in vitro (***Bieling et al., 2007***; ***des Georges et al., 2008***; ***Katsuki et al., 2009***; ***Matsuo et al., 2016***); the two members of the XMAP215 family, Dis1 and Alp14, which act as microtubule polymerases (***Al-Bassam et al., 2012***; ***Matsuo et al., 2016***); and the TACC protein Alp7, which interacts with Alp14 and enhances its polymerase activity (***Hussmann et al., 2016***; ***Sato et al., 2004***).

The deletion of *ase1*, *mal3*, *alp14*, and *alp7* still allowed the formation of comparatively long microtubule bundles in the *cut7-24* background (***Figure 3A,B***). In all cases, the growth velocity of microtubule bundles was significantly reduced (***Figure 3B,C***, ***Figure 3—source data 1***). However, only the deletion of *dis1* led to a decrease of the bundle growth velocity comparable to the deletion or shut-off condition of *klp9* (***Figure 3B,C***, ***Figure 3—source data 1***). Moreover, maximum bundle length was reduced upon deletion of *ase1*, *dis1*, and *alp7*, with the strongest decrease observed upon *dis1* deletion (***Figure 3D***, ***Figure 3—source data 1***).

We note that the deletion of *alp14* and *alp7* often resulted in the restoration of spindle bipolarity. This is in agreement with the model, that a balance between microtubule dynamics and the action of Cut7 is crucial for the establishment of spindle bipolarity (***Yukawa et al., 2019b***). Here, we analyzed the fraction of cells in which spindle bipolarity could not be restored, and spindles remained monopolar.

Taken together, of the tested candidates, the deletion of *dis1* gave rise to a similar phenotype as the deletion or shut-off condition of *klp9*. Similar to the deletion of *klp9*, upon *dis1* deletion the transition to anaphase B is not impaired, as indicated by the disappearance of the Cdc13-GFP signal (***Figure 3—figure supplement 1***). Thus, like Klp9, Dis1 seems to be involved in the regulation of microtubule growth during anaphase B and may act in the same pathway with Klp9.

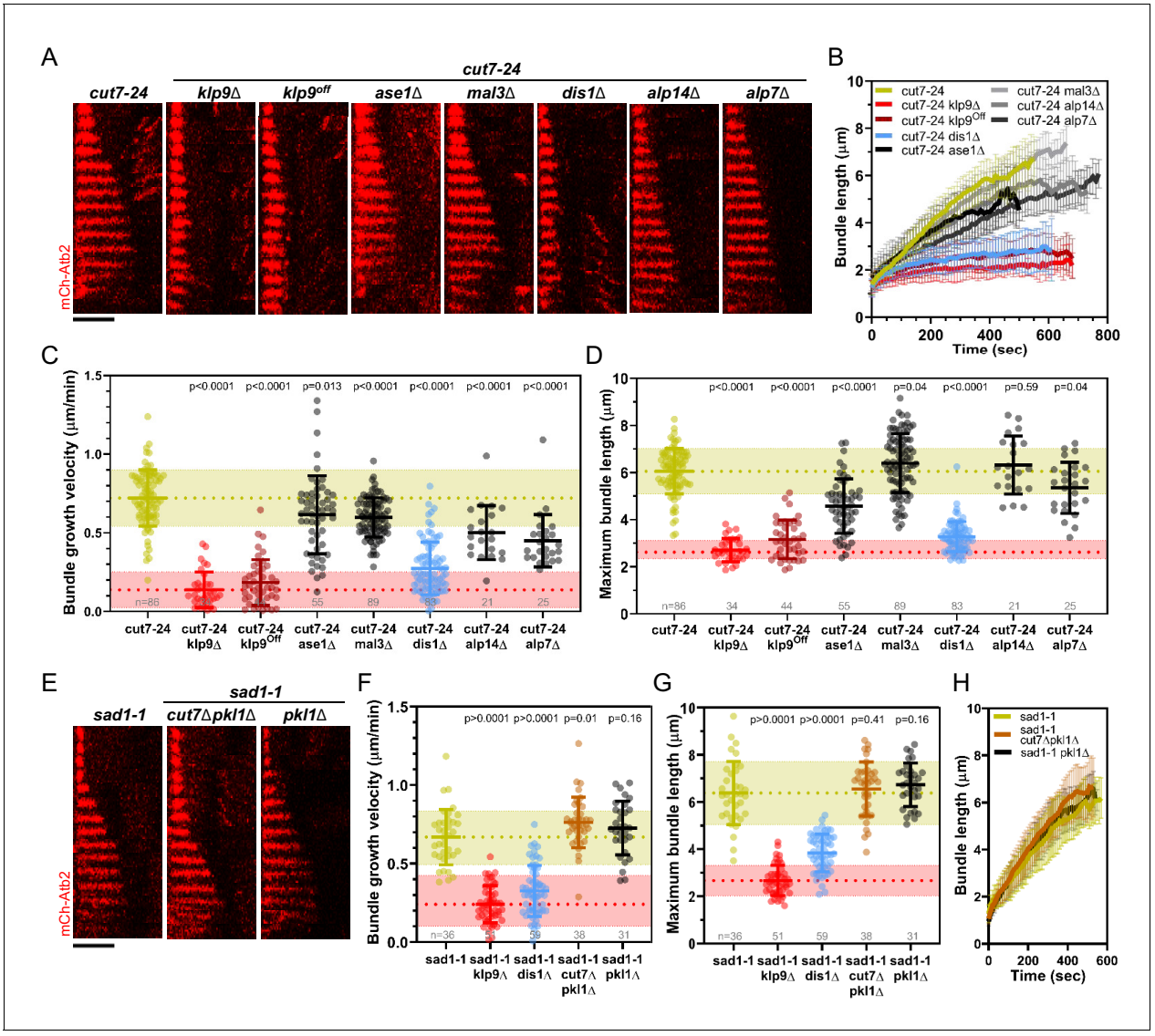


**Figure 3.** Deletion of *dis1* decreases microtubule bundle growth velocity and bundle length during anaphase B in monopolar spindles. (**A**) Time-lapse images of *cut7-24*, *cut7-24 klp9Δ*, *cut7-24 klp9$^{Off}$*, *klp9$^{Off}$ ase1Δ*, *cut7-24 mal3Δ*, *cut7-24 dis1Δ*, *cut7-24 alp14Δ*, and *cut7-24 alp7Δ* cells expressing mCherry-Atb2 (tubulin) at 37˚C. (**B**) Comparative plot of microtubule bundle dynamics in *cut7-24* (n = 40), *cut7-24 klp9Δ* (n = 40), *cut7-24 klp9$^{Off}$* (n = 40), *cut7-24 ase1Δ* (n = 39), *cut7-24 mal3Δ* (n = 40), *cut7-24 dis1Δ* (n = 39), *cut7-24 alp14Δ* (n = 20), and *cut7-24 alp7Δ* cells (n = 25) at 37˚C. (**C**) Dot plot comparison of microtubule bundle growth velocity during anaphase B. (**D**) Dot plot comparison of maximum microtubule bundle length during anaphase B. (**E**) Time-lapse images of *sad1-1*, *sad1-1 cut7ΔPkl1Δ* and *sad1-1 pkl1Δ* cells expressing mCherry-Atb2 (tubulin) at 37˚C. (**F**) Dot plot comparison of microtubule bundle growth velocity during anaphase B. (**G**) Dot plot comparison of maximum microtubule bundle length during anaphase B. (**H**) Comparative plot of microtubule bundle dynamics in *sad1-1* (n = 39), sad1-1 *cut7ΔPkl1Δ* (n = 38), and *sad1-1 pkl1Δ* (n = 31) at 37˚C. In (**A**) and (**E**), each frame corresponds to 1 min interval. Scale bar, 5 µm. In (**C**) and (**H**), bold curves correspond to the mean and error bars to the standard deviation. In (**C, D**) and (**F, G**), lines correspond to mean and standard deviation. p-values were calculated using Mann–Whitney U test. Data from n cells was collected from at least three independent experiments.

The online version of this article includes the following source data and figure supplement(s) for figure 3:

**Source data 1.** Numerical data used for ***Figure 3B,C,D,F,G, and H***.

**Figure supplement 1.** Time-lapse images of *dis1Δ* and *cut7-24* dis1Δ cells expressing mCherry-Atb2 (tubulin) and Cdc13-GFP (cyclin B) at 37˚C.

**Figure supplement 2.** Time-lapse images of *sad1-1* cells expressing mCherry-Atb2 (tubulin) and Sid1-GFP (SPBs), Klp9-GFP or Cut7-GFP at 37˚C.

*Figure 3 continued on next page*

*Figure 3 continued*

**Figure supplement 3.** Time-lapse images of wild-type and *klp9*Δ cells expressing mCherry-Atb2 (tubulin) and Cls1-3xGFP (CLASP) at 25˚C.
**Figure supplement 4.** Comparative plot of Cls1-3xGFP intensity throughout anaphase B spindle elongation of wild-type (n = 20) and *klp9*Δ (n = 20).
**Figure supplement 4—source data 1.** Numerical data used for ***Figure 3—figure supplement 4***.
**Figure supplement 5.** Time-lapse images of *cut7-24* cells expressing mCherry-Atb2 (tubulin) and Cls1-3xGFP (CLASP) at 37˚C.

Besides, we examined a possible involvement of the kinesin-5 Cut7 and CLASP Cls1 (also called Peg1). Cut7 has been shown to promote spindle elongation like Klp9, even though to a lower extent (***Rincon et al., 2017***; ***Yukawa et al., 2019b***), and a dimeric construct of the *X. laevis* kinesin-5 Eg5 promotes microtubule growth in vitro (***Chen et al., 2019***; ***Chen and Hancock, 2015***). To test the role of Cut7 we used the *sad1-1* temperature-sensitive mutant to generate monopolar spindles (***Hagan and Yanagida, 1995***). In this mutant, 9.3% of the spindles became bipolar and not all of the monopolar spindles proceeded to anaphase B. We analyzed the spindles that remained monopolar and initiated anaphase B. *Sad1-1* monopolar spindles also assembled long microtubule bundles during anaphase B (***Figure 3E***, ***Figure 3—figure supplement 2***), which grew with a similar velocity and to a similar maximum length as the anaphase B bundles in the *cut7-24* mutant (***Figure 3C,D,F,G***, ***Figure 3—source data 1***). Thus, *sad1-1* monopolar spindles can also be used to study microtubule dynamics during anaphase B. Deletion of *cut7* was performed in the background of *pkl1* (kinesin-14) deletion, since the deletion of the kinesin-5 alone is lethal (***Olmsted et al., 2014***; ***Rincon et al., 2017***; ***Syrovatkina and Tran, 2015***; ***Yukawa et al., 2018***). Unlike the deletion of *klp9* or *dis1*, the deletion of *cut7* (*cut7*Δ*pkl1*Δ) led to a slight increase of the growth velocity (***Figure 3F, H***) and no significant change of maximum bundle length (***Figure 3G***, ***Figure 3—source data 1***, ***Figure 3H***). The modest acceleration of bundle growth seemed to be a result of the absence of Cut7 and not Pkl1, since the deletion of *pkl1* alone did not affect growth velocity significantly (***Figure 3F***, ***Figure 3—source data 1***). Furthermore, we investigated the localization of Cut7-GFP in the *sad1-1* mutant. While, Klp9-GFP was detected at the tip of microtubule bundles, Cut7-GFP localized only to the unseparated spindle poles (***Figure 3—figure supplement 2***). Thus, even though both motors have been reported to be plus-end directed bipolar kinesins, and both localize to spindle microtubules in a bipolar spindle (***Fu et al., 2009***; ***Hagan and Yanagida, 1992***), only Klp9 tracks the tip of the microtubule bundles in monopolar spindles, and promotes their growth during anaphase B. Cut7, like other kinesin-5 members, has been shown to move bidirectionally along microtubule tracks (***Edamatsu, 2014***; ***Roostalu et al., 2011***). This bidirectional motility may be the basis for the differential localization of Cut7. Accordingly, Klp9 displays a much stronger affinity for the spindle midzone, where microtubules terminate with their plus-ends, in bipolar spindles than Cut7, which also localizes to regions closer to spindle poles (***Loncar et al., 2020***; ***Yukawa et al., 2020***).

Last, we examined if the phenotype upon *klp9* deletion could stem from an interaction with the fission yeast CLASP Cls1. Cls1 localizes to the spindle midzone during anaphase B and promotes microtubule rescues, thus preventing microtubules from depolymerizing back to the spindle poles and preserving spindle stability (***Bratman and Chang, 2007***). Since deletion of *cls1* is lethal, we tested a potential interaction with Klp9 during anaphase B by expressing Cls1-3xGFP in wild-type and *klp9* deleted cells. In bipolar spindles, Cls1-3xGFP localized to the spindle midzone in presence or absence of Klp9 (***Figure 3—figure supplement 3***) with similar intensities throughout anaphase B (***Figure 3—figure supplement 4***, ***Figure 3—figure supplement 4—source data 1***). Moreover, in monopolar *cut7-24* spindles, Cls1-3xGFP did not localize to the bundle tip but was rather spread all along the bundle (***Figure 3—figure supplement 5***). Therefore, we conclude that Cls1 is not involved in the underlying mechanism of Klp9-mediated microtubule growth during anaphase B.

## Dis1 regulates the recruitment of Klp9 to the anaphase B spindle

The XMAP215 family member Dis1 emerged as a possible candidate that acts in the pathway with Klp9. To probe this, we examined its role during anaphase B spindle elongation in bipolar spindles. Similar to the deletion of *klp9*, the deletion of *dis1* decreased the spindle elongation velocity (***Figure 4A,B***, ***Figure 4—source data 1***). Simultaneous deletion of both proteins did not display an additive effect, and decreased spindle elongation velocity to not significantly different values as the deletion of individual proteins (***Figure 4A,B***, ***Figure 4—source data 1***), suggesting that Klp9 and

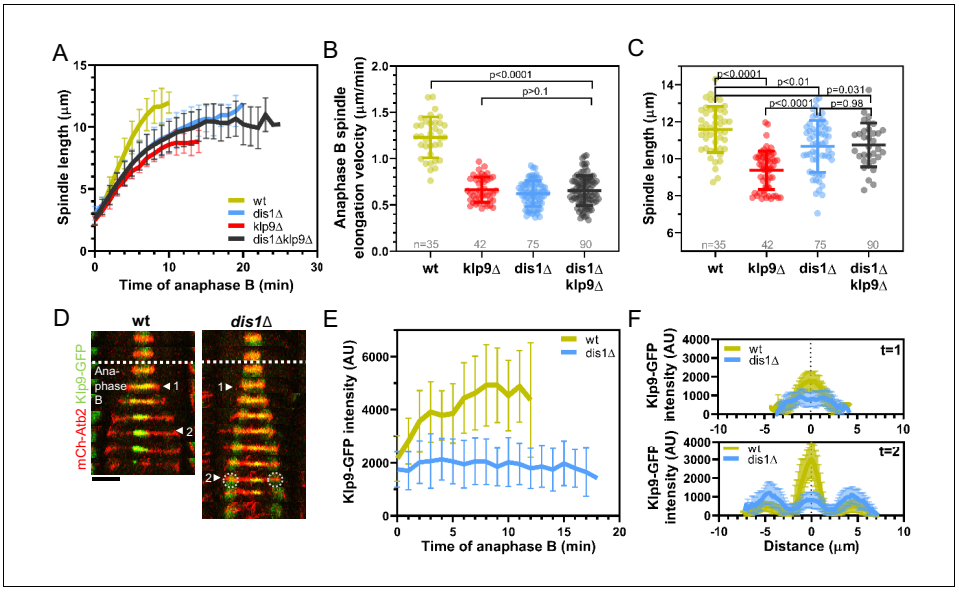


**Figure 4.** *Dis1* deletion impairs Klp9 recruitment to the anaphase B spindle. (**A**) Comparative plot of anaphase B spindle dynamics of wild-type (n = 35), *dis1*Δ (n = 75), *klp9*Δ (n = 38), and *dis1*Δ*klp9*Δ (n = 90) at 25˚C. (**B**) Dot plot comparison of spindle elongation velocity in wild-type, *dis1*Δ, *klp9*Δ, and *dis1*Δ*klp9*Δ cells. (**C**) Dot plot comparison of final anaphase B spindle length in wild-type, *dis1*Δ, *klp9*Δ, and *dis1*Δ*klp9*Δ cells. (**D**) Time-lapse images of wild-type and *dis1*Δ cells expressing mCherry-Atb2 (tubulin) and Klp9-GFP at 25˚C. Arrowheads 1 and 2 correspond to the time points used for linescan analysis at t = 1 (2 min after anaphase B onset), t = 2 (2 min before spindle disassembly). Circles mark the Klp9 pool that remained in the nucleoplasm. Scale bar, 5 µm. (**E**) Comparative plot of Klp9-GFP intensity throughout anaphase B spindle elongation of wild-type (n = 30) and *dis1*Δ cells (n = 33). (**F**) Intensity spectra obtained by linescan analysis of Klp9-GFP signals along the anaphase B spindle at early (t = 1) and late anaphase (t = 2). In (**A**), (**E**), and (**F**), bold curves correspond to the mean and error bars to the standard deviation. In (**B**) and (**C**), lines correspond to mean and standard deviation. Data from n cells was collected from at least three independent experiments.
The online version of this article includes the following source data and figure supplement(s) for figure 4:

**Source data 1.** Numerical data used for ***Figure 4A,B,C,E, and F***.
**Source data 2.** Numerical data used for ***Figure 4—figure supplements 1***, ***2***, ***4***, ***5,*** and ***6***.
**Figure supplement 1.** Dot plot comparison of cell length (µm) of wild-type, *klp9*Δ, and dis1Δ cells at mitosis onset.
**Figure supplement 2.** Dis1 recruitment to the anaphase B spindle is not impaired upon *klp9* deletion.
**Figure supplement 3.** Time-lapse images of *cut7-24* cells expressing mCherry-Atb2 (tubulin) and Dis1-EGFP at 37˚C.
**Figure supplement 4.** Dot plot comparison of Klp9-GFP intensity in the nucleoplasm at mitosis onset and mean Klp9-GFP intensity at the spindle midzone during anaphase B in wild-type and *dis1*Δ cells.
**Figure supplement 5.** Comparative plot of the relative Klp9 concentration at the spindle midzone (Klp9-GFP intensity normalized with the mCherry-Atb2 intensity) throughout anaphase B spindle elongation of wild-type (n = 29) and *dis1*Δ (n = 28).
**Figure supplement 6.** Mild overexpression of *dis1* increases Klp9-GFP levels at the spindle midzone during anaphase B.

Dis1 act in the same pathway. Furthermore, final spindle length is reduced in all three mutants (***Figure 4C***, ***Figure 4—source data 1***), further indicating an effect of Dis1 and Klp9 on microtubule growth in bipolar spindles.

The longer spindles in *dis1* deleted cells as compared to *klp9*Δ cells may be a result of an increased cell size upon *dis1* deletion (***Figure 4—figure supplement 1***, ***Figure 4—source data 2***) due to a slower growth rate in this mutant.

Dis1 was previously shown to be a microtubule polymerase (***Matsuo et al., 2016***). It was thus tempting to think that Klp9 transports Dis1 to the plus-ends of microtubules. However, during anaphase B, Dis1-EGFP localization to spindle poles and the lateral spindle microtubule lattice of bipolar spindles, and the Dis1-EGFP intensity on the spindle was not altered in the absence of Klp9 (***Figure 4—figure supplement 2***, ***Figure 4—source data 2***). Moreover, in monopolar spindles, Dis1-EGFP localized to the unseparated spindle poles and disperse along the microtubule bundle (***Figure 4—figure supplement 3***, ***Figure 4—source data 2***), but did not accumulate at the bundle tip.

These results suggest that Klp9 does neither regulate the recruitment of Dis1 nor its localization along the anaphase B spindle in bipolar or monopolar spindles. Dis1, thus, cannot be directly responsible for the reduced microtubule growth rate upon *klp9* deletion in monopolar spindles.

Therefore, we wondered if Dis1 could recruit Klp9. Indeed, we observed that the Klp9-GFP signal at the spindle midzone was strongly diminished upon *dis1* deletion (***Figure 4D***, ***Figure 4—source data 1***). While in the presence of Dis1, the intensity of Klp9-GFP increased with progressing spindle elongation, until a plateau was reached in late anaphase, the intensity remained low in *dis1*Δ cells (***Figure 4E***, ***Figure 4—source data 1***). This is not a consequence of overall lower Klp9 levels, since the total intensity of Klp9-GFP (measured at mitosis onset in the nucleoplasm, where Klp9 is localized before anaphase B onset) was not significantly altered (***Figure 4—figure supplement 4***, ***Figure 4—source data 2***). Intensity profiles along the spindle at early and late anaphase B showed that Klp9-GFP still localized preferentially to the midzone in absence of Dis1, but with reduced intensity (***Figure 4F***, ***Figure 4—source data 1***). The increased intensity of Klp9-GFP close to the spindle poles in late anaphase B in *dis1*Δ (***Figure 4F***, t = 2) corresponded to the pool of Klp9-GFP that remained in the nucleoplasm and was thus not recruited to the spindle (***Figure 4D***, circles). To further exclude the possibility, that the decreased Klp9-GFP intensity could be a result of a decreased spindle microtubule number, and thus fewer binding-sites for Klp9 upon *dis1* deletion, we normalized the Klp9-GFP intensity with the mCherry-Atb2 intensity. This relative Klp9 concentration at the midzone increased in wild-type cells, according to the increasing Klp9-GFP intensity, but remained low in *dis1*Δ cells (***Figure 4—figure supplement 5***, ***Figure 4—source data 2***). Hence, the impaired localization of Klp9-GFP did not stem from differences in microtubule number.

Moreover, mild overexpression of *dis1* by inserting the thiamine repressible nmt promoter *pnmt81* upstream of the *dis1* open-reading frame increased the intensity of Klp9-GFP throughout anaphase B at the midzone, while the total Klp9-GFP intensity was not significantly different (***Figure 4—figure supplement 6***, ***Figure 4—source data 2***). Thus, the microtubule polymerase Dis1 regulates the recruitment of the kinesin-6 motor Klp9 to the anaphase B spindle in a dose-dependent manner.

## Dis1 regulates the recruitment of Klp9 in a dephosphorylation-dependent manner

Klp9 localization during mitosis is regulated in a phosphorylation-dependent manner (***Figure 5A***). The motor is phosphorylated at mitosis onset by Cdc2, homolog of Cdk1, and dephosphorylated at the metaphase-to-anaphase B transition by Clp1, homolog of Cdc14 (***Fu et al., 2009***). Dephosphorylation was proposed to be required for Klp9 recruitment to the anaphase B spindle (***Fu et al., 2009***). The localization of Dis1 is also regulated via phosphorylation/dephosphorylation at Cdc2 phosphosites (***Aoki et al., 2006***; ***Figure 5A***). Cdc2-mediated phosphorylation of Dis1 promotes its localization to kinetochores during pro- and metaphase (***Aoki et al., 2006***), where it is involved in sister chromatid separation (***Nabeshima et al., 1995***; ***Ohkura et al., 1988***). Dephosphorylation of the Cdc2 phosphosites by an unknown phosphatase at the metaphase-to-anaphase B transition results in Dis1 relocalization to the lateral microtubule lattice of anaphase B spindles (***Figure 5A***; ***Aoki et al., 2006***). At this location, Dis1 may be required for bundling parallel microtubules (***Roque et al., 2010***). Accordingly, a phospho-mimetic Dis1 mutant cannot be detected on spindle microtubules, only at spindle poles, and a phospho-deficient Dis1 version localizes extensively to the parallel microtubule lattice of the mitotic spindle (***Aoki et al., 2006***).

We thus asked if Dis1 is also dephosphorylated by Clp1 and, furthermore, if this dephosphorylation is required for Dis1-mediated Klp9 recruitment.

Upon *clp1* deletion, Dis1-EGFP was only detected at spindle poles, and not on spindle microtubules during anaphase B (***Figure 5B–D***), resulting in a decreased Dis1-EGFP intensity along the spindle (***Figure 5E***, ***Figure 5—source data 1***). This localization pattern of Dis1-EGFP was equal to a phospho-mimetic Dis1 mutant (***Aoki et al., 2006***), indicating that in the absence of Clp1, Dis1 remained phosphorylated. Moreover, *clp1* deletion resulted in a significant reduction of the Klp9-mCherry intensity at the spindle midzone (***Figure 5B, D, and F***, ***Figure 5—source data 1***). Consequently, the spindle elongation velocity in anaphase B was reduced upon *clp1* deletion (***Figure 5—figure supplement 1***, ***Figure 5—source data 2***) as well as the growth of microtubule bundles in monopolar *cut7-24* spindles (***Figure 5—figure supplement 2***, ***Figure 5—source data 1***), in agreement with a reduced intensity of Klp9-GFP at the bundle tips (***Figure 5G***).

eLife Research article Cell Biology

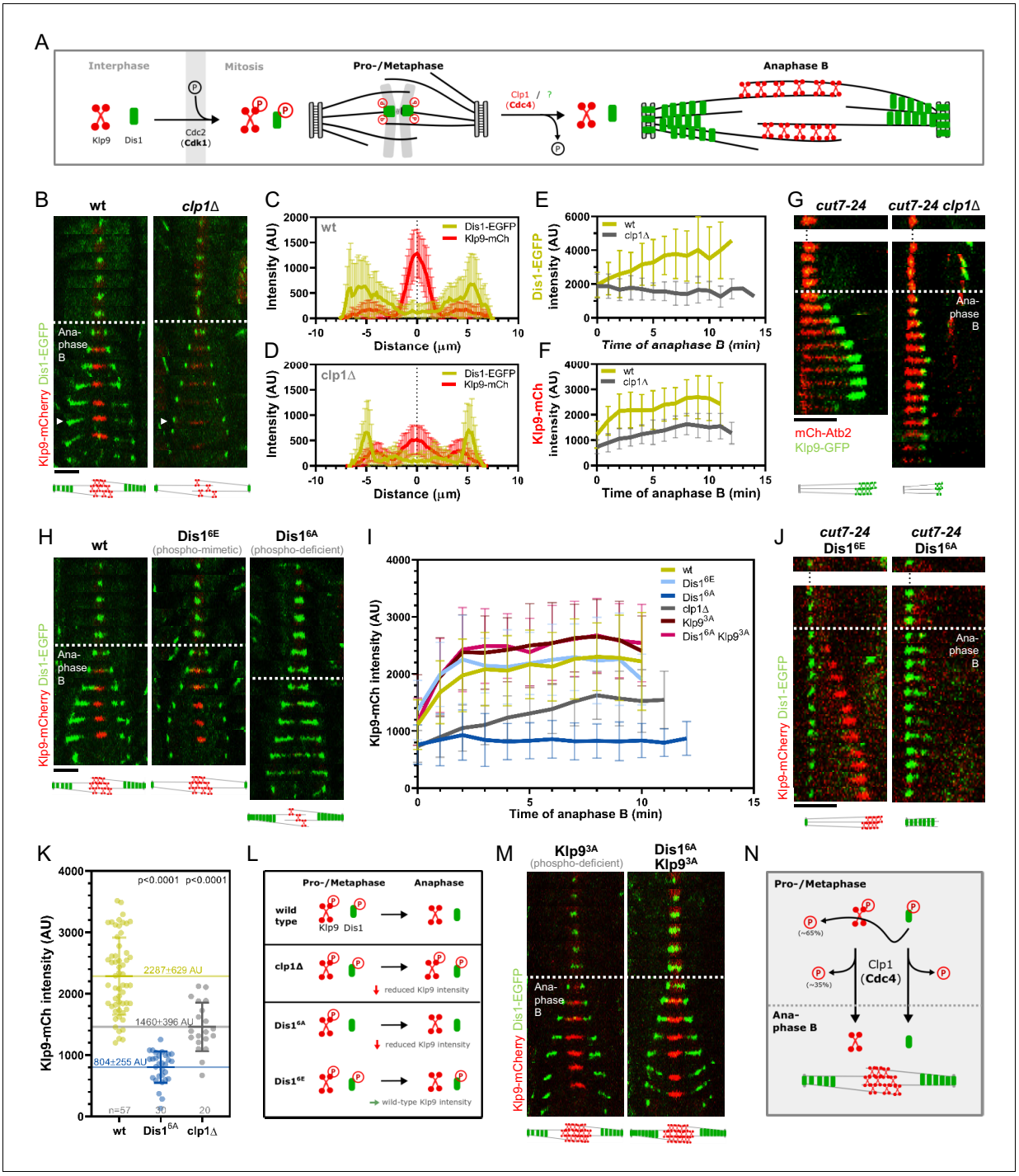


**Figure 5.** Phospho-dependent regulation of Dis1-mediated Klp9 recruitment. (**A**) Model of phosphorylation-dependent localization of Klp9 (red) and Dis1 (green) throughout mitosis mediated by the cyclin-dependent kinase Cdc2 (homolog of Cdk1) and the phosphatase Clp1 (homolog of Cdc14). (**B**) Time-lapse images of wild-type and *clp1*Δ cells expressing Klp9-mCherry and Dis1-EGFP at 25˚C. Arrowhead depicts the time point used for linescan analysis (2 min before spindle disassembly). Schemes of anaphase B spindles, illustrating the localization pattern of Klp9 (red) and Dis1 (green) along

*Figure 5 continued on next page*

*Figure 5 continued*

the spindle (gray). (**C**) Intensity spectra obtained by linescan analysis of Dis1-EGFP and Klp9-mCherry signals along the anaphase spindle at late anaphase in wild-type cells (n = 30). X = 0 µm equals the cell center. (**D**) Intensity spectra obtained by linescan analysis of Dis1-EGFP and Klp9-mCherry signals along the anaphase spindle at late anaphase in *clp1*Δ cells (n = 30). (**E**) Comparative plot of Dis1-EGFP intensity throughout anaphase B spindle elongation of wild-type (n = 30) and *clp1*Δ (n = 30). (**F**) Comparative plot of Klp9-mCherry intensity throughout anaphase B spindle elongation of wild-type (n = 30) and *clp1*Δ (n = 30). (**G**) Time-lapse images of *cut7-24*, and *cut7-24 clp1*Δ cells expressing Klp9-GFP and mCherry-Atb2. Time interval corresponds to 1 min. Schemes of monopolar anaphase B spindles, illustrating the localization pattern of Klp9 (green) along the spindle (grey). (**H**) Time-lapse images of cells expressing wild-type Dis1-GFP, phospho-mimetic Dis1$^{6E}$-GFP or phospho-deficient Dis1$^{6A}$-GFP together with Klp9-mCherry at 25˚C. (**I**) Comparative plot of Klp9-mCherry intensity throughout anaphase B spindle elongation of wild-type cells (n = 30) and cells expressing Dis1$^{6E}$-GFP (n = 30), Dis1$^{6A}$-GFP (n = 30), Klp9$^{3A}$-mCherry (n = 30), Dis1$^{6A}$-EGFP and Klp9$^{SA}$-mCherry (n = 30), and *clp1*Δ cells (n = 20). Schemes of anaphase B spindles, illustrating the localization pattern of Klp9 (red) and Dis1 (green) along the spindle (gray). (**J**) Time-lapse images of *cut7-24* cells expressing Klp9-mCherry and Dis1$^{6E}$-EGFP or Dis1$^{6A}$-EGFP. Time interval corresponds to 1 min. Schemes of monopolar anaphase B spindles, illustrating the localization pattern of Klp9 (red) and Dis1 (green) along the spindle (gray). (K) Dot plot comparison of the Klp9-mCherry intensity (AU) in wild-type, Dis1$^{6A}$, *clp1*Δ and Dis1$^{6E}$*clp1*Δ cells. Lines correspond to mean and standard deviation. Long lines depict the mean for each cell type. p-values were calculated using Mann-Whitney U test. (L) Summary of the results obtained upon *clp1* deletion and expression of phospho-deficient Dis1$^{6A}$ or phosphoimimetic Dis1$^{6E}$. (M) Time-lapse images of cells expressing phospho-deficient Klp9$^{3A}$-mCherry with wild-type Dis1-GFP, and phospho-deficient Klp9$^{3A}$-mCherry with phospho-deficient Dis1$^{6A}$-EGFP at 25˚C. Schemes of anaphase B spindles, illustrating the localization pattern of Klp9 (red) and Dis1 (green) along the spindle (gray). (**N**) Model of dephosphorylation-dependent regulation of Klp9 and Dis1 localization to the anaphase B spindle. In (**B**), (**H**), and (M), each frame corresponds to 2 min interval. Dotted lines denote the transition to anaphase B. Scale bar, 5 µm. In (**C–F**) and (**I**), bold curves correspond to the mean and error bars to the standard deviation. Data from n cells was collected from at least three independent experiments. The online version of this article includes the following source data and figure supplement(s) for figure 5:

**Source data 1.** Numerical data used for ***Figure 5C,D,E,F,I, and K***.
**Source data 2.** Numerical data used for ***Figure 5—figure supplements 1***, ***2,*** and ***4***.
**Figure supplement 1.** Comparative plot of spindle length dynamics during anaphase B and dot plot compairison of anaphase B spindle elongation velocity of wild-type (n = 20) and *clp1*Δ cells (n = 40).
**Figure supplement 2.** Comparative plot of microtubule bundle dynamics in *cut7-24* (n = 39), *cut7-24 clp1*Δ (n = 35), *and cut7-24 klp9*Δ (n = 40) at 37˚C.
**Figure supplement 3.** Time-lapse images of wild-type and *ase1*Δ cells expressing Klp9-mCherry and Dis1-EGFP at 25˚C.
**Figure supplement 4.** Comparative plot of Klp9-mCherry intensity throughout anaphase B spindle elongation of wild-type (n = 30) and *ase1*Δ (n = 30).

Thus, both Klp9 and Dis1 are dephosphorylated at the metaphase-to-anaphase B transition by Clp1, allowing Dis1 to bind to the parallel spindle microtubule lattice and Klp9 recruitment to anti-parallel midzone microtubules (***Figure 5L***).

Besides, Clp1 also dephosphorylates Ase1, and dephosphorylation of Ase1 and Klp9 has been proposed to allow their physical interaction, and eventually the recruitment of Klp9 to the spindle by Ase1 (***Fu et al., 2009***). Hence, we examined if the observed reduction of the Klp9-mCherry intensity in *clp1*Δ did not stem from a prevented Klp9-Ase1 interaction. We could not detect mis-localization of Klp9 or Dis1, nor a reduction of the Klp9-mCherry intensity upon *ase1* deletion (***Figure 5—figure supplements 3*** and ***4***, ***Figure 5—source data 2***). Thus, Ase1 does not appear to recruit Klp9 to the spindle upon dephosphorylation.

Our data suggests that this task is performed by Dis1, since *dis1* deletion disrupts Klp9 recruitment. We then asked if Dis1 dephosphorylation by Clp1 at anaphase B onset is required for Klp9 recruitment to the spindle.

To do so, we took advantage of previously generated phospho-mimetic and phospho-deficient mutants of Dis1. The six consensus Cdc2-phosphosites of Dis1 (T279, S293, S300, S551, S556, and S590) were either changed to alanine, to create a phospho-deficient mutant (Dis1$^{6A}$), or to glutamate, to obtain a phospho-mimetic version of Dis1 (Dis1$^{6E}$) (***Aoki et al., 2006***).

If dephosphorylation of Dis1 at anaphase B onset would be necessary for Klp9 recruitment, we would expect the expression of Dis1$^{6E}$-GFP, mimicking the metaphase phosphorylated state, to result in reduced Klp9-mCherry intensities, and expression of Dis1$^{6A}$-GFP, mimicking the anaphase B dephosphorylated state, to lead to unaltered Klp9-mCherry intensities at the spindle midzone. Contrarily, we found that the intensity of Klp9-mCherry was not altered in cells expressing the phospho-mimetic Dis1$^{6E}$-GFP, but was strongly reduced in cells expressing the phospho-deficient Dis1$^{6A}$-GFP compared to the expression of wild-type Dis1-GFP (***Figure 5H, I***, ***Figure 5—source data 1***). Accordingly, in *cut7-24* cells, expression of Dis1$^{6E}$-GFP allowed Klp9-mCherry recruitment to the growing microtubule bundle tip, whereas expression of Dis1$^{6A}$-GFP prevented Klp9-mCherry localization to the bundle and subsequently its growth (***Figure 5J***). This indicates that the recruitment of Klp9 by

Dis1 does not require Dis1 dephosphorylation but depends on its phosphorylation: For proper Klp9 recruitment, Dis1 has to be phosphorylated at Cdc2-phosphosites prior to anaphase B onset (***Figure 5L***).

This also suggests that, the reduced Klp9-mCherry intensity upon *clp1* deletion is not a result of the prevented dephosphorylation of Dis1. Two different pathways may regulate Klp9 localization to the anaphase B spindle: one depends on dephosphorylation of Klp9 by Clp1 and the other requires the presence of phosphorylated Dis1 during pro-/metaphase. Indeed, the decrease of the Klp9-mCherry intensity was milder upon *clp1* deletion, than it was upon expression of Dis1$^{6A}$ (***Figure 5I, K***, ***Figure 5—source data 1***). We noticed that the sum of the Klp9-mCherry intensity in cells expressing Dis1$^{6A}$-GFP (804 ± 255 AU) and *clp1*Δ cells (1460 ± 396 AU) yields a similar value as the intensity in wild-type cells (2287 ± 629 AU) (***Figure 5K***, ***Figure 5—source data 1***). Hence, Klp9 recruitment appears to be regulated by two pathways: one relying on phosphorylated Dis1 (~65%) and one on Clp1 (~35%).

Last, we asked how phosphorylated Dis1, present during pro- and metaphase, regulates the recruitment of Klp9 to spindle microtubules at anaphase B onset.

Similar to Clp1, Dis1 may promote Klp9 dephosphorylation. Phosphorylated Dis1 could initiate a pathway at the end of metaphase, which triggers Klp9 dephosphorylation at anaphase B onset, eventually enabling Klp9 binding to the spindle midzone.

To probe this hypothesis, we decided to test whether the expression of a phospho-deficient version of Klp9 could rescue the decreased Klp9 recruitment observed upon expression of phospho-deficient Dis1$^{6A}$-GFP. Previously, three Cdc2-dependent phosphorylation sites of Klp9 (S598, S605, and S611) have been mutated to alanine to obtain phospho-deficient Klp9 (Klp9$^{3A}$) (***Fu et al., 2009***). Indeed, the intensity of Klp9$^{3A}$-mCherry in cells expressing Dis1$^{6A}$-GFP was not significantly different compared to cells expressing wild-type Dis1-GFP and Klp9$^{3A}$-mCherry (***Figure 5I,M***, ***Figure 5—source data 1***). Thus, the reduced Klp9 recruitment upon expression of Dis1$^{6A}$-GFP could be rescued by simultaneous expression of Klp9$^{3A}$-mCherry (***Figure 5M***). Hence, Dis1 appears to regulate recruitment of the motor to anaphase B spindles by promoting Klp9 dephosphorylation.

The results at hand suggest the following mechanism for the recruitment of the kinesin-6 Klp9 to anaphase B spindles (***Figure 5N***): Klp9 and Dis1 are phosphorylated at Cdc2-phosphosites during pro- and metaphase. Phosphorylated Dis1, potentially at the end of metaphase, initiates a pathway that regulates dephosphorylation of approximately 65% of the recruited Klp9 pool at anaphase B onset. Dephosphorylation allows the motor to bind to the spindle midzone. The remaining 35% of Klp9 are dephosphorylated by Clp1, which also dephosphorylates Dis1 in order to allow its binding to parallel spindle microtubules during anaphase B.

## Klp9 sets the microtubule growth velocity in vitro

Since Dis1 acts upstream of Klp9, the effect of Klp9 on microtubule polymerization in monopolar spindles may arise from the motor function itself. To probe this hypothesis, we examined the effect of recombinant full-length Klp9 (***Figure 6—figure supplement 1***) on dynamic microtubules in vitro. The functionality of the kinesin-6 was verified using a microtubule gliding assay (***Figure 6A***). Klp9 was immobilized on a glass coverslip via a His6-antibody and red ATTO-647-labeled taxol-stabilized microtubules polymerized from bovine tubulin were added to the flowchamber (***Figure 6A***). Using total internal reflection fluorescence (TIRF) microscopy, microtubule motion was observed. Microtubules moved with an average velocity of 2.4 ± 0.4 µm/min (***Figure 6B,C***, ***Figure 6—source data 1***), which was consistent with previously observed Klp9-mediated microtubule gliding velocities (***Yukawa et al., 2019a***).

Subsequently, we examined the effect of Klp9 on dynamic microtubules growing from biotin- and ATTO-647-labeled, GMPCPP-stabilized microtubule seeds (***Figure 6D***). In the presence of 10 µM free tubulin (80% unlabeled, 20% ATTO-488 labeled), the addition of Klp9 increased the growth velocity in a dose-dependent manner from 1.0 ± 0.3 µm/min, in the absence of Klp9, to 1.7 ± 0.4 µm/min, in the presence of 25 nM Klp9 (***Figure 6E,F***, ***Figure 6—source data 1***). Moreover, microtubule length, measured just before a growing microtubule underwent catastrophe, increased (***Figure 6G***, ***Figure 6—source data 1***) and the catastrophe frequency decreased with increasing Klp9 concentration (***Figure 6H***, ***Figure 6—source data 1***). Taken together, the kinesin-6 Klp9 stabilized microtubules and enhanced microtubule growth by increasing the velocity of polymerization and by decreasing the catastrophe frequency. This has similarly been observed for the *S. cerevisiae*

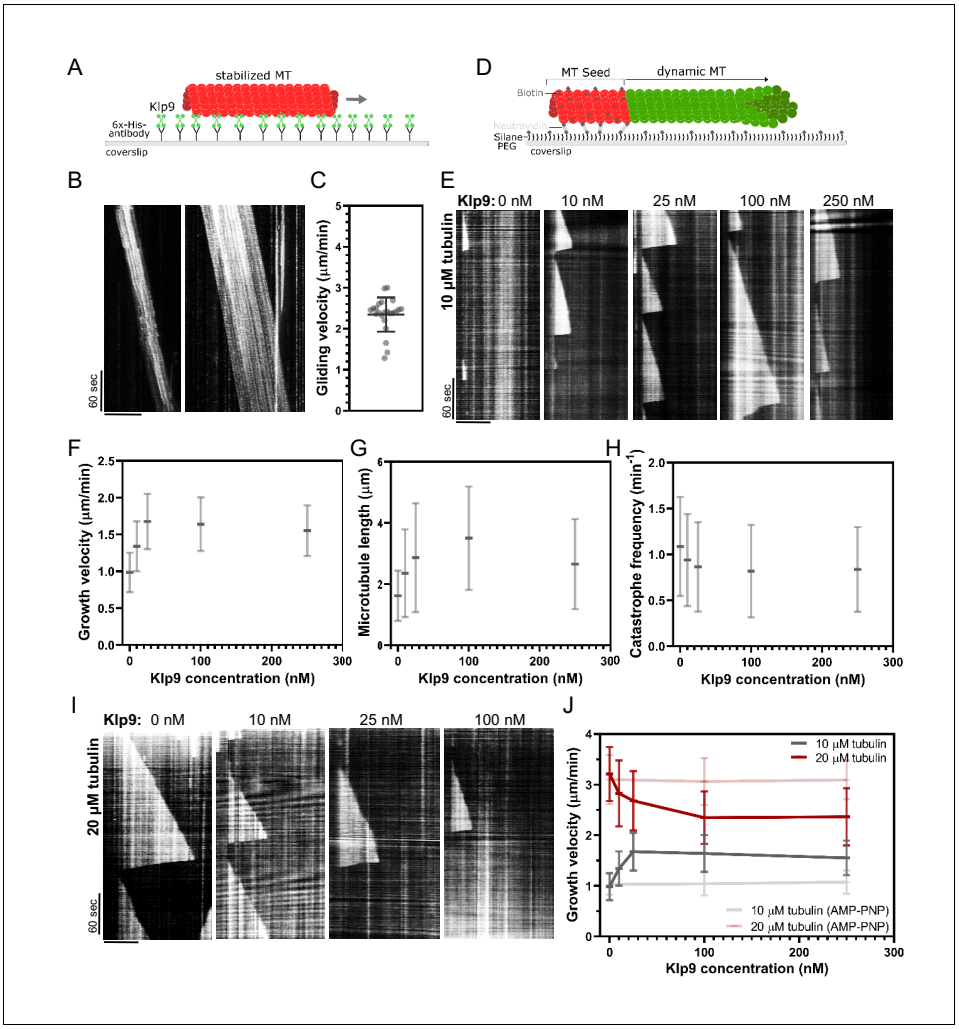


**Figure 6.** Recombinant Klp9 regulates the microtubule growth velocity in vitro. (**A**) Schematic set up of the microtubule gliding assay. His6 antibodies are shown in gray, Klp9 molecules in green, and taxol-stabilized microtubules in red. (**B**) Kymographs of gliding microtubules with the time on the y-axis and space on the x-axis. Scale bar, 10 µm. (**C**) Dot plot of microtubule gliding velocities. (**D**) Schematic of microtubule polymerization assay: GMPCPP-stabilized, ATTO-647-labeled microtubule seeds are shown in red and the dynamic microtubule grown from free tubulin (80% unlabeled, 20% ATTO-488-labeled tubulin) in green. (**E**) Kymographs of dynamic microtubules grown in presence of 10 µM free tubulin and 0, 10, 25, 100, and 250 nM Klp9. Scale bar, 5 µm. (**F**) Microtubule growth velocity (µm/min) shown as a function of the Klp9 concentration (nM); n = 190–325 microtubules per condition. (**G**) Microtubule length (µm) shown as a function of the Klp9 concentration (nM); n = 157–325 microtubules per condition. (**H**) Catastrophe frequency ($min^{-1}$) shown as a function of the Klp9 concentration (nM); n = 65–112 microtubules per condition. (**I**) Kymographs of dynamic microtubules grown in presence of 20 µM free tubulin (80% unlabeled, 20% ATTO-488-labeled tubulin), and 0, 10, 25, and 100 nM Klp9. Scale bar, 5 µm. (**J**) Microtubule growth velocity (µm/min) measured in the presence of 10 µM or 20 µM free tubulin, and ATP or AMP-PNP, shown as a function of the Klp9 concentration (nM); n = 190–399 microtubules per condition. For (**F–H**) and (**J**), mean values and standard deviations are shown. Data from n microtubules was collected from at least three independent experiments.
The online version of this article includes the following source data and figure supplement(s) for figure 6:

**Source data 1.** Numerical data used for ***Figure 6C,F,G,H, and J***.
**Source data 2.** Numerical data used for ***Figure 6—figure supplements 2*** and ***3***.
**Figure supplement 1.** SDS-gel of purified full-length Klp9 (71 kDa) stained with Instant Blue (Euromedex).
**Figure supplement 2.** Microtubule length (µm) measured in the presence of 10 µM or 20 µM free tubulin shown as a function of the Klp9 concentration (nM); n = 190–399 microtubules per condition.
*Figure 6 continued on next page*

*Figure 6 continued*

**Figure supplement 3.** Catastrophe frequency ($min^{-1}$) measured in presence of 10 µM or 20 µM free tubulin shown as a function of the Klp9 concentration (nM); n = 190–399 microtubules per condition.

plus-end directed kinesin Kip2 (***Hibbel et al., 2015***) and *X. laevis* kinesin-5 (***Chen and Hancock, 2015***).

Surprisingly, we found that at a higher tubulin concentration (20 µM), which allowed faster microtubule growth in the control condition (3.21 ± 0.53 µm/min), Klp9 displayed the opposite effect on microtubule growth (***Figure 6I,J***, ***Figure 6—source data 1***). With increasing Klp9 concentration, the microtubule growth velocity decreased until it reached a plateau, ranging around 2.4 ± 0.5 µm/min in the presence of 100 nM Klp9 (***Figure 6J***, ***Figure 6—source data 1***). Note that this velocity was similar to the Klp9-mediated microtubule gliding velocity (***Figure 6C***). Moreover, the microtubule length decreased with increasing Klp9 concentration (***Figure 6—figure supplement 2***, ***Figure 6—source data 2***), and the catastrophe frequency did not change significantly (***Figure 6—figure supplement 3***, ***Figure 6—source data 2***).

To probe, if the effect on the microtubule growth velocity was dependent on Klp9's motor activity, we performed the polymerization assays with 0, 100, and 250 nM Klp9 in the presence of the non-hydrolysable ATP analog AMP-PNP. In the presence of 10 µM or 20 µM free tubulin, the microtubule growth velocity was not significantly different in the absence or presence of Klp9 (***Figure 6J***, ***Figure 6—source data 1***). Hence, both the Klp9-dependent increase of the microtubule growth velocity when the tubulin concentration is low, and the Klp9-dependent decrease of the microtubule growth velocity when the tubulin concentration is high, require motor activity of the kinesin-6.

The results suggest that the kinesin-6 does not only promote microtubule polymerization it can also decrease the microtubule growth velocity depending on the tubulin concentration. The kinesin-6 may thus have adopted a mechanism that allows the motor to set a definite microtubule growth velocity, close to its walking speed. To our knowledge, such behavior has not yet been described for kinesins or other MAPs.

## Discussion

This study leads to two main conclusions: (i) The localization of the kinesin-6 Klp9 to spindle microtubules at anaphase B onset requires its dephosphorylation at Cdc2-phosphosites, mediated mostly by the XMAP215 family member Dis1 (phosphorylated at Cdc2-phosphosites) and with a smaller proportion by Clp1 (homolog of Cdc14). (ii) Klp9 promotes microtubule polymerization in vivo and in vitro in a dose-dependent manner. Moreover, in vitro at high tubulin concentration, where microtubules grow comparatively fast, an increasing Klp9 concentration caused a decrease of the microtubule growth speed, suggesting that Klp9 acts as a cruise control by setting a distinct microtubule growth velocity.

### Dis1-dependent localization of Klp9 to the anaphase spindle

Members of the XMAP215/Dis1 family have been identified as MAPs that accelerate the rate of microtubule growth from yeast to human (***Al-Bassam et al., 2012***; ***Brouhard et al., 2008***; ***Charrasse et al., 1998***; ***Gard and Kirschner, 1987***; ***Kinoshita et al., 2001***; ***Matsuo et al., 2016***; ***Podolski et al., 2014***; ***Tournebize et al., 2000***). Moreover, recently XMAP215 family members have been implicated in the regulation of microtubule nucleation (***Roostalu et al., 2015***; ***Thawani et al., 2018***; ***Wieczorek et al., 2015***). These functions make XMAP215 proteins essential for proper mitotic spindle functioning, with their knockdown leading to small or disorganized spindles (***Cassimeris and Morabito, 2004***; ***Cullen et al., 1999***; ***Garcia et al., 2001***; ***Gergely et al., 2003***; ***Goshima et al., 2005***; ***Kronja et al., 2009***; ***Matthews et al., 1998***; ***Ohkura et al., 1988***; ***Reber et al., 2013***; ***Severin et al., 2001***; ***Tournebize et al., 2000***). We found that Dis1 is moreover crucial due to its function in regulating the recruitment of the mitotic kinesin-6 Klp9. *X. laevis* XMAP215 has been implicated in the recruitment of Cdc2 to spindle microtubules via interaction with cyclin B (***Charrasse et al., 2000***), yet a direct effect on mitotic motors has not been reported so far. In general, the results suggest that XMAP215 proteins may also serve as a general regulatory unit of mitotic spindle composition. How Klp9 is dephosphorylated by the phosphorylated form of Dis1

remains elusive. Dis1, phosphorylated at Cdc2-phosphosites, could mediate the activation or release of a phosphatase. It is possible that Dis1, which is still phosphorylated in late metaphase, activates a phosphatase, which subsequently dephosphorylates Klp9 at anaphase onset. Recently, similar to Dis1, the inhibitor of PP2A protein phosphatases, Sds23, has been shown to act upstream of Klp9 and regulate Klp9 recruitment to the spindle (**Schutt and Moseley, 2020**). Dis1 and Sds23 may act in the same pathway.

Besides, we were wondering about the need for such an unconventional mechanism. Why is Dis1 implicated in the regulation of Klp9 localization to the anaphase B spindle? Previously, XMAP215 has been shown to regulate mitotic spindle length (**Milunovic-Jevtic et al., 2018**; **Reber et al., 2013**). In vitro and in vivo, XMAP215 sets spindle length in a dose-dependent manner, and may thus be a crucial factor for the scaling of spindle length to cell size (**Krüger and Tran, 2020**; **Milunovic-Jevtic et al., 2018**; **Reber et al., 2013**). Similarly, Klp9 sets the speed of anaphase B spindle elongation in a dose-dependent manner (**Krüger et al., 2019**), which allows scaling of anaphase B spindle elongation velocity to spindle length and cell size (**Krüger et al., 2019**). Thus, the mechanism of Dis1 regulating the recruitment of Klp9 to the anaphase spindle could link the regulation of spindle length to the regulation of spindle elongation velocity: an increased amount of Dis1 results in the formation of longer spindles and the recruitment of more Klp9, subsequently allowing faster spindle elongation of the longer spindles. To test this hypothesis, we investigated if Dis1 indeed regulates spindle length scaling, as it has been suggested by varying the XMAP215 amounts in *X. laevis* cell extracts (**Reber et al., 2013**) or in *X. laevis* cells of the same size (**Milunovic-Jevtic et al., 2018**). *Dis1* deletion did not affect spindle length scaling in metaphase (**Figure 7—figure supplement 1**, **Figure 7—figure supplement 1—source data 1**), but strongly impacted the scaling relationship in anaphase B (**Figure 7A**). *Klp9* deletion also diminished the scaling relationship (**Figure 7A**, **Figure 7—source data 1**), either due to its function in microtubule polymerization or sliding, but deletion of *dis1* displayed an even stronger effect, reducing the slope of the linear regression from 0.5 in wild-type cells to 0.21 in *dis1* deleted cells of different sizes (**Figure 7A**, **Figure 7—source data 1**). Thus, Dis1 regulating Klp9 recruitment during anaphase B could indeed link the regulation of spindle length to the regulation of spindle elongation velocity, ensuring that shorter spindles elongate with slower speeds, and longer spindles with higher speeds, as shown previously (**Figure 7B**; **Krüger et al., 2019**). Eventually, this ensures that longer spindles accomplish chromosome segregation within the same time frame as shorter spindles, thus preventing a prolongation of mitosis, which may be harmful for cell viability (**Krüger and Tran, 2020**).

## Regulation of microtubule dynamics by kinesin-6 Klp9

The in vivo and in vitro experiments at hand strongly suggest the kinesin-6 Klp9 to be a crucial regulator of microtubule dynamics. In monopolar spindles, in the presence of Klp9, microtubule bundles grew with a velocity that matches the microtubule growth velocity expected in bipolar spindles. In the absence of Klp9, the growth velocity and length of microtubule bundles was strongly diminished, indicating that the microtubule growth necessary for anaphase B spindle elongation is promoted by the kinesin-6. This is supported by the observation that Klp9 prominently localized to and accumulated at microtubule bundle tips with anaphase B progression. Microtubule plus-end accumulation appears to be an important function for microtubule dynamics regulating kinesins (**Chen and Hancock, 2015**; **Gudimchuk et al., 2013**; **Hibbel et al., 2015**; **Varga et al., 2006**; **Varga et al., 2009**). We have not observed such a strong tip-tracking activity for other anaphase B spindle components in monopolar spindles, namely the microtubule bundler Ase1, the microtubule rescue factor CLASP, the XMAP215 protein Dis1, or the other bipolar sliding motor kinesin-5. Klp9, thus, appears to be crucial for the regulation of microtubule growth during anaphase B.

We acknowledge that the effect of *klp9* deletion is more pronounced in monopolar as compared to bipolar spindles. Spindle length and elongation velocity are diminished to a smaller degree in bipolar spindles. Additional mechanisms regulating microtubule dynamics may be at play in spindles with a midzone. For instance, CLASP is localized strongly to the antiparallel-overlapping microtubules (**Bratman and Chang, 2007**) and promotes microtubule rescue to avoid microtubules depolymerizing back to spindle poles. Due to the absence of antiparallel microtubule bundles, the activity of CLASP may be reduced in monopolar spindles and thus the effect of Klp9 is more pronounced in monopolar spindles.

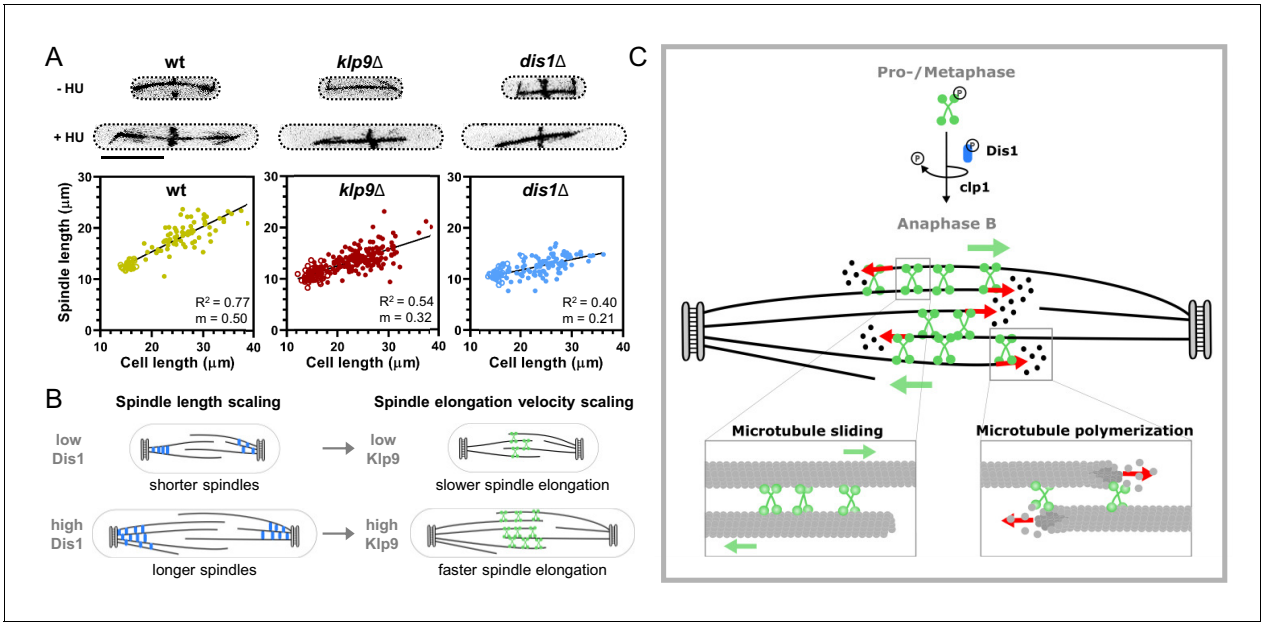


**Figure 7.** Model of Dis1-dependent Klp9 recruitment and Klp9 function during anaphase B spindle elongation. (**A**) Upper: Wild-type, *klp9*Δ and *dis1*Δ cells at the end of anaphase B expressing mCherry-Atb2 treated or not treated with hydroxyurea (HU). Addition of HU allows to block the cells in S-Phase, resulting in increased cell size. Lower: Final anaphase B spindle length plotted against cell length of wild-type, *klp9*Δ, and *dis1*Δ cells. Unfilled circles correspond to cells not treated with HU and filled circles to cells treated with HU. Data was fitted by linear regression, showing the regression coefficient $R^2$ and the slope m. (B) Schematic model of the link between spindle length and spindle elongation velocity scaling with cell size. In bigger cells the presence of higher Dis1 (blue) levels gives rise to the assembly of longer spindles as well as the recruitment of higher Klp9 (green) levels to the spindle midzone of anaphase B spindles, which subsequently results in faster spindle elongation of the longer spindles in bigger cells. (C) Model of Klp9 recruitment at anaphase onset and its function during anaphase B. Klp9 may promote spindle elongation by generating microtubule sliding forces and regulating the microtubule growth velocity.

The online version of this article includes the following source data and figure supplement(s) for figure 7:

**Source data 1.** Numerical data used for ***Figure 7A***.

**Figure supplement 1.** Wild-type, *klp9*Δ, and *dis1*Δ cells at the end of metaphase expressing mCherry-Atb2 treated or not treated with hydroxyurea (HU) and final metaphase spindle length plotted against cell length of wild-type, *klp9*Δ, and *dis1*Δ cells. .

**Figure supplement 1—source data 1.** Numerical data used for ***Figure 7—figure supplement 1***.

In vitro reconstitution experiments with recombinant full-length Klp9 provide further evidence for the sliding motors role in regulating microtubule dynamics. With low microtubule growth rates in the control condition, Klp9 increased the growth velocity in a dose-dependent manner. This has similarly been observed for the *X. laevis* kinesin-5 Eg5 (***Chen and Hancock, 2015***). The fact that not only a dimeric, but also a monomeric Eg5 construct promoted microtubule polymerization, suggests that the underlying mechanism is based on Eg5 stabilizing a straight tubulin conformation (***Chen et al., 2019***; ***Chen et al., 2016***; ***Chen and Hancock, 2015***). In solution, tubulin exhibits a curved conformation, which is not potent for microtubule lattice incorporation (***Ayaz et al., 2012***; ***McIntosh et al., 2018***; ***Rice et al., 2008***). The motor walks toward the microtubule plus-end, accumulates there by staying bound for time periods that greatly exceed the stepping duration (***Chen and Hancock, 2015***), and straightens newly added tubulin dimers, thus stabilizing lateral tubulin–tubulin interactions and promoting microtubule growth (***Chen et al., 2019***). This differs from the mechanism of microtubule polymerization proposed for members of the XMAP215 family. In contrast to kinesin-5, XMAP215 proteins show high affinity for free tubulin (***Ayaz et al., 2014***; ***Brouhard et al., 2008***). XMAP215 TOG domains are proposed to bring tubulin close to the plus-ends, so that it can be incorporated into the microtubule lattice (***Ayaz et al., 2014***; ***Brouhard et al., 2008***; ***Geyer et al., 2018***). The mode of action of kinesin-5 and XMAP215 may thus differ temporally: XMAP215 promotes tubulin dimer association with the protofilament and kinesin-5 stabilizes this association.

Interestingly, for kinesin-6, we observed that at higher microtubule growth velocities in the control condition, Klp9 displayed a negative effect on microtubule growth. Motor addition decreased the growth velocity in a dose-dependent manner at 20 µM free tubulin. Due to this observation, we hypothesize that the mechanism of microtubule growth regulation is different from the mechanisms that have been suggested for kinesin-5 (**Chen et al., 2019**; **Chen and Hancock, 2015**) or XMAP215 (**Ayaz et al., 2014**; **Brouhard et al., 2008**). First, for kinesin-5 and XMAP215, the addition of recombinant protein to higher tubulin concentrations further increases microtubule growth velocities (**Al-Bassam et al., 2012**; **Brouhard et al., 2008**; **Chen et al., 2019**). Second, the fact that microtubule growth velocities converge with the addition of Klp9 in the presence of low or high tubulin concentrations indicates that Klp9 sets a distinct microtubule growth velocity and suggests a mechanism beyond a stabilizing effect proposed for kinesin-5 (**Chen et al., 2019**) or an enhancement of tubulin dimer addition as regulated by XMAP215 (**Brouhard et al., 2008**). In contrast, to be able to accelerate and decelerate microtubule growth, Klp9 has to promote tubulin dimer addition at microtubule plus-ends, as well as to block it. This is reminiscent of the processive elongator of actin filaments formin (**Courtemanche, 2018**). Formins located at the barbed ends of actin filaments, consisting of a dimer of formin homology two domains (FH2), form a ring-like structure around the actin filament, and can accommodate a 'closed' conformation blocking actin subunit addition, or an 'open' conformation, which allows for subunit addition (**Vavylonis et al., 2006**). The equilibrium between the 'closed' and the 'open' conformation of FH2 dimers subsequently determines the rate of actin elongation (**Gurel et al., 2015**; **Kovar et al., 2006**; **Thompson et al., 2013**). Accordingly, one Klp9 molecule located at the end of each protofilament could promote the association of new tubulin dimers with a certain rate, but block the addition beyond that rate. One motorhead could be bound to the very last tubulin dimer, while the other motorhead binds free tubulin and promotes its incorporation into the microtubule lattice. How the inhibition of tubulin subunits occurs appears to be a complicated question. One possibility is that the binding of Klp9 to free curved tubulin induces a conformational change of tubulin dimers that is much more amenable for lattice incorporation. Like kinesin-5, kinesin-6 could promote tubulin dimer straightening, but unlike kinesin-5, not after lattice incorporation, but before. Even if a free tubulin dimer is in close proximity to the last tubulin dimer in the protofilament where one motorhead of Klp9 is bound, the straightened tubulin dimer bound to the other motorhead will be more potent for addition to the protofilament than a free curved tubulin dimer. Consequently, the velocity of microtubule growth may be set by the stepping rate of the motor. Accordingly, we found the reduced microtubule growth velocity in the presence of Klp9 at high tubulin concentrations to be comparable to the Klp9-mediated microtubule gliding velocity.

Given the observation that in monopolar spindles Klp9 primarily enhances microtubule growth, the question of how relevant the function of Klp9 to reduce the microtubule growth velocity of fast-growing microtubules is in vivo arises. In general, the ability of Klp9 to control the microtubule growth velocity and adjusts its speed, independent of encountering a comparatively fast- or slow-growing microtubule allows the motor to robustly coordinate the microtubule growth velocity to the microtubule sliding velocity. It is possible that in bipolar spindles additional mechanisms that regulate micrototubule dynamics are at play. Thus, also faster growing microtubules may be present in bipolar spindles. The kinesin-6 could reduce the velocity of these microtubules and adjust it to the sliding velocity. On the other hand, the motor can also increase the growth speed of slower growing microtubules and is thus able to adjust the velocity of microtubule growth to the velocity of microtubule sliding of different microtubule populations in the spindle.

Collectively, this work sheds light on the mechanism of Klp9 recruitment and function during anaphase B. Dephosphorylation of Klp9 mediated by Dis1 promotes its localization to the spindle midzone, where it can subsequently promote anaphase B spindle elongation (**Figure 7C**). This mechanism of Klp9 recruitment may link the regulation of mitotic spindle length and spindle elongation velocity to achieve scaling with cell size (**Figure 7B**). Moreover, we show that anaphase B spindle elongation is achieved not only by Klp9 generating microtubule sliding forces, as shown previously (**Fu et al., 2009**; **Rincon et al., 2017**), but also by regulating microtubule polymerization. This makes the kinesin-6 a perfect candidate responsible for the coordination of microtubule sliding and growth (**Figure 7C**). With Klp9 at the spindle midzone, the microtubule sliding velocity and the microtubule growth velocity of plus-ends located at the edge of the midzone are set with similar speeds. Last, the in vitro results suggest an unconventional mechanism of the regulation of microtubule growth. The kinesin-6 appears to not simply enhance tubulin dimer addition at microtubule

plus-ends, as suggested for other microtubule polymerases (**Ayaz et al., 2014**; **Brouhard et al., 2008**; **Chen et al., 2019**; **Chen and Hancock, 2015**), but also block tubulin dimer addition that exceeds a certain rate. Hence, Klp9 may have adopted a mechanism that is comparable to that of formins by being able to promote and block subunit addition to the filament. Eventually, Klp9 can thus set a well-defined microtubule growth velocity of slow- and fast-growing microtubules within the spindle and act as a 'cruise control' of microtubule polymerization.

## Materials and methods

### Production of *Schizosaccharomyces pombe* mutant strains

All used strains are isogenic to wild-type 972 and were obtained from genetic crosses, selected by random spore germination and replica on plates with appropriate drugs or supplements. All strains are listed in the supplementary strain list. Gene deletion and tagging was performed as described previously (**Bähler et al., 1998**).

### Fission yeast culture

All *Schizosaccharomyces pombe* strains were maintained at 25˚C and cultured in standard media. Strains were maintained on either YE5S plates or EMM plates supplemented with adenine, leucine, and uracil in the case of the Klp9 shut-off strain, at 25˚C and refreshed every third day. In general, cells were transferred into liquid YE5S and imaged the following day at exponential growth.

For overexpression of *dis1*, strains were transferred to liquid EMM supplemented with adenine, leucine, uracil, and thiamine 2 days before imaging. The following day cells were centrifuged at 3000 rpm for 5 min, washed three times with $H_2O$, and resuspended in EMM supplemented with adenine, leucine, and uracil. Following incubation at 25˚C for 18–20 hr, cells were imaged.

For shut-off of Klp9, cells were cultured in EMM supplemented with adenine, leucine, and uracil 2 days before imaging. The following day, cells were centrifuged at 3000 rpm for 5 min, resuspended in YE5S, and incubated at 25˚C for approximately 20 hr until imaging.

The generation of long cells was achieved by treatment with hydroxyurea (Sigma-Aldrich). Cells were transferred to liquid YE5S at 25˚C, and 10 mM 10 mM hydroxyurea was added when cells reached exponential growth. After incubation for 5 hr at 25˚C, cells were washed three times with $H_2O$ and resuspended in fresh YE5S. Following 1 hr at 25˚C, cells were imaged.

### Live microscopy of *S. pombe* cells

For live-cell imaging, fission yeast cells were mounted on YE5S agarose pads, containing 2% agarose (**Tran et al., 2004**). Temperature-sensitive *cut7-24* and *sad1-1* mutants were incubated at the microscope, which is equipped with a cage incubator (Life Imaging Services), at 37˚C for 1 hr before imaging was started. All other strains were imaged at 25˚C.

Images were acquired on an inverted Eclipse Ti-E microscope (Nikon) with a spinning disk CSU-22 (Yokogawa), equipped with a Plan Apochromat 100×/1.4 NA objective lens (Nikon), a PIFOC (perfect image focus) objective stepper, a Mad City Lab piezo stage, and an electron-multiplying charge-couple device camera (EMCCD 512 × 512 Evolve, Photometrics).

Stacks of seven planes spaced by 1 µm were acquired for each channel with 100 ms exposure time, binning one and an electronic gain of 300 for both wavelengths. For each time-lapse movie, an image was taken every minute for 90–120 min.

### Construction, expression, and purification of recombinant Klp9

For construction of a plasmid containing full-length Klp9, *klp9* cDNA was amplified from a cDNA library (**Hoffman et al., 2015**) and cloned into pET28a(+) between NcoI and NotI restriction sites, incorporating a C-terminal His6 tag.

For Klp9 purification *E. coli* NiCO21 (DE3), cells were transfected with pET28a-Klp9-His6 and grown in standard 2xYT medium. Following cell lysis and centrifugation, the supernatant was incubated with chitin resin (New England Biolabs) for 45 min at 4˚C and eluted on a gravity flow column. The protein solution was then loaded on an HiTrap IMAC HP column (GE Healthcare). Further purification of the Klp9-containing fractions was achieved by gel filtration using a Superdex 200 26/60

column equilibrated with a buffer containing 20 mM HEPES pH 8, 150 mM NaCl, 2 mM $MgCl_2$, 0.2 mM ADP, 0.5 mM TCEP, 0.5 mM PMSF, and 10% glycerol.

## Tubulin purification

Tubulin from fresh bovine brain was purified by three cycles of temperature-dependent assembly and disassembly in BRB80 buffer. Labeling of tubulin with ATTO-488, ATTO-647, or biotin was performed as previously described (***Hyman et al., 1991***).

## In vitro microtubule gliding assays

Taxol-stabilized microtubules were prepared by incubating 56 µM unlabeled tubulin and 14 µM ATTO-647-labeled tubulin in BRB80 (80 mM piperazineN,N[prime]-bis(2-ethanesulfonic acid [PIPES]) pH 6.8, 1 mM EGTA, 1 mM $MgCl_2$) with 20 mM $MgCl_2$, 10 mM GTP, and 25% DMSO in BRB80 at room temperature. The mixture was then diluted 1:111 with 10 µM taxol in BRB80.

The flow chamber was assembled from microscopy slides and glass coverslips cleaned sequentially in acetone in a sonication bath and in ethanol. Then, 0.1 mg/ml Anti-$His_6$ (Sigma-Aldrich) was added to the flow chamber, followed by 30 µM recombinant Klp9. Upon subsequent incubation of the flow chamber with taxol-stabilized microtubules, a buffer containing 0.5% methylcellulose, 125 mM KCl, 12.5 mM $MgCl_2$, 2.5 mM EGTA, 16.6 mM Hepes pH 7.5, 3 mg/ml glucose, 0.1 mg/ml glucose oxydase, 0.03 mg/ml catalase, 8.5 mM ATP, and 0.3% BSA was added and the flow chamber was sealed with vacuum grease. Imaging was performed immediately after at 30˚C at the TIRF microscope.

## In vitro microtubule dynamics assays

GMPCPP-stabilized microtubule seeds were prepared by incubating a mixture of 7 µM biotinylated tubulin, 3 µM ATTO-647-labeled tubulin, and 0.5 mM GMPCPP (Interchim) in 1xBRB80 for 1 hr at 37˚C. Following, 2.5 µM taxol was added and the mix was incubated for 20 min at room temperature (RT). After centrifugation at 14,000 rpm for 10 min the supernatant was removed and the pellet resuspended in a mix containing 2.5 µM taxol and 0.5 µM GMPCPP in 1xBRB80. The seeds were then snap frozen in liquid nitrogen and stored at −80˚C.

Flow chambers were assembled from microscopy slides and glass coverslips with double-sticky tape with three independent lanes, allowing the analysis of three different reaction mixtures in the same flow chamber. Slides and coverslips were cleaned sequentially in acetone in a sonication bath, in ethanol, in 2% Hellmanex (Sigma-Aldrich) and using a plasma-cleaner. Functionalization was achieved by sequential incubation with 1 mg/ml PEG-Silane (30 K, Creative PEGWorks) for microscopy slides or 0.8 mg/ml PEG-Silane and 0.2 mg/ml Biotin-PEG-Silane (5 K, Creative PEGWorks) for coverslips and 0.05 mg/ml NeutrAvidin (Invitrogen) in G-Buffer (2 mM Tris–Cl pH 8, 0.2 mM ATP, 0.5 mM DTT, 0.1 mM $CaCl_2$, 1 mM NaAzide, 6.7 mM Hepes pH 7.5, 50 mM KCl, 5 mM $MgCl_2$, and 1 mM EGTA). Attachment of microtubule seeds to the coverslip was achieved through biotin-neutrAvidin interaction. The reaction mixture with or without Klp9 in G-Buffer contained a tubulin mix (80% unlabeled tubulin, 20% 488-labeled tubulin in BRB80) 0.5% methylcellulose, 50 mM KCl, 5 mM $MgCl_2$, 1 mM EGTA, 6.6 mM Hepes pH 7.5, 3 mg/ml glucose, 0.1 mg/ml glucose oxydase, 0.03 mg/ml Catalase, 6.6 mM Tris–Cl pH 8, 0.65 mM ATP, 1 mM GTP, 11.5 mM DTT, 0.3 mM $CaCl_2$, 3.3 mM NaAzide, 0.1% BSA. The mixture was added to the flow chamber, which was then sealed with vacuum grease, and the dynamic microtubules were imaged immediately at 30˚C at the TIRF microscope.

## TIRF microscopy

In vitro reconstitution assays were imaged on an inverted Eclipse Ti-E (Nikon) equipped with Perfect Focus System (PFS 2, Nikon), a CFI Plan Apo TIRF 100×/1.49 N.A oil objective (Nikon), an TIRF-E motorized TIRF illuminator, and an EMCCD Evolve camera (Photometrics). For excitation, 491 nm 42 mW and 642 nm 480 mW (Gataca Systems) were used. The temperature was controlled with a cage incubator (Life Imaging Services).

For microtubule gliding and microtubule dynamics assays, movies of 5 min duration with 1 s interval were acquired.

### Image analysis

Using Metamorph 7.2, maximum projections of each stack were performed for the analysis of spindle dynamics and for presentation and sum projections for intensity measurements.

Spindle and bundle dynamics were examined by the length of the mCherry-Atb2 signal over time. Metaphase and anaphase spindle length refer to the final spindle length of each phase.

Intensity measurements were performed by drawing a region around the area of interest, reading out the average intensity per pixel, subtracting the background, and multiplying this value with the size of the area. Intensity profiles along microtubule bundles or along the bipolar spindle were obtained by drawing a line along the bundle/spindle and reading out the intensity values for each pixel along the line, from which the background intensity was subtracted.

The microtubule gliding velocity in the in vitro assays was revealed by constructing kymographs of the moving microtubules using Metamorph and calculation of the velocity by the microtubule displacement within each 5 min movie.

To analyze microtubule dynamics, parameters of individual microtubules growing from GMPCPP-seed kymographs were constructed with Metamorph. For each microtubule, a kymograph was constructed, and the slope of growth and shrinkage events as well as the microtubule length, corresponding to the length of a microtubule before undergoing catastrophe, was analyzed. The catastrophe frequency was calculated by the number of catastrophe events per microtubule within the 5 min movie divided by the total time the microtubule spent growing.

### Quantification and statistical analysis

Sample number, replicates, and error bars are indicated in the figure legends. All statistical analysis and regression analysis were performed using GraphPad Prism 7. Corresponding details for statistical tests and p-values are included in the figures and/or figure legends.

## Acknowledgements

We thank Manuel Lera Ramirez and Ana Loncar for discussions and critical reading of the manuscript. We thank Moutse Ranaivoson for help with the Klp9 purification. We thank Vincent Fraisier and Lucy Sengmanivong for the maintenance of microscopes at the PICT-IBiSA Imaging facility (Institut Curie), a member of the France-BioImaging national research infrastructure. We thank the Japan National BioResource Project – Yeast Genetic Resource Center (Osaka City University, Osaka University and Hiroshima University) for providing strains. We thank Chris Norbury (Oxford University) for generously providing the *S. pombe* cDNA library.

## Additional information

### Funding


| Funder | Grant reference number | Author |
|---|---|---|
| Ministère de l'enseignement supérieur et de la recherche | | Lara Katharina Krüger |
| Fondation ARC pour la Recherche sur le Cancer | | Lara Katharina Krüger<br>Phong T Tran |
| Ligue Contre le Cancer | | Phong T Tran |
| INCA | | Phong T Tran |
| European Research Council | Grant 771599 ICEBERG | Manuel Théry |

The funders had no role in study design, data collection and interpretation, or the decision to submit the work for publication.


### Author contributions

Lara Katharina Krüger, Conceptualization, Data curation, Formal analysis, Validation, Investigation, Visualization, Methodology, Writing - original draft, Writing - review and editing; Matthieu Gélin, Investigation, Methodology; Liang Ji, Resources; Carlos Kikuti, Methodology, Writing - review and

editing; Anne Houdusse, Resources, Writing - review and editing; Manuel Théry, Laurent Blanchoin, Resources, Supervision, Writing - review and editing; Phong T Tran, Resources, Supervision, Funding acquisition, Project administration, Writing - review and editing


### Author ORCIDs

Lara Katharina Krüger https://orcid.org/0000-0002-0439-951X
Anne Houdusse http://orcid.org/0000-0002-8566-0336
Laurent Blanchoin http://orcid.org/0000-0001-8146-9254
Phong T Tran https://orcid.org/0000-0002-2410-2277



### Decision letter and Author response

Decision letter https://doi.org/10.7554/eLife.67489.sa1
Author response https://doi.org/10.7554/eLife.67489.sa2


## Additional files

### Supplementary files

- Supplementary file 1. List of *S. pombe* strains used in this study.
- Transparent reporting form

### Data availability

A source data file for all data sets used in Figure 1–7 has been provided.

## References


**Aist JR**, Liang H, Berns MW. 1993. Astral and spindle forces in PtK2 cells during anaphase B: a laser microbeam study. *Journal of Cell Science* **104 ( Pt 4**:1207–1216. PMID: 8314902

**Al-Bassam J**, Kim H, Flor-Parra I, Lal N, Velji H, Chang F. 2012. Fission yeast Alp14 is a dose-dependent plus end-tracking microtubule polymerase. *Molecular Biology of the Cell* **23**:2878–2890. DOI: https://doi.org/10.1091/mbc.e12-03-0205, PMID: 22696680

**Aoki K**, Nakaseko Y, Kinoshita K, Goshima G, Yanagida M. 2006. CDC2 phosphorylation of the fission yeast dis1 ensures accurate chromosome segregation. *Current Biology* **16**:1627–1635. DOI: https://doi.org/10.1016/j.cub.2006.06.065, PMID: 16920624

**Avunie-Masala R**, Movshovich N, Nissenkorn Y, Gerson-Gurwitz A, Fridman V, Kõivomägi M, Loog M, Hoyt MA, Zaritsky A, Gheber L. 2011. Phospho-regulation of kinesin-5 during anaphase spindle elongation. *Journal of Cell Science* **124**:873–878. DOI: https://doi.org/10.1242/jcs.077396, PMID: 21378308

**Ayaz P**, Ye X, Huddleston P, Brautigam CA, Rice LM. 2012. A TOG:αβ-tubulin complex structure reveals conformation-based mechanisms for a microtubule polymerase. *Science* **337**:857–860. DOI: https://doi.org/10.1126/science.1221698, PMID: 22904013

**Ayaz P**, Munyoki S, Geyer EA, Piedra FA, Vu ES, Bromberg R, Otwinowski Z, Grishin NV, Brautigam CA, Rice LM. 2014. A tethered delivery mechanism explains the catalytic action of a microtubule polymerase. *eLife* **3**:e03069. DOI: https://doi.org/10.7554/eLife.03069, PMID: 25097237

**Bähler J**, Wu J-Q, Longtine MS, Shah NG, Mckenzie III A, Steever AB, Wach A, Philippsen P, Pringle JR. 1998. Heterologous modules for efficient and versatile PCR-based gene targeting in *Schizosaccharomyces pombe*. *Yeast* **14**:943–951. DOI: https://doi.org/10.1002/(SICI)1097-0061(199807)14:10<943::AID-YEA292>3.0.CO;2-Y

**Bieling P**, Laan L, Schek H, Munteanu EL, Sandblad L, Dogterom M, Brunner D, Surrey T. 2007. Reconstitution of a microtubule plus-end tracking system in vitro. *Nature* **450**:1100–1105. DOI: https://doi.org/10.1038/nature06386, PMID: 18059460

**Bratman SV**, Chang F. 2007. Stabilization of overlapping microtubules by fission yeast CLASP. *Developmental Cell* **13**:812–827. DOI: https://doi.org/10.1016/j.devcel.2007.10.015, PMID: 18061564

**Brouhard GJ**, Stear JH, Noetzel TL, Al-Bassam J, Kinoshita K, Harrison SC, Howard J, Hyman AA. 2008. XMAP215 is a processive microtubule polymerase. *Cell* **132**:79–88. DOI: https://doi.org/10.1016/j.cell.2007.11.043, PMID: 18191222

**Brust-Mascher I**, Sommi P, Cheerambathur DK, Scholey JM. 2009. Kinesin-5-dependent poleward flux and spindle length control in *Drosophila* embryo mitosis. *Molecular Biology of the Cell* **20**:1749–1762. DOI: https://doi.org/10.1091/mbc.e08-10-1033, PMID: 19158379

**Cande WZ**, McDonald KL. 1985. In vitro reactivation of anaphase spindle elongation using isolated diatom spindles. *Nature* **316**:168–170. DOI: https://doi.org/10.1038/316168a0

**Cande WZ**, McDonald K. 1986. Physiological and ultrastructural analysis of elongating mitotic spindles reactivated in vitro. *Journal of Cell Biology* **103**:593–604. DOI: https://doi.org/10.1083/jcb.103.2.593, PMID: 3733882

**Cassimeris L**, Morabito J. 2004. TOGp, the human homolog of XMAP215/Dis1, is required for centrosome integrity, spindle pole organization, and bipolar spindle assembly. *Molecular Biology of the Cell* **15**:1580–1590. DOI: https://doi.org/10.1091/mbc.e03-07-0544, PMID: 14718566

**Charrasse S**, Schroeder M, Gauthier-Rouviere C, Ango F, Cassimeris L, Gard DL, Larroque C. 1998. The TOGp protein is a new human microtubule-associated protein homologous to the *Xenopus* XMAP215. *Journal of Cell Science* **111 ( Pt 10**:1371–1383. DOI: https://doi.org/10.1242/jcs.111.10.1371, PMID: 9570755

**Charrasse S**, Lorca T, Dorée M, Larroque C. 2000. The *Xenopus* XMAP215 and its human homologue TOG proteins interact with cyclin B1 to target p34cdc2 to microtubules during mitosis. *Experimental Cell Research* **254**:249–256. DOI: https://doi.org/10.1006/excr.1999.4740, PMID: 10640423

**Cheerambathur DK**, Civelekoglu-Scholey G, Brust-Mascher I, Sommi P, Mogilner A, Scholey JM. 2007. Quantitative analysis of an anaphase B switch: predicted role for a microtubule catastrophe gradient. *Journal of Cell Biology* **177**:995–1004. DOI: https://doi.org/10.1083/jcb.200611113, PMID: 17576796

**Chen GY**, Mickolajczyk KJ, Hancock WO. 2016. The Kinesin-5 chemomechanical cycle is dominated by a Two-heads-bound state. *Journal of Biological Chemistry* **291**:20283–20294. DOI: https://doi.org/10.1074/jbc.M116.730697, PMID: 27402829

**Chen GY**, Cleary JM, Asenjo AB, Chen Y, Mascaro JA, Arginteanu DFJ, Sosa H, Hancock WO. 2019. Kinesin-5 promotes microtubule nucleation and assembly by stabilizing a Lattice-Competent conformation of tubulin. *Current Biology* **29**:2259–2269. DOI: https://doi.org/10.1016/j.cub.2019.05.075, PMID: 31280993

**Chen Y**, Hancock WO. 2015. Kinesin-5 is a microtubule polymerase. *Nature Communications* **6**:1–10. DOI: https://doi.org/10.1038/ncomms9160

**Costa J**, Fu C, Syrovatkina V, Tran PT. 2013. Imaging individual spindle microtubule dynamics in fission yeast. *Methods in Cell Biology* **115**:385–394. DOI: https://doi.org/10.1016/B978-0-12-407757-7.00024-4, PMID: 23973085

**Courtemanche N**. 2018. Mechanisms of formin-mediated actin assembly and dynamics. *Biophysical Reviews* **10**:1553–1569. DOI: https://doi.org/10.1007/s12551-018-0468-6, PMID: 30392063

**Cullen CF**, Deák P, Glover DM, Ohkura H. 1999. Mini spindles: a gene encoding a conserved microtubule-associated protein required for the integrity of the mitotic spindle in *Drosophila*. *The Journal of Cell Biology* **146**:1005–1018. DOI: https://doi.org/10.1083/jcb.146.5.1005, PMID: 10477755

**Decottignies A**, Zarzov P, Nurse P. 2001. In vivo localisation of fission yeast cyclin-dependent kinase cdc2p and cyclin B cdc13p during mitosis and meiosis. *Journal of Cell Science* **114**:2627–2640. DOI: https://doi.org/10.1242/jcs.114.14.2627, PMID: 11683390

**des Georges A**, Katsuki M, Drummond DR, Osei M, Cross RA, Amos LA. 2008. Mal3, the *Schizosaccharomyces pombe* homolog of EB1, changes the microtubule lattice. *Nature Structural & Molecular Biology* **15**:1102–1108. DOI: https://doi.org/10.1038/nsmb.1482, PMID: 18794845

**Ding R**, McDonald KL, McIntosh JR. 1993. Three-dimensional reconstruction and analysis of mitotic spindles from the yeast, *Schizosaccharomyces pombe*. *Journal of Cell Biology* **120**:141–151. DOI: https://doi.org/10.1083/jcb.120.1.141, PMID: 8416984

**Edamatsu M**. 2014. Bidirectional motility of the fission yeast kinesin-5, Cut7. *Biochemical and Biophysical Research Communications* **446**:231–234. DOI: https://doi.org/10.1016/j.bbrc.2014.02.106, PMID: 24589736

**Euteneuer U**, Jackson WT, McIntosh JR. 1982. Polarity of spindle microtubules in Haemanthus endosperm. *Journal of Cell Biology* **94**:644–653. DOI: https://doi.org/10.1083/jcb.94.3.644, PMID: 7130276

**Fink G**, Schuchardt I, Colombelli J, Stelzer E, Steinberg G. 2006. Dynein-mediated pulling forces drive rapid mitotic spindle elongation in *Ustilago maydis*. *The EMBO Journal* **25**:4897–4908. DOI: https://doi.org/10.1038/sj.emboj.7601354, PMID: 17024185

**Fu C**, Ward JJ, Loiodice I, Velve-Casquillas G, Nedelec FJ, Tran PT. 2009. Phospho-regulated interaction between kinesin-6 Klp9p and microtubule bundler Ase1p promotes spindle elongation. *Developmental Cell* **17**:257–267. DOI: https://doi.org/10.1016/j.devcel.2009.06.012, PMID: 19686686

**Garcia MA**, Vardy L, Koonrugsa N, Toda T. 2001. Fission yeast ch-TOG/XMAP215 homologue Alp14 connects mitotic spindles with the kinetochore and is a component of the Mad2-dependent spindle checkpoint. *The EMBO Journal* **20**:3389–3401. DOI: https://doi.org/10.1093/emboj/20.13.3389, PMID: 11432827

**Gard DL**, Kirschner MW. 1987. A microtubule-associated protein from *Xenopus* eggs that specifically promotes assembly at the plus-end. *Journal of Cell Biology* **105**:2203–2215. DOI: https://doi.org/10.1083/jcb.105.5.2203

**Gergely F**, Draviam VM, Raff JW. 2003. The ch-TOG/XMAP215 protein is essential for spindle pole organization in human somatic cells. *Genes & Development* **17**:336–341. DOI: https://doi.org/10.1101/gad.245603, PMID: 12569123

**Geyer EA**, Miller MP, Brautigam CA, Biggins S, Rice LM. 2018. Design principles of a microtubule polymerase. *eLife* **7**:e34574. DOI: https://doi.org/10.7554/eLife.34574, PMID: 29897335

**Goshima G**, Wollman R, Stuurman N, Scholey JM, Vale RD. 2005. Length control of the metaphase spindle. *Current Biology* **15**:1979–1988. DOI: https://doi.org/10.1016/j.cub.2005.09.054, PMID: 16303556

**Grill SW**, Gönczy P, Stelzer EHK, Hyman AA. 2001. Polarity controls forces governing asymmetric spindle positioning in the *Caenorhabditis elegans* embryo. *Nature* **409**:630–633. DOI: https://doi.org/10.1038/35054572

**Gudimchuk N**, Vitre B, Kim Y, Kiyatkin A, Cleveland DW, Ataullakhanov FI, Grishchuk EL. 2013. Kinetochore kinesin CENP-E is a processive bi-directional tracker of dynamic microtubule tips. *Nature Cell Biology* **15**:1079–1088. DOI: https://doi.org/10.1038/ncb2831, PMID: 23955301

**Gurel PS**, Mu A, Guo B, Shu R, Mierke DF, Higgs HN. 2015. Assembly and turnover of short actin filaments by the formin INF2 and profilin. *Journal of Biological Chemistry* **290**:22494–22506. DOI: https://doi.org/10.1074/jbc.M115.670166, PMID: 26124273

**Hagan I**, Yanagida M. 1990. Novel potential mitotic motor protein encoded by the fission yeast cut7+ gene. *Nature* **347**:563–566. DOI: https://doi.org/10.1038/347563a0, PMID: 2145514

**Hagan I**, Yanagida M. 1992. Kinesin-related cut7 protein associates with mitotic and meiotic spindles in fission yeast. *Nature* **356**:74–76. DOI: https://doi.org/10.1038/356074a0, PMID: 1538784

**Hagan I**, Yanagida M. 1995. The product of the spindle formation gene sad1+ associates with the fission yeast spindle pole body and is essential for viability. *Journal of Cell Biology* **129**:1033–1047. DOI: https://doi.org/10.1083/jcb.129.4.1033, PMID: 7744953

**Hibbel A**, Bogdanova A, Mahamdeh M, Jannasch A, Storch M, Schäffer E, Liakopoulos D, Howard J. 2015. Kinesin Kip2 enhances microtubule growth in vitro through length-dependent feedback on polymerization and catastrophe. *eLife* **4**:e10542. DOI: https://doi.org/10.7554/eLife.10542, PMID: 26576948

**Hoffman CS**, Wood V, Fantes PA. 2015. An ancient yeast for young geneticists: a primer on the *Schizosaccharomyces pombe* model system. *Genetics* **201**:403–423. DOI: https://doi.org/10.1534/genetics.115.181503, PMID: 26447128

**Hu CK**, Coughlin M, Field CM, Mitchison TJ. 2011. KIF4 regulates midzone length during cytokinesis. *Current Biology : CB* **21**:815–824. DOI: https://doi.org/10.1016/j.cub.2011.04.019, PMID: 21565503

**Hussmann F**, Drummond DR, Peet DR, Martin DS, Cross RA. 2016. Alp7/TACC-Alp14/TOG generates long-lived, fast-growing MTs by an unconventional mechanism. *Scientific Reports* **6**:1–15. DOI: https://doi.org/10.1038/srep20653, PMID: 26864000

**Hyman A**, Drechsel D, Kellogg D, Salser S, Sawin K, Steffen P, Wordeman L, Mitchison T. 1991. Preparation of modified tubulins. *Methods in enzymology* **196**:478–485. DOI: https://doi.org/10.1016/0076-6879(91)96041-o, PMID: 2034137

**Janson ME**, Loughlin R, Loïodice I, Fu C, Brunner D, Nédélec FJ, Tran PT. 2007. Crosslinkers and motors organize dynamic microtubules to form stable bipolar arrays in fission yeast. *Cell* **128**:357–368. DOI: https://doi.org/10.1016/j.cell.2006.12.030, PMID: 17254972

**Kapitein LC**, Peterman EJ, Kwok BH, Kim JH, Kapoor TM, Schmidt CF. 2005. The bipolar mitotic kinesin Eg5 moves on both microtubules that it crosslinks. *Nature* **435**:114–118. DOI: https://doi.org/10.1038/nature03503, PMID: 15875026

**Katsuki M**, Drummond DR, Osei M, Cross RA. 2009. Mal3 masks catastrophe events in *Schizosaccharomyces pombe* microtubules by inhibiting shrinkage and promoting rescue. *Journal of Biological Chemistry* **284**:29246–29250. DOI: https://doi.org/10.1074/jbc.C109.052159, PMID: 19740752

**Khodjakov A**, La Terra S, Chang F. 2004. Laser microsurgery in fission yeast; role of the mitotic spindle midzone in anaphase B. *Current Biology : CB* **14**:1330–1340. DOI: https://doi.org/10.1016/j.cub.2004.07.028, PMID: 15296749

**Kinoshita K**, Arnal I, Desai A, Drechsel DN, Hyman AA. 2001. Reconstitution of physiological microtubule dynamics using purified components. *Science* **294**:1340–1343. DOI: https://doi.org/10.1126/science.1064629, PMID: 11701928

**Kinoshita K**, Noetzel TL, Pelletier L, Mechtler K, Drechsel DN, Schwager A, Lee M, Raff JW, Hyman AA. 2005. Aurora A phosphorylation of TACC3/maskin is required for centrosome-dependent microtubule assembly in mitosis. *Journal of Cell Biology* **170**:1047–1055. DOI: https://doi.org/10.1083/jcb.200503023, PMID: 16172205

**Kiyomitsu T**, Cheeseman IM. 2013. Cortical dynein and asymmetric membrane elongation coordinately position the spindle in anaphase. *Cell* **154**:391–402. DOI: https://doi.org/10.1016/j.cell.2013.06.010, PMID: 23870127

**Kovar DR**, Harris ES, Mahaffy R, Higgs HN, Pollard TD. 2006. Control of the assembly of ATP- and ADP-actin by formins and profilin. *Cell* **124**:423–435. DOI: https://doi.org/10.1016/j.cell.2005.11.038, PMID: 16439214

**Kronja I**, Kruljac-Letunic A, Caudron-Herger M, Bieling P, Karsenti E. 2009. XMAP215-EB1 interaction is required for proper spindle assembly and chromosome segregation in *Xenopus* egg extract. *Molecular Biology of the Cell* **20**:2684–2696. DOI: https://doi.org/10.1091/mbc.e08-10-1051, PMID: 19369422

**Krüger LK**, Sanchez JL, Paoletti A, Tran PT. 2019. Kinesin-6 regulates cell-size-dependent spindle elongation velocity to keep mitosis duration constant in fission yeast. *eLife* **8**:e42182. DOI: https://doi.org/10.7554/eLife.42182, PMID: 30806623

**Krüger LK**, Tran PT. 2020. Spindle scaling mechanisms. *Essays in Biochemistry* **64**:383–396. DOI: https://doi.org/10.1042/EBC20190064, PMID: 32501481

**Lioutas A**, Vernos I. 2013. Aurora A kinase and its substrate TACC3 are required for central spindle assembly. *EMBO Reports* **14**:829–836. DOI: https://doi.org/10.1038/embor.2013.109, PMID: 23887685

**Loïodice I**, Staub J, Setty TG, Nguyen NP, Paoletti A, Tran PT. 2005. Ase1p organizes antiparallel microtubule arrays during interphase and mitosis in fission yeast. *Molecular Biology of the Cell* **16**:1756–1768. DOI: https://doi.org/10.1091/mbc.e04-10-0899, PMID: 15689489

**Loncar A**, Rincon SA, Lera Ramirez M, Paoletti A, Tran PT. 2020. Kinesin-14 family proteins and microtubule dynamics define *S. pombe* mitotic and meiotic spindle assembly, and elongation. *Journal of Cell Science* **133**:jcs240234. DOI: https://doi.org/10.1242/jcs.240234, PMID: 32327557

**Mallavarapu A**, Sawin K, Mitchison T. 1999. A switch in Microtubule dynamics at the onset of anaphase B in the mitotic spindle of *Schizosaccharomyces pombe*. *Current Biology* **9**:1423–1428. DOI: https://doi.org/10.1016/S0960-9822(00)80090-1, PMID: 10607565

**Mastronarde DN**, McDonald KL, Ding R, McIntosh JR. 1993. Interpolar spindle microtubules in PTK cells. *Journal of Cell Biology* **123**:1475–1489. DOI: https://doi.org/10.1083/jcb.123.6.1475, PMID: 8253845

**Masuda H**. 1995. The formation and functioning of yeast mitotic spindles. *BioEssays : news and reviews in molecular, cellular and developmental biology* **17**:45–51. DOI: https://doi.org/10.1002/bies.950170110, PMID: 7702593

**Masuda H**, Cande WZ. 1987. The role of tubulin polymerization during spindle elongation in vitro. *Cell* **49**:193–202. DOI: https://doi.org/10.1016/0092-8674(87)90560-5, PMID: 2882855

**Maton G**, Edwards F, Lacroix B, Stefanutti M, Laband K, Lieury T, Kim T, Espeut J, Canman JC, Dumont J. 2015. Kinetochore components are required for central spindle assembly. *Nature cell biology* **17**:697–705. DOI: https://doi.org/10.1038/ncb3150, PMID: 25866924

**Matsuo Y**, Maurer SP, Yukawa M, Zakian S, Singleton MR, Surrey T, Toda T. 2016. An unconventional interaction between Dis1/TOG and Mal3/EB1 promotes the fidelity of chromosome segregation. *Journal of Cell Science* **17**:4592–4606. DOI: https://doi.org/10.1242/jcs.197533

**Matthews LR**, Carter P, Thierry-Mieg D, Kemphues K. 1998. ZYG-9, A *Caenorhabditis elegans* protein required for microtubule organization and function, is a component of meiotic and mitotic spindle poles. *Journal of Cell Biology* **141**:1159–1168. DOI: https://doi.org/10.1083/jcb.141.5.1159

**McDonald K**, Pickett-Heaps JD, McIntosh JR, Tippit DH. 1977. On the mechanism of anaphase spindle elongation in Diatoma vulgare. *Journal of Cell Biology* **74**:377–388. DOI: https://doi.org/10.1083/jcb.74.2.377, PMID: 885908

**McIntosh JR**, O'Toole E, Morgan G, Austin J, Ulyanov E, Ataullakhanov F, Gudimchuk N. 2018. Microtubules grow by the addition of bent guanosine triphosphate tubulin to the tips of curved protofilaments. *Journal of Cell Biology* **217**:2691–2708. DOI: https://doi.org/10.1083/jcb.201802138, PMID: 29794031

**McIntosh JR**, Landis SC. 1971. The distribution of spindle microtubules during mitosis in cultured human cells. *Journal of Cell Biology* **49**:468–497. DOI: https://doi.org/10.1083/jcb.49.2.468, PMID: 19866774

**Meadows JC**, Lancaster TC, Buttrick GJ, Sochaj AM, Messin LJ, Del Mar Mora-Santos M, Hardwick KG, Millar JBA. 2017. Identification of a Sgo2-Dependent but Mad2-Independent pathway controlling anaphase onset in fission yeast. *Cell Reports* **18**:1422–1433. DOI: https://doi.org/10.1016/j.celrep.2017.01.032, PMID: 28178520

**Milunovic-Jevtic A**, Jevtic P, Levy DL, Gatlin JC. 2018. In vivo mitotic spindle scaling can be modulated by changing the levels of a single protein: the microtubule polymerase XMAP215. *Molecular Biology of the Cell* **29**:1311–1317. DOI: https://doi.org/10.1091/mbc.E18-01-0011, PMID: 29851557

**Nabeshima K**, Kurooka H, Takeuchi M, Kinoshita K, Nakaseko Y, Yanagida M. 1995. p93dis1, which is required for sister chromatid separation, is a novel microtubule and spindle pole body-associating protein phosphorylated at the Cdc2 target sites. *Genes & Development* **9**:1572–1585. DOI: https://doi.org/10.1101/gad.9.13.1572, PMID: 7628693

**Nabeshima K**, Nakagawa T, Straight AF, Murray A, Chikashige Y, Yamashita YM, Hiraoka Y, Yanagida M. 1998. Dynamics of centromeres during metaphase-anaphase transition in fission yeast: dis1 is implicated in force balance in metaphase bipolar spindle. *Molecular Biology of the Cell* **9**:3211–3225. DOI: https://doi.org/10.1091/mbc.9.11.3211, PMID: 9802907

**Oegema K**, Desai A, Rybina S, Kirkham M, Hyman AA. 2001. Functional analysis of kinetochore assembly in *Caenorhabditis elegans*. *Journal of Cell Biology* **153**:1209–1226. DOI: https://doi.org/10.1083/jcb.153.6.1209, PMID: 11402065

**Ohkura H**, Adachi Y, Kinoshita N, Niwa O, Toda T, Yanagida M. 1988. Cold-sensitive and caffeine-supersensitive mutants of the *Schizosaccharomyces pombe* dis genes implicated in sister chromatid separation during mitosis. *The EMBO Journal* **7**:1465–1473. DOI: https://doi.org/10.1002/j.1460-2075.1988.tb02964.x, PMID: 3409871

**Olmsted ZT**, Colliver AG, Riehlman TD, Paluh JL. 2014. Kinesin-14 and kinesin-5 antagonistically regulate microtubule nucleation by γ-TuRC in yeast and human cells. *Nature Communications* **5**:1–15. DOI: https://doi.org/10.1038/ncomms6339

**Pereira AL**, Pereira AJ, Maia AR, Drabek K, Sayas CL, Hergert PJ, Lince-Faria M, Matos I, Duque C, Stepanova T, Rieder CL, Earnshaw WC, Galjart N, Maiato H. 2006. Mammalian CLASP1 and CLASP2 cooperate to ensure mitotic fidelity by regulating spindle and kinetochore function. *Molecular Biology of the Cell* **17**:4526–4542. DOI: https://doi.org/10.1091/mbc.e06-07-0579, PMID: 16914514

**Peset I**, Seiler J, Sardon T, Bejarano LA, Rybina S, Vernos I. 2005. Function and regulation of Maskin, a TACC family protein, in microtubule growth during mitosis. *Journal of Cell Biology* **170**:1057–1066. DOI: https://doi.org/10.1083/jcb.200504037, PMID: 16172207

**Podolski M**, Mahamdeh M, Howard J. 2014. Stu2, the budding yeast XMAP215/Dis1 homolog, promotes assembly of yeast microtubules by increasing growth rate and decreasing catastrophe frequency. *Journal of Biological Chemistry* **289**:28087–28093. DOI: https://doi.org/10.1074/jbc.M114.584300, PMID: 25172511

**Reber SB**, Baumgart J, Widlund PO, Pozniakovsky A, Howard J, Hyman AA, Jülicher F. 2013. XMAP215 activity sets spindle length by controlling the total mass of spindle microtubules. *Nature Cell Biology* **15**:1116–1122. DOI: https://doi.org/10.1038/ncb2834, PMID: 23974040

**Redemann S**, Baumgart J, Lindow N, Shelley M, Nazockdast E, Kratz A, Prohaska S, Brugués J, Fürthauer S, Müller-Reichert T. 2017. *C. elegans* chromosomes connect to centrosomes by anchoring into the spindle network. *Nature Communications* **8**:1–13. DOI: https://doi.org/10.1038/ncomms15288, PMID: 28492281

**Rice LM**, Montabana EA, Agard DA. 2008. The lattice as allosteric effector: structural studies of alphabeta- and gamma-tubulin clarify the role of GTP in microtubule assembly. *PNAS* **105**:5378–5383. DOI: https://doi.org/10.1073/pnas.0801155105, PMID: 18388201

**Rincon SA**, Lamson A, Blackwell R, Syrovatkina V, Fraisier V, Paoletti A, Betterton MD, Tran PT. 2017. Kinesin-5-independent mitotic spindle assembly requires the antiparallel microtubule crosslinker Ase1 in fission yeast. *Nature Communications* **8**:1–12. DOI: https://doi.org/10.1038/ncomms15286, PMID: 28513584

**Roostalu J**, Schiebel E, Khmelinskii A. 2010. Cell cycle control of spindle elongation. *Cell Cycle* **9**:1084–1090. DOI: https://doi.org/10.4161/cc.9.6.11017, PMID: 20410686

**Roostalu J**, Hentrich C, Bieling P, Telley IA, Schiebel E, Surrey T. 2011. Directional switching of the kinesin Cin8 through motor coupling. *Science* **332**:94–99. DOI: https://doi.org/10.1126/science.1199945, PMID: 21350123

**Roostalu J**, Cade NI, Surrey T. 2015. Complementary activities of TPX2 and chTOG constitute an efficient importin-regulated microtubule nucleation module. *Nature Cell Biology* **17**:1422–1434. DOI: https://doi.org/10.1038/ncb3241, PMID: 26414402

**Roque H**, Ward JJ, Murrells L, Brunner D, Antony C. 2010. The fission yeast XMAP215 homolog Dis1p is involved in microtubule bundle organization. *PLOS ONE* **5**:e14201. DOI: https://doi.org/10.1371/journal.pone.0014201, PMID: 21151990

**Sato M**, Vardy L, Angel Garcia M, Koonrugsa N, Toda T. 2004. Interdependency of fission yeast Alp14/TOG and coiled coil protein Alp7 in microtubule localization and bipolar spindle formation. *Molecular Biology of the Cell* **15**:1609–1622. DOI: https://doi.org/10.1091/mbc.e03-11-0837, PMID: 14742702

**Saunders WS**, Koshland D, Eshel D, Gibbons IR, Hoyt MA. 1995. *Saccharomyces cerevisiae* kinesin- and dynein-related proteins required for anaphase chromosome segregation. *Journal of Cell Biology* **128**:617–624. DOI: https://doi.org/10.1083/jcb.128.4.617, PMID: 7860634

**Saxton WM**, McIntosh JR. 1987. Interzone microtubule behavior in late anaphase and telophase spindles. *Journal of Cell Biology* **105**:875–886. DOI: https://doi.org/10.1083/jcb.105.2.875, PMID: 3305523

**Scholey J**, Civelekoglu-Scholey G, Brust-Mascher I. 2016. Anaphase B. *Biology* **5**:1–30. DOI: https://doi.org/10.3390/biology5040051

**Schutt KL**, Moseley JB. 2020. The phosphatase inhibitor Sds23 promotes symmetric spindle positioning in fission yeast. *Cytoskeleton* **77**:544–557. DOI: https://doi.org/10.1002/cm.21648, PMID: 33280247

**Severin F**, Habermann B, Huffaker T, Hyman T. 2001. Stu2 promotes mitotic spindle elongation in anaphase. *Journal of Cell Biology* **153**:435–442. DOI: https://doi.org/10.1083/jcb.153.2.435, PMID: 11309422

**Sharp DJ**, Yu KR, Sisson JC, Sullivan W, Scholey JM. 1999. Antagonistic microtubule-sliding motors position mitotic centrosomes in *Drosophila* early embryos. *Nature Cell Biology* **1**:51–54. DOI: https://doi.org/10.1038/9025, PMID: 10559864

**Sharp DJ**, Brown HM, Kwon M, Rogers GC, Holland G, Scholey JM. 2000. Functional coordination of three mitotic motors in *Drosophila* embryos. *Molecular Biology of the Cell* **11**:241–253. DOI: https://doi.org/10.1091/mbc.11.1.241, PMID: 10637305

**Shimamoto Y**, Forth S, Kapoor TM. 2015. Measuring pushing and braking forces generated by ensembles of Kinesin-5 crosslinking two microtubules. *Developmental Cell* **34**:669–681. DOI: https://doi.org/10.1016/j.devcel.2015.08.017, PMID: 26418296

**Straight AF**, Sedat JW, Murray AW. 1998. Time-lapse microscopy reveals unique roles for kinesins during anaphase in budding yeast. *Journal of Cell Biology* **143**:687–694. DOI: https://doi.org/10.1083/jcb.143.3.687, PMID: 9813090

**Syrovatkina V**, Tran PT. 2015. Loss of kinesin-14 results in aneuploidy via kinesin-5-dependent microtubule protrusions leading to chromosome cut. *Nature Communications* **6**:1–8. DOI: https://doi.org/10.1038/ncomms8322

**Thawani A**, Kadzik RS, Petry S. 2018. XMAP215 is a microtubule nucleation factor that functions synergistically with the γ-tubulin ring complex. *Nature Cell Biology* **20**:575–585. DOI: https://doi.org/10.1038/s41556-018-0091-6, PMID: 29695792

**Thompson ME**, Heimsath EG, Gauvin TJ, Higgs HN, Kull FJ. 2013. FMNL3 FH2-actin structure gives insight into formin-mediated actin nucleation and elongation. *Nature Structural & Molecular Biology* **20**:111–118. DOI: https://doi.org/10.1038/nsmb.2462, PMID: 23222643

**Tolić-Nørrelykke IM**, Sacconi L, Thon G, Pavone FS. 2004. Positioning and elongation of the fission yeast spindle by microtubule-based pushing. *Current Biology* **14**:1181–1186. DOI: https://doi.org/10.1016/j.cub.2004.06.029, PMID: 15242615

**Tournebize R**, Popov A, Kinoshita K, Ashford AJ, Rybina S, Pozniakovsky A, Mayer TU, Walczak CE, Karsenti E, Hyman AA. 2000. Control of microtubule dynamics by the antagonistic activities of XMAP215 and XKCM1 in *Xenopus* egg extracts. *Nature Cell Biology* **2**:13–19. DOI: https://doi.org/10.1038/71330, PMID: 10620801

**Tran PT**, Paoletti A, Chang F. 2004. Imaging green fluorescent protein fusions in living fission yeast cells. *Methods* **33**:220–225. DOI: https://doi.org/10.1016/j.ymeth.2003.11.017, PMID: 15157889

**Varga V**, Helenius J, Tanaka K, Hyman AA, Tanaka TU, Howard J. 2006. Yeast kinesin-8 depolymerizes microtubules in a length-dependent manner. *Nature Cell Biology* **8**:957–962. DOI: https://doi.org/10.1038/ncb1462, PMID: 16906145

**Varga V**, Leduc C, Bormuth V, Diez S, Howard J. 2009. Kinesin-8 motors act cooperatively to mediate length-dependent microtubule depolymerization. *Cell* **138**:1174–1183. DOI: https://doi.org/10.1016/j.cell.2009.07.032, PMID: 19766569

**Vavylonis D**, Kovar DR, O'Shaughnessy B, Pollard TD. 2006. Model of formin-associated actin filament elongation. *Molecular Cell* **21**:455–466. DOI: https://doi.org/10.1016/j.molcel.2006.01.016, PMID: 16483928

**Vukušić K**, Buđa R, Bosilj A, Milas A, Pavin N, Tolić IM. 2017. Microtubule sliding within the bridging fiber pushes kinetochore fibers apart to segregate chromosomes. *Developmental Cell* **43**:11–23. DOI: https://doi.org/10.1016/j.devcel.2017.09.010, PMID: 29017027

**Vukušić K**, Buđa R, Tolić IM. 2019. Force-generating mechanisms of anaphase in human cells. *Journal of Cell Science* **132**:jcs.231985. DOI: https://doi.org/10.1242/jcs.231985

**Ward JJ**, Roque H, Antony C, Nédélec F. 2014. Mechanical design principles of a mitotic spindle. *eLife* **3**:e03398. DOI: https://doi.org/10.7554/eLife.03398, PMID: 25521247

**Wieczorek M**, Bechstedt S, Chaaban S, Brouhard GJ. 2015. Microtubule-associated proteins control the kinetics of microtubule nucleation. *Nature Cell Biology* **17**:907–916. DOI: https://doi.org/10.1038/ncb3188, PMID: 26098575

**Winey M**, Mamay CL, O'Toole ET, Mastronarde DN, Giddings TH, McDonald KL, McIntosh JR. 1995. Three-dimensional ultrastructural analysis of the *Saccharomyces cerevisiae* mitotic spindle. *Journal of Cell Biology* **129**:1601–1615. DOI: https://doi.org/10.1083/jcb.129.6.1601

**Yamashita A**, Sato M, Fujita A, Yamamoto M, Toda T. 2005. The roles of fission yeast ase1 in Mitotic cell division, meiotic nuclear oscillation, and cytokinesis checkpoint signaling. *Molecular Biology of the Cell* **16**:1378–1395. DOI: https://doi.org/10.1091/mbc.e04-10-0859, PMID: 15647375

**Yu CH**, Redemann S, Wu HY, Kiewisz R, Yoo TY, Conway W, Farhadifar R, Müller-Reichert T, Needleman D. 2019. Central-spindle microtubules are strongly coupled to chromosomes during both anaphase A and anaphase B. *Molecular Biology of the Cell* **30**:2503–2514. DOI: https://doi.org/10.1091/mbc.E19-01-0074, PMID: 31339442

**Yukawa M**, Kawakami T, Okazaki M, Kume K, Tang NH, Toda T. 2017. A microtubule polymerase cooperates with the kinesin-6 motor and a microtubule cross-linker to promote bipolar spindle assembly in the absence of kinesin-5 and kinesin-14 in fission yeast. *Molecular Biology of the Cell* **28**:3647–3659. DOI: https://doi.org/10.1091/mbc.e17-08-0497, PMID: 29021344

**Yukawa M**, Yamada Y, Yamauchi T, Toda T. 2018. Two spatially distinct kinesin-14 proteins, Pkl1 and Klp2, generate collaborative inward forces against kinesin-5 Cut7 in *S. pombe*. *Journal of Cell Science* **131**:jcs210740. DOI: https://doi.org/10.1242/jcs.210740, PMID: 29167352

**Yukawa M**, Okazaki M, Teratani Y, Furuta K, Toda T. 2019a. Kinesin-6 Klp9 plays motor-dependent and -independent roles in collaboration with Kinesin-5 Cut7 and the microtubule crosslinker Ase1 in fission yeast. *Scientific Reports* **9**:1–15. DOI: https://doi.org/10.1038/s41598-019-43774-7, PMID: 31089172

**Yukawa M**, Yamada Y, Toda T. 2019b. Suppressor Analysis Uncovers That MAPs and Microtubule Dynamics Balance with the Cut7/Kinesin-5 Motor for Mitotic Spindle Assembly in *Schizosaccharomyces pombe* . *G3: Genes, Genomes, Genetics* **9**:269–280. DOI: https://doi.org/10.1534/g3.118.200896

**Yukawa M**, Teratani Y, Toda T. 2020. How essential Kinesin-5 becomes Non-Essential in fission yeast: force balance and microtubule dynamics matter. *Cells* **9**:1154. DOI: https://doi.org/10.3390/cells9051154

# Discussion & Conclusion

Taken together, this work allows to draw the following main conclusions:

**(i)** Spindle length and dynamics scale with cell size throughout mitosis in *S. pombe*.
**(ii)** Cell size-dependent spindle dynamics keep mitosis duration constant.
**(iii)** Dis1/XMAP215 is a limiting component required for the cell size-dependent scaling of anaphase spindle length.
**(iv)** Dis1 promotes Klp9/kinesin-6 recruitment to the spindle midzone at anaphase onset via a dephosphorylation-dependent mechanism.
**(v)** Klp9 is a limiting component required for the cell size-dependent scaling of anaphase B spindle elongation velocity.
**(vi)** The microtubule sliding motor Klp9 promotes microtubule growth *in vivo* and *in vitro*.
**(vii)** Klp9 utilizes an unconventional mechanism for the regulation of microtubule growth: the motor can enhance and dampen microtubule growth speed depending on the tubulin concentration *in vitro*.

## 9 Cell size-dependent spindle length & spindle dynamics

***(i)** Spindle length and dynamics scale with cell size throughout mitosis in S. pombe.*

The scaling of spindle length during metaphase has been extensively studied in numerous organisms during early embryogenesis (see chapter 4.1) [440, 520, 524]. Here, I could show that spindle length scales with cell size at each mitotic phase (prophase, metaphase, and anaphase) in the single cell organism *S. pombe*.

Given that spindle length defines the distance between the two sister chromatid sets, localized to opposite spindle poles, and anaphase B spindle elongation substantially contributes to the separation of sister chromatids in many organisms [79, 184, 226, 488], scaling of final spindle

length is likely to ensure faithful chromosome separation in cells of different sizes (Figure 19). The adjustment of spindle length to cell size ensures that sister chromatids are separated by a sufficient distance away from each other, and, importantly, away from the site of cell cleavage. If chromosomes would remain in vicinity to the site of ring constriction, defined by the position of the spindle midzone at anaphase onset [568], the cytokinetic ring may cut chromosomes [389, 569], eventually resulting in the generation of aneuploid daughter cells.

An interesting observation, supporting this hypothesis, has been made in *Drosophila* larval neuroblasts, which contained abnormally long chromosome arms, which protruded into the cell division site [570]. To clear the site of ring constriction from genetic material, the cell and the mitotic spindle elongated [570].

On the other hand, the assembly of elongated spindles in small cells could perturb spindle architecture, and eventually chromosome separation (Figure 19). This has been observed upon kinesin-8 deletion in yeast cells [272] and after compression of Ptk2 cells [571].

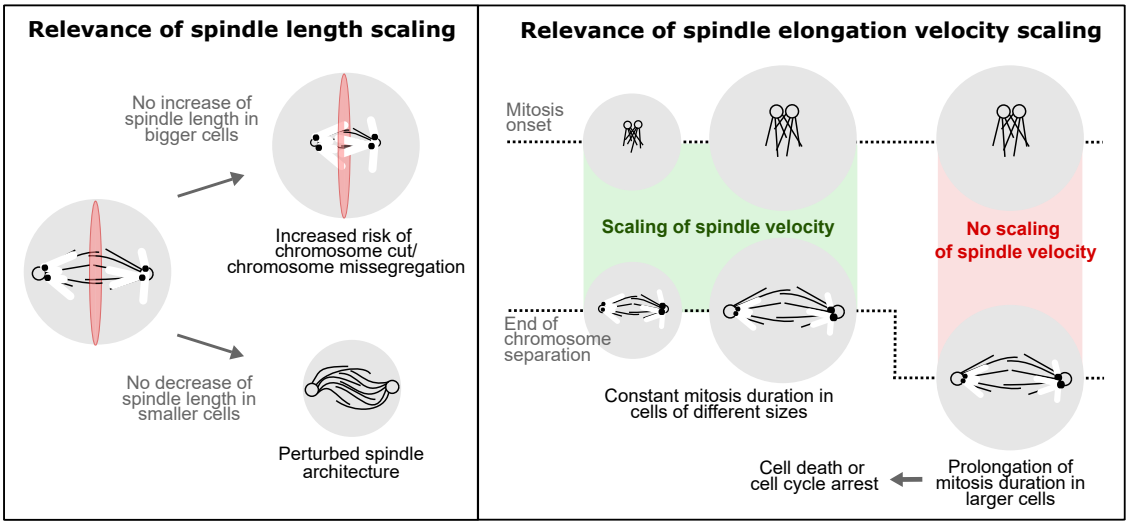


FIGURE 19: **Relevance of spindle scaling** - Scheme depicting the possible consequences of perturbed spindle length and spindle dynamics scaling. Left panel: If spindle length would not increase with cell size, this could lead to insufficient separation of sister chromatids away from the cytokinetic ring (red), which may cut chromosomes, that intrude into the site of cell cleavage. If spindle length would not decrease in smaller cells, this could lead to perturbed spindle architecture. Right panel: If the velocity of mitotic processes would not scale with cell size, mitosis would be prolonged in bigger cells, which could result in diminished cell viability. The image has been taken and adapted from [531].

Along with spindle length scaling, I observed a proportional increase of mitotic spindle dynamics with spindle length and cell size [513]. Cell size-dependent spindle elongation velocities are, therefore, not an exclusive feature of *C. elegans* embryos, where the speed of spindle

assembly and anaphase B spindle elongation adjusts to cell size [440, 454], but also apply to fission yeast cells of different sizes. Also in human cells, longer spindles have recently been shown to elongate faster [214]. This indicates that the adjustment of spindle velocities to spindle length and cell size, like spindle length scaling, is a general feature of mitotic spindles throughout evolution.

***(ii)*** *Cell size-dependent spindle dynamics keep mitosis duration constant.*

The proportional increase of mitotic spindle dynamics with spindle length or cell size allows fission yeast cells to maintain the duration of each mitotic phase, and eventually **mitosis duration constant** and independent of changes in spindle length and cell size [513]. Despite a 2-fold increase in cell and spindle length, maximum chromosome separation is achieved within approximately 30 minutes in small and big fission yeast cells [513].
Similarly, the time frame required for spindle assembly and anaphase B spindle elongation is independent of cell size in *C. elegans* embryos [440, 454].

A constant mitotic time frame may be particularly important during early embryogenesis, where several rounds of rapid cell divisions occur. However, a precise control of the mitotic time frame might be essential also for single cell organisms and somatic cells, since an extensive prolongation of mitosis often results in cell death or cell cycle arrest (Figure 19) [32, 563–567]. In addition, between various human cell lines where the duration of interphase varies dramatically, the duration of mitosis was found to be remarkably constant [563]. This suggests that, in general, control of mitosis duration may be crucial for faithful cell division.

Further evidence for the requirement of a tightly regulated mitotic time frame is provided by the observation that also the duration of cytokinesis is tightly controlled in cells of different sizes [572]. In *C. elegans* embryos and the filamentous fungus *Neurospora crassa* the constriction velocity of the actin-based cytokinetic ring increases with increasing ring perimeter and cell size. Eventually, this allows to maintain the duration of cytokinesis constant and independent of cell size [572, 573].

# 10 Mechanisms of anaphase spindle length and spindle dynamics scaling

Spindle length regulation has often been linked to the control of microtubule growth [440, 536, 541]. Accordingly, factors that control spindle microtubule dynamics have been proposed to act as limiting components, which promote spindle length scaling [272, 436, 437, 440, 522].

***(iii)*** *Dis1/XMAP215 is a limiting component required for the cell size-dependent scaling of anaphase spindle length.*

The microtubule plus-tip tracking polymerase XMAP215 [341] sets spindle length in a dose-dependent manner in *X. laevis*. The addition of XMAP215 with increasing concentration increased spindle length of *X. laevis* egg extract spindles, while microtubule density and spindle shape remained unaltered [437]. The dose-dependent effect of XMAP215 on spindle length was later confirmed *in vivo* by microinjection of additional XMAP215 into *X. laevis* embryos, which resulted in increased spindle length [436]. Strikingly, spindle length correlated with the polymerase activity of XMAP215 mutants in egg extracts [437].

Therefore, these studies present strong evidence for XMAP215 as a limiting component for the regulation of spindle length scaling. Yet, both set-ups include changes of the XMAP215 concentration. In fact, most studies that investigated the role of individual spindle components in spindle length scaling, perturbed the concentration of the protein of interest within the same cytoplasmic volume [436, 437, 440, 522].
However, particularly during embryogenesis, and in also in different sized yeast cells, the cytoplasmic composition remains constant [532, 533, 556]. Hence, it remains unclear whether XMAP215 indeed accounts for spindle length scaling, or if its absence would simply result in a similar decrease of spindle length in cells of different sizes.

Using fission yeast, I could demonstrate that **the XMAP215 homolog Dis1 indeed regulates spindle length scaling** [574]. Deletion of *dis1* strongly diminished the scaling relationship of anaphase spindle length with cell size [574]. The difference in final spindle length between wild type and *dis1* deleted cells was enhanced in bigger cells as compared to smaller cells.
Given the observation that *klp9* deletion had a less prominent effect on spindle length scaling [574], I argue that Dis1-mediated spindle length scaling does not, or does not exclusively,

originate from the Dis1-dependent recruitment of Klp9 to the spindle midzone. The regulation of spindle length scaling may rather be regulated by the activity of Dis1.

It is important to note, that upon *dis1* deletion, mitotic spindles still reach a significant length [574]. This suggests, that Dis1 may be required for spindle length scaling but additional spindle components assure assembly of mitotic anaphase spindles of a minimum length. The microtubule rescue factor CLASP (Cls1), is likely to assist the process of spindle length regulation. In absence of CLASP activity, microtubule rescue events are prevented, which leads to spindle collapse in fission yeast and *X. laevis* [118, 370]. Restricting CLASP to the spindle midzone by direct interaction with Ase1 prevents midzone-associated microtubules from depolymerizing back to spindle poles, since rescue events are induced within the midzone [370]. By this mechanism, Cls1 may ensure that anaphase spindles reach a certain length (Figure 20, upper panel).

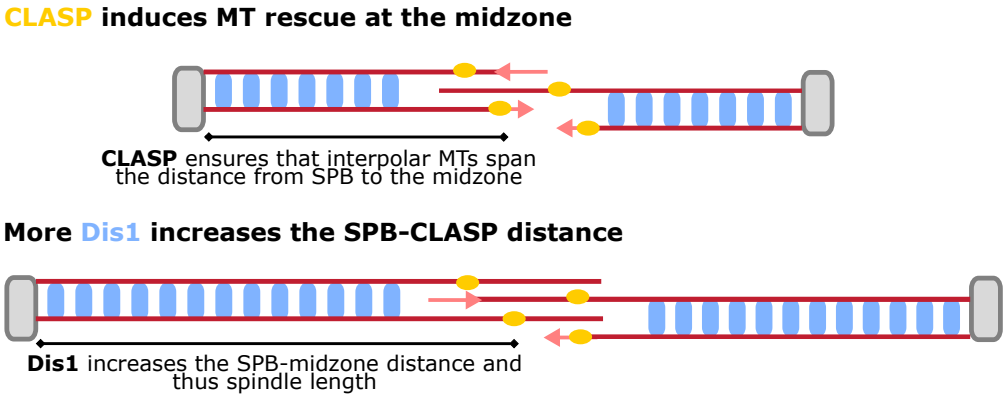


FIGURE 20: **Model for the mechanism of Dis1-mediated anaphase B spindle length scaling** - Scheme depicting a potential mechanism underlying spindle length scaling by Dis1. Cls1/CLASP (yellow) at the spindle midzone induces microtubule rescue events to prevent microtubules from shrinking back to the spindle poles (grey). Consequently, CLASP maintains spindle microtubules at a length spanning the distance from spindle poles to the midzone. Dis1 (blue) may restrict CLASP to the spindle midzone. An increased amount of Dis1 increases the distance between CLASP and SPBs and thus spindle length.

How Dis1 regulates spindle length scaling remains to be determined. Since Dis1, like Alp14, has been shown to be a microtubule polymerase *in vitro* [332, 339], it is tempting to think that this function enables the cell size-dependent regulation of spindle length. In particular since the polymerase activity of XMAP215 mutants in *X. laevis* egg extracts directly correlated with spindle length [437]. However, my results indicate that the primary function of Dis1 during anaphase B does not lie in the regulation of microtubule growth [574]. Also during interphase, Dis1 displays only minor effects on the microtubule dynamics [352].

On the other hand, XMAP215 has been shown to promote microtubule nucleation as well [100, 101, 123, 124, 358]. The microtubule nucleation profile along the spindle microtubule lattice determines spindle length in *X. laevis* and zebrafish [457, 535, 536]. However, in *S. pombe* microtubule minus-ends have only been found at SPBs [105, 156]. Therefore, spindle length rather depends on individual microtubule length, than on the spatial regulation of microtubule nucleation events.

An alternative mechanism is suggested by the particular localisation pattern of Dis1. Upon anaphase onset, Dis1-GFP relocalizes from kinetochores, where it is present during pro- and metaphase, to spindle microtubules on lateral sides of the spindle, while being excluded from the spindle midzone (Figure 20) [574, 575]. At the lateral spindle microtubule lattice Dis1 may promote microtubule bundling, since the protein has been implicated in the formation of parallel bundles during interphase [352].
With increasing levels of Dis1 in bigger cells, the region occupied by Dis1 likely expands towards the midzone. This could restrict the spindle midzone, and, in particular, spindle midzone components such as Cls1, farther away from spindle poles. As a result, the distance between spindle poles and the site of microtubule rescue induction by Cls1 at the midzone. Given that this would increase microtubule length, spindle length would be increased accordingly and scaling with cell size achieved.

To test this hypothesis, the detailed effect of Cls1 inactivation on anaphase B spindle length and microtubule dynamics in bipolar spindles has to be investigated. Moreover, the hypothesis builds on the assumption that Dis1 actively excludes CLASP along the microtubule lattice. This could be probed by analyzing the distribution of Cls1-GFP in absence of Dis1, as well as upon altered Dis1 levels, by expressing *dis1* under the control of nmt-promoters of different strength. An altered distribution of the Cls1-GFP signal along the anaphase B spindle microtubule lattice in absence, or upon altered expression of Dis1, would indicate that Dis1 restricts Cls1 to the spindle midzone. Furthermore, *in vitro* experiments encompassing purified Dis1, Cls1 and microtubules would reveal if Dis1 influences Cls1 binding to the microtubule lattice.

According to the proposed mechanism that can only account for anaphase B spindle length scaling, since Dis1 localizes to spindle microtubules only upon anaphase onset, *dis1* deletion did not impact metaphase spindle length scaling [574].
Hence, spindle length scaling before anaphase onset is likely regulated by a different spindle component. A potential candidate is Alp14, the second XMAP215 family member in fission

yeast. Possibly, Alp14's role is more prominent during early mitotic phases, while the Dis1 activity becomes crucial upon anaphase B onset. Corroborating this hypothesis, I observed that deletion of *alp14* often rescued bipolar spindle formation upon Cut7/kinesin-5 inactivation by restoring the balance between microtubule sliding/crosslinking and microtubule dynamics [395], while *dis1* deletion did not [574]. This suggests that rather Alp14 than Dis1 contributes to the control of microtubule dynamics during early mitotic phases. However, if Alp14 regulates spindle length scaling of the metaphase spindle remains to be tested. In general, this illustrates that spindle scaling may be regulated by a spindle component that is crucial for a given process at a given time.

*(iv) Dis1 promotes Klp9 recruitment to the spindle midzone at anaphase onset via a dephosphorylation-dependent mechanism.*

Importantly, Dis1 is not only involved in the regulation of spindle length scaling. At anaphase onset, Dis1 promotes recruitment of Klp9 to the spindle midzone via a dephosphorylation-dependent mechanism [574]. Moreover, an increased expression level of *dis1* resulted in increased Klp9 intensities at the midzone, suggesting that the recruitment of Klp9 is dependent on Dis1 levels. Since Dis1 sets spindle length [574] and Klp9 controls the velocity of spindle elongation [513], **Dis1-mediated Klp9 recruitment directly links the regulation of spindle length and spindle elongation velocity**.

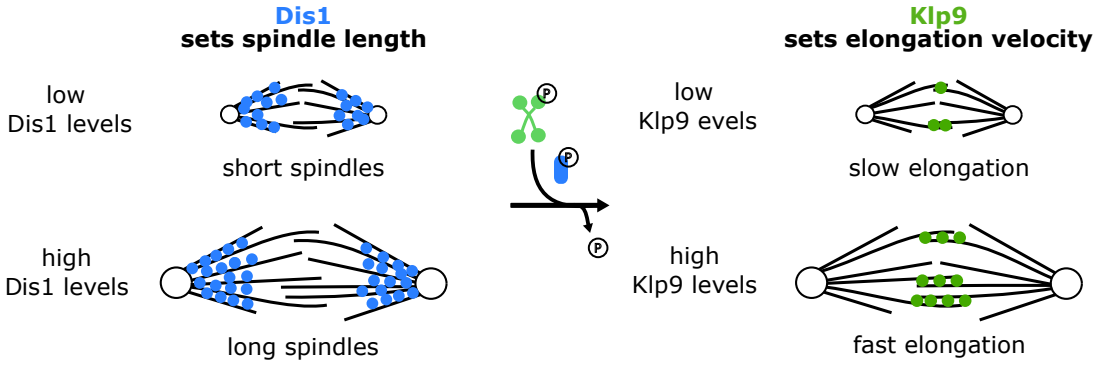


FIGURE 21: **Dis1-mediated Klp9 recruitment links the regulation of spindle length to spindle elongation velocity** - Scheme depicting the correlation of spindle length and elongation velocity mediated by Dis1-dependent recruitment of Klp9. Low levels of Dis1 (blue) in smaller cells lead to the assembly of smaller spindles and the recruitment of lower levels of Klp9 (green) to the spindle midzone. Less Klp9 motors at the spindle midzone results in slower spindle elongation as compared to longer spindles in bigger cells.

Hypothetically, the more Dis1 is present within bigger cells, the longer the assembled spindles are and the more Klp9 is recruited to the spindle midzone (Figure 21) [574]. Subsequently,

more midzone-associated Klp9 motors lead to faster spindle elongation [513]. Hence, the spindle elongation velocity is directly correlated with spindle length by Dis1-mediated Klp9 recruitment at anaphase onset. This ensures that longer spindles elongate with faster speeds when compared to shorter spindles.

***(v)*** *Klp9 is a limiting component required for the cell size-dependent scaling of anaphase B spindle elongation velocity.*

Klp9 adjusts the speed of spindle elongation during anaphase B to cell size. Therefore, as proposed for *C. elegans*, a force generator is the limiting component for spindle elongation velocity control in fission yeast. In the case of fission yeast, it is not a cortical pulling motor [454], but a microtubule sliding motor at the spindle midzone, which increases the distance between spindle poles [256, 513]. In line with this, midzone pushing is the dominant mechanism of anaphase spindle elongation in fission yeast, as in many other organisms [14–16, 162, 488, 492]. In absence of Klp9, the speed of spindle elongation is strongly diminished and not significantly different in cells of different sizes [256, 513]. Thus, mitosis duration increases with cell size and the constant mitosis duration is abolished. Contrarily, in presence of Klp9 the **spindle elongation velocity increases with elevated Klp9 levels in a dose-dependent manner** [513]. This has been recently confirmed by other studies in fission yeast [258, 576]. As a result, Klp9 acts as a limiting component in the mechanism underlying the cell size-dependent anaphase B spindle elongation velocity.

In addition, to the Klp9-mediated increase of the spindle elongation velocity of longer spindles appears to be assisted by an increased microtubule density [513]. Longer spindles contain more microtubules, and consequently, provide more binding sites for Klp9 at the spindle midzone. Since the microtubule overlap region is also longer, the increase of binding sites for Klp9 to spindle midzone microtubules is higher than the proportional increase if Klp9 levels. The prominent rise in the number of available binding sites results in a decrease of the motor concentration at the midzone, even though the absolute number of Klp9 increases. This leads to a situation where more motors act in a less crowded environment [513], which may enhance the efficiency of Klp9-mediated force production. In fact, other motors have been demonstrated to slow down when acting in crowded environments [233, 577].
Hence, while microtubule nucleation is not involved in spindle length regulation in fission yeast,

the process appears to be implicated in the regulation of spindle elongation velocities. I propose, that the **cell size-dependent microtubule number** assists the kinesin-6 mediated velocity control of anaphase B spindle elongation [513].
Microtubule nucleation may also be part of the mechanism that adjusts the speed of mitotic processes to cell size in animal cells. For instance, centrosome-independent microtubule nucleation and the corresponding increase in microtubule number reduces the time frame required for chromosome capture [578] and may similarly adjust duration of spindle assembly.

# 11 Klp9 - a dual function motor regulating microtubule sliding and growth

The investigation of the mechanism underlying the cell size-dependent spindle elongation velocity revealed the kinesin-6 Klp9 as the crucial regulator of spindle elongation velocity [513]. Klp9 is a known microtubule sliding motor [256–258], suggesting that the extent of sliding forces generated at the midzone directly sets the speed of spindle elongation. Accordingly, tetrameric motors have been shown to be cooperative and the forces generated by them add up [228].
However, previous studies suggested that **concomitant to the generation of microtubule sliding forces, midzone microtubules have to grow** to maintain the microtubule overlap while elongating and allow sustained spindle elongation (see chapter 3.4.5).

I, thus, set out to analyze microtubule dynamics during anaphase B. As a crucial anaphase B spindle component, I, thereby, focused on the kinesin-6 Klp9.

***(vi)*** *The microtubule sliding motor Klp9 promotes microtubule growth in vivo and in vitro.*

I combined monopolar spindles as a tool to study microtubule dynamics *in vivo* with *in vitro* reconstitution assays to decipher the role of Klp9 in the control of microtubule dynamics [574]. Despite the unseparated spindle poles and unsegregated chromosomes, monopolar spindles proceed to anaphase B, during which long microtubule bundles assemble. The bundles display growth velocities similar to the spindle elongation velocity observed in bipolar spindles.

Importantly, these monopolar spindles may be used in the future as useful tool to study anaphase B spindle component localization and their effect on microtubule dynamics. In particular, the absence of antiparallelly oriented microtubules may shed light on the otherwise

invisible behavior and function of spindle components. For instance, Ase1-GFP was spread along the parallel microtubule bundles and accumulated at the tips only at later stages of anaphase B [574]. This suggested that Ase1 compaction at the spindle midzone is regulated by a plus-end-directed motor, which was not evident from studies in bipolar spindles where Ase1 concentrates at the spindle midzone from anaphase onset on [550, 551].

Importantly, the plus-end-directed kinesin-6 **Klp9 tracks the growing bundle tips and accumulates** there. This has similarly been observed for MKLP1 in monopolar spindles in human cells [511]. Moreover, microtubule plus-end accumulation is a crucial characteristic of microtubule dynamics regulating kinesins [239, 265, 266, 579, 580]. Accordingly, *klp9* deletion strongly reduced microtubule bundle length, and growth velocity during anaphase B in monopolar spindles. Additionally, recombinant **Klp9 promoted microtubule growth *in vitro* in a dose-dependent manner** in presence of a low tubulin concentration [574]. Hence, Klp9 may regulate anaphase B spindle elongation via the dual function in regulating microtubule sliding and growth.

Thereby, Klp9 is not the only mitotic motor capable of performing both tasks. For instance, the other homotetrameric microtubule sliding motor, kinesin-5 [22], has also been demonstrated to regulate microtubule dynamics [239]. *X. laevis* kinesin-5, promotes microtubule polymerization *in vitro* [239]. Hence, the dual function of mitotic bipolar kinesins may be crucial throughout mitosis. During spindle assembly, kinesin-5 crosslinks microtubules, slides them apart, and may concomitantly promote growth of the bound microtubules to separate spindle poles. Subsequently, during anaphase B the dual function of kinesin-5, in most organisms, or kinesin-6, in fission yeast, might promote sustained spindle elongation.

The availability of mutants that can slide microtubules apart but are incapable to regulate microtubule dynamics, or vice versa, would be required to decipher the contribution of each of the functions to mitotic processes. For kinesin-5 this could be tested by expression of a mutant that can not form tetramers, for instance, by mutating the BASS domain. Dimeric or monomeric kinesin-5 is still able to promote microtubule growth *in vitro* [239, 240]. On the other hand, sustained microtubule sliding can, presumably, be promoted only by a tetrameric kinesin-5 motor.

Not to be ignored is the fact, that *klp9* deletion, like the deletion of *dis1*, strongly reduced the length of microtubule bundles in monopolar spindles but only mildly affected spindle length in

bipolar spindles [574]. This suggests that Klp9, despite controlling the microtubule growth velocity *in vivo* and *in vitro*, is not substantially implicated in the underlying mechanism of bipolar spindle length regulation.

The difference of the Klp9-mediated effect on bundle and spindle length may result from additional mechanisms regulating spindle length that are active in bipolar spindles but inactive in monopolar spindles. This is likely to include factors that bind to antiparallelly overlapping microtubules, that is the spindle midzone, which is absent in monopolar spindles.

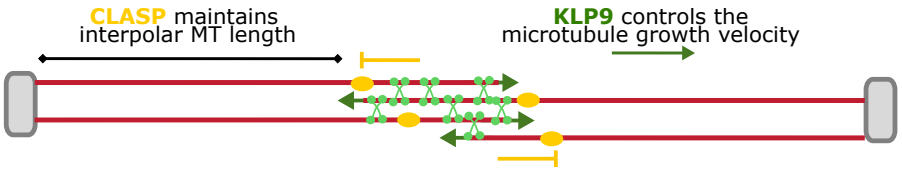


FIGURE 22: **Model for klp9-mediated microtubule growth control in bipolar spindles** - Scheme depicting the proposed mechanism for anaphase B spindle elongation mediated by CLASP (yellow), which maintains microtubules at a length spanning the distance from SPBs to the midzone and Klp9 (green), which controls the growth velocity of rescued microtubules.

As previously discussed, a promising candidate is Cls1, since it preferentially localizes to antiparallel overlaps and promotes rescue events [370]. According to this, the Cls1-3xGFP signal was very dim and spread all along the microtubule bundle in monopolar spindles while it strongly accumulates at the spindle midzone in bipolar spindles [574]. Cls1 potentially maintains a certain spindle microtubule length by promoting microtubule rescue at the spindle midzone. Concomitantly, Klp9 might precisely control the growth velocity of rescued microtubules to allow sustained spindle elongation (Figure 22).

# 12 Mechanisms that coordinate spindle microtubule sliding and growth

In theory, the dual function of Klp9 could allow inherent coordination of microtubule sliding and growth, which has been shown to be important for faithful chromosome separation [395, 471, 507, 508]. Conferring both functions to one motor protein can be a straightforward mechanism for the orchestration of both processes during spindle elongation.

Also kinesin-4 is a dual function motor, which has been proposed to coordinate microtubule sliding and growth by a mechanism termed **sliding-limited growth**: Upon overlap length reduction *in vitro*, the level of Xklp1 associated with the overlap is reduced, which eventually allows microtubules to grow [207]. In this study microtubules did not slide, since overlapping microtubules grew from immobilized microtubule seeds [207]. However, when microtubule bundles that self-organized in solution in presence of PRC1 and KIF4A were analyzed, KIF4A, recruited by PRC1 to the overlap, was shown to slide microtubules and subsequently suppresses their dynamics [213]. KIF4A-mediated microtubule sliding reduces the overlap length, and consequently the overlap-associated motor number. Accordingly, microtubule sliding was slowed when the overlap length decreased [213]. The reduced amount of KIF4A in the overlap then allows microtubules to grow [511].
In human cells, KIF4A depletion alone only mildly effected spindle elongation, but strongly decreased the speed of spindle elongation upon simultaneous inactivation of kinesin-5 [214]. This corroborates the proposed function of KIF4A in the promotion of microtubule sliding during anaphase B, which occurs in a redundant manner to Eg5/kinesin-5 [214]. How, the function of KIF4A in regulating microtubule dynamics contributes to the regulation of anaphase B spindle elongation *in vivo* remains to be determined. Yet, the ability to regulate both microtubule sliding and dynamics make KIF4A a promising candidate for the coordinated control of both processes.

Alternatively, **growth-limited microtubule sliding** could regulate sustained spindle elongation (see chapter 3.4.5). In this scenario, the spindle elongation velocity is dependent on the microtubule growth velocity. Indeed, in fission yeast, which does not possess kinesin-4, a reduction of microtubule dynamics by low doses of microtubule-destabilizing drugs reduced the speed of spindle elongation [257]. Moreover, deletion of the microtubule polymerase Stu2 (XMAP215) in budding yeast displayed a similar effect [515], and silencing of the transforming acid coiled-coil (TACC) protein TACC3, which stabilizes microtubules together with XMAP215 [581–583], has been reported to reduce the rate of spindle elongation in HeLa cells [514].
Accordingly, deletion of the microtubule depolymerase kinesin-8 increased the spindle elongation velocity in *S. cerevisiae* and *Drosophila* [272, 584]. In conclusion, several lines of evidence suggest that the velocity of microtubule growth directly translates into the velocity of spindle elongation.

Yet, elucidating the precise mechanism underlying the coordination of microtubule growth and sliding *in vivo* requires direct measurements of individual spindle microtubules within bipolar

anaphase spindles. However, so far this data is not available.

Due to the kinesin-6's dual function in promoting microtubule sliding and growth, instead of sliding and suppression of microtubule dynamics as shown for kinesin-4, the mechanism by which Klp9 could coordinate both processes may be different. Furthermore, while the previous models describe one process as limiting, Klp9 could simply promote microtubule sliding and growth with equal velocities (Figure 23).

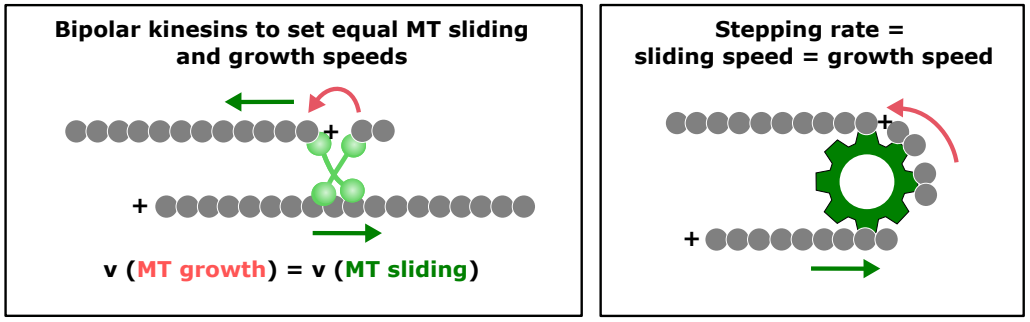


FIGURE 23: **Model for the kinesin-6-mediated coordination of microtubule sliding and growth** - Left panel: Scheme depicting a possible mechanism employed by kinesin-6 (light green) to coordinate microtubule sliding (green arrow) and growth (red arrow). Right panel: If the velocity of microtubule sliding and growth are determined by the stepping rate of the motor (depicted as a gearwheel) both processes would be inherently coordinated.

How Klp9 might perform this task remains to be determined. However, one can envision two mechanisms underlying the equal control of the sliding and growth velocity.

Either both processes are dose-dependent by the same extent, meaning that a certain number of Klp9 molecules at the midzone promotes microtubule sliding and growth with the same velocity.

Yet, a more robust control is achieved when the velocity of both processes is set by the motor's stepping rate (Figure 23, right panel). The best illustration for this mechanism may be a gearwheel, which turns with a distinct rate and this rate determines both the speed of tubulin subunit addition and the speed of microtubule sliding (Figure 23). The gearwheel's turning rate, thereby illustrates the motor's stepping velocity. Consequently, the motor would inherently set equal speeds of microtubule growth and sliding.

# 13 Shovel-model for the kinesin-6 mediated regulation of microtubule dynamics

***(vii)*** *Klp9 utilizes an unconventional mechanism for the regulation of microtubule growth: it can enhance and dampen microtubule growth speed depending on the tubulin concentration in vitro.*

*In vitro*, recombinant Klp9 is able to either increase or decrease the microtubule growth velocity [574]. At low tubulin concentration, where microtubules grow comparatively slowly, Klp9 addition increases the growth speed in a dose-dependent manner. Contrarily, at high tubulin concentration, where microtubule growth is fast, Klp9 decreases the growth velocity in a dose-dependent manner [574]. Importantly, upon addition of purified Klp9, the microtubule growth velocity at high tubulin concentration converges towards the microtubule growth velocity measured in presence of a low tubulin concentration [574]. This indicates that Klp9 is able to set a well-defined microtubule growth velocity, independently of encountering a fast- or slow-growing microtubule.
Importantly, this distinct growth velocity is similar to the Klp9-mediated microtubule gliding velocity, suggesting that the motor's stepping rate may dictate the velocity of microtubule growth. As discussed above, such a mechanism would allow for an inherent coordination of microtubule sliding and growth (Figure 23).

Nevertheless, to draw this conclusion further experiments need to be done. Of particular importance would be to perform the microtubule gliding assay and dynamics assay under the exact same conditions. The buffers used for each assay have been different making a comparison of the microtubule gliding and polymerization velocity difficult. Ideally, both assays should be combined: Klp9 immobilized on the coverslip binds to microtubule seeds free in solution, from which microtubules can grow from free tubulin dimers assisted by Klp9 free in solution. In this case, microtubule sliding and growth could be observed within the same assay. Furthermore, the stepping rate of Klp9 should be determined by single molecule assays.

However, the performed experiments clearly suggest that Klp9 sets a well-defined microtubule growth velocity. The mechanism by which Klp9 achieves such a precise and robust control of microtubule growth remains to be determined. Importantly, this requires a functional fluorescently labeled recombinant Klp9, which I did not obtain so far. However, comparison with the

mechanism utilized by other microtubule growth promoting factors allows to speculate on the mechanism underlying the Klp9-mediated regulation of microtubule growth.

In general, microtubule polymerization can be regulated by different mechanisms (see chapter 2.4 and 2.5). For instance, XMAP215 at the outermost microtubule tip [330] was proposed to bind free curved tubulin dimers via the TOG domains [340, 341, 345, 346]. Consequently, XMAP215, which tracks the growing tip [341, 349], promotes microtubule growth by increasing the local tubulin concentration at the microtubule tip [341, 344]. Accordingly, the addition of XMAP215 proteins *in vitro* consistently accelerats microtubule growth over a large range of tubulin concentrations [339, 341]. Therefore, this mechanism can not explain the observed Klp9-mediated reduction of the microtubule growth velocity as it can only account for an increase of the microtubule growth rate by the protein.

Kinesin-5, which preferentially binds lattice-incorporated tubulin, has been shown to promote microtubule growth by virtue of a stabilizing effect [240]. At the microtubule tip, kinesin-5 from *X. laevis* induces a curved-to-straight conformational change of newly added tubulin dimers and consequently stabilizes the growing tip *in vitro* [240]. However, stabilisation of microtubule tips only explains an enhancement of microtubule growth and can therefore not account for the Klp9-mediated regulation of microtubule growth.

The kinesin-6 most likely utilizes a different mechanism for the regulation of microtubule dynamics. In fact, to set a well-defined growth velocity independent of the tubulin concentration, Klp9 must be able to **promote and block tubulin subunit addition** to the microtubule lattice.

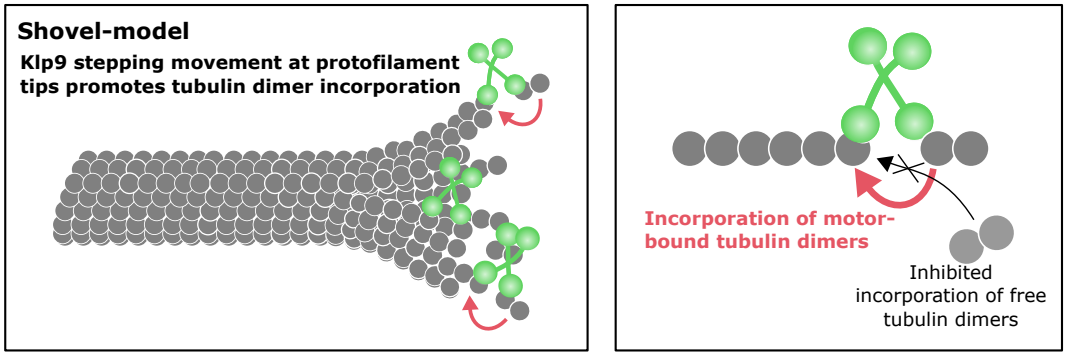


FIGURE 24: **Shovel-model for Klp9-mediated regulation of microtubule growth** - Scheme depicting the proposed model for Klp9-mediated regulation of microtubule dynamics. Klp9 (green) localizes to the end of each protofilament and promotes tubulin dimer association by bringing free tubulin dimers to the protofilament tip via its stepping movement. To set a well-defined growth velocity independent of the tubulin concentration, Klp9 has to be able to block addition of free tubulin dimers, that are not bound to the motor.

This is reminiscent of the mechanism employed by Formin, the processive elongator of actin filaments. Formin, which associates in a ring-like structure around actin polymers can accommodate an open or a closed conformation, which allows for or prevents subunit addition [585]. The balance between the open and the closed conformation, then, dictates the rate of filament elongation [586–588].
Based on this mechanism proposed for Formin, and the observation that the mean microtubule growth velocity in presence of Klp9 converges towards its hypothetical stepping rate in presence of low or high tubulin concentration [574], I envision a **shovel-model** for the Klp9-mediated regulation of microtubule growth (Figure 24): One Klp9 motor localizes to the end of each protofilament in the microtubule lattice, bound via one motor head to the last incorporated tubulin dimer, and **adds tubulin subunits to the growing protofilament via its stepping-movements** with the second motor head, that binds free tubulin dimers. Thus, the **stepping rate dictates the microtubule growth velocity**.

To examine the role of the motor's stepping rate within the underlying mechanism, Klp9 mutants could be generated which display altered motor velocity [589, 590]. If these purified Klp9 mutants would promote microtubule growth with accordingly different velocities than wild-type Klp9, this would indicate that the motor's stepping rate sets the speed of microtubule growth. Furthermore, the shovel mechanism can only explain microtubule growth mediated by tetrameric or dimeric Klp9 motors. Hence, a purification of a Klp9 mutant that cannot dimerize would provide further insight into the underlying mechanism.

The proposed mechanism, likewise, requires Klp9 to be able to block tubulin subunit addition to the microtubule lattice. Motor-independent incorporation of tubulin dimers should be prevented, as otherwise the microtubule growth rate would become sensitive to the tubulin concentration. To achieve a fixed microtubule growth rate, only tubulin dimers bound to the motor head should be able to associate with the last tubulin dimer in the protofilament. A possible mechanism for this selectivity could lie in the 'activation' of tubulin dimers for incorporation. The Klp9 motor head may bind free curved tubulin dimers, and induce a curved-to-straight conformational transition, like kinesin-5 [240]. However, in contrast to kinesin-5, Klp9 may do so before the motor promotes lattice incorporation. The straight tubulin dimer would be more amenable for lattice incorporation due to the facilitated formation of longitudinal and lateral bonds, as compared to free curved tubulin dimers in solution. As a result, Klp9-bound tubulin may be preferably added to the protofilament. If this mechanism would be active, growing

microtubule ends would potentially exhibit an altered structure. Eventually, protofilaments display reduced curvature.
Alternatively, by occupying the end of each protofilament the motor could block addition of non-motor bound tubulin dimers via steric hindrance.

A potential function of kinesin-6 motors in the regulation of microtubule dynamics is also hinted by its sequence and structure. The mammalian MKLP2 motor domain contains several unique aminoacid insertions [246]. These include a 60 residue N-terminal extension, an 18 aa long sequence insertion in loop 2, an 99 aa long insertion in loop 6, an 5 aa long insertion in loop 8, and an 6 aa long insertion in loop 12, as well as an extended neck-linker region [246].
Effectively, insertions within loop 2 have been associated with a depolymerizing activity, for instance of kinesin-13 proteins [591]. Moreover, the insertions in loop 2, 8 and 12 create additional contact sites between the MKLP2 motor domain and microtubules [246], which may allow binding of free tubulin dimers or tubulin dimer straightening and, consequently, assist microtubule growth control.
Finally, the kinesin-6 family characteristic insertions in loop 6 could be involved in the unconventional mechanism underlying the Klp9-mediated microtubule growth control. Structural studies of MKLP2 have shown that this loop 6 insertion forms a discrete additional subdomain, which protrudes from the motor core and away from the microtubule [246]. It would be interesting to test if this modification of the kinesin-6 motor domain is implicated in the regulation of microtubule dynamics. Potentially, the domain could block microtubule lattice incorporation of non-motor bound tubulin dimers via steric hindrance. Removal of the loop 6 insertion in the fission yeast kinesin-6 would allow deciphering its contribution to motor function.
In general, systematic removal or shortening of the typical loop insertions, would be highly informative for the determination of kinesin-6 function.

# 14 Conclusion - Klp9 regulates sustained anaphase B spindle elongation & scaling

Collectively, these studies highlight the kinesin-6 Klp9 as a crucial regulator of anaphase B spindle elongation and scaling in *S. pombe*. My work sheds light on the mechanism of anaphase B from Klp9 recruitment at anaphase onset to the Klp9-mediated regulation of spindle elongation, and its adjustment to cell size (Figure 25).

Klp9 targeting to the spindle midzone upon the metaphase-anaphase transition depends on its dephosphorylation, in part mediated by Dis1 [574]. Since Dis1 adjusts anaphase spindle length [574], and Klp9 adapts the spindle elongation velocity to cell size [513], the mechanism directly links the regulation of spindle length and spindle elongation velocity (Figure 25). This ensures that within bigger cells, longer spindles elongate with proportionally faster speeds. Subsequently, the mitotic time frame is maintained constant within cells of different sizes [513].

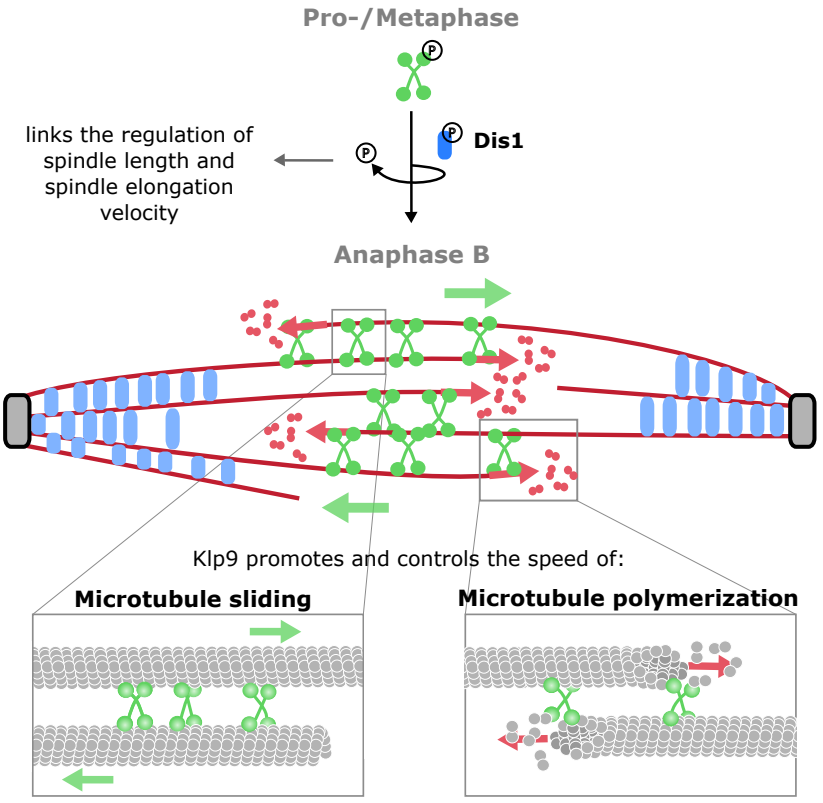


FIGURE 25: **Mechanism of Klp9-mediated anaphase B spindle elongation & scaling** - Scheme depicting the mechanism of anaphase B spindle elongation. Klp9 (green) recruitment to the spindle midzone at anaphase onset is regulated by Dis1-mediated dephosphorylation of the motor. This mechanism correlates the regulation of spindle length, mediated by Dis1 (blue), with the regulation of the spindle elongation velocity, mediated by Klp9. At the spindle midzone Klp9 regulates microtubule sliding and growth. By setting equal sliding and growth velocities the motor may coordinate both processes to keep the spindle midzone at a constant length and allow sustained spindle elongation.

At the spindle midzone, Klp9 promotes sustained spindle elongation by regulating microtubule sliding and growth. Potentially, Klp9 controls the speed of midzone microtubule sliding and the growth of their plus-ends at midzone edges with equal velocities. Therefore, both processes are inherently coordinated, and a constant microtubule overlap length is maintained throughout spindle elongation. Hence, this work proposes a mechanism for the coordination of

microtubule sliding and growth, which is essential for mitotic processes but remains scarcely understood.

However, although this work emphasizes the important role of Klp9 and Dis1 for anaphase B spindle elongation and scaling, bipolar spindles still reach a significant length in their absence [574]. Hence, another spindle component may be essential for this mitotic phase. As discussed, a promising candidate is the midzone-associated microtubule rescue factor CLASP [370].
In conclusion, **Klp9 and Dis1, together with Cls1/CLASP, may constitute a sufficient module for anaphase B spindle elongation**. CLASP maintains spindle microtubules at a length that spans the distance from SPBs to the midzone, Dis1 adjusts the spindle length to cell size and recruits Klp9, while Klp9 controls the velocity of microtubule growth and sliding.

Lastly, the obtained *in vitro* results suggest an unconventional mechanism for the Klp9-mediated regulation of microtubule dynamics. The kinesin-6 appears to have adopted a mechanism that resembles that utilized by Formins. Formins promote and block subunit addition to actin filaments [586–588]. I envision that the Klp9-mediated microtubule growth regulation can be explained by a shovel mechanism: by being bound to the last tubulin dimer of each protofilament, Klp9 shovels free tubulin dimers towards the tip and promotes their incorporation by a distinct rate.
To my knowledge, such a mechanism would be new in the microtubule field, since motors or MAPs have generally been shown to either promote, block or diminish microtubule growth [331, 334]. So far, a motor has not been reported to be able to enhance and dampen microtubule growth, depending on the condition.

It would be highly interesting to investigate if other kinesin-6 family members or other microtubule-based motors employ a similar mechanism and how this function precisely contributes to mitotic processes *in vivo*.

# Resumé

## 15 Introduction - le fuseau mitotique & l'anaphase B

La division cellulaire - la génération de deux cellules filles à partir d'une cellule mère - est un processus essentiel dans toutes les cellules vivantes. Au cours de la mitose, l'ADN précédemment dupliquée, sous la forme de chromosomes contenant deux chromatides soeurs égales, est séparée en deux ensembles identiques. Des erreurs dans ce processus conduisent à une séparation erronée des chromosomes et, par conséquent, à la génération de cellules filles dont le contenu en ADN est inégal. Cette aneuploïdie est souvent observé dans les cellules cancéreuse. Il est donc essentiel d'acquérir une compréhension approfondie des mécanismes sous-jacents de la séparation des chromosomes.

La séparation des chromosomes est orchestrée par le fuseau mitotique dans un processus hautement dynamique. Le fuseau mitotique comprend les microtubules, les pôles du fuseau et de nombreux moteurs moléculaires et d'autres protéines associées aux microtubules (MAPs) [115].

Le bon assemblage et la fonction correcte du fuseau mitotique reposent essentiellement sur les caractéristiques des microtubules du fuseau. Ces dernièrs présentent une instabilité dynamique, c'est à dire des périodes alternées de croissance et de raccourcissement [12]. De plus, les microtubules sont polaires, ils possèdent une extrémité positive (terminaison $\beta$-tubulin) et une extrémité negative (terminaison $\alpha$-tubulin). En début de mitose (pendant la prophase), la nucléation des microtubules est initiée aux pôles du fuseau, des centrosomes chez les vertébrés ou des corps polaires du fuseau (SPB) chez la levure [592, 593]. Les extrémités negatives sont ancrées aux pôles, tandis que les extrémités positives des microtubules explorent le cytoplasme pour aller à l'encontre des microtubules de l'autre pôle. Les sites de contact des microtubules sont reconnus par des moteurs moléculaires, principalement

de la famille de la kinésine-5 [20, 22, 221, 223, 229]. Ces moteurs bipolaires se lient aux microtubules orientés de manière antiparallèle. En se dirigeant vers les extrémités positives, ils les font glisser les uns par rapport aux autres [22]. Cela génère un mouvement de séparation des pôles et permet d'établir un fuseau á structure bipolaire [20, 22, 221, 223, 229]. La présence de forces opposées, génèrés par les moteurs des familles kinésine-14 ou dynéine, dirigées vers les extrémités negatives, crée un équilibre au sein du fuseau qui stabilise le mécanisme de séparation. [224, 225, 389–391].

Pendant la prophase dans les levures ou pendant la prometaphase dans les animaux, les microtubules s'attachent aux kinétochores, situés sur les chromosomes. Ceci permet l'alignement des chromosomes sur la plaque équatoriale [12, 592] et le déplacement vers les pôles des chromatides sœurs pendant l'anaphase A [516, 594, 595]. Pendant l'anaphase B le fuseau s'allonge [506–508], ce qui contribue de manière substantielle à la séparation des chromosomes dans les cellules de la levure, de *C. elegans*, de *Drosophila* et de l'homme [156, 214, 278, 596]. Dans ces organismes, la principale force motrice engendrant l'élongation du fuseau est générée au niveau de sa zone médiane [596], la région des microtubules provenant des pôles opposés qui se chevauchent de facon antiparallèle [8, 105, 156]. En effet, la destruction par impulsion laser des microtubules interpolaires au niveau de la zone médiane empêche l'élongation du fuseau, ce qui n'a pas été observé lors de la coupure des microtubules astraux [14–16, 162, 488].

Cette structure est stabilisée par les protéines de la famille Ase1/PRC1, qui se lient préférentiellement aux microtubules antiparallèles [207, 223, 310, 311, 550]. La déphosphorylation de Ase1/PRC1 au niveau des sites de phosphorylation du Cdk1 favorise sa liaison aux microtubules interpolaires [256, 315, 318, 489, 490], et donc la formation d'une zone médiane stable. Les membres de la famille PRC1 favorisent ensuite le recrutement de nombreuses protéines, comme les membres de la kinésine-6 MKLP1 et MKLP2 dans les cellules de mammifères, et Klp9 chez *S. pombe*, la kinésine-4 KIF4 qui régule la dynamique des microtubules dans les vertébrés et le facteur de sauvetage des microtubules CLASP [256, 315, 318, 370, 491].

Il est communément admis que l'allongement du fuseau à partir de la zone médiane est induit par la génération de forces de glissement des microtubules [492]. Typiquement, les protéines kinésine-5, qui forment des homotétramères bipolaires, peuvent accomplir cette tâche [22, 223]. En conséquence, la l'inactivation des protéines kinésine-5 réduit la vitesse

d'élongation du fuseau dans *S. cerevisae*, *S. pombe*, *Drosophila* et les cellules humaines [214, 226, 278, 425, 476, 495, 496]. Alors que les protéines kinésine-5 sont les seuls moteurs mitotiques qui forment des homotéramères dans la plupart des organismes, la kinésine-6 Klp9 de la levure de fission a également été identifiée comme une kinésine bipolaire [198, 256]. Comme la kinésine-5, Klp9 est un moteur qui se dirigé vers l'extrémité positive et qui est capable de faire glisser les microtubules [256–259]. Contrairement à la kinésine-5, Klp9 se lie au fuseau mitotique seulement pendant l'anaphase B [256, 258, 259]. Le recrutement au niveau de la zone médiane du fuseau est régulé par la déphosphorylation aux sites CDK1(Cdc2) par l'homologue de Cdc14, Clp1 [256].

Dans les cellules humaines, les protéines de kinésine-6 MKLP1 et MKLP2 forment des dimères et il a été démontré qu'elles transportent le complexe chromosome de passagers (CPC) vers la zone médiane du fuseau. Elles sont donc impliquées dans les voies de signalisation qui contrôlent la cytokinèse [244, 252].

Contrairement à d'autres organismes, chez la levure à fission, la kinésine-6 Klp9 est un régulateur crucial du glissement des microtubules au cours de l'anaphase B [214, 256, 258, 259]. Lors de la suppression de *klp9*, la vitesse d'élongation du fuseau est fortement réduite, comme observé en l'absence d'activité de la kinésine-5 dans d'autres organismes [256]. La suppression de *klp9* et l'inactivation simultanée de la kinésine-5 Cut7 abolissent complètement l'élongation du fuseau, ce qui indique que la kinésine-5 contribue également à ce processus [259]. Cependant, Klp9 y contribue plus fortement, puisque sa suppression entraîne une plus grande diminution de la vitesse d'élongation du fuseau que l'inactivation de Cut7 [259].

Néanmoins, la génération de force sans élongation des microtubule n'est pas suffisante pour permettre au fuseau de la levure à fission de s'allonger d'environ 2 à 12 µm. Il en est de même dans les cellules humaines qui présentent une élongation de 6 - 9 µm avec une longueur moyenne de zone médiane de 5 µm [105, 156, 273, 504]. Par conséquent, la polymérisation interpolaire des microtubules est nécessaire à l'allongement du fuseau. En effet, les premières expériences de photoblanchiment dans les cellules Ptk1 ont montré que les sous-unités de tubuline sont ajoutées aux extrémités positives des microtubules, pendant que le fuseau s'allonge [506]. De plus, dans les fuseaux isolés de diatomées, l'élongation du fuseau est supprimée et l'élongation est activé lorsque les sous-unités de tubuline sont ajoutées [507–509].

Il a été proposé que la croissance de l'extrémité positive pendant l'anaphase B est régulée par CLASP dans les zygotes de *C. elegans* et les cellules de mammifères. Le facteur de

sauvetage des microtubules est également nécessaire pour maintenir une structure stable du fuseau en anaphase chez la levure à fission [370, 442, 510]. Par ailleurs, la kinésine-4 KIF4A empêche la polymérisation et limite la longueur du chevauchement, ce qui est nécessaire pour mettre fin à l'élongation du fuseau en anaphase B chez les vertébrés [207, 511]. Cependant, les détails concernant la régulation précise de la dynamique des microtubules au cours de l'anaphase B reste peux compris.

La simple promotion de la polymérisation du réseau de microtubules peut ne pas être suffisante pour permettre une élongation soutenue du fuseau. Lorsque les microtubules sont séparés par glissement au niveau de la zone médiane, le chevauchement se rétrécit, ce qui inhibe le mouvement de glissement suite á la diminution des sites de liaison du moteur. Par conséquent, la croissance des microtubules doit être coordonnée avec leur glissement pour maintenir un chevauchement constant au niveau de la zone médiane du fuseau [507–509]. De plus, il a été démontré que, au cours de l'assemblage du fuseau, un équilibre précis entre la dynamique des microtubules et la réticulation/le glissement des microtubules est crucial pour la séparation des pôles du fuseau [395]. Pourtant, le mécanisme par lequel le glissement et la croissance des microtubules sont cordonnés reste inconnu.

Le fuseau mitotique depend également de son environnement cellulaire. Par exemple, il s'adapte á la taille de la cellule. En effet, le rapport entre la longueur du fuseau et la taille de la cellule a été étudiée dans de nombreux organismes [440, 454, 519–524]. Le développement embryonnaire permet d'observer les structures cellulaires en fonction de la taille des cellules, comme celle-ci diminue progressivement, parfois de plusieurs ordres de grandeur, tandis que l'embryon subit des cycles successifs de division cellulaire. Au cours de l'embryogenèse précoce de *X. leavis*, *C. elegans*, de l'oursin *P. lividus*, de la souris et d'autres métazoaires, la longueur du fuseau augmente de facon linéaire avec la taille des cellules jusqu'à atteindre une certaine limite supérieure [440, 454, 520, 521, 523, 524]. En dehors de l'embryogenèse, l'adaptation de la longueur du fuseau á la taille de la cellule a été demontrée chez *S. cerevisae* [272], et dans différentes lignées de cellules cancéreuses [525].

Au cours de l'embryogenèse, la composition du cytoplasme, c'est a dire, la teneur et la concentration en protéines, est supposée constante. En conséquence, il a été proposé que l'échelonnement de la longueur du fuseau est régulé par un mécanisme à composants limitants [532, 533]: la quantite d'un ou de plusieurs régulateurs cruciaux impactant la longueur

du fuseau est limitant. De plus, des expériences utilisant des extraits d'œufs de *X. leavis* encapsulés dans des liposomes de différents diamètres, ont démontré que l'augmentation du volume cytoplasmique est suffisant pour réguler la longueur du fuseau [527, 528]. Une augmentation de la taille de la cellule conduit à une augmentation de la quantité absolue de protéines. Lorsqu'un fuseau s'assemble, le composant limitant est incorporé dans la structure de la cellule, ce qui entraîne une diminution de sa quantité dans le cytoplasme. Pendant que le fuseau mitotique s'assemble, la réduction de la concentration du composant libre entraîne une réduction de la vitesse d'assemblage du fuseau. Puisque le composant limitant est moins abondant dans les cellules plus petites, le taux de croissance sera réduit plus rapidement lors de l'assemblage du fuseau, par rapport aux cellules plus grandes. Par conséquent, la taille du fuseau est ajustée à la taille de la cellule [533].
Plusieurs composants du fuseau ont été proposés comme composants limitants pour la régulation de la longueur du fuseau: la polymérase des microtubules XMAP215 chez *C. leavis* [436, 437], le facteur de promotion et de sauvetage de la croissance des microtubules CLASP chez *C. elegans* [440], la dépolymérase des microtubules Kip3 de la famille de la kinésine-8 chez *S. cerevisae* [272] et le facteur de nucléation des microtubules TPX2 dans les cellules *X. leavis* et U2OS [458, 459].

Bien que l'on se soit plus concentré sur la régulation de la longueur du fuseau mitotique en fonction de la taille des cellules, quelques études ont mis en lumière le phénomène de la vitesse d'élongation du fuseau en fonction de la taille des cellules.

Dans les embryons de *C. elegans* la vitesse de croissance des microtubules augmente avec la taille de la cellule. En consequence la vitesse d'assemblage du fuseau s'adapte á la taille de la cellule [440]. De plus, la vitesse d'élongation du fuseau en anaphase B varie en fonction de la taille de la cellule. Les fuseaux plus longs dans des cellules plus grandes sont allongés avec des vitesses proportionnellement plus élevées [454]. La combinaison de données expérimentales et de simulations numériques suggére que ceci dépend des forces de traction corticales influencées par la dynéine. Avec une densité constante de générateurs de force au niveau du cortex cellulaire, le nombre de dynéines corticales augmente avec la taille de la cellule. Donc les forces de traction exercées sur les pôles du fuseau sont plus élevées plus la cellule grandit, ce qui entraîne une élongation plus rapide du fuseau [454]. Cependant, les forces de traction astrales ne semblent pas constituer la principale force motrice de l'anaphase B chez la plupart des organismes.

# 16 Article I - La kinésine-6 contrôle la vitesse d'élongation du fuseau en fonction de la taille de la cellule pour constante maintenir la durée de la mitose chez la levure de fission.

Inspirée ces phénomènes, j'ai entrepris de déterminer si l'adaptation de la longueur et de la vitesse du fuseau á la taille des cellules, peut être observé dans l'organisme unicellulaire *S. pombe*. De plus, je me suis questionnée sur la raison d'une telle adaptation de la vitesse des processus mitotiques à la taille des cellules.

*S. pombe* représente un système modèle approprié pour étudier le fuseau mitotique en raison de sa composition et de sa dynamique relativement simples [156, 187]. De plus divers composants et mécanismes sont similaires á ceux observés dans des organismes plus complexes. En outre, la disponibilité de mutants qui presentent une longueur inférieure (*wee1-50*) ou supérieure (*cdc25-22*) aux cellules de type sauvage lors de la division cellulaire permet d'étudier les mécanismes de l'adaptation á la taille de cellule [18]. Étant donné que les cellules de levure de fission possédent une forme en bâtonnet á diamètre constant [555], la taille des cellules peut être facilement quantifiée en mesurant la longueur des cellules d'une extrémité à l'autre.

En utilisant ces cellules, j'ai découvert que la longueur du fuseau est aussi corrélée à leur taille: plus ces cellules sont longues, plus leurs fuseaux mitotiques le sont aussi [513]. De plus, j'ai observé que la vitesse des processus mitotiques, tels que l'assemblage du fuseau et l'élongation du fuseau en anaphase B, dépend de la taille de la cellule. Par conséquent, la durée de la mitose est maintenue constante. Elle est indépendante de la taille de la cellule et de la longueur du fuseau. Ceci peut être crucial pour la santé des cellules. En effet, il a été démontré que la prolongation de la mitose a un impact négatif sur la viabilité des cellules [563–567].

J'ai donc entrepris de déterminer le mécanisme qui régule la vitesse d'élongation du fuseau en fonction de la taille des cellules en me concentrant sur l'anaphase B.
Chez *C. elegans*, il a été proposé que la vitesse d'élongation du fuseau est régulée par la quantité de générateurs de force au niveau du cortex cellulaire [454]. Cependant, chez la levure à fission, comme dans les cellules humaines et plusieurs autres organismes, les forces nécessaires à l'élongation du fuseau sont générées dans la zone médiane [15, 16, 162, 488].

Par conséquent, j'ai analysé le rôle de la kinésine-6 Klp9, le moteur responsable du glissement des microtubules pendant l'anaphase B chez la levure à fission, dans ce mécanisme d'adaptation.
J'ai pu montrer que la suppression de *klp9* réduit la vitesse d'élongation du fuseau à des valeurs similaires dans des cellules de différentes tailles. Par conséquent, l'adaptation de la vitesse d'élongation du fuseau en fonction de la taille de la cellule a été complètement abolie en l'absence du moteur de glissement. La durée de la mitose augmente avec la taille de la cellule et la longueur du fuseau suite á la suppression de *klp9*.
Comme la régulation de la longueur du fuseau a été expliquée par un mécanisme à composants limitants, il était tentant de suggérer que la quantité de Klp9 détermine la vitesse d'élongation du fuseau. En effet, dans mes expériences, la quantité de moteur sur le fuseau et les niveaux totaux de Klp9-GFP augmentaient avec la taille de la cellule. Pour vérifier si la quantité accrue de Klp9 peut expliquer l'augmentation de la vitesse d'élongation du fuseau, j'ai surexprimé le moteur en utilisant des promoteurs de différentes niveaux. Avec des niveaux d'expression élevés de Klp9, la vitesse d'élongation du fuseau était actuellement augmentée.

En conclusion, le moteur de glissement des microtubules Klp9 ajuste la vitesse d'élongation du fuseau en anaphase B à la taille de la cellule en agissant comme un composant limitant : couplée à la taille de la cellule, la quantité de molécules de kinésine-6 Klp9 augmente dans les grandes cellules, ce qui entraîne une accélération de l'élongation du fuseau.
De surcroît, j'ai constaté que, bien que les niveaux absolus de Klp9 associé à la zone médiane augmentent, le taux d'occupation, défini par le rapport entre l'intensité de Klp9-GFP et l'intensité des microtubules de la zone médiane, diminue avec la longueur du fuseau. Ceci peut être expliqué par une augmentation surproportionnelle des sites de liaison pour Klp9. Les fuseaux plus longs forment des zones médianes plus longues et sont composés de plus de microtubules.

L'occupation de la zone médiane par le moteur Klp9 peut contribuer à la régulation de la vitesse d'élongation du fuseau en anaphase B. Il a été démontré que plusieurs protéines motrices se déplacent plus lentement lorsque la densité des moteurs est élevée. Par conséquent, puisque la zone médiane des petits fuseaux est plus encombrée, Klp9 allonge le fuseau à des vitesses plus lentes en comparaison avec des fuseaux plus longs, où Klp9 agit dans un environnement moins encombré.

En conclusion, cette étude démontre que la vitesse d'élongation du fuseau pendant l'anaphase

B dépend de la taille de la cellule. Elle est controlée par la kinésine-6 Klp9: plus le fuseau est long, plus la quantité de Klp9 est élevé. En outre Klp9 agit dans un environnement moins encombré au sein des fuseaux plus longs qui sont présents dans les cellules plus grandes. La combinaison de ces deux effets induit une augmentation de la vitesse d'élongation du fuseau.

# 17 Article II - La kinésine-6 Klp9 controle l'élongation du fuseau en anaphase B en régulant le glissement et la croissance des microtubules.

L'étude précédente a identifié la kinésine-6 homotétramérique Klp9 comme un régulateur principal de la vitesse d'élongation du fuseau en anaphase B chez la levure de fission. Il était donc tentant à ce stade de suggérer que le contrôle de la vitesse de glissement des microtubules est suffisant pour réguler la vitesse d'élongation du fuseau.
Cependant, la longueur de chevauchement des microtubules au niveau de la zone médiane du fuseau reste constante tout au long de l'élongation du fuseau, comme en témoignent les signaux de la tubuline et de l'Ase1 [513]. Ceci suggère que le glissement des microtubules et la croissance se produisent à des vitesses égales et doivent être précisément coordonnés.

J'ai donc essayé de comprendre comment la croissance des microtubules est régulée pendant l'anaphase B et comment elle est coordonnée avec le glissement des microtubules. Il est important de souligner que la régulation de la dynamique des microtubules pendant l'élongation du fuseau n'est pas bien comprise dans la plupart des organismes.

Étant donné le rôle proéminent de Klp9 pendant l'élongation du fuseau, j'ai émis l'hypothèse que le moteur lui-même pouvait simultanément réguler le glissement et la croissance des microtubules pour établir des vitesses égales et ainsi coordonner ces deux processus.
Cependant, la détermination des paramètres de dynamique des microtubules individuels dans le fuseau de l'anaphase B est difficile en raison de la structure trés dense de ce dérnier. Pour tester le rôle de Klp9 sur la dynamique des microtubules pendant l'anaphase B *in vivo*, j'ai développé des fuseaux monopolaires comme outil. Ce montage *in vivo* combiné à des expériences de reconstitution *in vitro* utilisant le Klp9 purifié a permis de déterminer l'effet du moteur sur la dynamique des microtubules [574].

Des fuseaux monopolaires ont été générés par l'inactivation de la kinésine-5 Cut7, en utilisant le mutant *cut7-24* sensible à la température. Malgré l'absence de séparation de leurs pôles et donc des chromosomes, les fuseaux monopolaires ont progressé jusqu'à l'anaphase B. Au cours de cette phase mitotique, de longs faisceaux de microtubules ont été assemblés. Les faisceaux de fuseaux monopolaires se sont développés à une vitesse qui correspondait à la moitié de la vitesse d'élongation des fuseaux bipolaires en anaphase B, atteignant une longueur totale égale á la moitié de la longueur des fuseaux bipolaires.
Pendant l'anaphase B, la kinésine-6 Klp9 marquée par la GFP s'est accumulée à l'extrémité croissante des faisceaux de microtubules. Cette accumulation à l'extrémité des microtubules est une caractéristique importante des protéines régulatrices de la dynamique des microtubules.
En conséquence, la suppression de klp9 dans les cellules *cut7-24* a fortement réduit la croissance des faisceaux pendant l'anaphase B. Les faisceaux de microtubules ont grandi avec une vitesse fortement réduite et leur longueur maximale a été significativement diminuée. Ceci indique que le moteur kinesin-6 favorise la polymérisation des microtubules pendant l'anaphase B.

Cependant, en tant que moteur qui se dirige vers l'extrémité positive, Klp9 peut également transporter des protéines régulatrices vers l'extrémité du faisceau de microtubules et ainsi favoriser indirectement la croissance des microtubules.
J'ai donc testé le rôle de quelques candidats qui sont des composants cruciaux de la zone médiane du fuseau ou bien connus comme régulateurs de la dynamique des microtubules. Il s'agit notamment de l'agent de mise en faisceau des microtubules Ase1 [550, 551], de l'homologue d'EB1 et de la polymérase des microtubules Mal3 [327, 332], des deux polymérases de la famille XMAP215 Dis1 et Alp14 [332, 339], de l'homologue de la protéine TACC et du facteur ciblant Alp14 Alp7 [357], ainsi que de la kinésine-5 Cut7 [20]. Seule la suppression de *dis1* dans les fuseaux monopolaires a entraîné une réduction de la croissance et de la longueur des faisceaux de microtubules à un degré comparable à celui de la suppression de *klp9*.
De plus, CLASP [370] ne semble pas impliqué dans la régulation de la croissance des microtubules médiée par Klp9, puisque l'intensité ou la localisation de Cls1-GFP ne sont pas affectées en absence de Klp9.

En consequence j'ai testé si Klp9 contrôle la localisation de Dis1 pendant l'anaphase B.

Cependant, contrairement aux hypothèses, le moteur Klp9 qui se dirige vers l'extrémité positive ne semble pas réguler la localisation et le recrutement de la polymérase Dis1. La suppression de *klp9* n'a pas altéré l'intensité ou la localisation de Dis1-GFP le long des fuseaux bipolaires de l'anaphase B. À contrario, la suppression de *dis1* a fortement réduit l'intensité de Klp9-GFP au niveau de la zone médiane du fuseau. En utilisant des mutants phosphomimiques et phospho-déficients de Dis1 et Klp9, j'ai démontré que le mécanisme derrière le recrutement de Klp9 médié par Dis1 inclut la déphosphorylation de Klp9 aux phosphosites de Cdc2, qui est, en partie, médiée par Dis1.
Il s'agit d'un résultat inattendu qui souléve la question pourquoi une polymérase régulerait le recrutement d'un moteur microtubulaire.

Chez *X. leavis*, XMAP215 a été suggéré comme un composant limitant pour l'adaptation de la longueur du fuseau á ;a taille de la cellule [436, 437]. Par conséquent, j'ai émis l'hypothèse que le recrutement de Klp9 médié par Dis1 peut lier la régulation de la longueur du fuseau (régulée par XMAP215) à la régulation de la vitesse d'élongation du fuseau (régulée par Klp9) et ainsi permettre aux fuseaux plus longs de s'allonger plus rapidement, comme le montre l'étude précédente.
En effet, j'ai observé que l'homologue de XMAP215, Dis1, régule l'adaptation de la longueur du fuseau chez la levure de fission. Après la suppression de *dis1*, la corrélation entre la longueur du fuseau en anaphase B et la taille de la cellule disparaît.

De plus, il reste intéressant de comprendre si Klp9 peut réguler directement la croissance des microtubules ou si d'autres protéines sont impliquées. Pour répondre à cette question, j'ai réalisé des expériences de reconstitution *in vitro* incluant Klp9 et des microtubules dynamiques. L'ajout de Klp9, lorsque les microtubules croissent lentement (à faible concentration de tubuline) a augmenté la vitesse de croissance des microtubules. Ainsi, ce moteur est effectivement capable de stimuler la croissance des microtubules. J'ai observé que Klp9 montre l'effet opposé en présence de concentrations élevées de tubuline: lorsque les microtubules croissent rapidement Klp9 diminue leur vitesse de croissance. Il est important de noter qu'en augmentant la concentration de Klp9, la vitesse de croissance des microtubules en présence d'une concentration élevée de tubuline converge vers la vitesse de croissance des microtubules mesurée en présence d'une faible concentration de tubuline. Ceci indique que Klp9 peut fixer une vitesses de croissance bien définie. A ma connaissance, un tel comportement n'a pas encore été décrit pour les kinésines ou d'autres MAPs.

# 18 Discussion - La kinésine-6 Klp9 comme facteur clé de l'élongation du fuseau en anaphase B

En considérant l'ensemble de ces résultats, nous pouvons tirer les conclusions suivantes:
(i) La longueur du fuseau et la vitesse d'élongation varient en fonction de la taille de la cellule tout au long de la mitose chez *S. pombe*.
(ii) Les vitesses des processus mitotiques, qui dépendent de la taille des cellules, permettent à des cellules de tailles différentes de conserver un temps mitotique constant.
(iv) Dis1 est un composant limitant pour l'adaptation de la longueur du fuseau.
(iii) La kinésine-6 Klp9 est une composante limitant pour la régulation de la vitesse d'élongation du fuseau en anaphase B dépendant de la taille de la cellule.
(v) Dis1 favorise le recrutement de Klp9 au niveau de la zone médiane du fuseau en début d'anaphase par un mécanisme de déphosphorylation.
(vi) Le moteur de glissement des microtubules Klp9 favorise la croissance des microtubules *in vivo* et *in vitro*.
(vii) Klp9 utilise un mécanisme non conventionnel pour la régulation de la croissance des microtubules : le moteur peut augmenter ou diminuer la vitesse de croissance des microtubules en fonction de la concentration en tubuline in vitro.

Ces études mettent en évidence la kinésine-6 Klp9 comme le régulateur principal de l'élongation du fuseau en anaphase B chez *S. pombe*. De plus, ces travaux mettent en lumière le mécanisme sous-jacent: depuis le recrutement de Klp9 au début de l'anaphase jusqu'à la régulation, médiée par Klp9, de l'élongation du fuseau, et son ajustement à la taille de la cellule. Le recrutement de Klp9 au niveau la zone médiane du fuseau de l'anaphase B est régulé par la déphosphorylation, en partie, médiée par l'homolgue Dis1 de XMAP215. Étant donné que Dis1 est responsable de la régulation de la longueur du fuseau et que Klp9 est responsable de la régulation de sa vitesse d'élongation en fonction de la taille de la cellule, ce mécanisme relie les deux processus et garantit que les fuseaux plus longs s'allongent plus rapidement afin de maintenir une durée mitotique constante dans les cellules de différentes tailles. Il a été suggeré que XMAP215 contrôle l'adaptation de la longueur du fuseau chez *X. laevis* [436, 437]. Cependant, ces études ont été réalisées dans des conditions non physiologiques, puisqu'elles comprenaient une augmentation de la concentration

de XMAP215 dans des volumes cytoplasmiques non modifiés. Ceci est en contraste avec la situation pendant l'embryogenèse, où la composition cytoplasmique est supposée rester constante, alors que la taille des cellules diminue. Mon travail démontre que dans des cellules de tailles différentes avec une composition cytoplasmique constante, XMAP215 peut effectivement réguler l'adaptation de la longueur du fuseau en agissant comme un composant limitant.

En outre, ces travaux révèlent une double function de la kinésine-6 Klp9: le moteur controle la vitesse de glissement et de croissance des microtubules. Klp9 peut donc coordonner de manière inhérente ces deux processus et promouvoir une élongation soutenue du fuseau. Ainsi, mon travail indique comment ces deux processus, qui sont essentiels pour la fonction du fuseau, peuvent être orchestrés pendant la mitose.

Il a aussi été démontré que la kinésine-5 de *X. leavis*, également une kinésine bipolaire, favorise la croissance des microtubules *in vitro* [239]. Cette double fonction pourrait être une caractéristique générale des kinésines bipolaires et pourait assurer la bonne fonction du fuseau mitotique.

Enfin, les résultats obtenus *in vitro* suggèrent un mécanisme non conventionnel pour la régulation de la dynamique des microtubules par Klp9. Klp9 semble être capable de fixer une vitesse de croissance bien définie, indépendante de la concentration en tubuline et indépendante de la vitesse de croissance en absence de Klp9. Cela indique que la kinésine-6 peut favoriser et bloquer l'addition de dimères de tubuline au réseau de microtubules.
Ceci était surprenant puisque les moteurs ou MAPs sont généralement connus pour favoriser ou empêcher la polymérisation des microtubules.
Par conséquent, le moteur semble avoir adopté un mécanisme qui ressemble à celui utilisé par le régulateur de l'élongation des filaments d'actine, la formine. Les formines favorisent et bloquent l'ajout de sous-unités aux filaments d'actine, ce qui permet de fixer une vitesse de croissance des filaments actine à une valeur bien définie [585–588]. Je propose que la régulation de la croissance des microtubules médiée par Klp9 peut être expliquée par le mécanisme suivant: en se liant au dernier dimère de tubuline de chaque protofilament, Klp9 déplace les dimères de tubuline libres vers la pointe du microtubule et favorise son incorporation à sa fréquence de pas.
En fait, ce mécanisme permet à Klp9 de coordonner intrinsèquement le glissement et la croissance des microtubules en fixant des vitesses égales.

# Bibliography


[1] R. Hooke. *Micrographia: Or Some Physiological Descriptions of Minute Bodies Made by Magnifying Glasses with Observations and Inquiries Thereupon*. James Allestry: London, UK, 1667.

[2] R. Virchow. *Die Cellularpathologie in Ihrer Begründung auf Physiologische und Pathologische Gewebelehre*. Verlag von August Hirschwald: Berlin, Deutschland, 1858.

[3] Walther Flemming. *Beiträge zur Kenntniss der Zelle und ihrer Lebenserscheinungen.* Archiv für mikroskopische Anatomie., 1880.

[4] A. F. Hughes and M. M. Swann. Anaphase Movements in the Living Cell. *Journal of Experimental Biology*, 25(1):45–72, 1948. doi: 10.1242/jeb.25.1.45.

[5] Shinya Inoue. Polarization optical studies of the mitotic spindle. *Chromosoma*, 5:487–500, 1953.

[6] B. R. Brinkley and Elton Stubblefield. The fine structure of the kinetochore of a mammalian cell in vitro. *Chromosoma*, 19(1):28–43, 1966. doi: 10.1007/BF00332792.

[7] Patricia Harris. Some observations concerning metakinesis in sea urchin eggs. *Journal of Cell Biology*, 25 (6):73–77, 1965. doi: 10.1083/jcb.25.1.73.

[8] Richard J. McIntosh and Story C. Landis. The distribution of spindle microtubules during mitosis in cultured human cells. *Journal of Cell Biology*, 49(6):468–497, 1971. doi: 10.1083/jcb.49.2.468.

[9] Kent Mcdonald, Jeremy D Pickett-Heaps, J Richard Mcintosh, and David H. Tippit. On the mechanism of anaphase spindle elongation in diatom vulgare. *Journal of Cell Biology*, 74:377–388, 1977. doi: 10.1083/jcb.74.2.377.

[10] Richard C Weisenberg. Microtubule formation in vitro in solutions containing low calcium concentrations. *Science*, 177(4054):1104–1105, 1972. doi: 10.1126/science.177.4054.1104.

[11] J. V. Kilmartin and A. E. M. Adams. Structural rearrangements of tubulin and actin during the cell cycle of the yeast saccharomyces. *Journal of Cell Biology*, 98:922–933, 1984. doi: 10.1083/jcb.98.3.922.

[12] Tim Mitchison and Marc Kirschner. Dynamic instability of microtubule growth. *Nature*, 312(14):237–242, 1984. doi: 10.1002/bies.950070403.

[13] Mark Winey, Cynthia L. Mamay, Eileen T. O'Toole, David N. Mastronarde, Jr. Thomas H. Giddings, Kent L. McDonald, and J. Richard McIntosh. Three-Dimensional Ultrastructural Analysis of the Saccharomyces cerevisiae Mitotic Spindle. *The Journal of cell biology*, 129(6):1601–1615, 1995. doi: 10.7868/s0869803118010010.

[14] R. J. Leslie and J. D. Pickett Heaps. Ultraviolet microbeam irradiations of mitotic diatoms: Investigation of spindle elongation. *Journal of Cell Biology*, 96(2):548–561, 1983. doi: 10.1083/jcb.96.2.548.

[15] Alexey Khodjakov, Sabrina La Terra, and Fred Chang. Laser Microsurgery in Fission Yeast: Role of the Mitotic Spindle Midzone in Anaphase B. *Current Biology*, 14(10):1330–1340, 2004. doi: 10.1016/j.cub.2004.07.028.

[16] Iva Tolic-Norrelykke, Leonardo Sacconi, Geneviève Thon, and Francesco S. Pavone. Positioning and Elongation of the Fission Yeast Spindle by Microtubule-Based Pushing. *Current Biology*, 14(13):1181–1186, 2004. doi: 10.1016/j.cub.2004.06.029.

[17] Leland H. Hartwell, Joseph Culotti, John R. Pringle, and Brian J. Reid. Genetic control of the cell division cycle in yeast. *Science*, 183(4120):46–51, 1974. doi: 10.1126/science.183.4120.46.

[18] Paul Nurse. Genetic control of cell size at the cell division in yeast. *Nature*, 256:547–551, 1975. doi: 10.1007/BF00268085.

[19] J. V. Kilmartin and A. E. M. Adams. Structural rearrangements of tubulin and actin during the cell cycle of the yeast saccharomyces. *Journal of Cell Biology*, 98:922–933, 1984.

[20] Iain M. Hagan and M. Yanagida. Kinesin-related cut7 protein associates with mitotic and meiotic spindles in fission yeast. *Nature*, 356:74–76, 1992. doi: 10.1038/356074a0.

[21] Iain M. Hagan and M. Yanagida. Novel potential mitotic motor protein encoded by the fission yeast cut7+ gene. *Nature*, 347:563–566, 1990. doi: 10.1038/347563a0.

[22] Lukas C. Kapitein, Erwin J.G. Peterman, Benjamin H. Kwok, Jeffrey H. Kim, Tarun M. Kapoor, and Christoph F. Schmidt. The bipolar mitotic kinesin Eg5 moves on both microtubules that it crosslinks. *Letter to Nature*, 435(5):114–118, 2005. doi: 10.1038/nature03493.

[23] G. G. Borisy and E. W. Taylor. The mechanism of action of colchicine. Binding of colchincine-3H to cellular protein. *The Journal of cell biology*, 34(2):525–533, 1967. doi: 10.1083/jcb.34.2.525.

[24] Jacques Dubochet, Marc Adrian, Jiin-Ju Chang, Jean-Claude Homo, Jean Lepault, Alasdair W. McDowall, and Patrick Schultz. Cryo-electron microscopy of vitrified specimens. *Quarterly Reviews of Biophysics*, 21 (2):129–228, 1988. doi: 10.1017/S0033583500004297.

[25] R. H. Wade and D. Chretien. Cryoelectron microscopy of microtubules. *Journal of Structural Biology*, 110 (1):1–27, 1993. doi: 10.1006/jsbi.1993.1001.

[26] Eva Nogales and Sjors H.W. Scheres. Cryo-EM: A Unique Tool for the Visualization of Macromolecular Complexity. *Molecular Cell*, 58(4):677–689, 2015. doi: 10.1016/j.molcel.2015.02.019.

[27] Marileen Dogterom and Thomas Surrey. Microtubule organization in vitro. *Current Opinion in Cell Biology*, 25(1):23–29, 2013. doi: 10.1016/j.ceb.2012.12.002.

[28] Chii Shyang Fong, Gregory Mazo, Tuhin Das, Joshua Goodman, Minhee Kim, Brian P. O'Rourke, Denisse Izquierdo, and Meng Fu Bryan Tsou. 53BP1 and USP28 mediate p53- dependent cell cycle arrest in response to centrosome loss and prolonged mitosis. *eLife*, 5(e16270):1–18, 2016. doi: 10.7554/eLife.16270.

[29] Neil J. Ganem, Susana A. Godinho, and David Pellman. A mechanism linking extra centrosomes to chromosomal instability. *Nature*, 460(7252):278–282, 2009. doi: 10.1038/nature08136.

[30] Franz Meitinger, John V. Anzola, Manuel Kaulich, Amelia Richardson, Joshua D. Stender, Christopher Benner, Christopher K. Glass, Steven F. Dowdy, Arshad Desai, Andrew K. Shiau, and Karen Oegema. 53BP1 and USP28 mediate p53 activation and G1 arrest after centrosome loss or extended mitotic duration. *Journal of Cell Biology*, 214(2):155–166, 2016. doi: 10.1083/jcb.201604081.

[31] Yumi Uetake and Greenfield Sluder. Activation of the apoptotic pathway during prolonged prometaphase blocks daughter cell proliferation. *Molecular Biology of the Cell*, 29(22):2632–2643, 2018. doi: 10.1091/mbc.E18-01-0026.

[32] Yumi Uetake and Greenfield Sluder. Prolonged prometaphase blocks daughter cell proliferation despite normal completion of mitosis. *Current Biology*, 20(18):1666–1671, 2010. doi: 10.1016/j.cub.2010.08.018.

[33] Michel Bornens. Centrosome organization and functions. *Current Opinion in Structural Biology*, 66:199–206, 2021. doi: 10.1016/j.sbi.2020.11.002.

[34] Robert E. Palazzo, Jacalyn M. Vogel, Bradley J. Schnackenberg, Dawn R. Hull, and Xingyong Wu. Centrosome maturation. *Current Topics in Developmental Biology*, 49:449–470, 1999. doi: 10.1016/s0070-2153(99)49021-0.

[35] V. Mennella, B. Keszthelyi, K. L. Mcdonald, B. Chhun, F. Kan, G. C. Rogers, B. Huang, and D. A. Agard. Subdiffraction-resolution fluorescence microscopy reveals a domain of the centrosome critical for pericentriolar material organization. *Nature Cell Biology*, 14(11):1159–1168, 2012. doi: 10.1038/ncb2597.

[36] Steffen Lawo, Monica Hasegan, Gagan D. Gupta, and Laurence Pelletier. Subdiffraction imaging of centrosomes reveals higher-order organizational features of pericentriolar material. *Nature Cell Biology*, 14(11):1148–1158, 2012. doi: 10.1038/ncb2591.

[37] Justin M. Kollman, Andreas Merdes, Lionel Mourey, and David A. Agard. Microtubule nucleation by γ-tubulin complexes. *Nature Reviews Molecular Cell Biology*, 12(11):709–721, 2011. doi: 10.1038/nrm3209.

[38] Roy M. Golsteyn, Kirsten E. Mundt, Andrew M. Fry, and Erich A. Nigg. Cell cycle regulation of the activity and subcellular localization of PLK1, a human protein kinase implicated in mitotic spindle function. *Journal of Cell Biology*, 129(6):1617–1628, 1995. doi: 10.1083/jcb.129.6.1617.

[39] Heidi A. Lane and Erich A. Nigg. Antibody microinjection reveals an essential role for human polo-like kinase 1 (Plk1) in the functional maturation of mitotic centrosomes. *Journal of Cell Biology*, 135(6):1701–1713, 1996. doi: 10.1083/jcb.135.6.1701.

[40] Tien Chen Lin, Annett Neuner, Dirk Flemming, Peng Liu, Takumi Chinen, Ursula Jäkle, Robert Arkowitz, and Elmar Schiebel. MOZ ART1 and γ-tubulin complex receptors are both required to turn $\gamma$-TuSC into an active microtubule nucleation template. *Journal of Cell Biology*, 215(6):823–840, 2016. doi: $10.1083/\mathrm{jcb}.201606092$.

[41] Midori Ohta, Zhiling Zhao, Di Wu, Shaohe Wang, Jennifer L. Harrison, J. Sebastián Gómez-Cavazos, Arshad Desai, and Karen F. Oegema. Polo-like kinase 1 independently controls microtubule-nucleating capacity and size of the centrosome. *Journal of Cell Biology*, 220(2), 2021. doi: $10.1083/\mathrm{JCB}.202009083$.

[42] Michal Wieczorek, Tzu Lun Huang, Linas Urnavicius, Kuo Chiang Hsia, and Tarun M. Kapoor. MZT Proteins Form Multi-Faceted Structural Modules in the $\gamma$-Tubulin Ring Complex. *Cell Reports*, 31(13):107791, 2020. doi: $10.1016/\mathrm{j.celrep}.2020.107791$.

[43] Oliver Wueseke, David Zwicker, Anne Schwager, Yao Liang Wong, Karen Oegema, Frank Jülicher, Anthony A. Hyman, and Jeffrey B. Woodruff. Polo-like kinase phosphorylation determines Caenorhabditis elegans centrosome size and density by biasing SPD-5 toward an assembly-competent conformation. *Biology Open*, 5(10):1431–1440, 2016. doi: $10.1242/\mathrm{bio}.020990$.

[44] Andrew Muroyama, Lindsey Seldin, and Terry Lechler. Characterization and reconstitution of Drosophila γ-tubulin ring complex subunits. *Journal of Cell Biology*, 151(7):1513–1523, 2000.

[45] Laurence Haren, Marie Hélène Remy, Ingrid Bazin, Isabelle Callebaut, Michel Wright, and Andreas Merdes. NEDD1-dependent recruitment of the $\gamma$-tubulin ring complex to the centrosome is necessary for centriole duplication and spindle assembly. *Journal of Cell Biology*, 172(4):505–515, 2006. doi: $10.1083/\mathrm{jcb}.200510028$.

[46] James R.A. Hutchins, Yusuke Toyoda, Björn Hegemann, Ina Poser, Jean Karim Hériché, Martina M. Sykora, Martina Augsburg, Otto Hudecz, Bettina A. Buschhorn, Jutta Bulkescher, Christian Conrad, David Comartin, Alexander Schleiffer, Mihail Sarov, Andrei Pozniakovsky, Mikolaj Michal Slabicki, Siegfried Schloissnig, Ines Steinmacher, Marit Leuschner, Andrea Ssykor, Steffen Lawo, Laurence Pelletier, Holger Stark, Kim Nasmyth, Jan Ellenberg, Richard Durbin, Frank Buchholz, Karl Mechtler, Anthony A. Hyman, and Jan Michael Peters. Systematic analysis of human protein complexes identifies chromosome segregation proteins. *Science*, 328(5978):593–599, 2010. doi: $10.1126/\mathrm{science}.1181348$.

[47] Jens Lüders, Urvashi K. Patel, and Tim Stearns. GCP-WD is a $\gamma$-tubulin targeting factor required for centrosomal and chromatin-mediated microtubule nucleation. *Nature Cell Biology*, 8(2):137–147, 2006. doi: $10.1038/\mathrm{ncb}1349$.

[48] Neus Teixidó-Travesa, Joan Roig, and Jens Lüders. The where, when and how of microtubule nucleation - one ring to rule them all. *Journal of Cell Science*, 125(19):4445–4456, 2012. doi: $10.1242/\mathrm{jcs}.106971$.

[49] Yuk Kwan Choi, Pengfei Liu, Siu Kwan Sze, Chao Dai, and Robert Z. Qi. CDK5RAP2 stimulates microtubule nucleation by the $\gamma$-tubulin ring complex. *Journal of Cell Biology*, 191(6):1089–1095, 2010. doi: $10.1083/\mathrm{jcb}.201007030$.

[50] Mikiko Takahasi, Akiko Yamagiwa, Tamako Nishimura, Hideyuki Mukai, and Yoshitaka Ono. Functional Proteomic Analysis of Human Nucleolus. *Molecular Biology of the Cell*, 13(September):3235–3245, 2002. doi: $10.1091/\mathrm{mbc.E02}$.

[51] Mónica Bettencourt-Dias. Q&A: Who needs a centrosome? *BMC Biology*, 11:1–7, 2013. doi: 10.1186/1741-7007-11-28.

[52] Alexey Khodjakov, Richard W. Cole, Berl R. Oakley, and Conly L. Rieder. Centrosome-independent mitotic spindle formation in vertebrates. *Current Biology*, 10(2):59–67, 2000. doi: 10.1016/S0960-9822(99)00276-6.

[53] Melina Schuh and Jan Ellenberg. Self-Organization of MTOCs Replaces Centrosome Function during Acentrosomal Spindle Assembly in Live Mouse Oocytes. *Cell*, 130(3):484–498, 2007. doi: 10.1016/j.cell.2007.06.025.

[54] Renata Basto, Joyce Lau, Tatiana Vinogradova, Alejandra Gardiol, C. Geoffrey Woods, Alexey Khodjakov, and Jordan W. Raff. Flies without Centrioles. *Cell*, 125(7):1375–1386, 2006. doi: 10.1016/j.cell.2006.05.025.

[55] Takumi Chinen, Shohei Yamamoto, Yutaka Takeda, Koki Watanabe, Kanako Kuroki, Kaho Hashimoto, Daisuke Takao, and Daiju Kitagawa. NuMA assemblies organize microtubule asters to establish spindle bipolarity in acentrosomal human cells. *The EMBO Journal*, 39(2):1–18, 2020. doi: 10.15252/embj.2019102378.

[56] Alain Debec, William Sullivan, and Monica Bettencourt-Dias. Centrioles: Active players or passengers during mitosis? *Cellular and Molecular Life Sciences*, 67(13):2173–2194, 2010. doi: 10.1007/s00018-010-0323-9.

[57] Ann M. Cavanaugh and Sue L. Jaspersen. Big Lessons from Little Yeast: Budding and Fission Yeast Centrosome Structure, Duplication, and Function. *Annual Review of Genetics*, 51(1):361–383, 2017. doi: 10.1146/annurev-genet-120116-024733.

[58] Barbara Boettcher and Yves Barral. The cell biology of open and closed mitosis. *Nucleus (United States)*, 4(3), 2013. doi: 10.4161/nucl.24676.

[59] E. K. McCully and C. F. Robinow. Mitosis in the fission yeast Schizosaccharomyces pombe: a comparative study with light and electron microscopy. *Journal of Cell Science*, 9(2):475–507, 1971. doi: 10.1242/jcs.9.2.475.

[60] Rubai Ding, Robert R. West, Mary Morphew, Berl R. Oakley, and J. Richard McIntosh. The spindle pole body of Schizosaccharomyces pombe enters and leaves the nuclear envelope as the cell cycle proceeds. *Molecular Biology of the Cell*, 8(8):1461–1479, 1997. doi: 10.1091/mbc.8.8.1461.

[61] Chii Shyang Fong, Masamitsu Sato, and Takashi Toda. Fission yeast Pcp1 links polo kinase-mediated mitotic entry to γ-tubulin-dependent spindle formation. *EMBO Journal*, 29(1):120–130, 2010. doi: 10.1038/emboj.2009.331.

[62] Richard C. Weisenberg, William J. Deery, and Peter J. Dickinson. Tubulin-Nucleotide Interactions during the Polymerization and Depolymerization of Microtubules. *Biochemistry*, 15(19):4248–4254, 1976. doi: 10.1021/bi00664a018.

[63] Marie France Carlier and Dominique Pantaloni. Kinetic Analysis of Guanosine 5'-Triphosphate Hydrolysis Associated with Tubulin Polymerization. *Biochemistry*, 20(7):1918–1924, 1981. doi: 10.1021/bi00510a030.

[64] Louise Evans, Tim Mitchison, and Marc Kirschner. Influence of the centrosome on the structure of nucleated microtubules. *Journal of Cell Biology*, 100(4):1185 1191, 1985. doi: 10.1083/jcb.100.4.1185.

[65] Lewis G. Tilney, Joseph Bryan, Doris J. Bush, Keigi Fujiwara, Mark S. Mooseker, Douglas B. Murphy, and Daniel H. Snyder. Microtubules: Evidence for 13 protofilaments. *Journal of Cell Biology*, 59(2):267–275, 1973. doi: 10.1083/jcb.59.2.267.

[66] Eva-Maria -M Mandelkow, Roberto Rapp, and Eckhard Mandelkow. Microtubule structure studied by quick freezing: Cryo-electron microscopy and freeze fracture. *Journal of Microscopy*, 141(3):361–373, 1986. doi: 10.1111/j.1365-2818.1986.tb02729.x.

[67] Bruce McEwen and Stuart J. Edelstein. Evidence for a mixed lattice in microtubules reassembled in vitro. *Journal of Molecular Biology*, 139(2):123–143, 1980. doi: 10.1016/0022-2836(80)90300-9.

[68] L. A. Amos and A. Klug. Arrangement of subunits in flagellar microtubules. *Journal of Cell Science*, 14(3): 523–549, 1974. doi: 10.1242/jcs.14.3.523.

[69] Carol Allen and Gary G. Borisy. Structural polarity and directional growth of microtubules of Chlamydomonas flagella. *Journal of Molecular Biology*, 90(2):381–402, 1974. doi: 10.1016/0022-2836(74)90381-7.

[70] D. Kuchnir Fygenson, H. Flyvbjerg, K. Sneppen, A. Libchaber, and S. Leibler. Spontaneous nucleation of microtubules. *Physical Review E*, 51(5):5058–5063, 1995. doi: 10.1103/PhysRevE.51.5058.

[71] W. A. Voter and H. P. Erickson. The kinetics of microtubule assembly. Evidence for a two-stage nucleation mechanism. *Journal of Biological Chemistry*, 259(16):10430–10438, 1984. doi: 10.1016/s0021-9258(18)90982-8.

[72] Michal Wieczorek, Susanne Bechstedt, Sami Chaaban, and Gary J. Brouhard. Microtubule-associated proteins control the kinetics of microtubule nucleation. *Nature Cell Biology*, 17(7):907–916, 2015. doi: 10.1038/ncb3188.

[73] Denis Chrétien and Richard H. Wade. New data on the microtubule surface lattice. *Biology of the Cell*, 71 (1-2):161–174, 1991. doi: 10.1016/0248-4900(91)90062-R.

[74] Myron C. Ledbetter and Keith R. Porter. Morphology of microtubules of plant cells. *Science*, 144(3620): 872–874, 1964. doi: 10.1126/science.144.3620.872.

[75] T. Horio, S. Uzawa, M. K. Jung, B. R. Oakley, K. Tanaka, and M. Yanagida. The fission yeast $\gamma$-tubulin is essential for mitosis and is localized at microtubule organizing centres. *Journal of Cell Science*, 99(4): 693–700, 1991. doi: 10.1242/jcs.99.4.693.

[76] Tien chen Lin, Annett Neuner, and Elmar Schiebel. Targeting of $\gamma$-tubulin complexes to microtubule organizing centers: Conservation and divergence. *Trends in Cell Biology*, 25(5):296–307, 2015. doi: 10.1016/j.tcb.2014.12.002.

[77] Andrew Muroyama, Lindsey Seldin, and Terry Lechler. Role of $\gamma$-tubulin in mitosis-specific microtubule nucleation from the Schizosaccharomyces pombe spindle pole body. *Journal of Cell Science*, 109(1):165–177, 1996.

[78] Michael Knop, Gislene Pereira, Silke Geissler, Katrin Grein, and Elmar Schiebel. The spindle pole body component Spc97p interacts with the $\gamma$-tubulin of Saccharomyces cerevisiae and functions in microtubule organization and spindle pole body duplication. *EMBO Journal*, 16(7):1550–1564, 1997. doi: $10.1093/\mathrm{emboj}/16.7.1550$.

[79] Karen Oegema, Arshad Desai, Sonja Rybina, Matthew Kirkham, and Anthony A. Hyman. Functional analysis of kinetochore assembly in Caenorhabditis elegans. *Journal of Cell Biology*, 153(6):1209–1225, 2001. doi: $10.1083/\mathrm{jcb}.153.6.1209$.

[80] Leah Vardy and Takashi Toda. The fission yeast γ-tubulin complex is required in G1 phase and is a component of the spindle assembly checkpoint. *The EMBO Journal*, 19(22):6098–6111, 2000. doi: $10.1093/\mathrm{emboj}/19.22.6098$.

[81] Dani B.N. Vinh, Joshua W. Kern, William O. Hancock, Jonathon Howard, and Trisha N. Davis. Reconstitution and Characterization of Budding Yeast γ-Tubulin Complex. *Molecular Biology of the Cell*, 13(April):114–1157, 2002. doi: $10.1091/\mathrm{mbc}.02$.

[82] Justin M. Kollman, Jessica K. Polka, Alex Zelter, Trisha N. Davis, and David A. Agard. Microtubule nucleating $\gamma$-TuSC assembles structures with 13-fold microtubule-like symmetry. *Nature*, 466(7308):879–882, 2010. doi: $10.1038/\mathrm{nature}09207$.

[83] Hector Aldaz, Luke M. Rice, Tim Stearns, and David A. Agard. Insights into microtubule nucleation from the crystal structure of human $\gamma$-tubulin. *Nature*, 435(7041):523–527, 2005. doi: $10.1038/\mathrm{nature}03586$.

[84] Michelle Moritz, Michael B. Braunfeld, Vincent Guénebaut, John Heuser, and David A. Agard. Structure of the $\gamma$-tubulin ring complex: A template for microtubule nucleation. *Nature Cell Biology*, 2(6):365–370, 2000. doi: $10.1038/35014058$.

[85] Tim Stearns and Marc Kirschner. In vitro reconstitution of centrosome assembly and function: The central role of $\gamma$-tubulin. *Cell*, 76(4):623–637, 1994. doi: $10.1016/0092\text{-}8674(94)90503\text{-}7$.

[86] C. Wiese and Y. Zheng. A new function for the $\gamma$-tubulin ring complex as a microtubule minus-end cap. *Nature Cell Biology*, 2(6):358–364, 2000. doi: $10.1038/35014051$.

[87] Yixian Zheng, Mei Lie Wong, Bruce Alberts, and Tim Mitchison. Nucleation of microtubule assembly by a y-tubulin-containing ring complex. *Nature*, 378(7):578–583, 1995. doi: $10.1038/378578\mathrm{a}0$.

[88] Andreas Anders, Paula C.C. Lourenco, and Kenneth E. Sawin. Noncore Components of the Fission Yeast γ-Tubulin Complex. *Molecular Biology of the Cell*, 17:5075–5093, 2006. doi: $10.1091/\mathrm{mbc}.\mathrm{E}05$.

[89] Deepsharan K. Dhani, Benjamin T. Goult, Gifty M. George, Daniel T. Rogerson, Danny A. Bitton, Crispin J. Miller, John W.R. Schwabe, and Kayoko Tanaka. Mzt1/Tam4, a fission yeast MOZART1 homologue, is an essential component of the γ-tubulin complex and directly interacts with GCP3/Alp6. *Molecular Biology of the Cell*, 24(21):3337–3349, 2013. doi: $10.1091/\mathrm{mbc}.\mathrm{E}13\text{-}05\text{-}0253$.

[90] Akiko Fujita, Leah Vardy, Miguel Angel Garcia, and Takashi Toda. A Fourth Component of the Fission Yeast γ-Tubulin Complex, Alp16, Is Required for Cytoplasmic Microtubule Integrity and Becomes Indispensable

When γ-Tubulin Function Is Compromised. *Molecular Biology of the Cell*, 13(July):2360–2373, 2002. doi: 10.1091/mbc.02.

[91] T. J. Keating and G. G. Borisy. Immunostructural evidence for the template mechanism of microtubule nucleation. *Nature Cell Biology*, 2(6):352–357, 2000. doi: 10.1038/35014045.

[92] Srinivas Venkatram, Joseph J. Tasto, Anna Feoktistova, Jennifer L. Jennings, Andrew J. Link, and Kathleen L. Gould. Identification and Characterization of Two Novel Proteins Affecting Fission Yeast γ-tubulin Complex Function. *Molecular Biology of the Cell*, 15(May):2287–2301, 2004. doi: 10.1091/mbc.E03.

[93] Tanja Consolati, Julia Locke, Johanna Roostalu, Zhuo Angel Chen, Julian Gannon, Jayant Asthana, Wei Ming Lim, Fabrizio Martino, Milos A. Cvetkovic, Juri Rappsilber, Alessandro Costa, and Thomas Surrey. Microtubule Nucleation Properties of Single Human γTuRCs Explained by Their Cryo-EM Structure. *Developmental Cell*, 53(5):603–617.e8, 2020. doi: 10.1016/j.devcel.2020.04.019.

[94] Dorian Farache, Laurent Emorine, Laurence Haren, and Andreas Merdes. Assembly and regulation of γ-tubulin complexes. *Open Biology*, 8(3), 2018. doi: 10.1098/rsob.170266.

[95] Valérie Guillet, Martine Knibiehler, Lynn Gregory-Pauron, Marie Héléne Remy, Cécile Chemin, Brigitte Raynaud-Messina, Cécile Bon, Justin M. Kollman, David A. Agard, Andreas Merdes, and Lionel Mourey. Crystal structure of γ-tubulin complex protein GCP4 provides insight into microtubule nucleation. *Nature Structural and Molecular Biology*, 18(8):915–919, 2011. doi: 10.1038/nsmb.2083.

[96] Justin M. Kollman, Charles H. Greenberg, Sam Li, Michelle Moritz, Alex Zelter, Kimberly K. Fong, Jose Jesus Fernandez, Andrej Sali, John Kilmartin, Trisha N. Davis, and David A. Agard. Ring closure activates yeast γTuRC for species-specific microtubule nucleation. *Nature Structural and Molecular Biology*, 22(2):132–137, 2015. doi: 10.1038/nsmb.2953.

[97] Andrew Muroyama, Lindsey Seldin, and Terry Lechler. Divergent regulation of functionally distinct γ-tubulin complexes during differentiation. *Journal of Cell Biology*, 213(6):679–692, 2016. doi: 10.1083/jcb.201601099.

[98] Jacopo Scrofani, Teresa Sardon, Sylvain Meunier, and Isabelle Vernos. Microtubule nucleation in mitosis by a RanGTP-dependent protein complex. *Current Biology*, 25(2):131–140, 2015. doi: 10.1016/j.cub.2014.11.025.

[99] Raymundo Alfaro-Aco and Sabine Petry. How TPX2 helps microtubules branch out. *Cell Cycle*, 16(17):1560–1561, 2017. doi: 10.1080/15384101.2017.1348080.

[100] Andrei V. Popov, Fedor Severin, and Eric Karsenti. XMAP215 is required for the microtubule-nucleating activity of centrosomes. *Current Biology*, 12(15):1326–1330, 2002. doi: 10.1016/S0960-9822(02)01033-3.

[101] Akanksha Thawani, Rachel S. Kadzik, and Sabine Petry. XMAP215 is a microtubule nucleation factor that functions synergistically with the γ-tubulin ring complex. *Nature Cell Biology*, 20(5):575–585, 2018. doi: 10.1038/s41556-018-0091-6.

[102] Jan Brugués, Valeria Nuzzo, Eric Mazur, and Daniel J. Needleman. Nucleation and transport organize microtubules in metaphase spindles. *Cell*, 149(3):554–564, 2012. doi: 10.1016/j.cell.2012.03.027.

[103] Nicole M. Mahoney, Gohta Goshima, Adam D. Douglass, and Ronald D. Vale. Making microtubules and mitotic spindles in cells without functional centrosomes. *Current Biology*, 16(6):564–569, 2006. doi: 10.1016/j.cub.2006.01.053.

[104] Takashi Murata, Seiji Sonobe, Tobias I. Baskin, Susumu Hyodo, Seiichiro Hasezawa, Toshiyuki Nagata, Tetsuya Horio, and Mitsuyasu Hasebe. Microtubule-dependent microtubule nucleation based on recruitment of $\gamma$-tubulin in higher plants. *Nature Cell Biology*, 7(10):961–968, 2005. doi: 10.1038/ncb1306.

[105] Jonathan J. Ward, Hélio Roque, Claude Antony, and François Nédélec. Mechanical design principles of a mitotic spindle. *eLife*, 3:e03398:1–28, 2014. doi: 10.7554/eLife.03398.

[106] Gohta Goshima, Mirjam Mayer, Nan Zhang, Nico Stuurman, and Ronald D. Vale. Augmin: A protein complex required for centrosome-independent microtubule generation within the spindle. *Journal of Cell Biology*, 181 (3):421–429, 2008. doi: 10.1083/jcb.200711053.

[107] Gohta Goshima, Roy Wollman, Sarah S. Goodwin, Nan Zhang, Jonathan M. Scholey, Ronald D. Vale, and Nico Stuurman. Genes required for mitotic spindle assembly in Drosophila S2 cells. *Science*, 316(5823): 417–421, 2007. doi: 10.1126/science.1141314.

[108] Steffen Lawo, Mikhail Bashkurov, Michael Mullin, Mariana Gomez Ferreria, Ralf Kittler, Bianca Habermann, Andrea Tagliaferro, Ina Poser, James R.A. Hutchins, Björn Hegemann, Deborah Pinchev, Frank Buchholz, Jan Michael Peters, Anthony A. Hyman, Anne Claude Gingras, and Laurence Pelletier. HAUS, the 8-Subunit Human Augmin Complex, Regulates Centrosome and Spindle Integrity. *Current Biology*, 19(10):816–826, 2009. doi: 10.1016/j.cub.2009.04.033.

[109] Sabine Petry, Celine Pugieux, Francois J. Nedelec, and Ronald D. Vale. Augmin promotes meiotic spindle formation and bipolarity in Xenopus egg extracts. *Proceedings of the National Academy of Sciences of the United States of America*, 108(35):14473–14478, 2011. doi: 10.1073/pnas.1110412108.

[110] Ryota Uehara, Ryu Suke Nozawa, Akiko Tomioka, Sabine Petry, Ronald D. Vale, Chikashi Obuse, and Gohta Goshima. The augmin complex plays a critical role in spindle microtubule generation for mitotic progression and cytokinesis in human cells. *Proceedings of the National Academy of Sciences of the United States of America*, 106(17):6998–7003, 2009. doi: 10.1073/pnas.0901587106.

[111] Ana F. David, Philippe Roudot, Wesley R. Legant, Eric Betzig, Gaudenz Danuser, and Daniel W. Gerlich. Augmin accumulation on long-lived microtubules drives amplification and kinetochore-directed growth. *Journal of Cell Biology*, 218(7):2150–2168, 2019. doi: 10.1083/jcb.201805044.

[112] Sabine Petry, Aaron C. Groen, Keisuke Ishihara, Timothy J. Mitchison, and Ronald D. Vale. Branching microtubule nucleation in xenopus egg extracts mediated by augmin and TPX2. *Cell*, 152(4):768–777, 2013. doi: 10.1016/j.cell.2012.12.044.

[113] Oliver J. Gruss, Rafael E. Carazo-Salas, Christoph A. Schatz, Giulia Guarguaglini, Jürgen Kast, Matthias Wilm, Nathalie Le Bot, Isabelle Vernos, Eric Karsenti, and Iain W. Mattaj. Ran induces spindle assembly by reversing the inhibitory effect of importin $\alpha$ on TPX2 activity. *Cell*, 104(1):83–93, 2001. doi: 10.1016/S0092-8674(01)00193-3.

[114] Petr Kalab and Rebecca Heald. The RanGTP gradient - A GPS for the mitotic spindle. *Journal of Cell Science*, 121(10):1577–1586, 2008. doi: 10.1242/jcs.005959.

[115] Suzanna L. Prosser and Laurence Pelletier. Mitotic spindle assembly in animal cells: A fine balancing act. *Nature Reviews Molecular Cell Biology*, 18(3):187–201, 2017. doi: 10.1038/nrm.2016.162.

[116] Paul D. Andrews, Yulia Ovechkina, Nick Morrice, Michael Wagenbach, Karen Duncan, Linda Wordeman, and Jason R. Swedlow. Aurora B regulates MCAK at the mitotic centromere. *Developmental Cell*, 6(2): 253–268, 2004. doi: 10.1016/S1534-5807(04)00025-5.

[117] Thomas J. Maresca, Aaron C. Groen, Jesse C. Gatlin, Ryoma Ohi, Timothy J. Mitchison, and Edward D. Salmon. Spindle Assembly in the Absence of a RanGTP Gradient Requires Localized CPC Activity. *Current Biology*, 19(14):1210–1215, 2009. doi: 10.1016/j.cub.2009.05.061.

[118] Eva Hannak, Karen Oegema, Matthew Kirkham, Pierre Gönczy, Bianca Habermann, and Anthony A. Hyman. The kinetically dominant assembly pathway for centrosomal asters in Caenorhabditis elegans is $\gamma$-tubulin dependent. *Journal of Cell Biology*, 157(4):591–602, 2002. doi: 10.1083/jcb.200202047.

[119] Eileen O'Toole, Garrett Greenan, Karen I. Lange, Martin Srayko, and Thomas Müller-Reichert. The role of $\gamma$-tubulin in centrosomal microtubule organization. *PLoS ONE*, 7(1):1–11, 2012. doi: 10.1371/journal.pone.0029795.

[120] Paula Sampaio, Elena Rebollo, Hanne Varmark, Claudio E. Sunkel, and Cayetano González. Organized microtubule arrays in $\gamma$-tubulin-depleted Drosophila spermatocytes. *Current Biology*, 11(22):1788–1793, 2001. doi: 10.1016/S0960-9822(01)00561-9.

[121] S. Strome, J. Powers, M. Dunn, K. Reese, C. J. Malone, J. White, G. Seydoux, and W. Saxton. Spindle dynamics and the role of $\gamma$-tubulin in early Caenorhabditis elegans embryos. *Molecular Biology of the Cell*, 12(6):1751–1764, 2001. doi: 10.1091/mbc.12.6.1751.

[122] Kah Wai Yau, Sam F.B. VanBeuningen, Inês Cunha-Ferreira, Bas M.C. Cloin, Eljo Y. VanBattum, Lena Will, Philipp Schätzle, Roderick P. Tas, Jaap VanKrugten, Eugene A. Katrukha, Kai Jiang, Phebe S. Wulf, Marina Mikhaylova, Martin Harterink, R. Jeroen Pasterkamp, Anna Akhmanova, Lukas C. Kapitein, and Casper C. Hoogenraad. Microtubule minus-end binding protein CAMSAP2 controls axon specification and dendrite development. *Neuron*, 82(5):1058–1073, 2014. doi: 10.1016/j.neuron.2014.04.019.

[123] Aaron C. Groen, Thomas J. Maresca, Jesse C. Gatlin, Edward D. Salmon, and Timothy J. Mitchison. Functional Overlap of Microtubule Assembly Factors in Chromatin-Promoted Spindle Assembly. *Molecular Biology of the Cell*, 20(June):2766–2773, 2009. doi: 10.1091/mbc.E09.

[124] Johanna Roostalu, Nicholas I. Cade, and Thomas Surrey. Complementary activities of TPX2 and chTOG constitute an efficient importin-regulated microtubule nucleation module. *Nature Cell Biology*, 17(11):1422–1434, 2015. doi: 10.1038/ncb3241.

[125] Christoph A. Schatz, Rachel Santarella, Andreas Hoenger, Eric Karsenti, Iain W. Mattaj, Oliver J. Gruss, and Rafael E. Carazo-Salas. Importin $\alpha$-regulated nucleation of microtubules by TPX2. *EMBO Journal*, 22 (9):2060–2070, 2003. doi: 10.1093/emboj/cdg195.

[126] Andrey Efimov, Alexey Kharitonov, Nadia Efimova, Jadranka Loncarek, Paul M. Miller, Natalia Andreyeva, Paul Gleeson, Niels Galjart, Ana R.R. Maia, Ian X. McLeod, John R. Yates, Helder Maiato, Alexey Khodjakov, Anna Akhmanova, and Irina Kaverina. Asymmetric CLASP-Dependent Nucleation of Noncentrosomal Microtubules at the trans-Golgi Network. *Developmental Cell*, 12(6):917–930, 2007. doi: 10.1016/j.devcel.2007.04.002.

[127] Jingchao Wu, Cecilia de Heus, Qingyang Liu, Benjamin P. Bouchet, Ivar Noordstra, Kai Jiang, Shasha Hua, Maud Martin, Chao Yang, Ilya Grigoriev, Eugene A. Katrukha, A. F.Maarten Altelaar, Casper C. Hoogenraad, Robert Z. Qi, Judith Klumperman, and Anna Akhmanova. Molecular Pathway of Microtubule Organization at the Golgi Apparatus. *Developmental Cell*, 39(1):44–60, 2016. doi: 10.1016/j.devcel.2016.08.009.

[128] Dmitry Nashchekin, Artur Ribeiro Fernandes, and Daniel St Johnston. Patronin/Shot Cortical Foci Assemble the Noncentrosomal Microtubule Array that Specifies the Drosophila Anterior-Posterior Axis. *Developmental Cell*, 38(1):61–72, 2016. doi: 10.1016/j.devcel.2016.06.010.

[129] Vanya Vasileva, Marek Gierlinski, Zuojun Yue, Nicola O'Reilly, Etsushi Kitamura, and Tomoyuki U. Tanaka. Molecular mechanisms facilitating the initial kinetochore encounter with spindle microtubules. *Journal of Cell Biology*, 216(6):1609–1622, 2017. doi: 10.1083/jcb.201608122.

[130] R. A. Walker, E. T. O'Brien, N. K. Pryer, M. F. Soboeiro, W. A. Voter, H. P. Erickson, and E. D. Salmon. Dynamic instability of individual microtubules analyzed by video light microscopy: rate constants and transition frequencies. *The Journal of cell biology*, 107(4):1437–1448, 1988. doi: 10.1083/jcb.107.4.1437.

[131] Eva Nogales, S.G. Wolf, and K.H. Downing . Structure of the a-b tubulin dimer by electron crystallography. *Nature*, 6(8):786–787, 1998. doi: 10.1038/34465.

[132] Eva Nogales, Michael Whittaker, Ronald A. Milligan, and Kenneth H. Downing. High-resolution model of the microtubule. *Cell*, 96(1):79–88, 1999. doi: 10.1016/S0092-8674(00)80961-7.

[133] J. Howard and Anthony A. Hyman. Dynamics and mechanics of the microtubule plus end. *Nature*, 422 (6933):753–8, 2003. doi: 10.1038/nature01600.

[134] Johanna Roostalu, Claire Thomas, Nicholas Ian Cade, Simone Kunzelmann, Ian A. Taylor, and Thomas Surrey. The speed of GTP hydrolysis determines GTP cap size and controls microtubule stability. *eLife*, 9: 1–22, 2020. doi: 10.7554/eLife.51992.

[135] Rubén M. Buey, J. Fernando Díaz, and José M. Andreu. The nucleotide switch of tubulin and microtubule assembly: A polymerization-driven structural change. *Biochemistry*, 45(19):5933–5938, 2006. doi: 10.1021/bi060334m.

[136] Agata Nawrotek, Marcel Knossow, and Benoît Gigant. The determinants that Govern microtubule assembly from the atomic structure of GTP-tubulin. *Journal of Molecular Biology*, 412(1):35–42, 2011. doi: 10.1016/j.jmb.2011.07.029.

[137] Luke M. Rice, Elizabeth A. Montabana, and David A. Agard. The lattice as allosteric effector: Structural studies of $\alpha\beta$- and $\gamma$-tubulin clarify the role of GTP in microtubule assembly. *PNAS*, 105(14):5378–5383, 2008. doi: 10.1073/pnas.0801155105.

[138] Gregory M. Alushin, Gabriel C. Lander, Elizabeth H. Kellogg, Rui Zhang, David Baker, and Eva Nogales. High-Resolution microtubule structures reveal the structural transitions in $\alpha\beta$-tubulin upon GTP hydrolysis. *Cell*, 157(5):1117–1129, 2014. doi: 10.1016/j.cell.2014.03.053.

[139] A. A. Hyman, D. Chretien, I. Arnal, and R. H. Wade. Structural changes accompanying GTP hydrolysis in microtubules: Information from a slowly hydrolyzable analogue guanylyl-($\alpha$,$\beta$)-methylene- diphosphonate. *Journal of Cell Biology*, 128(1-2):117–125, 1995. doi: 10.1083/jcb.128.1.117.

[140] E. M. Mandelkow, E. Mandelkow, and R. A. Milligan. Microtubule dynamics and microtubule caps: A time-resolved cryo-electron microscopy study. *Journal of Cell Biology*, 114(5):977–991, 1991. doi: 10.1083/jcb.114.5.977.

[141] R. A. Walker, Shinya Inoué, and E. D. Salmon. Asymmetric behavior of severed microtubule ends after ultraviolet-microbeam irradiation of individual microtubules in vitro. *Journal of Cell Biology*, 108(3):931–937, 1989. doi: 10.1083/jcb.108.3.931.

[142] A. A. Hyman, S. Salser, D. N. Drechsel, N. Unwin, and T. J. Mitchison. Role of GTP hydrolysis in microtubule dynamics: Information from a slowly hydrolyzable analogue, GMPCPP. *Molecular Biology of the Cell*, 3(10):1155–1167, 1992. doi: 10.1091/mbc.3.10.1155.

[143] Melissa K. Gardner, Marija Zanic, Christopher Gell, Volker Bormuth, and Jonathon Howard. Depolymerizing kinesins Kip3 and MCAK shape cellular microtubule architecture by differential control of catastrophe. *Cell*, 147(5):1092–1103, 2011. doi: 10.1016/j.cell.2011.10.037.

[144] Hugo Bowne-Anderson, Marija Zanic, Monika Kauer, and Jonathon Howard. Microtubule dynamic instability: A new model with coupled GTP hydrolysis and multistep catastrophe. *BioEssays*, 35(5):452–461, 2013. doi: 10.1002/bies.201200131.

[145] Courtney E. Coombes, Ami Yamamoto, Madeline R. Kenzie, David J. Odde, and Melissa K. Gardner. Evolving tip structures can explain age-dependent microtubule catastrophe. *Current Biology*, 23(14):1342–1348, 2013. doi: 10.1016/j.cub.2013.05.059.

[146] Ariane Dimitrov, Mélanie Quesnoit, Sandrine Moutel, Isabelle Cantaloube, Christian Poüs, and Franck Perez. Detection of GTP-tubulin conformation in vivo reveals a role for GTP remnants in microtubule rescues. *Science*, 322(5906):1353–1356, 2008. doi: 10.1126/science.1165401.

[147] Carolina Tropini, Elizabeth A. Roth, Marija Zanic, Melissa K. Gardner, and Jonathon Howard. Islands containing slowly hydrolyzable GTP analogs promote microtubule rescues. *PLoS ONE*, 7(1):1–5, 2012. doi: 10.1371/journal.pone.0030103.

[148] Manuel Théry and Laurent Blanchoin. Microtubule self-repair. *Current Opinion in Cell Biology*, 68:144–154, 2021. doi: 10.1016/j.ceb.2020.10.012.

[149] Charlotte Aumeier, Laura Schaedel, Jérémie Gaillard, Karin John, Laurent Blanchoin, and Manuel Théry. Self-repair promotes microtubule rescue. *Nature Cell Biology*, 18(10):1054–1064, 2016. doi: 10.1038/ncb3406.

[150] Laura Schaedel, Karin John, Jeremie Gaillard, Maxence V. Nachury, Laurent Blanchoin, and Manuel Thery. Microtubules self-repair in response to mechanical stress. *Nature Materials*, 14(11):1156–1163, 2015. doi: 10.1038/nmat4396.

[151] Laura Schaedel, Sarah Triclin, Denis Chrétien, Ariane Abrieu, Charlotte Aumeier, Jérémie Gaillard, Laurent Blanchoin, Manuel Théry, and Karin John. Lattice defects induce microtubule self-renewal. *Nature Physics*, 15(8):830–838, 2019. doi: 10.1038/s41567-019-0542-4.

[152] Annapurna Vemu, Ewa Szczesna, Elena A. Zehr, Jeffrey O. Spector, Nikolaus Grigorieff, Alexandra M. Deaconescu, and Antonina Roll-Mecak. Severing enzymes amplify microtubule arrays through lattice GTP-tubulin incorporation. *Science*, 361(6404), 2018. doi: 10.1126/science.aau1504.

[153] B R Brinkley and Joiner Cartwright. Ultrastructural Analysis of Mitotic Spindle. *The Journal of Cell Biology*, 50(1969):416–431, 1971.

[154] K. L. McDonald, E. T. O'Toole, D. N. Mastronarde, and J. R. McIntosh. Kinetochore microtubules in PTK cells. *Journal of Cell Biology*, 118(2):369–383, 1992. doi: 10.1083/jcb.118.2.369.

[155] Bruce F. McEwen, Amy B. Heagle, Grisel O. Cassels, Karolyn F. Buttle, and Conly L. Rieder. Kinetochore fiber maturation in PtK1 cells and its implications for the mechanisms of chromosome congression and anaphase onset. *Journal of Cell Biology*, 137(7):1567–1580, 1997. doi: 10.1083/jcb.137.7.1567.

[156] R. Ding, K. L. McDonald, and J. R. McIntosh. Three-Dimensional Reconstruction and Analysis of Mitotic Spindles from the Yeast, Schizosaccharomyces pombe. *Journal of Cell Biology*, 120(1):141–151, 1993. doi: 10.1083/jcb.120.1.141.

[157] B. R. Brinkley. Cold-labile and cold-stable microtubules in the mitotic spindle of mammalian cells. *Annals of the New York Academy of Science*, 253:428–439, 1975. doi: 10.1111/j.1749-6632.1975.tb19218.x.

[158] Cony L. Rieder. The Structure of the Cold-stable Kinetochore Fiber in Metaphase PtK1 Cells. *Chromosoma*, 84:145–158, 1981. doi: 10.1254/fpj.69.571.

[159] Danilo Lopes and Helder Maiato. The Tubulin Code in Mitosis and Cancer. *Cells*, 9(11), 2020. doi: 10.3390/cells9112356.

[160] Carsten Janke and Maria M. Magiera. The tubulin code and its role in controlling microtubule properties and functions. *Nature Reviews Molecular Cell Biology*, 21:307–326, 2020. doi: 10.1038/s41580-020-0214-3.

[161] D. N. Mastronarde, K. L. McDonald, R. Ding, and J. R. McIntosh. Interpolar spindle microtubules in PTK cells. *Journal of Cell Biology*, 123(6):1475–1489, 1993. doi: 10.1083/jcb.123.6.1475.

[162] Che-hang Yu, Stefanie Redemann, Hai-yin Wu, Robert Kiewisz, and Tae Yeon. Central-spindle microtubules are strongly coupled to chromosomes during both anaphase A and anaphase B. *Molecular Biology of the Cell*, 30:2503–2514, 2019. doi: 10.1091/mbc.E19-01-0074.

[163] Janko Kajtez, Anastasia Solomatina, Maja Novak, Bruno Polak, Kruno Vukušić, Jonas Rüdiger, Gheorghe Cojoc, Ana Milas, Ivana Šumanovac Šestak, Patrik Risteski, Federica Tavano, Anna H. Klemm, Emanuele Roscioli, Julie Welburn, Daniela Cimini, Matko Glunčić, Nenad Pavin, and Iva M. Tolić. Overlap microtubules

link sister k-fibres and balance the forces on bi-oriented kinetochores. *Nature Communications*, 7:1–11, 2016. doi: 10.1038/ncomms10298.

[164] Jeffrey K. Moore, Melissa D. Stuchell-Brereton, and John A. Cooper. Function of dynein in budding yeast: Mitotic spindle positioning in a polarized cell. *Cell Motility and the Cytoskeleton*, 66(8):546–555, 2009. doi: 10.1002/cm.20364.

[165] Stephan W Grill, Jonathon Howard, Erik Scha, Ernst H K Stelzer, and Anthony A Hyman. The Distribution of Active Force Generators Controls Mitotic Spindle Position. *Science*, 301(5632):518–521, 2003. doi: 10.1126/science.1086560.

[166] Thomas Müller-Reichert, Garrett Greenan, Eileen O'Toole, and Martin Srayko. The elegans of spindle assembly. *Cellular and Molecular Life Sciences*, 67(13):2195–2213, 2010. doi: 10.1007/s00018-010-0324-8.

[167] H. Funabiki, I. Hagan, S. Uzawa, and M. Yanagida. Cell cycle-dependent specific positioning and clustering of centromeres and telomeres in fission yeast. *Journal of Cell Biology*, 121(5):961–976, 1993. doi: 10.1083/jcb.121.5.961.

[168] Christian H. Haering, Ana Maria Farcas, Prakash Arumugam, Jean Metson, and Kim Nasmyth. The cohesin ring concatenates sister DNA molecules. *Nature*, 454(7202):297–301, 2008. doi: 10.1038/nature07098.

[169] Gunjan D. Mehta, Syed Meraj Azhar Rizvi, and Santanu Kumar Ghosh. Cohesin: A guardian of genome integrity. *Biochimica et Biophysica Acta - Molecular Cell Research*, 1823(8):1324–1342, 2012. doi: 10.1016/j.bbamcr.2012.05.027.

[170] Andrea Musacchio and Arshad Desai. A molecular view of kinetochore assembly and function. *Biology*, 6 (1):1–47, 2017. doi: 10.3390/biology6010005.

[171] Andrew D. McAinsh, Jessica D. Tytell, and Peter K. Sorger. Structure, Function, And Regulation Of Budding Yeast Kinetochores. *Annual Review of Cell and Developmental Biology*, 19:519–539, 2003. doi: 10.1146/annurev.cellbio.19.111301.155607.

[172] Janet L. Paluh, Eva Nogales, Berl R. Oakley, Kent McDonald, Alison L. Pidoux, and W. Z. Cande. A mutation in $\gamma$-tubulin alters microtubule dynamics and organization and is synthetically lethal with the kinesin-like protein Pkl1p. *Molecular Biology of the Cell*, 11(4):1225–1239, 2000. doi: 10.1091/mbc.11.4.1225.

[173] Noemi C. Steiner and Louise Clarke. A novel epigenetic effect can alter centromere function in fission yeast. *Cell*, 79(5):865–874, 1994. doi: 10.1016/0092-8674(94)90075-2.

[174] Iain M. Cheeseman, Joshua S. Chappie, Elizabeth M. Wilson-Kubalek, and Arshad Desai. The Conserved KMN Network Constitutes the Core Microtubule-Binding Site of the Kinetochore. *Cell*, 127(5):983–997, 2006. doi: 10.1016/j.cell.2006.09.039.

[175] Jennifer G. DeLuca, Walter E. Gall, Claudio Ciferri, Daniela Cimini, Andrea Musacchio, and E. D. Salmon. Kinetochore Microtubule Dynamics and Attachment Stability Are Regulated by Hec1. *Cell*, 127(5):969–982, 2006. doi: 10.1016/j.cell.2006.09.047.

[176] Claudio Ciferri, Jennifer De Lucall, Silvia Monzani, Karin J. Ferrari, Dejan Ristic, Claire Wyman, Holger Stark, John Kilmartin, Edward D. Salmon, and Andrea Musacchio. Architecture of the human Ndc80-Hec1 complex, a critical constituent of the outer kinetochore. *Journal of Biological Chemistry*, 280(32):29088–29095, 2005. doi: 10.1074/jbc.M504070200.

[177] Ronnie R. Wei, Jawdat Al-Bassam, and Stephen C. Harrison. The Ndc80/HEC1 complex is a contact point for kinetochore-microtubule attachment. *Nature Structural and Molecular Biology*, 14(1):54–59, 2007. doi: 10.1038/nsmb1186.

[178] Ronnie R. Wei, Peter K. Sorger, and Stephen C. Harrison. Molecular organization of the Ndc80 complex, an essential kinetochore component. *Proceedings of the National Academy of Sciences of the United States of America*, 102(15):5363–5367, 2005. doi: 10.1073/pnas.0501168102.

[179] Charles L. Asbury, Daniel R. Gestaut, Andrew F. Powers, Andrew D. Franck, and Trisha N. Davis. The Dam1 kinetochore complex harnesses microtubule dynamics to produce force and movement. *Proceedings of the National Academy of Sciences of the United States of America*, 103(26):9873–9878, 2006. doi: 10.1073/pnas.0602249103.

[180] Alejandro Franco, John C. Meadows, and Jonathan B.A. Millar. The Dam1/DASH complex is required for the retrieval of unclustered kinetochores in fission yeast. *Journal of Cell Science*, 120(19):3345–3351, 2007. doi: 10.1242/jcs.013698.

[181] Ekaterina L. Grishchuk, A. Efremov, V. A. Volkov, Ilia S. Spiridonov, Nikita Gudimchuk, Stefan Westermann, D. Drubin, G. Barnes, J Richard Mclntosh, Fazly I. Ataullakhanov, J Richard Mcintosh, and Fazly I. Ataullakhanov. The Dam1 ring binds microtubules strongly enough to be a processive as well as energy-efficient coupler for chromosome motion. *106*, 105(40):15423–15428, 2009. doi: 10.1073/pnas.0807859105.

[182] Jens C. Schmidt, Haribabu Arthanari, Andras Boeszoermenyi, Natalia M. Dashkevich, Elizabeth M. Wilson-Kubalek, Nilah Monnier, Michelle Markus, Monika Oberer, Ron A. Milligan, Mark Bathe, Gerhard Wagner, Ekaterina L. Grishchuk, and Iain M. Cheeseman. The Kinetochore-Bound Ska1 Complex Tracks Depolymerizing Microtubules and Binds to Curved Protofilaments. *Developmental Cell*, 23(5):968–980, 2012. doi: 10.1016/j.devcel.2012.09.012.

[183] Sara Moutinho-Pereira, Nico Stuurman, Olga Afonso, Marten Hornsveld, Paulo Aguiar, Gohta Goshima, Ronald D. Vale, and Helder Maiato. Genes involved in centrosome-independent mitotic spindle assembly in Drosophila S2 cells. *Proceedings of the National Academy of Sciences of the United States of America*, 110(49):19808–19813, 2013. doi: 10.1073/pnas.1320013110.

[184] Aneil Mallavarapu, Ken Sawin, and Tim Mitchison. A switch in microtubule dynamics at the onset of anaphase B in the mitotic spindle of Schizosaccharomyces pombe. *Current Biology*, 9(23):1423–1428, 1999. doi: 10.1016/S0960-9822(00)80090-1.

[185] Yutaka Shirasugi and Masamitsu Sato. Kinetochore-mediated outward force promotes spindle pole separation in fission yeast. *Molecular Biology of the Cell*, 30(22):2802–2813, 2019. doi: 10.1091/mbc.E19-07-0366.

[186] Zachary R. Gergely, Ammon Crapo, Loren E. Hough, J. Richard McIntosh, and Meredith D. Betterton. Kinesin-8 effects on mitotic microtubule dynamics contribute to spindle function in fission yeast. *Molecular Biology of the Cell*, 27(22):3490–3514, 2016. doi: 10.1091/mbc.E15-07-0505.

[187] K. Nabeshima, T. Nakagawa, A. F. Straight, A. Murray, Y. Chikashige, Y. M. Yamashita, Y. Hiraoka, and M. Yanagida. Dynamics of Centromeres during Metaphase-Anaphase Transition in Fission Yeast: Dis1 Is Implicated in Force Balance in Metaphase Bipolar Spindle. *Molecular Biology of the Cell*, 9(11):3211–3225, 1998. doi: 10.1091/mbc.9.11.3211.

[188] Isabel Sanchez-Perez, Steven J. Renwick, Karen Crawley, Inga Karig, Vicky Buck, John C. Meadows, Alejandro Franco-Sanchez, Ursula Fleig, Takashi Toda, and Jonathan B.A. Millar. The DASH complex and Klp5/Klp6 kinesin coordinate bipolar chromosome attachment in fission yeast. *EMBO Journal*, 24(16):2931–2943, 2005. doi: 10.1038/sj.emboj.7600761.

[189] F. Jon Kull, Ronald D. Vale, and Robert J. Flettrick. The case for a common ancestor: kinesin and myosin motor proteins and G proteins. *Journal of Muscle Research and Cell Motility*, 19:877–886, 1998. doi: 10.1023/a:1005489907021.

[190] Ronald D. Vale, Thomas S. Reese, and Michael P. Sheetz. Identification of a novel force-generating protein, kinesin, involved in microtubule-based motility. *Cell*, 42(1):39–50, 1985. doi: 10.1016/S0092-8674(85)80099-4.

[191] Isabelle Arnal and Richard H. Wade. Nucleotide-dependent conformations of the kinesin dimer interacting with microtubules. *Structure*, 6(1):33–38, 1998. doi: 10.1016/S0969-2126(98)00005-7.

[192] D. D. Hackney. Evidence for alternating head catalysis by kinesin during microtubule- stimulated ATP hydrolysis. *Proceedings of the National Academy of Sciences of the United States of America*, 91(15):6865–6869, 1994. doi: 10.1073/pnas.91.15.6865.

[193] Keiko Hirose, Erika Akimaru, Toshihiko Akiba, Sharyn A. Endow, and Linda A. Amos. Large Conformational Changes in a Kinesin Motor Catalyzed by Interaction with Microtubules. *Molecular Cell*, 23(6):913–923, 2006. doi: 10.1016/j.molcel.2006.07.020.

[194] Masahide Kikkawa, Elena P. Sablin, Yasushi Okada, Hiroaki Yajima, Robert J. Fletterick, and Nobutaka Hirokawa. Switch-based mechanism of kinesin motors. *Nature*, 411(6836):439–445, 2001. doi: 10.1038/35078000.

[195] Yong Ze Ma and Edwin W. Taylor. Interacting head mechanism of microtubule-kinesin ATPase. *Journal of Biological Chemistry*, 272(2):724–730, 1997. doi: 10.1074/jbc.272.2.724.

[196] Mikyung Yun, Xiaohua Zhang, Cheon Gil Park, Hee Won Park, and Sharyn A. Endow. A structural pathway for activation of the kinesin motor ATPase. *EMBO Journal*, 20(11):2611–2618, 2001. doi: 10.1093/emboj/20.11.2611.

[197] Carolyn J. Lawrence, R. Kelly Dawe, Karen R. Christie, Don W. Cleveland, Scott C. Dawson, Sharyn A. Endow, Lawrence S.B. Goldstein, Holly V. Goodson, Nobutaka Hirokawa, Jonathon Howard, Russell L. Malmberg, J. Richard McIntosh, Harukata Miki, Timothy J. Mitchison, Yasushi Okada, Anireddy S.N. Reddy,

William M. Saxton, Manfred Schliwa, Jonathan M. Scholey, Ronald D. Vale, Claire E. Walczak, and Linda Wordeman. A standardized kinesin nomenclature. *Journal of Cell Biology*, 167(1):19–22, 2004. doi: 10.1083/jcb.200408113.

[198] Robert A. Cross and Andrew McAinsh. Prime movers: The mechanochemistry of mitotic kinesins. *Nature Reviews Molecular Cell Biology*, 15(4):257–271, 2014. doi: 10.1038/nrm3768.

[199] Kristen J. Verhey and Jennetta W. Hammond. Traffic control: Regulation of kinesin motors. *Nature Reviews Molecular Cell Biology*, 10(11):765–777, 2009. doi: 10.1038/nrm2782.

[200] Yulia Ovechkina and Linda Wordeman. Unconventional motoring: An overview of the Kin C and Kin I kinesins. *Traffic*, 4(6):367–375, 2003. doi: 10.1034/j.1600-0854.2003.00099.x.

[201] Ryan B. Case, Daniel W. Pierce, Nora Hom-Booher, Cynthia L. Hart, and Ronald D. Vale. The directional preference of kinesin motors is specified by an element outside of the motor catalytic domain. *Cell*, 90(5): 959–966, 1997. doi: 10.1016/S0092-8674(00)80360-8.

[202] Sharyn A. Endow and Kimberly W. Waligora. Determinants of kinesin motor polarity. *Science*, 281(5380): 1200–1202, 1998. doi: 10.1126/science.281.5380.1200.

[203] Masaki Edamatsu. Bidirectional motility of the fission yeast kinesin-5, Cut7. *Biochemical and Biophysical Research Communications*, 446(1):231–234, 2014. doi: 10.1016/j.bbrc.2014.02.106.

[204] Johanna Roostalu, Christian Hentrich, Peter Bieling, Ivo A. Telley, Elmar Schiebel, and Thomas Surrey. Directional switching of the kinesin Cin8 through motor coupling. *Science*, 332(6025):94–99, 2011. doi: 10.1126/science.1199945.

[205] Sudhir Kumar Singh, Himanshu Pandey, Jawdat Al-Bassam, and Larisa Gheber. Bidirectional motility of kinesin-5 motor proteins: structural determinants, cumulative functions and physiological roles. *Cellular and Molecular Life Sciences*, 75(10):1757–1771, 2018. doi: 10.1007/s00018-018-2754-7.

[206] Ricardo Nunes Bastos, Sapan R. Gandhi, Ryan D. Baron, Ulrike Gruneberg, Erich A. Nigg, and Francis A. Barr. Aurora B suppresses microtubule dynamics and limits central spindle size by locally activating KIF4A. *Journal of Cell Biology*, 202(4):605–621, 2013. doi: 10.1083/jcb.201301094.

[207] Peter Bieling, Ivo A. Telley, and Thomas Surrey. A minimal midzone protein module controls formation and length of antiparallel microtubule overlaps. *Cell*, 142(3):420–432, 2010. doi: 10.1016/j.cell.2010.06.033.

[208] Henrik Bringmann, Georgios Skiniotis, Annina Spilker, Stefanie Kandels-Lewis, Isabelle Vernos, and Thomas Surrey. A Kinesin-like Motor Inhibits Microtubule Dynamic Instability. *Science*, 303(5663):1519–1522, 2004. doi: 10.1126/science.1094838.

[209] Mu He, Radhika Subramanian, Fiona Bangs, Tatiana Omelchenko, Karel F. Liem, Tarun M. Kapoor, and Kathryn V. Anderson. The kinesin-4 protein Kif7 regulates mammalian Hedgehog signalling by organizing the cilium tip compartment. *Nature Cell Biology*, 16(7):663–672, 2014. doi: 10.1038/ncb2988.

[210] Wilhelmina E van Riel, Ankit Rai, Sarah Bianchi, Eugene A Katrukha, Qingyang Liu, Albert JR Heck, Casper C Hoogenraad, Michel O Steinmetz, Lukas C Kapitein, and Anna Akhmanova. Kinesin-4 KIF21B is a potent microtubule pausing factor. *eLife*, 6:1–30, 2017. doi: 10.7554/elife.24746.

[211] Radhika Subramanian, Shih Chieh Ti, Lei Tan, Seth A. Darst, and Tarun M. Kapoor. Marking and measuring single microtubules by PRC1 and kinesin-4. *Cell*, 154(2):377–390, 2013. doi: 10.1016/j.cell.2013.06.021.

[212] Yasuhiro Kurasawa, William C. Earnshaw, Yuko Mochizuki, Naoshi Dohmae, and Kazuo Todokoro. Essential roles of KIF4 and its binding partner PRC1 in organized central spindle midzone formation. *EMBO Journal*, 23(16):3237–3248, 2004. doi: 10.1038/sj.emboj.7600347.

[213] Jonathon Hannabuss, Manuel Lera-Ramirez, Nicholas I. Cade, Franck J. Fourniol, François Nédélec, and Thomas Surrey. Self-Organization of Minimal Anaphase Spindle Midzone Bundles. *Current Biology*, 29(13): 2120–2130.e7, 2019. doi: 10.1016/j.cub.2019.05.049.

[214] Kruno Vukušić, Ivana Ponjavić, Renata Buđa, Patrik Risteski, and Iva M. Tolić. Microtubule-sliding modules based on kinesins EG5 and PRC1-dependent KIF4A drive human spindle elongation. *Developmental Cell*, 56(9):1253–1267.e10, 2021. doi: 10.1016/j.devcel.2021.04.005.

[215] Sithara Wijeratne and Radhika Subramanian. Geometry of antiparallel microtubule bundles regulates relative sliding and stalling by PRC1 and Kif4A. *eLife*, 7:e32595:1–28, 2018. doi: 10.7554/eLife.32595.

[216] Helder Maiato, Ana Margarida Gomes, Filipe Sousa, and Marin Barisic. Mechanisms of chromosome congression during mitosis. *Biology*, 6(1):1–56, 2017. doi: 10.3390/biology6010013.

[217] Manjari Mazumdar and Tom Misteli. Chromokinesins: Multitalented players in mitosis. *Trends in Cell Biology*, 15(7):349–355, 2005. doi: 10.1016/j.tcb.2005.05.006.

[218] Seyda Acar, David B. Carlson, Madhu S. Budamagunta, Vladimir Yarov-Yarovoy, John J. Correia, Milady R. Niñonuevo, Weitao Jia, Li Tao, Julie A. Leary, John C. Voss, James E. Evans, and Jonathan M. Scholey. The bipolar assembly domain of the mitotic motor kinesin-5. *Nature Communications*, 4:1343:1–11, 2013. doi: 10.1038/ncomms2348.

[219] Donna M. Gordon and David M. Roof. The kinesin-related protein Kip1p of Saccharomyces cerevisiae is bipolar. *Journal of Biological Chemistry*, 274(40):28779–28786, 1999. doi: 10.1074/jbc.274.40.28779.

[220] Emily R. Hildebrandt, Larisa Gheber, Tami Kingsbury, and M. Andrew Hoyt. Homotetrameric form of Cin8p, a Saccharomyces cerevisiae kinesin-5 motor, is essential for its in Vivo function. *Journal of Biological Chemistry*, 281(36):26004–26013, 2006. doi: 10.1074/jbc.M604817200.

[221] A. S. Kashina, R. J. Baskin, D. G. Cole, K. P. Wedaman, W. M. Saxton, and J. M. Scholey. A bipolar kinesin. *Nature*, 379(6562):270–272, 1996. doi: 10.1038/379270a0.

[222] Jessica E. Scholey, Stanley Nithianantham, Jonathan M. Scholey, and Jawdat Al-Bassam. Structural basis for the assembly of the mitotic motor kinesin-5 into bipolar tetramers. *eLife*, 2014(3):1–19, 2014. doi: 10.7554/eLife.02217.

[223] Lukas C. Kapitein, Benjamin H. Kwok, Joshua S. Weinger, Christoph F. Schmidt, Tarun M. Kapoor, and Erwin J G Peterman. Microtubule cross-linking triggers the directional motility of kinesin-5. *Journal of Cell Biology*, 182(3):421–428, 2008. doi: 10.1083/jcb.200801145.

[224] William S Saunders and M. Andrew Hoyt. Kinesin-related proteins required for structural integrity of the mitotic spindle. *Cell*, 70:451–458, 1992. doi: 10.1016/0092-8674(92)90169-d.

[225] David J. Sharp, Kent L. McDonald, Heather M. Brown, Heinrich J. Matthies, Claire Walczak, Ron D. Vale, Timothy J. Mitchison, and Jonathan M. Scholey. The bipolar kinesin, KLP61F, cross-links microtubules within interpolar microtubule bundles of Drosophila embryonic mitotic spindles. *Journal of Cell Biology*, 144 (1):125–138, 1999. doi: 10.1083/jcb.144.1.125.

[226] Aaron F. Straight, John W. Sedat, and Andrew W. Murray. Time-lapse microscopy reveals unique roles for kinesins during anaphase in budding yeast. *Journal of Cell Biology*, 143(3):687–694, 1998. doi: 10.1083/jcb.143.3.687.

[227] Siet M.J.L. van den Wildenberg, Li Tao, Lukas C. Kapitein, Christoph F. Schmidt, Jonathan M. Scholey, and Erwin J.G. Peterman. The Homotetrameric Kinesin-5 KLP61F Preferentially Crosslinks Microtubules into Antiparallel Orientations. *Current Biology*, 18(23):1860–1864, 2008. doi: 10.1016/j.cub.2008.10.026.

[228] Yuta Shimamoto, Scott Forth, and Tarun M. Kapoor. Measuring Pushing and Braking Forces Generated by Ensembles of Kinesin-5 Crosslinking Two Microtubules. *Developmental Cell*, 34(6):669–681, 2015. doi: 10.1016/j.devcel.2015.08.017.

[229] Douglas G. Cole, William M. Saxton, Kathy B. Sheehan, and Jonathan M. Scholey. A "slow" Homotetrameric Kinesin-related Motor Protein Purified from Drosophila Embryos. *Journal of Biological Chemistry*, 269(37): 22913–22916, 1994. doi: 10.1016/j.surg.2006.10.010.

[230] André Düselder, Christina Thiede, Christoph F. Schmidt, and Stefan Lakämper. Neck-linker length dependence of processive kinesin-5 motility. *Journal of Molecular Biology*, 423(2):159–168, 2012. doi: 10.1016/j.jmb.2012.06.043.

[231] Vladimir Fridman, Adina Gerson-Gurwitz, Ofer Shapira, Natalia Movshovich, Stefan Lakämper, Christoph F. Schmidt, and Larisa Gheber. Kinesin-5 Kip1 is a bi-directional motor that stabilizes microtubules and tracks their plus-ends in vivo. *Journal of Cell Science*, 126(18):4147–4159, 2013. doi: 10.1242/jcs.125153.

[232] Kuniyoshi Kaseda, Isabelle Crevel, Keiko Hirose, and Robert A. Cross. Single-headed mode of kinesin-5. *EMBO Reports*, 9(8):761–765, 2008. doi: 10.1038/embor.2008.96.

[233] Mishan Britto, Adeline Goulet, Syeda Rizvi, Ottilie von Loeffelholz, Carolyn A. Moores, and Robert A. Cross. Schizosaccharomyces pombe kinesin-5 switches direction using a steric blocking mechanism. *Proceedings of the National Academy of Sciences*, 113(47):E7483–E7489, 2016. doi: 10.1073/pnas.1611581113.

[234] Adina Gerson-Gurwitz, Christina Thiede, Natalia Movshovich, Vladimir Fridman, Maria Podolskaya, Tsafi Danieli, Stefan Lakämper, Dieter R. Klopfenstein, Christoph F. Schmidt, and Larisa Gheber. Directionality of individual kinesin-5 Cin8 motors is modulated by loop 8, ionic strength and microtubule geometry. *EMBO Journal*, 30(24):4942–4954, 2011. doi: 10.1038/emboj.2011.403.

[235] Christina Thiede, Vladimir Fridman, Adina Gerson-Gurwitz, Larisa Gheber, and Christoph F. Schmidt. Regulation of bi-directional movement of single kinesin-5 Cin8 molecules. *BioArchitecture*, 2(2):70–74, 2012. doi: 10.4161/bioa.20395.

[236] Ofer Shapira, Alina Goldstein, Jawdat Al-Bassam, and Larisa Gheber. A potential physiological role for bi-directional motility and motor clustering of mitotic kinesin-5 Cin8 in yeast mitosis. *Journal of Cell Science*, 130(4):725–734, 2017. doi: 10.1242/jcs.195040.

[237] Marianne Uteng, Christian Hentrich, Kota Miura, Peter Bieling, and Thomas Surrey. Poleward transport of Eg5 by dynein-dynactin in Xenopus laevis egg extract spindles. *Journal of Cell Biology*, 182(4):715–726, 2008. doi: 10.1083/jcb.200801125.

[238] Torsten Wittmann, Matthias Wilm, Eric Karsenti, and Isabelle Vernos. TPX2, a novel Xenopus MAP involved in spindle pole organization. *Journal of Cell Biology*, 149(7):1405–1418, 2000. doi: 10.1083/jcb.149.7.1405.

[239] Yalei Chen and William O. Hancock. Kinesin-5 is a microtubule polymerase. *Nature Communications*, 6 (8160):1–10, 2015. doi: 10.1038/ncomms9160.

[240] Geng Yuan Chen, Joseph M. Cleary, A. B. Asenjo, Y. Chen, Jacob A. Mascaro, David F.J. Arginteanu, Hernando Sosa, and William O. Hancock. Kinesin-5 Promotes Microtubule Nucleation and Assembly by Stabilizing a Lattice-Competent Conformation of Tubulin. *Current Biology*, 29(14):2259–2269, 2019. doi: 10.1016/j.cub.2019.05.075.

[241] Vladimir Fridman, Adina Gerson-Gurwitz, Natalia Movshovich, Martin Kupiec, and Larisa Gheber. Midzone organization restricts interpolar microtubule plus-end dynamics during spindle elongation. *EMBO Reports*, 10(4):387–393, 2009. doi: 10.1038/embor.2009.7.

[242] Melissa K. Gardner, David C. Bouck, Leocadia V. Paliulis, Janet B. Meehl, Eileen T. O'Toole, Julian Haase, Adelheid Soubry, Ajit P. Joglekar, Mark Winey, Edward D. Salmon, Kerry Bloom, and David J. Odde. Chromosome Congression by Kinesin-5 Motor-Mediated Disassembly of Longer Kinetochore Microtubules. *Cell*, 135(5):894–906, 2008. doi: 10.1016/j.cell.2008.09.046.

[243] Emily Tubman, Yungui He, Thomas S. Hays, and David J. Odde. Kinesin-5 Mediated Chromosome Congression in Insect Spindles. *Cellular and Molecular Bioengineering*, 11(1):25–36, 2018. doi: 10.1007/s12195-017-0500-0.

[244] Ingrid E. Adriaans, Peter Jan Hooikaas, Amol Aher, Martijn J.M. Vromans, Robert M. van Es, Ilya Grigoriev, Anna Akhmanova, and Susanne M.A. Lens. MKLP2 Is a Motile Kinesin that Transports the Chromosomal Passenger Complex during Anaphase. *Current Biology*, 30(13):2628–2637.e9, 2020. doi: 10.1016/j.cub.2020.04.081.

[245] Tim Davies, Noriyuki Kodera, Gabriele S. Kaminski Schierle, Eric Rees, Miklos Erdelyi, Clemens F. Kaminski, Toshio Ando, and Masanori Mishima. CYK4 Promotes Antiparallel Microtubule Bundling by Optimizing MKLP1 Neck Conformation. *PLoS Biology*, 13(4):1–26, 2015. doi: 10.1371/journal.pbio.1002121.

[246] Joseph Atherton, I. Mei Yu, Alexander Cook, Joseph M. Muretta, Agnel Joseph, Jennifer Major, Yannick Sourigues, Jeffrey Clause, Maya Topf, Steven S. Rosenfeld, Anne Houdusse, and Carolyn A. Moores. The

divergent mitotic kinesin MKLP2 exhibits atypical structure and mechanochemistry. *eLife*, 6:1–27, 2017. doi: 10.7554/eLife.27793.

[247] Yohei Maruyama, Mitsuhiro Sugawa, Shin Yamaguchi, Tim Davies, Toshihisa Osaki, Takuya Kobayashi, Masahiko Yamagishi, Shoji Takeuchi, Masanori Mishima, and Junichiro Yajima. CYK4 relaxes the bias in the off-axis motion by MKLP1 kinesin-6. *Communications Biology*, 4(1), 2021. doi: 10.1038/s42003-021-01704-2.

[248] Masanori Mishima, Susanne Kaitna, and Michael Glotzer. Central spindle assembly and cytokinesis require a kinesin-like protein/RhoGAP complex with microtubule bundling activity. *Developmental Cell*, 2(1):41–54, 2002. doi: 10.1016/S1534-5807(01)00110-1.

[249] Visnja Pavicic-Kaltenbrunner, Masanori Mishima, and Michael Glotzer. Cooperative Assembly of CYK-4/MgcRacGAP and ZEN-4/MKLP1 to Form the Centralspindlin Complex. *Molecular Biology of the Cell*, 18 (December):4992–5993, 2007. doi: 10.1091/mbc.E07.

[250] Arnaud Echard, Florence Jollivet, Olivier Martinez, Jean-Jacques Lacapere, Annie Rousselet, Isabelle Janoueix-Lerosey, and Bruno Goud. Interaction of a golgi-associated kinesin-like protein with Rab6. *Science*, 279(5350):580–585, 1998. doi: 10.1126/science.279.5350.580.

[251] Michael Glotzer. The 3Ms of central spindle assembly: Microtubules, motors and MAPs. *Nature Reviews Molecular Cell Biology*, 10(1):9–20, 2009. doi: 10.1038/nrm2609.

[252] Mayumi Kitagawa, Suet Yin Sarah Fung, Nobuyuki Onishi, Hideyuki Saya, and Sang Hyun Lee. Targeting Aurora B to the Equatorial Cortex by MKlp2 Is Required for Cytokinesis. *PLoS ONE*, 8(6), 2013. doi: 10.1371/journal.pone.0064826.

[253] Stefan Hümmer and Thomas U. Mayer. Cdk1 Negatively Regulates Midzone Localization of the Mitotic Kinesin Mklp2 and the Chromosomal Passenger Complex. *Current Biology*, 19(7):607–612, 2009. doi: 10.1016/j.cub.2009.02.046.

[254] Mayumi Kitagawa, Suet Yin Sarah Fung, Umar Farook Shahul Hameed, Hidemasa Goto, Masaki Inagaki, and Sang Hyun Lee. Cdk1 coordinates timely activation of MKlp2 kinesin with relocation of the chromosome passenger complex for cytokinesis. *Cell Reports*, 7(1):166–179, 2014. doi: 10.1016/j.celrep.2014.02.034.

[255] John C. Meadows, Theresa C. Lancaster, Graham J. Buttrick, Alicja M. Sochaj, Liam J. Messin, Maria del Mar Mora-Santos, Kevin G. Hardwick, and Jonathan B.A. Millar. Identification of a Sgo2-Dependent but Mad2-Independent Pathway Controlling Anaphase Onset in Fission Yeast. *Cell Reports*, 18(6):1422–1433, 2017. doi: 10.1016/j.celrep.2017.01.032.

[256] Chuanhai Fu, Jonathan J. Ward, Isabelle Loiodice, Guilhem Velve-Casquillas, Francois J. Nedelec, and Phong T. Tran. Phospho-Regulated Interaction between Kinesin-6 Klp9p and Microtubule Bundler Ase1p Promotes Spindle Elongation. *Developmental Cell*, 17(2):257–267, 2009. doi: 10.1016/j.devcel.2009.06.012.

[257] Aniek Jongerius. Control mechanisms of microtubule overlap regions. *PhD Thesis*, 2017. URL `https://library.wur.nl/WebQuery/wurpubs/523659`.

[258] Masashi Yukawa, Masaki Okazaki, Yasuhiro Teratani, Ken Furuta, and Takashi Toda. Kinesin-6 Klp9 plays motor- dependent and -independent roles in collaboration with Kinesin-5 Cut7 and the microtubule crosslinker Ase1 in fission yeast. *Scientific Reports*, 9(1):1–15, 2019. doi: 10.1038/s41598-019-43774-7.

[259] Sergio A. Rincon, Adam Lamson, Robert Blackwell, Viktoriya Syrovatkina, Vincent Fraisier, Anne Paoletti, Meredith D. Betterton, and Phong T. Tran. Kinesin-5-independent mitotic spindle assembly requires the antiparallel microtubule crosslinker Ase1 in fission yeast. *Nature Communications*, 8:1–12, 2017. ISSN 20411723. doi: 10.1038/ncomms15286.

[260] Masashi Yukawa, Tomoki Kawakami, Masaki Okazaki, Kazunori Kume, Ngang Heok Tang, and Takashi Toda. A microtubule polymerase cooperates with the kinesin-6 motor and a microtubule cross-linker to promote bipolar spindle assembly in the absence of kinesin-5 and kinesin-14 in fission yeast. *Molecular Biology of the Cell*, 28(25):3647–3659, 2017. doi: 10.1091/mbc.E17-08-0497.

[261] Masashi Yukawa, Yusuke Yamada, Tomoaki Yamauchi, and Takashi Toda. Two spatially distinct kinesin-14 proteins, Pkl1 and Klp2, generate collaborative inward forces against kinesin-5 Cut7 in S. pombe. *Journal of Cell Science*, 131(1):jcs210740, 2018. doi: 10.1242/jcs.210740.

[262] Mohan L. Gupta, Pedro Carvalho, David M. Roof, and David Pellman. Plus end-specific depolymerase activity of Kip3, a kinesin-8 protein, explains its role in positioning the yeast mitotic spindle. *Nature Cell Biology*, 8(9):913–923, 2006. doi: 10.1038/ncb1457.

[263] Monika I. Mayr, Stefan Hümmer, Jenny Bormann, Tamara Grüner, Sarah Adio, Guenther Woehlke, and Thomas U. Mayer. The Human Kinesin Kif18A Is a Motile Microtubule Depolymerase Essential for Chromosome Congression. *Current Biology*, 17(6):488–498, 2007. doi: 10.1016/j.cub.2007.02.036.

[264] Amy Unsworth, Hirohisa Masudaa, Susheela Dhut, and Takashi Toda. Fission Yeast Kinesin-8 Klp5 and Klp6 Are Interdependent for Mitotic Nuclear Retention and Required for Proper Microtubule Dynamics. *Molecular biology of the cell*, 19(December):5104–5115, 2008. doi: 10.1091/mbc.E08.

[265] Vladimir Varga, Jonne Helenius, Kozo Tanaka, Anthony A Hyman, Tomoyuki U Tanaka, and Jonathon Howard. Yeast kinesin-8 depolymerizes microtubules in a length-dependent manner. *Nature Cell Biology*, 8 (9):957–962, 2006. doi: 10.1038/ncb1462.

[266] Vladimir Varga, Cecile Leduc, Volker Bormuth, Stefan Diez, and Jonathon Howard. Kinesin-8 Motors Act Cooperatively to Mediate Length-Dependent Microtubule Depolymerization. *Cell*, 138(6):1174–1183, 2009. doi: 10.1016/j.cell.2009.07.032.

[267] Julia Locke, Agnel Praveen Joseph, Alejandro Peña, Martin M. Möckel, Thomas U. Mayer, Maya Topf, and Carolyn A. Moores. Structural basis of human kinesin-8 function and inhibition. *Proceedings of the National Academy of Sciences of the United States of America*, 114(45):E9539–E9548, 2017. doi: 10.1073/pnas.1712169114.

[268] Hugo Arellano-Santoyo, Elisabeth A. Geyer, Ema Stokasimov, Geng Yuan Chen, Xiaolei Su, William Hancock, Luke M. Rice, and David Pellman. A Tubulin Binding Switch Underlies Kip3/Kinesin-8 Depolymerase Activity. *Developmental Cell*, 42(1):37–51, 2017. doi: 10.1016/j.devcel.2017.06.011.

[269] Muriel Erent, Douglas R. Drummond, and Robert A. Cross. S. pombe kinesins-8 promote both nucleation and catastrophe of microtubules. *PLoS ONE*, 7(2), 2012. doi: 10.1371/journal.pone.0030738.

[270] Anna H. Klemm, Agneza Bosilj, Matko Glunčic, Nenad Pavin, and Iva M. Tolic. Metaphase kinetochore movements are regulated by kinesin-8 motors and microtubule dynamic instability. *Molecular Biology of the Cell*, 29(11):1332–1345, 2018. doi: 10.1091/mbc.E17-11-0667.

[271] Christian Tischer, Damian Brunner, and Marileen Dogterom. Force- and kinesin-8-dependent effects in the spatial regulation of fission yeast microtubule dynamics. *Molecular Systems Biology*, 5(250):1–10, 2009. doi: 10.1038/msb.2009.5.

[272] Rania S. Rizk, Katherine A. DiScipio, Kathleen G. Proudfoot, and Mohan L. Gupta. The kinesin-8 Kip3 scales anaphase spindle length by suppression of midzone microtubule polymerization. *Journal of Cell Biology*, 204(6):965–975, 2014. doi: 10.1083/jcb.201312039.

[273] Xiaolei Su, Hugo Arellano-Santoyo, Didier Portran, Jeremie Gaillard, Marylin Vantard, Manuel Thery, and David Pellman. Microtubule-sliding activity of a kinesin-8 promotes spindle assembly and spindle-length control. *Nature Cell Biology*, 15(8):948–957, 2013. doi: 10.1038/ncb2801.

[274] Miguel Angel Garcia, Nirada Koonrugsa, and Takashi Toda. Spindle-kinetochore attachment requires the combined action of Kin I-like Klp5/6 and Alp14/Dis1-MAPs in fission yeast. *EMBO Journal*, 21(22):6015–6024, 2002. doi: 10.1093/emboj/cdf611.

[275] Hadrien Mary, Jonathan Fouchard, Guillaume Gay, Céline Reyes, Tiphaine Gauthier, Clémence Gruget, Jacques Pécréaux, Sylvie Tournier, and Yannick Gachet. Fission yeast kinesin-8 controls chromosome congression independently of oscillations. *Journal of Cell Science*, 128(20):3720–3730, 2015. doi: 10.1242/jcs.160465.

[276] Jason Stumpff, Yaqing Du, Chauca A. English, Zoltan Maliga, Michael Wagenbach, Charles L. Asbury, Linda Wordeman, and Ryoma Ohi. A Tethering Mechanism Controls the Processivity and Kinetochore-Microtubule Plus-End Enrichment of the Kinesin-8 Kif18A. *Molecular Cell*, 43(5):764–775, 2011. doi: 10.1016/j.molcel.2011.07.022.

[277] I. Brust-Mascher and Jonathan M. Scholey. Microtubule Flux and Sliding in Mitotic Spindles of Drosophila Embryos. *Molecular Biology of the Cell*, 13(June):3967–3975, 2002. doi: 10.1091/mbc.02.

[278] I. Brust-Mascher, G. Civelekoglu-Scholey, M. Kwon, A. Mogilner, and J. M. Scholey. Model for anaphase B: Role of three mitotic motors in a switch from poleward flux to spindle elongation. *Proceedings of the National Academy of Sciences*, 101(45):15938–15943, 2004. doi: 10.1073/pnas.0407044101.

[279] Neil J. Ganem, Kristi Upton, and Duane A. Compton. Efficient mitosis in human cells lacking poleward microtubule flux. *Current Biology*, 15(20):1827–1832, 2005. doi: 10.1016/j.cub.2005.08.065.

[280] Gregory C. Rogers, Stephen L. Rogers, Tamara A. Schwimmer, Stephanie C. Ems-McClung, Claire E. Walczak, Ronald D. Vale, Jonathan M. Scholey, and David J. Sharp. Two mitotic kinesins cooperate to drive sister chromatid separation during anaphase. *Nature*, 427(6972):364–370, 2004. doi: 10.1038/nature02256.

[281] Elena P. Sablin, Ryan B. Case, Shirleko C. Dai, Cynthia L. Hart, Aaron Ruby, Ronald D. Vale, and Robert J. Fletterick. Direction determination in the minus-end-directed kinesin motor ncd. *Nature*, 395(6704):813–816, 1998. doi: 10.1038/27463.

[282] R. Chandra, E. D. Salmon, H. P. Erickson, A. Lockhart, and S. A. Endow. Structural and functional domains of the Drosophila ncd microtubule motor protein. *Journal of Biological Chemistry*, 268(12):9005–9013, 1993. doi: 10.1016/s0021-9258(18)52971-9.

[283] Ken'ya Furuta, Masaki Edamatsu, Yurina Maeda, and Yoko Y. Toyoshima. Diffusion and directed movement: In vitro motile properties of fission yeast kinesin-14 Pkl1. *Journal of Biological Chemistry*, 283(52):36465–36473, 2008. doi: 10.1074/jbc.M803730200.

[284] Marcus Braun, Douglas R. Drummond, Robert A. Cross, and Andrew D. McAinsh. The kinesin-14 Klp2 organizes microtubules into parallel bundles by an ATP-dependent sorting mechanism. *Nature Cell Biology*, 11(6):724–730, 2009. doi: 10.1038/ncb1878.

[285] Gero Fink, Lukasz Hajdo, Krzysztof J. Skowronek, Cordula Reuther, Andrzej A. Kasprzak, and Stefan Diez. The mitotic kinesin-14 Ncd drives directional microtubule-microtubule sliding. *Nature Cell Biology*, 11(6): 717–723, 2009. doi: 10.1038/ncb1877.

[286] Marcus Braun, Zdenek Lansky, Agata Szuba, Friedrich W. Schwarz, Aniruddha Mitra, Mengfei Gao, Annemarie Lüdecke, Pieter Rein Ten Wolde, and Stefan Diez. Changes in microtubule overlap length regulate kinesin-14-driven microtubule sliding. *Nature Chemical Biology*, 13(12):1245–1252, 2017. doi: 10.1038/nchembio.2495.

[287] Christian Hentrich and Thomas Surrey. Microtubule organization by the antagonistic mitotic motors kinesin-5 and kinesin-14. *Journal of Cell Biology*, 189(3):465–480, 2010. doi: 10.1083/jcb.200910125.

[288] Zdenek Lansky, Marcus Braun, Annemarie Lüdecke, Michael Schlierf, Pieter Rein Ten Wolde, Marcel E. Janson, and Stefan Diez. Diffusible crosslinkers generate directed forces in microtubule networks. *Cell*, 160 (6):1159–1168, 2015. doi: 10.1016/j.cell.2015.01.051.

[289] Stefan Highsmith, Michael Thoene, Elena Sablin, and Katherine Polosukhina. NCD activation of tubulin polymerization. *Biophysical Chemistry*, 92(1-2):127–139, 2001. doi: 10.1016/S0301-4622(01)00197-1.

[290] Zachary T. Olmsted, Andrew G. Colliver, Timothy D. Riehlman, and Janet L. Paluh. Kinesin-14 and kinesin-5 antagonistically regulate microtubule nucleation by $\gamma$-TuRC in yeast and human cells. *Nature Communications*, 5(May):1–15, 2014. doi: 10.1038/ncomms6339.

[291] Lisa R. Sproul, Daniel J. Anderson, Andrew T. Mackey, William S. Saunders, and Susan P. Gilbert. Cik1 targets the minus-end Kinesin depolymerase Kar3 to microtubule plus ends. *Current Biology*, 15(15):1420–1427, 2005. doi: 10.1016/j.cub.2005.06.066.

[292] Gohta Goshima, François Nédélec, and Ronald D. Vale. Mechanisms for focusing mitotic spindle poles by minus end-directed motor proteins. *Journal of Cell Biology*, 171(2):229–240, 2005. doi: 10.1083/jcb.200505107.

[293] Claire E. Walczak, Suzie Verma, and Timothy J. Mitchison. XCTK2: A kinesin-related protein that promotes mitotic spindle assembly in Xenopus laevis egg extracts. *Journal of Cell Biology*, 136(4):859–870, 1997. doi: 10.1083/jcb.136.4.859.

[294] Alison L. Pidoux, Michel LeDizet, and W. Zacheus Cande. Fission yeast pkl1 is a kinesin-related protein involved in mitotic spindle function. *Molecular Biology of the Cell*, 7(10):1639–1655, 1996. doi: 10.1091/mbc.7.10.1639.

[295] Masashi Yukawa, Chiho Ikebe, and Takashi Toda. The Msd1-Wdr8-Pkl1 complex anchors microtubule minus ends to fission yeast spindle pole bodies. *Journal of Cell Biology*, 209(4):549–562, 2015. doi: 10.1083/jcb.201412111.

[296] Ana Loncar, Sergio A. Rincon, Manuel Lera Ramirez, Anne Paoletti, and Phong T. Tran. Kinesin-14 family proteins and microtubule dynamics define S. pombe mitotic and meiotic spindle assembly, and elongation. *Journal of Cell Science*, 133(11), 2020. doi: 10.1242/jcs.240234.

[297] Michael A. Cianfrocco, Morgan E. Desantis, Andres E. Leschziner, and Samara L. Reck-Peterson. Mechanism and Regulation of Cytoplasmic Dynein. *Annual Review of Cell and Developmental Biology*, 31:83–108, 2015. doi: 10.1146/annurev-cellbio-100814-125438.

[298] J. A. Raaijmakers and R. H. Medema. Function and regulation of dynein in mitotic chromosome segregation. *Chromosoma*, 123(5):407–422, 2014. doi: 10.1007/s00412-014-0468-7.

[299] Julia R. Kardon and Ronald D. Vale. Regulators of the cytoplasmic dynein motor. *Nature Reviews Molecular Cell Biology*, 10(12):854–865, 2009. doi: 10.1038/nrm2804.

[300] K. Kevin Pfister, Elizabeth M.C. Fisher, Ian R. Gibbons, Thomas S. Hays, Erika L.F. Holzbaur, J. Richard McIntosh, Mary E. Porter, Trina A. Schroer, Kevin T. Vaughan, George B. Witman, Stephen M. King, and Richard B. Vallee. Cytoplasmic dynein nomenclature. *Journal of Cell Biology*, 171(3):411–413, 2005. doi: 10.1083/jcb.200508078.

[301] Christophe J. Echeverri, Bryce M. Paschal, Kevin T. Vaughan, and Richard B. Vallee. Molecular characterization of the 50-kD subunit of dynactin reveals function for the complex in chromosome alignment and spindle organization during mitosis. *Journal of Cell Biology*, 132(4):617–633, 1996. doi: 10.1083/jcb.132.4.617.

[302] Jonne A. Raaijmakers, Marvin E. Tanenbaum, and René H. Medema. Systematic dissection of dynein regulators in mitosis. *Journal of Cell Biology*, 201(2):201–215, 2013. doi: 10.1083/jcb.201208098.

[303] Daniël Splinter, David S. Razafsky, Max A. Schlager, Andrea Serra-Marques, Ilya Grigoriev, Jeroen Demmers, Nanda Keijzer, Kai Jiang, Ina Poser, Anthony A. Hyman, Casper C. Hoogenraad, Stephen J. King, and Anna Akhmanova. BICD2, dynactin, and LIS1 cooperate in regulating dynein recruitment to cellular structures. *Molecular Biology of the Cell*, 23(21):4226–4241, 2012. doi: 10.1091/mbc.E12-03-0210.

[304] Sachin Kotak, Coralie Busso, and Pierre Gönczy. NuMA phosphorylation by CDK1 couples mitotic progression with cortical dynein function. *EMBO Journal*, 32(18):2517–2529, 2013. doi: 10.1038/emboj.2013.172.

[305] Tu Nguyen-Ngoc, Katayoun Afshar, and Pierre Gönczy. Coupling of cortical dynein and G$\alpha$ proteins mediates spindle positioning in Caenorhabditis elegans. *Nature Cell Biology*, 9(11):1294–1302, 2007. doi: 10.1038/ncb1649.

[306] Eric R. Griffis, Nico Stuurman, and Ronald D. Vale. Spindly, a novel protein essential for silencing the spindle assembly checkpoint, recruits dynein to the kinetochore. *Journal of Cell Biology*, 177(6):1005–1015, 2007. doi: 10.1083/jcb.200702062.

[307] Wai Chan Ying, Luca L. Fava, Andreas Uldschmid, Michael H.A. Schmitz, Daniel W. Gerlich, Erich A. Nigg, and Anna Santamaria. Mitotic control of kinetochore-associated dynein and spindle orientation by human Spindly. *Journal of Cell Biology*, 185(5):859–874, 2009. doi: 10.1083/jcb.200812167.

[308] Samara L. Reck-Peterson, Ahmet Yildiz, Andrew P. Carter, Arne Gennerich, Nan Zhang, and Ronald D. Vale. Single-Molecule Analysis of Dynein Processivity and Stepping Behavior. *Cell*, 126(2):335–348, 2006. doi: 10.1016/j.cell.2006.05.046.

[309] Jérémie Gaillard, Emmanuelle Neumann, Daniel Van Damme, Virginie Stoppin-Mellet, Christine Ebel, Elodie Barbier, Danny Geelen, and Marylin Vantard. Two Microtubule-associated Proteins of Arabidopsis MAP65s Promote Antiparallel Microtubule Bundling. *Molecular biology of Cell*, 19:4534–4544, 2008. doi: 10.1091/mbc.E08.

[310] Marcel E. Janson, Rose Loughlin, Isabelle Loïodice, Chuanhai Fu, Damian Brunner, François J. Nédélec, and Phong T. Tran. Crosslinkers and Motors Organize Dynamic Microtubules to Form Stable Bipolar Arrays in Fission Yeast. *Cell*, 128(2):357–368, 2007. doi: 10.1016/j.cell.2006.12.030.

[311] Radhika Subramanian, Elizabeth M. Wilson-Kubalek, Christopher P. Arthur, Matthew J. Bick, Elizabeth A. Campbell, Seth A. Darst, Ronald A. Milligan, and Tarun M. Kapoor. Insights into antiparallel microtubule crosslinking by PRC1, a conserved nonmotor microtubule binding protein. *Cell*, 142(3):433–443, 2010. doi: 10.1016/j.cell.2010.07.012.

[312] Qian Zhu, Fan Zheng, Allen P. Liu, Jin Qian, Chuanhai Fu, and Yuan Lin. Shape Transformation of the Nuclear Envelope during Closed Mitosis. *Biophysical Journal*, 111(10):2309–2316, 2016. doi: http://dx.doi.org/10.1016/j.bpj.2016.10.004.

[313] Marcus Braun, Zdenek Lansky, Gero Fink, Felix Ruhnow, Stefan Diez, and Marcel E. Janson. Adaptive braking by Ase1 prevents overlapping microtubules from sliding completely apart. *Nature Cell Biology*, 13 (10):1259–1264, 2011. doi: 10.1038/ncb2323.

[314] Wei Jiang, Gretchen Jimenez, Nicholas J. Wells, Thomas J. Hope, Geoffrey M. Wahl, Tony Hunter, and Rikiro Fukunaga. PRC1: A human mitotic spindle-associated CDK substrate protein required for cytokinesis. *Molecular Cell*, 2(6):877–885, 1998. doi: 10.1016/s1097-2765(00)80302-0.

[315] Anton Khmelinskii, Johanna Roostalu, Helio Roque, Claude Antony, and Elmar Schiebel. Phosphorylation-Dependent Protein Interactions at the Spindle Midzone Mediate Cell Cycle Regulation of Spindle Elongation. *Developmental Cell*, 17(2):244–256, 2009. doi: 10.1016/j.devcel.2009.06.011.

[316] Rüdiger Neef, Ulrike Gruneberg, Robert Kopajtich, Xiuling Li, Erich A. Nigg, Herman Sillje, and Francis A. Barr. Choice of Plk1 docking partners during mitosis and cytokinesis is controlled by the activation state of Cdk1. *Nature Cell Biology*, 9(4):436–444, 2007. doi: 10.1038/ncb1557.

[317] Andrei Smertenko, Norihan Saleh, Hisako Igarashi, Hitoshi Mori, Isolde Hauser-Hahn, Chang Jie Jiang, Seiji Sonobe, Clive W. Lloyd, and Patrick J. Hussey. A new class of microtubule-associated proteins in plants. *Nature Cell Biology*, 2(10):750–753, 2000. doi: 10.1038/35036390.

[318] Johanna Roostalu, Elmar Schiebel, and Anton Khmelinskii. Cell cycle control of spindle elongation. *Cell Cycle*, 9(6):1084–1090, 2010. doi: 10.4161/cc.9.6.11017.

[319] Christian O. De Groot, Ilian Jelesarov, Fred F. Damberger, Saša Bjelić, Martin A. Schärer, Neel S. Bhavesh, Ilia Grigoriev, Ruben M. Buey, Kurt Wüthrich, Guido Capitani, Anna Akhmanova, and Michel O. Steinmetz. Molecular insights into mammalian end-binding protein heterodimerization. *Journal of Biological Chemistry*, 285(8):5802–5814, 2010. doi: 10.1074/jbc.M109.068130.

[320] Ikuko Hayashi and Mitsuhiko Ikura. Crystal structure of the amino-terminal microtubule-binding domain of end-binding protein 1 (EB1). *Journal of Biological Chemistry*, 278(38):36430–36434, 2003. doi: 10.1074/jbc.M305773200.

[321] Yulia Komarova, Christian O. De Groot, Ilya Grigoriev, Susana Montenegro Gouveia, E. Laura Munteanu, Joseph M. Schober, Srinivas Honnappa, Rubén M. Buey, Casper C. Hoogenraad, Marileen Dogterom, Gary G. Borisy, Michel O. Steinmetz, and Anna Akhmanova. Mammalian end binding proteins control persistent microtubule growth. *Journal of Cell Biology*, 184(5):691–706, 2009. doi: 10.1083/jcb.200807179.

[322] Kevin C. Slep, Stephen L. Rogers, Sarah L. Elliott, Hiroyuki Ohkura, Peter A. Kolodziej, and Ronald D. Vale. Structural determinants for EB1-mediated recruitment of APC and spectraplakins to the microtubule plus end. *Journal of Cell Biology*, 168(4):587–598, 2005. doi: 10.1083/jcb.200410114.

[323] Ram Dixit, Brian Barnett, Jacob E. Lazarus, Mariko Tokito, Yale E. Goldman, and Erika L.F. Holzbaur. Microtubule plus-end tracking by CLIP-170 requires EB1. *Proceedings of the National Academy of Sciences of the United States of America*, 106(2):492–497, 2009. doi: 10.1073/pnas.0807614106.

[324] Sebastian P. Maurer, Peter Bieling, Julia Cope, Andreas Hoenger, and Thomas Surrey. GTP$\gamma$S microtubules mimic the growing microtubule end structure recognized by end-binding proteins (EBs). *Proceedings of the National Academy of Sciences of the United States of America*, 108(10):3988–3993, 2011. doi: 10.1073/pnas.1014758108.

[325] Daniel Roth, Benjamin P. Fitton, Nikola P. Chmel, Natalia Wasiluk, and Anne Straube. Spatial positioning of EB family proteins at microtubule tips involves distinct nucleotide-dependent binding properties. *Journal of Cell Science*, 132(4), 2018. doi: 10.1242/jcs.219550.

[326] Dominique Seetapun, Brian T. Castle, Alistair J. McIntyre, Phong T. Tran, and David J. Odde. Estimating the microtubule GTP cap size in vivo. *Current Biology*, 22(18):1681–1687, 2012. doi: 10.1016/j.cub.2012.06.068.

[327] Peter Bieling, Liedewij Laan, Henry Schek, E. Laura Munteanu, Linda Sandblad, Marileen Dogterom, Damian Brunner, and Thomas Surrey. Reconstitution of a microtubule plus-end tracking system in vitro. *Nature*, 450(7172):1100–1105, 2007. doi: 10.1038/nature06386.

[328] Yuko Mimori-Kiyosue, Nobuyuki Shiina, and Shoichiro Tsukita. The dynamic behavior of the APC-binding protein EB1 on the distal ends of microtubules. *Current Biology*, 10(14):865–868, 2000. doi: 10.1016/S0960-9822(00)00600-X.

[329] Rui Zhang, Gregory M. Alushin, Alan Brown, and Eva Nogales. Mechanistic origin of microtubule dynamic instability and its modulation by EB proteins. *Cell*, 162(4):849–859, 2015. doi: 10.1016/j.cell.2015.07.012.

[330] Sebastian P. Maurer, Nicholas I. Cade, Gergö Bohner, Nils Gustafsson, Emmanuel Boutant, and Thomas Surrey. EB1 accelerates two conformational transitions important for microtubule maturation and dynamics. *Current Biology*, 24(4):372–384, 2014. doi: 10.1016/j.cub.2013.12.042.

[331] Anna Akhmanova and Michel O. Steinmetz. Control of microtubule organization and dynamics: Two ends in the limelight. *Nature Reviews Molecular Cell Biology*, 16(12):711–726, 2015. doi: 10.1038/nrm4084.

[332] Yuzy Matsuo, Sebastian P. Maurer, Masashi Yukawa, Silva Zakian, Martin R. Singleton, Thomas Surrey, and Takashi Toda. An unconventional interaction between Dis1/TOG and Mal3/EB1 promotes the fidelity of chromosome segregation. *Journal of Cell Science*, 129(24):4592–4606, 2016. doi: 10.1242/jcs.197533.

[333] Marija Zanic, Per O Widlund, Anthony A Hyman, and Jonathon Howard. Synergy between XMAP215 and EB1 increases microtubule growth rates to physiological levels. *Nature Cell Biology*, 15(5):1–8, 2013. doi: 10.1038/ncb2744.

[334] Anna Akhmanova and Michel O. Steinmetz. Tracking the ends: A dynamic protein network controls the fate of microtubule tips. *Nature Reviews Molecular Cell Biology*, 9(4):309–322, 2008. doi: 10.1038/nrm2369.

[335] Anne Nehlig, Angie Molina, Sylvie Rodrigues-Ferreira, Stéphane Honoré, and Clara Nahmias. Regulation of end-binding protein EB1 in the control of microtubule dynamics. *Cellular and Molecular Life Sciences*, 74 (13):2381–2393, 2017. doi: 10.1007/s00018-017-2476-2.

[336] Agnes Grallert, Christoph Beuter, Rachel A. Craven, Steve Bagley, Deepti Wilks, Ursula Fleig, and Iain M. Hagan. S. pombe CLASP needs dynein, not EB1 or CLIP170, to induce microtubule instability and slows polymerization rates at cell tips in a dynein-dependent manner. *Genes and Development*, 20(17):2421–2436, 2006. doi: 10.1101/gad.381306.

[337] Karl Emanuel Busch, Jacky Hayles, Paul Nurse, and Damian Brunner. Tea2p kinesin is involved in spatial microtubule organization by transporting Tip1p on microtubules. *Developmental Cell*, 6(6):831–843, 2004. doi: 10.1016/j.devcel.2004.05.008.

[338] Sebastian Mana-Capelli, Janel R. McLean, Chun Ti Chen, Kathleen L. Gould, and Dannel McCollum. The kinesin-14 Klp2 is negatively regulated by the SIN for proper spindle elongation and telophase nuclear positioning. *Molecular Biology of the Cell*, 23(23):4592–4600, 2012. doi: 10.1091/mbc.E12-07-0532.

[339] Jawdat Al-Bassam, Hwajin Kim, Ignacio Flor-Parra, Neeraj Lal, Hamida Velji, and Fred Chang. Fission yeast Alp14 is a dose-dependent plus end-tracking microtubule polymerase. *Molecular Biology of the Cell*, 23(15): 2878–2890, 2012. doi: 10.1091/mbc.E12-03-0205.

[340] Jawdat Al-Bassam, Mark Van Breugel, Stephen C. Harrison, and Anthony Hyman. Stu2p binds tubulin and undergoes an open-to-closed conformational change. *Journal of Cell Biology*, 172(7):1009–1022, 2006. doi: 10.1083/jcb.200511010.

[341] Gary J. Brouhard, Jeffrey H. Stear, Tim L. Noetzel, Jawdat Al-Bassam, Kazuhisa Kinoshita, Stephen C. Harrison, Jonathon Howard, and Anthony A. Hyman. XMAP215 Is a Processive Microtubule Polymerase. *Cell*, 132(1):79–88, 2008. doi: 10.1016/j.cell.2007.11.043.

[342] Sophie Charrasse, Marianne Schroeder, Cécile Gauthier-Rouviere, Fabrice Ango, Lynne Cassimeris, David L. Gard, and Christian Larroque. The TOGp protein is a new human microtubule-associated protein homologous to the Xenopus XMAP215. *Journal of Cell Science*, 111(10):1371–1383, 1998.

[343] D. L. Gard and M. W. Kirschner. A microtubule-associated protein from Xenopus eggs that specifically promotes assembly at the plus-end. *Journal of Cell Biology*, 105(5):2203–2215, 1987. doi: 10.1083/jcb.105.5.2203.

[344] Jawdat Al-Bassam, Nicholas A. Larsen, Anthony A. Hyman, and Stephen C. Harrison. Crystal Structure of a TOG Domain: Conserved Features of XMAP215/Dis1-Family TOG Domains and Implications for Tubulin Binding. *Structure*, 15(3):355–362, 2007. doi: 10.1016/j.str.2007.01.012.

[345] Pelin Ayaz, Xuecheng Ye, Patrick Huddelston, Chad A. Brautigam, and Luke M. Rice. A TOG:ab-tubulin Complex Structure Reveals Conformation-Based Mechanisms for a Microtubule Polymerase. *Science*, 337: 857–860, 2012. doi: 10.1126/science.1221698.

[346] Pelin Ayaz, Sarah Munyoki, Elisabeth A. Geyer, Felipe Andrés Piedra, Emily S. Vu, Raquel Bromberg, Zbyszek Otwinowski, Nick V. Grishin, Chad A. Brautigam, and Luke M. Rice. A tethered delivery mechanism explains the catalytic action of a microtubule polymerase. *eLife*, 3(e03069):1–19, 2014. doi: 10.7554/eLife.03069.

[347] Per O Widlund, Jeffrey H Stear, Andrei Pozniakovsky, Marija Zanic, Simone Reber, and Gary J Brouhard. XMAP215 polymerase activity is built by combining multiple tubulin-binding TOG domains and a basic lattice-binding region. *PNAS*, 14(7), 2010. doi: 10.1073/pnas.1016498108.

[348] Satoko Nakamura, Ilya Grigoriev, Taisaku Nogi, Tomoko Hamaji, Lynne Cassimeris, and Yuko Mimori-Kiyosue. Dissecting the Nanoscale Distributions and Functions of Microtubule-End-Binding Proteins EB1 and ch-TOG in Interphase HeLa Cells. *PLoS ONE*, 7(12):1–20, 2012. doi: 10.1371/journal.pone.0051442.

[349] Elisabeth A. Geyer, Matthew P. Miller, Chad A. Brautigam, Sue Biggins, and Luke M. Rice. Design principles of a microtubule polymerase. *eLife*, 7:1–23, 2018. doi: 10.7554/eLife.34574.

[350] M. A. Garcia, L. Vardy, N. Koonrugsa, and T. Toda. Fission yeast ch-TOG/XMAP215 homologue Alp14 connects mitotic spindles with the kinetochore and is a component of the Mad2-dependent spindle checkpoint. *EMBO Journal*, 20(13):3389–3401, 2001. doi: 10.1093/emboj/20.13.3389.

[351] Yukinobu Nakaseko, Gohta Goshima, Jun Morishita, and Mitsuhiro Yanagida. M phase-specific kinetochore proteins in fission yeast: Microtubule-associating Dis1 and Mtc1 display rapid separation and segregation during anaphase. *Current Biology*, 11(8):537–549, 2001. doi: 10.1016/S0960-9822(01)00155-5.

[352] Hélio Roque, Jonathan J. Ward, Lindsay Murrells, Damian Brunner, and Claude Antony. The fission yeast XMAP215 homolog dis1p is involved in microtubule bundle organization. *PLoS ONE*, 5:1–12, 2010. doi: 10.1371/journal.pone.0014201.

[353] Gohta Goshima, Shigeaki Saitoh, and Mitsuhiro Yanagida. Proper metaphase spindle length is determined by centromere proteins Mis12 and Mis6 required for faithful chromosome segregation. *Genes and Development*, 13(13):1664–1677, 1999. doi: 10.1101/gad.13.13.1664.

[354] Kuo-shun Shun Hsu and Takashi Toda. Ndc80 internal loop interacts with Dis1/TOG to ensure proper kinetochore-spindle attachment in fission yeast. *Current Biology*, 21(3):214–220, 2011. doi: 10.1016/j.cub.2010.12.048.

[355] Yusuke Toyoda, Kanji Furuya, Gohta Goshima, Koji Nagao, Kohta Takahashi, and Mitsuhiro Yanagida. Requirement of chromatid cohesion proteins Rad21/Scc1 and Mis4/Scc2 for normal spindle-kinetochore interaction in fission yeast. *Current Biology*, 12(5):347–358, 2002. doi: 10.1016/S0960-9822(02)00692-9.

[356] Ngang Heok Tang, Hirofumi Takada, Kuo Shun Hsu, and Takashi Toda. The internal loop of fission yeast Ndc80 binds Alp7/TACC-Alp14/TOG and ensures proper chromosome attachment. *Molecular Biology of the Cell*, 24(8):1122–1133, 2013. doi: 10.1091/mbc.E12-11-0817.

[357] Masamitsu Sato, Leah Vardy, Miguel Angel Garcia, Nirada Koonrugsa, and Takashi Toda. Interdependency of Fission Yeast Alp14/TOG and Coiled Coil Protein Alp7 in Microtubule Localization and Bipolar Spindle Formation. *Molecular Biology of the Cell*, 15(April):1609–1622, 2004. doi: 10.1091/mbc.E03.

[358] Ignacio Flor-Parra, Ana Belén Iglesias-Romero, and Fred Chang. The XMAP215 Ortholog Alp14 Promotes Microtubule Nucleation in Fission Yeast. *Current Biology*, 28(11):1681–1691.e4, 2018. doi: 10.1016/j.cub.2018.04.008.

[359] Amol Aher, Maurits Kok, Ashwani Sharma, Ankit Rai, Natacha Olieric, Ruddi Rodriguez-Garcia, Eugene A. Katrukha, Tobias Weinert, Vincent Olieric, Lukas C. Kapitein, Michel O. Steinmetz, Marileen Dogterom, and Anna Akhmanova. CLASP Suppresses Microtubule Catastrophes through a Single TOG Domain. *Developmental Cell*, 46(1):40–58, 2018. doi: 10.1016/j.devcel.2018.05.032.

[360] Jawdat Al-bassam, Hwajin Kim, Gary Brouhard, Antoine van Oijen, Stephen C. Harrison, Fred Chang, Antoine Van Oijen, Stephen C. Harrison, and Fred Chang. CLASP Promotes Microtubule Rescue by Recruiting Tubulin Dimers to the Microtubule. *Developmental Cell*, 19(2):245–258, 2010. doi: 10.1016/j.devcel.2010.07.016.

[361] Elizabeth J. Lawrence, Göker Arpag, Stephen R. Norris, and Marija Zanic. Human CLASP2 specifically regulates microtubule catastrophe and rescue. *Molecular Biology of the Cell*, 29(10):1168–1177, 2018. doi: 10.1091/mbc.E18-01-0016.

[362] E. J. Lawrence and M. Zanic. Rescuing microtubules from the brink of catastrophe: CLASPs lead the way. *Current Opinion in Cell Biology*, 56:94–101, 2019. doi: 10.1016/j.ceb.2018.10.011.

[363] Takashi Moriwaki and Gohta Goshima. Five factors can reconstitute all three phases of microtubule polymerization dynamics. *Journal of Cell Biology*, 215(3):357–368, 2016. doi: 10.1083/jcb.201604118.

[364] Anna Akhmanova, Hoogenraad CC, Drabek K, Stepanova T, Dortland B, Verkerk T, Vermeulen W, Burgering BM, De Zeeuw CI, Grosveld F, and Galjart N. Clasps are CLIP-115 and -170 associating proteins involved in the regional regulation of microtubule dynamics in motile fibroblasts. *Cell*, 104:923–935, 2001.

[365] Jonathan B. Leano, Stephen L. Rogers, and Kevin C. Slep. A cryptic TOG domain with a distinct architecture underlies CLASP-dependent bipolar spindle formation. *Structure*, 21(6):939–950, 2013. doi: 10.1016/j.str.2013.04.018.

[366] Shreoshi Majumdar, Tae Kim, Zhe Chen, Sarah Munyoki, Shih Chia Tso, Chad A. Brautigam, and Luke M. Rice. An isolated CLASP TOG domain suppresses microtubule catastrophe and promotes rescue. *Molecular Biology of the Cell*, 29(11):1359–1375, 2018. doi: 10.1091/mbc.E17-12-0748.

[367] Takahisa Maki, Ashley D. Grimaldi, Sotaro Fuchigami, Irina Kaverina, and Ikuko Hayashi. CLASP2 has two distinct TOG domains that contribute differently to microtubule dynamics. *Journal of Molecular Biology*, 427(14):2379–2395, 2015. doi: 10.1016/j.jmb.2015.05.012.

[368] Amol Aher, Dipti Rai, Laura Schaedel, Jeremie Gaillard, Karin John, Qingyang Liu, Maarten Altelaar, Laurent Blanchoin, Manuel Thery, and Anna Akhmanova. CLASP Mediates Microtubule Repair by Restricting Lattice Damage and Regulating Tubulin Incorporation. *Current Biology*, 30(11):2175–2183, 2020. doi: 10.1016/j.cub.2020.03.070.

[369] Yuko Mimori-Kiyosue, Ilya Grigoriev, Hiroyuki Sasaki, Chiyuki Matsui, Anna Akhmanova, Shoichiro Tsukita, and Ivan Vorobjev. Mammalian CLASPs are required for mitotic spindle organization and kinetochore alignment. *Genes to Cells*, 11(8):845–857, 2006. doi: 10.1111/j.1365-2443.2006.00990.x.

[370] Scott V. Bratman and Fred Chang. Stabilization of Overlapping Microtubules by Fission Yeast CLASP. *Developmental Cell*, 13(6):812–827, 2007. doi: 10.1016/j.devcel.2007.10.015.

[371] Daishi Kitazawa, Tatsuru Matsuo, Kana Kaizuka, Chie Miyauchi, Daisuke Hayashi, and Yoshihiro H. Inoue. Orbit/CLASP is required for myosin accumulation at the cleavage furrow in Drosophila male meiosis. *PLoS ONE*, 9(5), 2014. doi: 10.1371/journal.pone.0093669.

[372] Jing Liu, Zhikai Wang, Kai Jiang, Liangyu Zhang, Lingli Zhao, Shasha Hua, Feng Yan, Yong Yang, Dongmei Wang, Chuanhai Fu, Xia Ding, Zhen Guo, and Xuebiao Yao. PRC1 cooperates with CLASP1 to organize central spindle plasticity in mitosis. *Journal of Biological Chemistry*, 284(34):23059–23071, 2009. doi: 10.1074/jbc.M109.009670.

[373] Jean Gautier, Chris Norbury, Manfred Lohka, Paul Nurse, and James Maller. Purified maturation-promoting factor contains the product of a Xenopus homolog of the fission yeast cell cycle control gene cdc2+. *Cell*, 54(3):433–439, 1988. doi: 10.1016/0092-8674(88)90206-1.

[374] M. J. Lohka, M. K. Hayes, and J. L. Maller. Purification of maturation-promoting factor, an intracellular regulator of early mitotic events. *Proceedings of the National Academy of Sciences of the United States of America*, 85(9):3009–3013, 1988. doi: 10.1073/pnas.85.9.3009.

[375] Yoshio Masui. Oscillatory activity of maturation promoting factor (MPF) in extracts of Rana pipiens eggs. *Journal of Experimental Zoology*, 224(3):389–399, 1982. doi: 10.1002/jez.1402240312.

[376] K. Kinoshita, I. Arnal, A. Desai, D. N. Drechsel, and A. A. Hyman. Reconstitution of physiological microtubule dynamics using purified components. *Science*, 294(5545):1340–1343, 2001. doi: 10.1126/science.1064629.

[377] Nunu Mchedlishvili, Helen K. Matthews, Adam Corrigan, and Buzz Baum. Two-step interphase microtubule disassembly aids spindle morphogenesis. *BMC Biology*, 16(1):1–16, 2018. doi: 10.1186/s12915-017-0478-z.

[378] Margarete M. S. Heck, Andrea Pereira, Patty Pesavento, Yvonne Yannoni, Allan C. Spradling, and Lawrence S. B. Goldstein. The Kinesin-like Protein KLP6IF Is Essential for Mitosis in Drosophila. *Journal of Cell Biology*, 123(3):665–679, 1993. doi: 10.1083/jcb.123.3.665.

[379] Tarun M. Kapoor, Thomas U. Mayer, Margaret L. Coughlin, and Timothy J. Mitchison. Probing spindle assembly mechanisms with monastrol, a small molecule inhibitor of the mitotic kinesin, Eg5. *Journal of Cell Biology*, 150(5):975–988, 2000. doi: 10.1083/jcb.150.5.975.

[380] Ken Sawin, Katherine LeGuellec, Michel Philippe, and Timothy J. Mitchison. Mitotic spindle organization by a plus-end-directed microtubule motor. *Nature*, 359:540–543, 1992. doi: 10.1038/359540a0.

[381] Lora Winters, Ivana Ban, Marcel Prelogović, Iana Kalinina, Nenad Pavin, and Iva M. Tolić. Pivoting of microtubules driven by minus-end-directed motors leads to spindle assembly. *BMC Biology*, 17(1):1–18, may 2019. doi: 10.1186/s12915-019-0656-2.

[382] Benjamin H. Kwok, Lukas C. Kapitein, Jeffrey H. Kim, Erwin J.G. Peterman, Christoph F. Schmidt, and Tarun M. Kapoor. Allosteric inhibition of kinesin-5 modulates its processive directional motility. *Nature Chemical Biology*, 2(9):480–485, 2006. doi: 10.1038/nchembio812.

[383] Emma G. Sturgill, Stephen R. Norris, Yan Guo, and Ryoma Ohi. Kinesin-5 inhibitor resistance is driven by kinesin-12. *Journal of Cell Biology*, 213(2):213–227, 2016. doi: 10.1083/jcb.201507036.

[384] Marvin E. Tanenbaum, Libor Macůrek, Aniek Janssen, Erica F. Geers, Mónica Alvarez-Fernández, and René H. Medema. Kif15 Cooperates with Eg5 to Promote Bipolar Spindle Assembly. *Current Biology*, 19 (20):1703–1711, 2009. doi: 10.1016/j.cub.2009.08.027.

[385] William Saunders, Valerie Lengyel, and M. Andrew Hoyt. Mitotic spindle function in Saccharomyces cerevisiae requires a balance between different types of kinesin-related motors. *Molecular Biology of the Cell*, 8 (6):1025–1033, 1997. doi: 10.1091/mbc.8.6.1025.

[386] Nick P. Ferenz, Raja Paul, Carey Fagerstrom, Alex Mogilner, and Patricia Wadsworth. Dynein Antagonizes Eg5 by Crosslinking and Sliding Antiparallel Microtubules. *Current Biology*, 19(21):1833–1838, 2009. doi: 10.1016/j.cub.2009.09.025.

[387] Vicki Mountain, Calvin Simerly, Louisa Howard, Asako Ando, Gerald Schatten, and Duane A Compton. The Kinesin-related Protein, HSET, Opposes the Activity of Eg5 and Cross-links Microtubules in the Mammalian Mitotic Spindle. *J. Cell Biol.*, 147(2):351–365, 1999. doi: 10.1083/jcb.147.2.351.

[388] David J. Sharp, Kristina R. Yu, John C. Sisson, William Sullivan, and Jonathan M. Scholey. Antagonistic microtubule-sliding motors position mitotic centrosomes in Drosopnifa early embryos. *Nature Cell Biology*, 1(1):51–54, 1999. doi: 10.1038/9025.

[389] Viktoriya Syrovatkina and Phong T. Tran. Loss of kinesin-14 results in aneuploidy via kinesin-5-dependent microtubule protrusions leading to chromosome cut. *Nature Communications*, 6:1–8, 2015. doi: 10.1038/ncomms8322.

[390] David Vanneste, Masatoshi Takagi, Naoko Imamoto, and Isabelle Vernos. The Role of Hklp2 in the Stabilization and Maintenance of Spindle Bipolarity. *Current Biology*, 19(20):1712–1717, 2009. doi: 10.1016/j.cub.2009.09.019.

[391] Claire E. Walczak, Isabelle Vernos, Timothy J. Mitchison, Eric Karsenti, and Rebecca Heald. A model for the proposed roles of different microtubule-based motor proteins in establishing spindle bipolarity. *Current Biology*, 8(16):903–913, 1998. doi: 10.1016/S0960-9822(07)00370-3.

[392] Duane A. Compton. Focusing on spindle poles. *Journal of Cell Science*, 111(11):1477–1481, 1998. doi: 10.1242/jcs.111.11.1477.

[393] Thomas Surrey, François Nédélec, Stanislas Leibler, and Eric Karsenti. Physical properties determining self-organization of motors and microtubules. *Science*, 292(5519):1167–1171, 2001. doi: 10.1126/science.1059758.

[394] Robert Blackwell, Christopher Edelmaier, Oliver Sweezy-Schindler, Adam Lamson, Zachary R. Gergely, Eileen O'Toole, Ammon Crapo, Loren E. Hough, J. Richard McIntosh, Matthew A. Glaser, and Meredith D. Betterton. Physical determinants of bipolar mitotic spindle assembly and stability in fission yeast. *Science Advances*, 3(1):e1601603, 2017. doi: 10.1126/sciadv.1601603.

[395] Masashi Yukawa, Yusuke Yamada, and Takashi Toda. Suppressor analysis uncovers that maps and microtubule dynamics balance with the Cut7/Kinesin-5 motor for mitotic spindle assembly in schizosaccharomyces pombe. *G3: Genes, Genomes, Genetics*, 9(1):269–280, 2019. doi: 10.1534/g3.118.200896.

[396] Rebecca Heald and Alexey Khodjakov. Thirty years of search and capture: The complex simplicity of mitotic spindle assembly. *Journal of Cell Biology*, 211(6):1103–1111, 2015. doi: 10.1083/jcb.201510015.

[397] R. Wollman, E. N. Cytrynbaum, J. T. Jones, T. Meyer, J. M. Scholey, and A. Mogilner. Efficient chromosome capture requires a bias in the 'search-and-capture' process during mitotic-spindle assembly. *Current Biology*, 15(9):828–832, 2005. doi: 10.1016/j.cub.2005.03.019.

[398] Petr Kalab, Karsten Weis, and Rebecca Heald. Visualization of a Ran-GTP gradient in interphase and mitotic Xenopus egg extracts. *Science*, 295(5564):2452–2456, 2002. doi: 10.1126/science.1068798.

[399] Ekaterina L. Grishchuk and J. Richard McIntosh. Microtubule depolymerization can drive poleward chromosome motion in fission yeast. *EMBO Journal*, 25(20):4888–4896, 2006. doi: 10.1038/sj.emboj.7601353.

[400] Iana Kalinina, Amitabha Nandi, Petrina Delivani, Mariola R. Chacón, Anna H. Klemm, Damien Ramunno-Johnson, Alexander Krull, Benjamin Lindner, Nenad Pavin, and Iva M. Tolić-Nørrelykke. Pivoting of microtubules around the spindle pole accelerates kinetochore capture. *Nature Cell Biology*, 15(1):82–87, 2013. doi: 10.1038/ncb2640.

[401] Indrani Nayak, Dibyendu Das, and Amitabha Nandi. Kinetochore capture by spindle microtubules: why fission yeast may prefer pivoting to search-and-capture. *bioRxive*, page 673723, 2019. doi: 10.1101/673723.

[402] Hirohisa Masuda, Takashi Toda, Rumi Miyamoto, Tokuko Haraguchi, and Yasushi Hiraoka. Modulation of Alp4 function in Schizosaccharomyces pombe induces novel phenotypes that imply distinct functions for nuclear and cytoplasmic γ-tubulin complexes. *Genes to Cells*, 11(4):319–336, 2006. doi: 10.1111/j.1365-2443.2006.00946.x.

[403] Miguel Angel Garcia, Nirada Koonrugsa, and Takashi Toda. Two kinesin-like Kin I family proteins in fission yeast regulate the establishment of metaphase and the onset of anaphase A. *Current Biology*, 12(8):610–621, 2002. doi: 10.1016/S0960-9822(02)00761-3.

[404] Celia Antonio, Ingvar Ferby, Heike Wilhelm, Margaret Jones, Eric Karsenti, Angel R. Nebreda, and Isabelle Vernos. Xkid, a chromokinesin required for chromosome alignment on the metaphase plate. *Cell*, 102(4):425–435, 2000. doi: 10.1016/S0092-8674(00)00048-9.

[405] Marin Barisic, Paulo Aguiar, Stephan Geley, and Helder Maiato. Kinetochore motors drive congression of peripheral polar chromosomes by overcoming random arm-ejection forces. *Nature Cell Biology*, 16(12):1249–1256, 2014. doi: 10.1038/ncb3060.

[406] Tarun M. Kapoor, Michael A. Lampson, Polla Hergert, Lisa Cameron, Daniela Cimini, E. D. Salmon, Bruce F. McEwen, and Alexey Khodjakov. Chromosomes can congress to the metaphase plate before biorientation. *Science*, 311(5759):388–391, 2006. doi: 10.1126/science.1122142.

[407] C. L. Rieder, E. A. Davison, L. C.W. Jensen, L. Cassimeris, and E. D. Salmon. Oscillatory movements of monooriented chromosomes and their position relative to the spindle pole result from the ejection properties of the aster and half-spindle. *Journal of Cell Biology*, 103(2):581–591, 1986. doi: 10.1083/jcb.103.2.581.

[408] B. T. Schaar, G. K.T. Chan, P. Maddox, E. D. Salmon, and T. J. Yen. CENP-E function at kinetochores is essential for chromosome alignment. *Journal of Cell Biology*, 139(6):1373–1382, 1997. doi: 10.1083/jcb.139.6.1373.

[409] Cornelia Wandke, Marin Barisic, Reinhard Sigl, Veronika Rauch, Frank Wolf, Ana C. Amaro, Chia H. Tan, Antonio J. Pereira, Ulrike Kutay, Helder Maiato, Patrick Meraldi, and Stephan Geley. Human chromokinesins promote chromosome congression and spindle microtubule dynamics during mitosis. *Journal of Cell Biology*, 198(5):847–863, 2012. doi: 10.1083/jcb.201110060.

[410] Zhenye Yang, U. Serdar Tulu, Patricia Wadsworth, and Conly L. Rieder. Kinetochore Dynein Is Required for Chromosome Motion and Congression Independent of the Spindle Checkpoint. *Current Biology*, 17(11):973–980, 2007. doi: 10.1016/j.cub.2007.04.056.

[411] C. L. Rieder and S. P. Alexander. Kinetochores are transported poleward along a single astral microtubule during chromosome attachment to the spindle in newt lung cells. *Journal of Cell Biology*, 110(1):81–95, 1990. doi: 10.1083/jcb.110.1.81.

[412] Tomoyuki U. Tanaka. Kinetochore-microtubule interactions: Steps towards bi-orientation. *EMBO Journal*, 29(24):4070–4082, 2010. doi: 10.1038/emboj.2010.294.

[413] Tomoyuki U. Tanaka, Michael J.R. Stark, and Kozo Tanaka. Kinetochore capture and bi-orientation on the mitotic spindle. *Nature Reviews Molecular Cell Biology*, 6(12):929–942, 2005. doi: 10.1038/nrm1764.

[414] Ekaterina L. Grishchuk, Ilia S. Spiridonov, and J Richard Mcintosh. Mitotic Chromosome Biorientation in Fission Yeast Is Enhanced by Dynein and a Minus-end–directed, Kinesin-like Protein. *Molecular biology of the cell*, 18(June):2216–2225, 2007. doi: 10.1091/mbc.E06.

[415] Kazuhide Asakawa, Mika Toya, Masamitsu Sato, Muneyoshi Kanai, Kazunori Kume, Tetsuya Goshima, Miguel Angel Garcia, Dai Hirata, and Takashi Toda. Mal3, the fission yeast EB1 homologue, cooperates with Bub1 spindle checkpoint to prevent monopolar attachment. *EMBO Reports*, 6(12):1194–1200, 2005. doi: 10.1038/sj.embor.7400540.

[416] Jason Stumpff, Michael Wagenbach, Andrew Franck, Charles L. Asbury, and Linda Wordeman. Kif18A and Chromokinesins Confine Centromere Movements via Microtubule Growth Suppression and Spatial Control of Kinetochore Tension. *Developmental Cell*, 22(5):1017–1029, 2012. doi: 10.1016/j.devcel.2012.02.013.

[417] Sue Biggins and Andrew W. Murray. The budding yeast protein kinase Ipl1/Aurora allows the absence of tension to activate the spindle checkpoint. *Genes and Development*, 15(23):3118–3129, 2001. doi: 10.1101/gad.934801.

[418] Andrea Musacchio. The Molecular Biology of Spindle Assembly Checkpoint Signaling Dynamics. *Current Biology*, 25(20):R1002–R1018, 2015. doi: 10.1016/j.cub.2015.08.051.

[419] Iain M. Cheeseman, Scott Anderson, Miri Jwa, Erin M. Green, Jung seog Kang, John R. Yates, Clarence S.M. Chan, David G. Drubin, and Georjana Barnes. Phospho-regulation of kinetochore-microtubule attachments by the Aurora kinase Ipl1p. *Cell*, 111(2):163–172, 2002. doi: 10.1016/S0092-8674(02)00973-X.

[420] Silke Hauf, Richard W. Cole, Sabrina LaTerra, Christine Zimmer, Gisela Schnapp, Rainer Walter, Armin Heckel, Jacques Van Meel, Conly L. Rieder, and Jan Michael Peters. The small molecule Hesperadin reveals a role for Aurora B in correcting kinetochore-microtubule attachment and in maintaining the spindle assembly checkpoint. *Journal of Cell Biology*, 161(2):281–294, 2003. doi: 10.1083/jcb.200208092.

[421] Marko J. Kallio, Mark L. McCleland, P. Todd Stukenberg, and Gary J. Gorbsky. Inhibition of Aurora B kinase blocks chromosome segregation, overrides the spindle checkpoint, and perturbs microtubule dynamics in mitosis. *Current Biology*, 12(11):900–905, 2002. doi: 10.1016/S0960-9822(02)00887-4.

[422] Michael A. Lampson and Ekaterina L. Grishchuk. Mechanisms to avoid and correct erroneous kinetochore-microtubule attachments. *Biology*, 6(1), 2017. doi: 10.3390/biology6010001.

[423] Sung Hugh Choi and Dannel McCollum. A role for metaphase spindle elongation forces in correction of merotelic kinetochore attachments. *Current Biology*, 22(3):225–230, 2012. doi: 10.1016/j.cub.2011.12.022.

[424] Viktoriya Syrovatkina, Chuanhai Fu, and Phong T. Tran. Antagonistic spindle motors and MAPs regulate metaphase spindle length and chromosome segregation. *Current Biology*, 23(23):2423–2429, 2013. doi: 10.1016/j.cub.2013.10.023.

[425] Ingrid Brust-Mascher, Patrizia Sommi, Dhanya K. Cheerambathur Jonathan M. Scholey, Dhanya K. Cheerambathur, and Jonathan M. Scholey. Kinesin-5–dependent Poleward Flux and Spindle Length Control in Drosophila Embryo Mitosis. *Molecular Biology of the Cell*, 20(4):1749–1762, 2009. doi: 10.1091/mbc.E08.

[426] Yulia Steblyanko, Girish Rajendraprasad, Mariana Osswald, Susana Eibes, Ariana Jacome, Stephan Geley, António J Pereira, Helder Maiato, and Marin Barisic. Microtubule poleward flux in human cells is driven by the coordinated action of four kinesins. *The EMBO Journal*, 39(23):1–22, 2020. doi: 10.15252/embj.2020105432.

[427] Austin J. Hepperla, Patrick T. Willey, Courtney E. Coombes, Breanna M. Schuster, Maryam Gerami-Nejad, Mark McClellan, Soumya Mukherjee, Janet Fox, Mark Winey, David J. Odde, Eileen O'Toole, and Melissa K. Gardner. Minus-end-directed kinesin-14 motors align antiparallel microtubules to control metaphase spindle length. *Developmental Cell*, 31(1):61–72, 2014. doi: 10.1016/j.devcel.2014.07.023.

[428] Zachary T. Olmsted, Timothy D. Riehlman, Carmen N. Branca, Andrew G. Colliver, Leilani O. Cruz, and Janet L. Paluh. Kinesin-14 Pkl1 targets $\gamma$-tubulin for release from the $\gamma$-tubulin ring complex ($\gamma$-TuRC). *Cell Cycle*, 12(5):842–848, 2013. doi: 10.4161/cc.23822.

[429] Adrianna S. Rodriguez, Joseph Batac, Alison N. Killilea, Jason Filopei, Dimitre R. Simeonov, Ida Lin, and Janet L. Paluh. Protein complexes at the microtubule organizing center regulate bipolar spindle assembly. *Cell Cycle*, 7(9):1246–1253, 2008. doi: 10.4161/cc.7.9.5808.

[430] Marvin E. Tanenbaum, Libor Macůrek, Niels Galjart, and René H. Medema. Dynein, Lis1 and CLIP-170 counteract Eg5-dependent centrosome separation during bipolar spindle assembly. *EMBO Journal*, 27(24):3235–3245, 2008. doi: 10.1038/emboj.2008.242.

[431] Roy G.H.P. van Heesbeen, Marvin E. Tanenbaum, René H. Medema, Roy G.H.P. VanHeesbeen, Marvin E. Tanenbaum, and René H. Medema. Balanced activity of three mitotic motors is required for bipolar spindle assembly and chromosome segregation. *Cell Reports*, 8(4):948–956, 2014. doi: 10.1016/j.celrep.2014.07.015.

[432] R. R. West, T. Malmstrom, C. L. Troxell, and J. R. McIntosh. Two related kinesins, klp5+ and klp6+, foster microtubule disassembly and are required for meiosis in fission yeast. *Molecular Biology of the Cell*, 12(12):3919–3932, 2001. doi: 10.1091/mbc.12.12.3919.

[433] Gohta Goshima and Ronald D. Vale. The roles of microtubule-based motor proteins in mitosis: Comprehensive RNAi analysis in the Drosophila S2 cell line. *Journal of Cell Biology*, 162(6):1003–1016, 2003. doi: 10.1083/jcb.200303022.

[434] Sanjay Shrestha, Mark Hazelbaker, Amber L. Yount, and Claire E. Walczak. Emerging insights into the function of kinesin-8 proteins in microtubule length regulation. *Biomolecules*, 9(1):1–18, 2019. doi: 10.3390/biom9010001.

[435] Régis Tournebize, Andrei Popov, Kazuhisa Kinoshita, Anthony J. Ashford, Sonja Rybina, Andrei Pozniakovsky, Thomas U. Mayer, Claire E. Walczak, Eric Karsenti, and Anthony A. Hyman. Control of microtubule dynamics by the antagonistic activities of XMAP215 and XKCM1 in Xenopus egg extracts. *Nature Cell Biology*, 2(1):13–19, 2000. doi: 10.1038/71330.

[436] Ana Milunovic-Jevtic, Predrag Jevtic, Daniel L. Levy, and J. C. Gatlin. In vivo mitotic spindle scaling can be modulated by changing the levels of a single protein: the microtubule polymerase XMAP215. *Molecular Biology of the Cell*, 29(11):1311–1317, 2018. doi: 10.1091/mbc.E18-01-0011.

[437] Simone B. Reber, Johannes Baumgart, Per O. Widlund, Andrei Pozniakovsky, Jonathon Howard, Anthony A. Hyman, and Frank Jülicher. XMAP215 activity sets spindle length by controlling the total mass of spindle microtubules. *Nature Cell Biology*, 15(9):1116–1122, 2013. doi: 10.1038/ncb2834.

[438] Hirohisa Ebina, Liang Ji, and Masamitsu Sato. CLASP promotes microtubule bundling in metaphase spindle independently of Ase1/PRC1 in fission yeast. *Biology Open*, 8(10):1–10, 2019. doi: 10.1242/bio.045716.

[439] Hugo Girão, Naoyuki Okada, Tony A. Rodrigues, Alexandra O. Silva, Ana C. Figueiredo, Zaira Garcia, Tatiana Moutinho-Santos, Ikuko Hayashi, Jorge E. Azevedo, Sandra Macedo-Ribeiro, and Helder Maiato. CLASP2 binding to curved microtubule tips promotes flux and stabilizes kinetochore attachments. *Journal of Cell Biology*, 219(2), 2020. doi: 10.1083/jcb.201905080.

[440] Benjamin Lacroix, Gaëlle Letort, Laras Pitayu, Jérémy Sallé, Marine Stefanutti, Gilliane Maton, Anne-Marie Ladouceur, Julie C. Canman, Paul S. Maddox, Amy S. Maddox, Nicolas Minc, François Nédélec, and Julien Dumont. Microtubule Dynamics Scale with Cell Size to Set Spindle Length and Assembly Timing. *Developmental Cell*, 45(4):496–511, 2018. doi: 10.1016/j.devcel.2018.04.022.

[441] Catarina L. Lemos, Paula Sampaio, Helder Maiato, Madalena Costa, Leonid V. Omel'yanchuk, Vasco Liberal, and Claudio E. Sunkel. Mast, a conserved microtubule-associated protein required for bipolar mitotic spindle organization. *EMBO Journal*, 19(14):3668–3682, 2000. doi: 10.1093/emboj/19.14.3668.

[442] Ana L Pereira, António J. Pereira, Ana R.R. Maia, Ksenija Drabek, C. Laura Sayas, Polla J. Hergert, Mariana Lince-Faria, Irina Matos, Cristina Duque, Tatiana Stepanova, Cony L. Rieder, William C. Earnshaw, Niels Galjart, and Helder Maiato. Mammalian CLASP1 and CLASP2 Cooperate to Ensure Mitotic Fidelity by Regulating Spindle and Kinetochore Function. *Molecular biology of the cell*, 17(October):4526–4542, 2006. doi: 10.1091/mbc.E06.

[443] Sarah S. Goodwin and Ronald D. Vale. Patronin Regulates the Microtubule Network by Protecting Microtubule Minus Ends. *Cell*, 143(2):263–274, 2010. doi: 10.1016/j.cell.2010.09.022.

[444] Shanhui Liao, Girish Rajendraprasad, Na Wang, Susana Eibes, Jun Gao, Huijuan Yu, Gao Wu, Xiaoming Tu, Hongda Huang, Marin Barisic, and Chao Xu. Molecular basis of vasohibins-mediated detyrosination and its impact on spindle function and mitosis. *Cell Research*, 29(7):533–547, 2019. doi: 10.1038/s41422-019-0187-y.

[445] Rose Loughlin, Jeremy D. Wilbur, Francis J. McNally, Franois J. Nédélec, and Rebecca Heald. Katanin contributes to interspecies spindle length scaling in xenopus. *Cell*, 147(6):1397–1407, 2011. doi: 10.1016/j.cell.2011.11.014.

[446] Karen Perry McNally, Michelle T. Panzica, Taekyung Kim, Daniel B. Cortes, and Francis J. McNally. A novel chromosome segregation mechanism during female meiosis. *Molecular Biology of the Cell*, 27(16): 2576–2589, 2016. doi: 10.1091/mbc.E16-05-0331.

[447] Martin Srayko, Eileen T. O'Toole, Anthony A. Hyman, and Thomas Müller-Reichert. Katanin Disrupts the Microtubule Lattice and Increases Polymer Number in C. elegans Meiosis. *Current Biology*, 16(19):1944–1949, 2006. doi: 10.1016/j.cub.2006.08.029.

[448] Jedidiah Gaetz and Tarun M. Kapoor. Dynein/dynactin regulate metaphase spindle length by targeting depolymerizing activities to spindle poles. *Journal of Cell Biology*, 166(4):465–471, 2004. doi: 10.1083/jcb.200404015.

[449] T. J. Mitchison. Polewards microtubule flux in the mitotic spindle: Evidence from photoactivation of fluorescence. *Journal of Cell Biology*, 109(2):637–652, 1989. doi: 10.1083/jcb.109.2.637.

[450] Arthur Forer. Local reduction of spindle fiber birefringence in living Nephrotoma suturalis (loew) spermatocytes induced by ultraviolet microbeam irradiation. *The Journal of Cell Biology*, 25:95–117, 1965. doi: 10.1083/jcb.25.1.95.

[451] Helder Maiato, Alexey Khodjakov, and Conly L. Rieder. Drosophila CLASP is required for the incorporation of microtubule subunits into fluxing kinetochore fibres. *Nature Cell Biology*, 7(1):42–47, 2005. doi: 10.1038/ncb1207.

[452] Dong Zhang, Gregory C. Rogers, Daniel W. Buster, and David J. Sharp. Three microtubule severing enzymes contribute to the "Pacman- flux" machinery that moves chromosomes. *Journal of Cell Biology*, 177 (2):231–242, 2007. doi: 10.1083/jcb.200612011.

[453] Haifeng Wang, Ingrid Brust-Mascher, Gul Civelekoglu-Scholey, and Jonathan M. Scholey. Patronin mediates a switch from kinesin-13-dependent poleward flux to anaphase b spindle elongation. *Journal of Cell Biology*, 203(1):35–46, 2013. doi: 10.1083/jcb.201306001.

[454] Yuki Hara and Akatsuki Kimura. Cell-Size-Dependent Spindle Elongation in the Caenorhabditis elegans Early Embryo. *Current Biology*, 19(18):1549–1554, 2009. doi: 10.1016/j.cub.2009.07.050.

[455] Stefanie Redemann, Johannes Baumgart, Norbert Lindow, Michael Shelley, Ehssan Nazockdast, Andrea Kratz, Steffen Prohaska, Jan Brugués, Sebastian Fürthauer, and Thomas Müller-Reichert. C. elegans chromosomes connect to centrosomes by anchoring into the spindle network. *Nature Communications*, 8 (May):1–13, 2017. doi: 10.1038/ncomms15288.

[456] Fulvia Verde, Marileen Dogterom, Ernst Stelzer, Eric Karsenti, and Stanislas Leibler. Control of microtubule dynamics and length by cyclin A- and cyclin B-dependent kinases in Xenopus egg extracts. *Journal of Cell Biology*, 118(5):1097–1108, 1992. doi: 10.1083/jcb.118.5.1097.

[457] Franziska Decker, David Oriola, Benjamin Dalton, and Jan Brugue. Autocatalytic microtubule nucleation determines the size and mass of Xenopus laevis egg extract spindles. *eLife*, 7:e31149:1–20, 2018. doi: 10.7554/eLife.31149.

[458] Doogie Oh, Che Hang Yu, and Daniel J. Needleman. Spatial organization of the Ran pathway by microtubules in mitosis. *Proceedings of the National Academy of Sciences of the United States of America*, 113 (31):8729–8734, 2016. doi: 10.1073/pnas.1607498113.

[459] Alexander W. Bird and Anthony A. Hyman. Building a spindle of the correct length in human cells requires the interaction between TPX2 and Aurora A. *Journal of Cell Biology*, 182(2):289–300, 2008. doi: 10.1083/jcb.200802005.

[460] Daniel J. Burke and P. Todd Stukenberg. Linking Kinetochore-Microtubule Binding to the Spindle Checkpoint. *Developmental Cell*, 14(4):474–479, 2008. doi: 10.1016/j.devcel.2008.03.015.

[461] Xianxian Han and Ziyin Li. Comparative analysis of chromosome segregation in human, yeasts and trypanosome. *Frontiers in Biology*, 9(6):472–480, 2014. doi: 10.1007/s11515-014-1334-y.

[462] S. Hauf, I. C. Waizenegger, and J. M. Peters. Cohesin cleavage by separase required for anaphase and cytokinesis in human cells. *Science*, 293(5533):1320–1323, 2001. doi: 10.1126/science.1061376.

[463] H. Jäger, A. Herzig, C. F. Lehner, and S. Heidmann. Drosophila separase is required for sister chromatid separation and binds to PIM and THR. *Genes and Development*, 15(19):2572–2584, 2001. doi: 10.1101/gad.207301.

[464] Frank Uhlmann, Dominik Wernic, Eugene V Koonin, and Kim Nasmyth. Cleavage of Cohesin by the CD Clan Protease Separin Triggers Anaphase in Yeast. *Cell*, 103(3):375–386, 2000. doi: 10.1016/s0092-8674(00)00130-6.

[465] Devin H. Parry and Patrick H. O'Farrell. The schedule of destruction of three mitotic cyclins can dictate the timing of events during exit from mitosis. *Current Biology*, 11(9):671–683, 2001. doi: 10.1016/S0960-9822(01)00204-4.

[466] Matt Sullivan and Frank Uhlmann. A non-proteolytic function of separase links the onset of anaphase to mitotic exit. *Nature Cell Biology*, 5(3):249–254, 2003. doi: 10.1038/ncb940.

[467] Claudia Wurzenberger and Daniel W. Gerlich. Phosphatases: Providing safe passage through mitotic exit. *Nature Reviews Molecular Cell Biology*, 12(8):469–482, 2011. doi: 10.1038/nrm3149.

[468] M Mishima, V Pavicic, U Gruneberg, E a Nigg, and M Glotzer. Cell cycle regulation of central spindle assembly. *Nature*, 430(7002):908–913, 2004. doi: 10.1038/nature02763.

[469] Régis Tournebize, Søren S.L. Andersen, Fulvia Verde, Marcel Dorée, Eric Karsenti, and Anthony A. Hyman. Distinct roles of PP1 and PP2A-like phosphatases in control of microtubule dynamics during mitosis. *EMBO Journal*, 16(18):5537–5549, 1997. doi: 10.1093/emboj/16.18.5537.

[470] Benjamin A. Wolfe, W. Hayes McDonald, John R R. Yates, and Kathleen L. Gould. Phospho-Regulation of the Cdc14/Clp1 Phosphatase Delays Late Mitotic Events in S. pombe. *Developmental Cell*, 11(3):423–430, 2006. doi: 10.1016/j.devcel.2006.07.016.

[471] Dhanya K. Cheerambathur, Gul Civelekoglu-Scholey, Ingrid Brust-Mascher, Patrizia Sommi, Alex Mogilner, and Jonathan M. Scholey. Quantitative analysis of an anaphase B switch: Predicted role for a microtubule catastrophe gradient. *Journal of Cell Biology*, 177(6):995–1004, 2007. doi: 10.1083/jcb.200611113.

[472] P. S. Maddox, K. S. Salmon, and E. D. Bloom. The polarity and dynamics of microtubule assembly in the budding yeast Saccharomyces cerevisae. *Nature Cell Biology*, 2(1):36–41, 2000. doi: 10.1038/71357.

[473] Matt Sullivan and David O. Morgan. Finishing mitosis, one step at a time. *Nature Reviews Molecular Cell Biology*, 8(11):894–903, 2007. doi: 10.1038/nrm2276.

[474] Kozo Tanaka, Etsushi Kitamura, Yoko Kitamura, and Tomoyuki U. Tanaka. Molecular mechanisms of microtubule-dependent kinetochore transport toward spindle poles. *Journal of Cell Biology*, 178(2):269–281, 2007. doi: 10.1083/jcb.200702141.

[475] B. J. Howell, B. F. McEwen, J. C. Canman, D. B. Hoffman, E. M. Farrar, C. L. Rieder, and E. D. Salmon. Cytoplasmic dynein/dynactin drives kinetochore protein transport to the spindle poles and has a role in mitotic spindle checkpoint inactivation. *Journal of Cell Biology*, 155(7):1159–1172, 2001. doi: 10.1083/jcb.200105093.

[476] D. J. Sharp, G. C. Rogers, and J. M. Scholey. Cytoplasmic dyein is required for poleward chromosome movement during mitosis in Drosophila embryos. *Nature Cell Biology*, 2(12):922–930, 2000. doi: 10.1038/35046574.

[477] Meredith J. Sagolla, Satoru Uzawa, and W. Zacheus Cande. Individual microtubule dynamics contribute to the function of mitotic and cytoplasmic arrays in fission yeast. *Journal of Cell Science*, 116(24):4891–4903, 2003. doi: 10.1242/jcs.00796.

[478] Xiangwei He, Daniel R. Rines, Christopher W. Espelin, and Peter K. Sorger. Molecular analysis of kinetochore-microtubule attachment in budding yeast. *Cell*, 106(2):195–206, 2001. doi: 10.1016/S0092-8674(01)00438-X.

[479] Carsten Janke, Jennifer Ortíz, Tomoyuki U. Tanaka, Johannes Lechner, and Elmar Schiebel. Four new subunits of the Dam1-Duo1 complex reveal novel functions in sister kinetochore biorientation. *EMBO Journal*, 21(1-2):181–193, 2002. ISSN 02614189. doi: 10.1093/emboj/21.1.181.

[480] J. J.L. Miranda, Peter De Wulf, Peter K. Sorger, and Stephen C. Harrison. The yeast DASH complex forms closed rings on microtubules. *Nature Structural and Molecular Biology*, 12(2):138–143, 2005. doi: 10.1038/nsmb896.

[481] Stefan Westermann, Agustin Avila-Sakar, Hong Wei Wang, Hanspeter Niederstrasser, Jonathan Wong, David G. Drubin, Eva Nogales, and Georjana Barnes. Formation of a dynamic kinetochore-microtubule interface through assembly of the Dam1 ring complex. *Molecular Cell*, 17(2):277–290, 2005. doi: 10.1016/j.molcel.2004.12.019.

[482] E. L. Grishchuk, I. S. Spiridonov, V. A. Volkov, A. Efremov, S. Westermann, D. Drubin, G. Barnes, F. I. Ataullakhanov, and J. R. McIntosh. Different assemblies of the DAM1 complex follow shortening microtubules by distinct mechanisms. *Proceedings of the National Academy of Sciences of the United States of America*, 105(19):6918–6923, 2008. doi: 10.1073/pnas.0801811105.

[483] Arockia A. Jeyaprakash, Anna Santamaria, Uma Jayachandran, Ying Wai Chan, Christian Benda, Erich A. Nigg, and Elena Conti. Structural and Functional Organization of the Ska Complex, a Key Component of the Kinetochore-Microtubule Interface. *Molecular Cell*, 46(3):274–286, 2012. doi: 10.1016/j.molcel.2012.03.005.

[484] Julie P.I. Welburn, Ekaterina L. Grishchuk, Chelsea B. Backer, Elizabeth M. Wilson-Kubalek, John R. Yates, and Iain M. Cheeseman. The Human Kinetochore Ska1 Complex Facilitates Microtubule Depolymerization-Coupled Motility. *Developmental Cell*, 16(3):374–385, 2009. doi: 10.1016/j.devcel.2009.01.011.

[485] Jason Stumpff, George von Dassow, Michael Wagenbach, Charles Asbury, and Linda Wordeman. The Kinesin-8 Motor Kif18A Suppresses Kinetochore Movements to Control Mitotic Chromosome Alignment. *Developmental Cell*, 14(2):252–262, 2008. doi: 10.1016/j.devcel.2007.11.014.

[486] Amity L. Manning, Neil J. Ganem, Samuel F Bakhoum, Michael Wagenbach, Linda Wordeman, and Duane A. Compton. The Kinesin-13 Proteins Kif2a, Kif2b, and Kif2c/MCAK Have Distinct Roles during Mitosis in Human Cells. *Molecular Biology of the Cell*, 18(August):2970–2979, 2007. doi: 10.1091/mbc.E07.

[487] Arshad Desai, Paul S. Maddox, Timothy J. Mitchison, and E. D. Salmon. Anaphase a chromosome movement and poleward spindle microtubule flux occur at similar rates in Xenopus extract spindles. *Journal of Cell Biology*, 141(3):703–713, 1998. doi: 10.1083/jcb.141.3.703.

[488] Kruno Vukušić, Renata Buđa, Agneza Bosilj, Ana Milas, Nenad Pavin, and Iva M. Tolić. Microtubule Sliding within the Bridging Fiber Pushes Kinetochore Fibers Apart to Segregate Chromosomes. *Developmental Cell*, 43(1):11–23.e6, 2017. doi: 10.1016/j.devcel.2017.09.010.

[489] Zhen Yu She, Ya Lan Wei, Yang Lin, Yue Ling Li, and Ming Hui Lu. Mechanisms of the Ase1/PRC1/MAP65 family in central spindle assembly. *Biological Reviews*, 94(6):2033–2048, 2019. doi: 10.1111/brv.12547.

[490] Changjun Zhu, Eric Lau, Robert Schwarzenbacher, Ella Bossy-Wetzel, and Wei Jiang. Spatiotemporal control of spindle midzone formation by PRC1 in human cells. *Proceedings of the National Academy of Sciences of the United States of America*, 103(16):6196–6201, 2006. doi: 10.1073/pnas.0506926103.

[491] Ulrike Gruneberg, Rüdiger Neef, Xiuling Li, Eunice H.Y. Chan, Ravindra B. Chalamalasetty, Erich A. Nigg, and Francis A. Barr. KIF14 and citron kinase act together to promote efficient cytokinesis. *Journal of Cell Biology*, 172(3):363–372, 2006. doi: 10.1083/jcb.200511061.

[492] J. R. McIntosh, P. K. Hepler, and D. G. Van Wie. Model for mitosis. *Nature*, 224(5220):659–663, 1969. doi: 10.1038/224659a0.

[493] Kruno Vukušić, Renata Buđa, Ivana Ponjavić, Patrik Risteski, and Iva Tolić. Microtubule-sliding modules based on kinesins EG5 and PRC1-dependent KIF4A drive human spindle elongation. *Developmental Cell*, 56(9):1253–1267, 2019. doi: 10.1016/j.devcel.2021.04.005.

[494] Iva M. Tolić. Mitotic spindle: kinetochore fibers hold on tight to interpolar bundles. *European Biophysics Journal*, 47(3):191–203, 2018. doi: 10.1007/s00249-017-1244-4.

[495] R. Avunie-Masala, N. Movshovich, Y. Nissenkorn, A. Gerson-Gurwitz, V. Fridman, M. Koivomagi, M. Loog, M. A. Hoyt, A. Zaritsky, and L. Gheber. Phospho-regulation of kinesin-5 during anaphase spindle elongation. *Journal of Cell Science*, 124(6):873–878, 2011. doi: 10.1242/jcs.077396.

[496] W Saunders, D Koshland, D Eshel, I Gibbons, and A Hoyt. Saccharomycescerevisiae kinesin- and dynein-related protein required for anaphase chromosome segregation. *J. Cell Biol.*, 128(4):617–624, 1995. doi: 10.1083/jcb.128.4.617.

[497] Tomomi Kiyomitsu and Iain M. Cheeseman. Cortical dynein and asymmetric membrane elongation coordinately position the spindle in anaphase. *Cell*, 154(2):391, 2013. doi: 10.1016/j.cell.2013.06.010.

[498] James R Aist, Hong Liang, and Michael W Berns. Astral and spindle forces in PtK 2 cells during anaphase B : a laser microbeam study. *Journal of Cell Science*, 104(4):1207–1216, 1993.

[499] Gero Fink, Isabel Schuchardt, Julien Colombelli, Ernst Stelzer, and Gero Steinberg. Dynein-mediated pulling forces drive rapid mitotic spindle elongation in Ustilago maydis. *The EMBO Journal*, 25(20):4897–4908, 2006. doi: 10.1038/sj.emboj.7601354.

[500] Nenad Pavin and Iva M. Tolíc-Nørrelykke. Dynein, microtubule and cargo: A ménage à trois. *Biochemical Society Transactions*, 41(6):1731–1735, 2013. doi: 10.1042/BST20130235.

[501] Ekaterina L. Grishchuk, Maxim I. Molodtsov, Fazly I. Ataullakhanov, and J. Richard McIntosh. Force production by disassembling microtubules. *Nature*, 438(7066):384–388, 2005. doi: 10.1038/nature04132.

[502] Adam M. Saunders, James Powers, Susan Strome, and William M. Saxton. Kinesin-5 acts as a brake in anaphase spindle elongation. *Current Biology*, 17(12):453–454, 2007. doi: 10.1016/j.cub.2007.05.001.

[503] Reza Farhadifar, Che Hang Yu, Gunar Fabig, Hai Yin Wu, David B. Stein, Matthew Rockman, Thomas Müller-Reichert, Michael J. Shelley, and Daniel J. Needleman. Stoichiometric interactions explain spindle dynamics and scaling across 100 million years of nematode evolution. *eLife*, 9:1–26, 2020. doi: 10.7554/ELIFE.55877.

[504] Melissa C. Pamula, Lina Carlini, Scott Forth, Priyanka Verma, Subbulakshmi Suresh, Wesley R. Legant, Alexey Khodjakov, Eric Betzig, and Tarun M. Kapoor. High-resolution imaging reveals how the spindle midzone impacts chromosome movement. *Journal of Cell Biology*, 218(8):2529–2544, 2019. doi: 10.1083/JCB.201904169.

[505] Kuan Chung Su, Zachary Barry, Nina Schweizer, Helder Maiato, Mark Bathe, and Iain Mc Pherson Cheeseman. A Regulatory Switch Alters Chromosome Motions at the Metaphase-to-Anaphase Transition. *Cell Reports*, 17(7):1728–1738, 2016. doi: 10.1016/j.celrep.2016.10.046.

[506] William M Saxton and J Richard McIntosh. Interzone Microtubule Behavior in Late Anaphase and Telophase Spindles. *Journal of Cell Biology*, 105:875–886, 1987. doi: 10.1083/jcb.105.2.875.

[507] W Zacheus Cande and Kent Mcdonald. Physiological and Ultrastructural Analysis of Elongating Mitotic Spindles Reactivated In Vitro. *Journal of Cell Biology*, 103(2):593–604, 1986. doi: 10.1083/jcb.103.2.593.

[508] W Zacheus Cande and Kent L. McDonald. In vitro reactivation of anaphase spindle elongation using isolated diatom spindles. *Letter to Nature*, 316(11):168–170, 1985. doi: 10.1038/316168a0.

[509] Hirohiss Masuda and W Zacheus. The Role of Tubulin Polymerization during Spindle Elongation In Vitro. *Cell*, 49(2):193–202, 1987. doi: 10.1016/0092-8674(87)90560-5.

[510] Gilliane Maton, Frances Edwards, Benjamin Lacroix, Marine Stefanutti, Kimberley Laband, Tiffany Lieury, Taekyung Kim, Julien Espeut, Julie C. Canman, and Julien Dumont. Kinetochore components are required for central spindle assembly. *Nature Cell Biology*, 17(5):697–705, 2015. doi: 10.1038/ncb3150.

[511] Chi-kuo Kuo Hu, Margaret Coughlin, Christine M. Field, and Timothy J. Mitchison. KIF4 regulates midzone length during cytokinesis. *Current Biology*, 21(10):815–824, 2011. doi: 10.1016/j.cub.2011.04.019.

[512] Marileen Dogterom, Jacob W.J. Kerssemakers, Guillaume Romet-Lemonne, and Marcel E. Janson. Force generation by dynamic microtubules. *Current Opinion in Cell Biology*, 17(1):67–74, 2005. doi: 10.1016/j.ceb.2004.12.011.

[513] Lara Katharina Krüger, Jérémie Luc Sanchez, Anne Paoletti, and Phong Thanh Tran. Kinesin-6 regulates cell-size-dependent spindle elongation velocity to keep mitosis duration constant in fission yeast. *eLife*, 8: 1–22, feb 2019. doi: 10.7554/eLife.42182.

[514] Antonios Lioutas and Isabelle Vernos. Aurora A kinase and its substrate TACC3 are required for central spindle assembly. *EMBO Reports*, 14(9):829–836, 2013. doi: 10.1038/embor.2013.109.

[515] Fedor Severin, Bianca Habermann, Tim Huffaker, and Tony Hyman. Stu2 Promotes Mitotic Spindle Elongation in Anaphase. *Journal of Cell Biology*, 153(2):435–442, 2001. doi: 10.1083/jcb.153.2.435.

[516] Daniela Cimini, Lisa A. Cameron, and E.D. Salmon. Anaphase Spindle Mechanics Prevent Mis-Segregation of Merotelically Oriented Chromosomes. *Current Biology*, 14:2149–2155, 2004. doi: 10.1016/j.

[517] Thibault Courtheoux, Guillaume Gay, Yannick Gachet, and Sylvie Tournier. Ase1/Prc1-dependent spindle elongation corrects merotely during anaphase in fission yeast. *Journal of Cell Biology*, 187(3):399–412, 2009. doi: 10.1083/jcb.200902093.

[518] A. L. Pidoux, S. Uzawa, P. E. Perry, W. Z. Cande, and R. C. Allshire. Live analysis of lagging chromosomes during anaphase and their effect on spindle elongation rate in fission yeast. *Journal of Cell Science*, 113 (23):4177–4191, 2000.

[519] Aurélien Courtois, Melina Schuh, Jan Ellenberg, and Takashi Hiiragi. The transition from meiotic to mitotic spindle assembly is gradual during early mammalian development. *Journal of Cell Biology*, 198(3):357–370, 2012. doi: 10.1083/jcb.201202135.

[520] Marina E. Crowder, Magdalena Strzelecka, Jeremy D. Wilbur, Matthew C. Good, George Von Dassow, and Rebecca Heald. A Comparative Analysis of Spindle Morphometrics across Metazoans. *Current Biology*, 25 (11):1542–1550, 2015. doi: 10.1016/j.cub.2015.04.036.

[521] Reza Farhadifar, Charles F. Baer, Aurore Cécile Valfort, Erik C. Andersen, Thomas Müller-Reichert, Marie Delattre, and Daniel J. Needleman. Scaling, selection, and evolutionary dynamics of the mitotic spindle. *Current Biology*, 25(6):732–740, 2015. doi: 10.1016/j.cub.2014.12.060.

[522] Garrett Greenan, Clifford P. Brangwynne, Steffen Jaensch, Jöbin Gharakhani, Frank Jülicher, and Anthony A. Hyman. Centrosome Size Sets Mitotic Spindle Length in Caenorhabditis elegans Embryos. *Current Biology*, 20(4):353–358, 2010. doi: 10.1016/j.cub.2009.12.050.

[523] Aurore Cécile Valfort, Caroline Launay, Marie Sémon, and Marie Delattre. Evolution of mitotic spindle behavior during the first asymmetric embryonic division of nematodes. *PLoS Biology*, 16(1), 2018. doi: 10.1371/journal.pbio.2005099.

[524] Martin Wühr, Yao Chen, Sophie Dumont, Aaron C Groen, Daniel J Needleman, Adrian Salic, and Timothy J Mitchison. Evidence for an Upper Limit to Mitotic Spindle Length. *Current Biology*, 18(16):1256–1261, 2008. doi: 10.1016/j.cub.2008.07.092.

[525] Ching Feng Yang, Wan Yu Tsai, Wei An Chen, Kai Wen Liang, Cheng Ju Pan, Pei Lun Lai, Pan Chyr Yang, and Hsiao Chun Huang. Kinesin-5 Contributes to Spindle-length Scaling in the Evolution of Cancer toward Metastasis. *Scientific Reports*, 6(October):1–9, 2016. doi: 10.1038/srep35767.

[526] Katherine S. Brown, Michael D. Blower, Thomas J. Maresca, Timothy C. Grammer, Richard M. Harland, and Rebecca Heald. Xenopus tropicalis egg extracts provide insight into scaling of the mitotic spindle. *Journal of Cell Biology*, 176(6):765–770, 2007. doi: 10.1083/jcb.200610043.

[527] M. C. Good, M. D. Vahey, A. Skandarajah, D. A. Fletcher, and R. Heald. Cytoplasmic Volume Modulates Spindle Size During Embryogenesis. *Science*, 342:856–860, 2013. doi: 10.1126/science.1243147.

[528] J. Hazel, K. Krutkramelis, P. Mooney, M. Tomschik, K. Gerow, J. Oakey, and J. C. Gatlin. Changes in Cytoplasmic Volume Are Sufficient to Drive Spindle Scaling. *Science*, 342(November):853–857, 2013. doi: 10.1126/science.1243110.

[529] Hirohisa Kyogoku and Tomoya S. Kitajima. Large Cytoplasm Is Linked to the Error-Prone Nature of Oocytes. *Developmental Cell*, 41(3):287–298.e4, 2017. doi: 10.1016/j.devcel.2017.04.009.

[530] Lucia Novakova, Kristina Kovacovicova, Thanh Quang Dang-Nguyen, Martin Sodek, Michal Skultety, and Martin Anger Anger. A balance between nuclear and cytoplasmic volumes controls spindle length. *PLoS ONE*, 11(2):1–11, 2016. doi: 10.1371/journal.pone.0149535.

[531] Lara K. Krüger and Phong T. Tran. Spindle scaling mechanisms. *Essays in biochemistry*, 64(2):383–396, 2020. doi: 10.1042/EBC20190064.

[532] Markus Decker, Steffen Jaensch, Andrei Pozniakovsky, Andrea Zinke, Kevin F. O'Connell, Wolfgang Zachariae, Eugene Myers, and Anthony A. Hyman. Limiting amounts of centrosome material set centrosome size in C. elegans embryos. *Current Biology*, 21(15):1259–1267, 2011. doi: 10.1016/j.cub.2011.06.002.

[533] Nathan W. Goehring and Anthony A. Hyman. Organelle growth control through limiting pools of cytoplasmic components. *Current Biology*, 22(9):R330–R339, 2012. doi: 10.1016/j.cub.2012.03.046.

[534] Jingyan Fu, Minglei Bian, Guangwei Xin, Zhaoxuan Deng, Jia Luo, Xiao Guo, Hao Chen, Yao Wang, Qing Jiang, and Chuanmao Zhang. TPX2 phosphorylation maintains metaphase spindle length by regulating microtubule flux. *Journal of Cell Biology*, 210(3):373–383, 2015. doi: 10.1083/jcb.201412109.

[535] Elisa Maria Rieckhoff, Keisuke Ishihara, and Jan Brugués. How to tune spindle size relative to cell size? *Current Opinion in Cell Biology*, 60:139–144, 2019. doi: 10.1016/j.ceb.2019.06.007.

[536] Elisa Maria Rieckhoff, Frederic Berndt, Maria Elsner, Stefan Golfier, Franziska Decker, Keisuke Ishihara, and Jan Brugués. Spindle Scaling Is Governed by Cell Boundary Regulation of Microtubule Nucleation. *Current Biology*, 30(24):4973–4983.e10, 2020. doi: 10.1016/j.cub.2020.10.093.

[537] Jeremy D. Wilbur and Rebecca Heald. Mitotic spindle scaling during Xenopus development by kif2a and importin $\alpha$. *eLife*, 2:e00290:1–17, 2013. doi: 10.7554/eLife.00290.

[538] Christopher Brownlee and Rebecca Heald. Importin $\alpha$ Partitioning to the Plasma Membrane Regulates Intracellular Scaling. *Cell*, 176(4):805–815.e8, 2019. doi: 10.1016/j.cell.2018.12.001.

[539] Kara J. Helmke and Rebecca Heald. TPX2 levels modulate meiotic spindle size and architecture in Xenopus egg extracts. *Journal of Cell Biology*, 206(3):385–393, 2014. doi: 10.1083/jcb.201401014.

[540] Kelly E. Miller, Adam M. Session, and Rebecca Heald. Kif2a Scales Meiotic Spindle Size in Hymenochirus boettgeri. *Current Biology*, 29(21):3720–3727.e5, 2019. doi: 10.1016/j.cub.2019.08.073.

[541] William G. Hirst, Abin Biswas, Kishore K. Mahalingan, and Simone Reber. Differences in Intrinsic Tubulin Dynamic Properties Contribute to Spindle Length Control in Xenopus Species. *Current Biology*, 30(11): 2184–2190.e5, 2020. doi: 10.1016/j.cub.2020.03.067.

[542] Hirohisa Masuda, Martine Sevik, and W. Zacheus Cande. In Vitro Microtubule-nucleating Activity of Spindle Pole Bodies in Fission Yeast Schizosaccharomyces pombe: Cell Cycle-dependent Activation in Xenopus Cell-free Extracts. *Journal of Cell Biology*, 117(5):1055–1066, 1992. doi: 10.1083/jcb.117.5.1055.

[543] Hirohisa Masuda, Risa Mori, Masashi Yukawa, and Takashi Toda. Fission yeast MOZART1/Mzt1 is an essential γ-tubulin complex component required for complex recruitment to the microtubule organizing center, but not its assembly. *Molecular Biology of the Cell*, 24(18):2894–2906, 2013. doi: 10.1091/mbc.E13-05-0235.

[544] Mika Toya, Masamitsu Sato, Uta Haselmann, Kazuhide Asakawa, Damian Brunner, Claude Antony, and Takashi Toda. γ-Tubulin complex-mediated anchoring of spindle microtubules to spindle-pole bodies requires Msd1 in fission yeast. *Nature Cell Biology*, 9(6):646–653, 2007. doi: 10.1038/ncb1593.

[545] K. Tanaka and T. Kanbe. Mitosis in the fission yeast Schizosaccharomyces pombe as revealed by freeze-substitution electron microscopy. *Journal of Cell Science*, 80:253–268, 1986.

[546] Christopher J. Edelmaier, Adam R. Lamson, Zachary R. Gergely, Saad Ansari, Robert Blackwell, J. Richard McIntosh, Matthew A. Glaser, and Meredith D. Betterton. Mechanisms of chromosome biorientation and bipolar spindle assembly analyzed by computational modeling. *eLife*, 9:e48787:1–48, 2020. doi: 10.1101/649913.

[547] Babhrubahan Roy, Neha Varshney, Vikas Yadav, and Kaustuv Sanyal. The process of kinetochore assembly in yeasts. *FEMS Microbiology Letters*, 338(2):107–117, 2013. doi: 10.1111/1574-6968.12019.

[548] Kentaro Nabeshima, Hisanori Kurooka, Masahiro Takeuchi, Kazuhisa Kinoshita, Yukinobu Nakaseko, and Mitsuhiro Yanagida. p93dis1, which is required for sister chromatid separation, is a novel microtubule and spindle pole body-associating protein phosphorylated at the Cdc2 target sites. *Genes and Development*, 9 (13):1572–1585, 1995. doi: 10.1101/gad.9.13.1572.

[549] Andrew D. Franck, Andrew F. Powers, Daniel R. Gestaut, Tamir Gonen, Trisha N. Davis, and Charles L. Asbury. Tension applied through the Dam1 complex promotes microtubule elongation providing a direct mechanism for length control in mitosis. *Nature Cell Biology*, 9(7):832–837, 2007. doi: 10.1038/ncb1609.

[550] Isabelle Loiodice, Jayme Staub, Thanauja Gangi Setty, Nam-Phuong T. Nguyen, Anne Paoletti, and P. T. Tran. Ase1p Organizes Antiparallel Microtubule Arrays during Interphase and Mitosis in Fission Yeast. *Molecular biology of the cell*, 16(1):1756–1768, 2005. doi: 10.1091/mbc.E04.

[551] Akira Yamashita, Masamitsu Sato, Akiko Fujita, Masakyuki Yamamoto, and Takashi Toda. The Roles of Fission Yeast Ase1 in Mitotic Cell Division, Meiotic Nuclear Oscillation, and Cytokinesis Checkpoint Signaling. *Molecular biology of the cell*, 16:1378–1395, 2005. doi: 10.1091/mbc.E04.

[552] Scott V. Bratman and Fred Chang. Mechanisms for maintaining microtubule bundles. *Trends in Cell Biology*, 18(12):580–586, 2008. doi: 10.1016/j.tcb.2008.09.004.

[553] Sherilyn Goldstone, Céline Reyes, Guillaume Gay, Thibault Courthéoux, Marion Dubarry, Sylvie Tournier, and Yannick Gachet. Tip1/clip-170 protein is required for correct chromosome poleward movement in fission yeast. *PLoS ONE*, 5(5), 2010. doi: 10.1371/journal.pone.0010634.

[554] Frank R Neumann and Paul Nurse. Nuclear size control in fission yeast. *The Journal of Cell Biology*, 179 (4):593–600, 2007. doi: 10.1083/jcb.200708054.

[555] F. D. Kelly and P. Nurse. Spatial control of Cdc42 activation determines cell width in fission yeast. *Molecular Biolofy of the Cell*, 22(20):3801–3811, 2011. doi: 10.1091/mbc.E11-01-0057.

[556] Jacob Zhurinsky, Klaus Leonhard, Stephen Watt, Samuel Marguerat, Jürg Bähler, and Paul Nurse. A coordinated global control over cellular transcription. *Current Biology*, 20(22):2010–2015, 2010. doi: 10.1016/j.cub.2010.10.002.

[557] Ray Alfaro-Aco and Sabine Petry. Building the microtubule cytoskeleton piece by piece. *Journal of Biological Chemistry*, 290(28):17154–17162, 2015. doi: 10.1074/jbc.R115.638452.

[558] D. Axelrod. Cell-substrate contacts illuminated by total internal reflection fluorescence. *Journal of Cell Biology*, 89(1):141–145, 1981. doi: 10.1083/jcb.89.1.141.

[559] D. Axelrod. Total Internal Reflection Fluorescence Microscopy. *Encyclopedia of Cell Biology*, 2(2):62–69, 2016. doi: 10.1016/B978-0-12-394447-4.20089-8.

[560] J. W.J. Kerssemakers, M. E. Janson, A. Van Der Horst, and M. Dogterom. Optical trap setup for measuring microtubule pushing forces. *Applied Physics Letters*, 83(21):4441–4443, 2003. doi: 10.1063/1.1629796.

[561] Amit D. Mehta, Matthias Rief, James A. Spudich, David A. Smith, and Robert M. Simmons. Single-molecule biomechanics with optical methods. *Science*, 283(5408):1689–1695, 1999. doi: 10.1126/science.283.5408.1689.

[562] Kasimira T. Stanhope and Jennifer L. Ross. *Microtubules, MAPs, and motor patterns*, volume 128. Elsevier Ltd, 2015. doi: 10.1016/bs.mcb.2015.02.003.

[563] Ana Rita Araujo, Lendert Gelens, Rahuman S.M. Sheriff, and Silvia D.M. Santos. Positive Feedback Keeps Duration of Mitosis Temporally Insulated from Upstream Cell-Cycle Events. *Molecular Cell*, 64(2):362–375, 2016. doi: 10.1016/j.molcel.2016.09.018.

[564] J S Lanni and T Jacks. Characterization of the p53-dependent postmitotic checkpoint following spindle disruption. *Molecular and cellular biology*, 18(2):1055–64, 1998. doi: 10.1128/MCB.18.2.1055.

[565] J. D. Orth, A. Loewer, G. Lahav, and T. J. Mitchison. Prolonged mitotic arrest triggers partial activation of apoptosis, resulting in DNA damage and p53 induction. *Molecular Biology of the Cell*, 23(4):567–576, 2012. doi: 10.1091/mbc.E11-09-0781.

[566] F. Quignon, L. Rozier, A. M. Lachages, A. Bieth, M. Simili, and M. Debatisse. Sustained mitotic block elicits DNA breaks: One-step alteration of ploidy and chromosome integrity in mammalian cells. *Oncogene*, 26(2):165–172, 2007. doi: 10.1038/sj.onc.1209787.

[567] Conly L Rieder and Robert E Palazzo. Colcemid and the mitotic cycle. *Journal of Cell Science*, 102(1):387–92, 1992.

[568] David R. Burgess and Fred Chang. Site selection for the cleavage furrow at cytokinesis. *Trends in Cell Biology*, 15(3):156–162, 2005. doi: 10.1016/j.tcb.2005.01.006.

[569] I. Schubert and J. L. Oud. There is an upper limit of chromosome size for normal development of an organism. *Cell*, 88(4):515–520, 1997. doi: 10.1016/S0092-8674(00)81891-7.

[570] Shaila Kotadia, Emilie Montembault, William Sullivan, and Anne Royou. Cell elongation is an adaptive response for clearing long chromatid arms from the cleavage plane. *Journal of Cell Biology*, 199(5):745–753, 2012. doi: 10.1083/jcb.201208041.

[571] Sophie Dumont and Timothy J. Mitchison. Compression Regulates Mitotic Spindle Length by a Mechanochemical Switch at the Poles. *Current Biology*, 19(13):1086–1095, 2009. doi: 10.1016/j.cub.2009.05.056.

[572] Ana Carvalho, Arshad Desai, and Karen Oegema. Structural Memory in the Contractile Ring Makes the Duration of Cytokinesis Independent of Cell Size. *Cell*, 137(5):926–937, 2009. doi: 10.1016/j.cell.2009.03.021.

[573] Meredith E.K. Calvert, Graham D. Wright, Fong Yew Leong, Keng Hwee Chiam, Yinxiao Chen, Gregory Jedd, and Mohan K. Balasubramanian. Myosin concentration underlies cell size-dependent scalability of actomyosin ring constriction. *Journal of Cell Biology*, 195(5):799–813, 2011. doi: 10.1083/jcb.201101055.

[574] Lara Katharina Krüger, Matthieu Gélin, Liang Ji, Carlos Kikuti, Anne Houdusse, Manuel Théry, Laurent Blanchoin, and Phong T Tran. Kinesin-6 Klp9 orchestrates spindle elongation by regulating microtubule sliding and growth. *eLife*, 10(10:e67489):1–27, 2021. doi: 10.7554/elife.67489.

[575] Keita Aoki, Yukinobu Nakaseko, Kazuhisa Kinoshita, Gohta Goshima, and Mitsuhiro Yanagida. Cdc2 Phosphorylation of the Fission Yeast Dis1 Ensures Accurate Chromosome Segregation. *Current Biology*, 16(16): 1627–1635, 2006. doi: 10.1016/j.cub.2006.06.065.

[576] Katherine L Schutt and James B Moseley. The phosphatase inhibitor Sds23 promotes symmetric spindle positioning in fission yeast. *Cytoskeleton*, 77(12):1–14, 2020. doi: 10.1002/cm.21648.

[577] Cecile Leduc, Kathrin Padberg-Gehle, Vladimir Varga, Dirk Helbing, Stefan Diez, and Jonathon Howard. Molecular crowding creates traffic jams of kinesin motors on microtubules. *PNAS*, 109(16):6100–6105, 2012. doi: 10.1073/pnas.1107281109.

[578] Timothy E. Holy and Stanislas Leibler. Dynamic instability of microtubules as an efficient way to search in space. *Proceedings of the National Academy of Sciences of the United States of America*, 91(12):5682–5685, 1994. doi: 10.1073/pnas.91.12.5682.

[579] Nikita Gudimchuk, Benjamin Vitre, Yumi Kim, Anatoly Kiyatkin, Don W. Cleveland, Fazly I. Ataullakhanov, and Ekaterina L. Grishchuk. Kinetochore kinesin CENP-E is a processive bi-directional tracker of dynamic microtubule tips. *Nature Cell Biology*, 15(9):1079–1088, 2013. doi: 10.1038/ncb2831.

[580] Anneke Hibbel, Aliona Bogdanova, Mohammed Mahamdeh, Anita Jannasch, Marko Storch, Erik Schäffer, Dimitris Liakopoulos, and Jonathon Howard. Kinesin Kip2 enhances microtubule growth in vitro through length-dependent feedback on polymerization and catastrophe. *eLife*, 4:e10542:1–11, 2015. doi: 10.7554/eLife.10542.

[581] Fanni Gergely, Viji M. Draviam, and Jordan W. Raff. The ch-TOG/XMAP215 protein is essential for spindle pole organization in human somatic cells. *Genes and Development*, 17(3):336–341, 2003. doi: 10.1101/gad.245603.

[582] Kazuhisa Kinoshita, Tim L. Noetzel, Laurence Pelletier, Karl Mechtler, David N. Drechsel, Anne Schwager, Mike Lee, Jordan W. Raff, and Anthony A. Hyman. Aurora A phosphorylation of TACC3/maskin is required for centrosome-dependent microtubule assembly in mitosis. *Journal of Cell Biology*, 170(7):1047–1055, 2005. doi: 10.1083/jcb.200503023.

[583] Isabel Peset, Jeanette Seiler, Teresa Sardon, Luis A. Bejarano, Sonja Rybina, and Isabelle Vernos. Function and regulation of Maskin, a TACC family protein, in microtubule growth during mitosis. *Journal of Cell Biology*, 170(7):1057–1066, 2005. doi: 10.1083/jcb.200504037.

[584] Haifeng Wang, Ingrid Brust-mascher, Dhanya Cheerambathur, and Jonathan M. Scholey. Coupling between microtubule sliding, plus-end growth and spindle length revealed by kinesin-8 depletion. *Cytoskeleton*, 67 (1):715–728, 2010. doi: 10.1002/cm.20482.

[585] Dimitrios Vavylonis, David R. Kovar, Ben O'Shaughnessy, and Thomas D. Pollard. Model of formin-associated actin filament elongation. *Molecular Cell*, 21(4):455–466, 2006. doi: 10.1016/j.molcel.2006.01.016.

[586] Pinar S. Gurel, A. Mu, Bingqian Guo, Rui Shu, Dale F. Mierke, and Henry N. Higgs. Assembly and turnover of short actin filaments by the formin INF2 and profilin. *Journal of Biological Chemistry*, 290(37):22494–22506, 2015. doi: 10.1074/jbc.M115.670166.

[587] David R. Kovar, Elizabeth S. Harris, Rachel Mahaffy, Henry N. Higgs, and Thomas D. Pollard. Control of the assembly of ATP- and ADP-actin by formins and profilin. *Cell*, 124(2):423–435, 2006. doi: 10.1016/j.cell.2005.11.038.

[588] Morgan E. Thompson, Ernest G. Heimsath, Timothy J. Gauvin, Henry N. Higgs, and F. Jon Kull. FMNL3 FH2-actin structure gives insight into formin-mediated actin nucleation and elongation. *Nature Structural and Molecular Biology*, 20(1):111–118, 2013. doi: 10.1038/nsmb.2462.

[589] Ahmet Yildiz, Michio Tomishige, Arne Gennerich, and Ronald D. Vale. Intramolecular Strain Coordinates Kinesin Stepping Behavior along Microtubules. *Cell*, 134(6):1030–1041, 2008. doi: 10.1016/j.cell.2008.07.018.

[590] Hideo Higuchi, Christian Eric Bronner, Hee Won Park, and Sharyn A. Endow. Rapid double 8-nm steps by a kinesin mutant. *EMBO Journal*, 23(15):2993–2999, 2004. doi: 10.1038/sj.emboj.7600306.

[591] Tadayuki Ogawa, Ryo Nitta, Yasushi Okada, and Nobutaka Hirokawa. A Common Mechanism for Microtubule Destabilizers - M Type Kinesins Stabilize Curling of the Protofilament Using the Class-Specific Neck and Loops. *Cell*, 116(4):591–602, 2004. doi: 10.1016/S0092-8674(04)00129-1.

[592] Luísa T. Ferreira and Helder Maiato. Prometaphase. *Seminars in Cell & Developmental Biology*, (in press), 2021. doi: 10.1016/j.semcdb.2021.06.004.

[593] Tarun M. Kapoor. Metaphase spindle assembly. *Biology*, 6(1), 2017. doi: 10.3390/biology6010008.

[594] G. J. Gorbsky, P. J. Sammak, and G. G. Borisy. Chromosomes move poleward in anaphase along stationary microtubules that coordinately diassemble from their kinetochore ends. *Journal of Cell Biology*, 104(1):9–18, 1987. doi: 10.1083/jcb.104.1.9.

[595] Tim Mitchison, Louise Evans, Eric Schulze, and Marc Kirschner. Sites of microtubule assembly and disassembly in the mitotic spindle. *Cell*, 45(4):515–527, 1986. doi: 10.1016/0092-8674(86)90283-7.

[596] Jonathan Scholey, Gul Civelekoglu-Scholey, and Ingrid Brust-Mascher. Anaphase B. *Biology*, 5(51):1–30, 2016. doi: 10.3390/biology5040051.

# Publications

1. **L. K. Krüger**, J.-L. Sanchez, A. Paoletti, and P. T. Tran. Kinesin-6 regulates cell-size-dependent spindle elongation velocity to keep mitosis duration constant in fission yeast. *eLife*, 8:e42182, 2019.
2. **L. K. Krüger** and P. T. Tran. Spindle scaling mechanisms. *Essays in Biochemistry*, 2:64, 2020.
3. **L. K. Krüger**, M. Gélin, C. Kikuti, A. Houdusse, M. Théry, L. Blanchoin and P. T. Tran. Kinesin-6 Klp9 orchestrates spindle elongation by regulating microtubule sliding and growth. *eLife*, 10:e67489, 2021.
4. O. Finet, C. Yague-Sanz, **L. K. Krüger**, P. T. Tran, V. Migeot, M. Louski, A. Nevers, M. Rougemaille, J. Sun, F. G. M. Ernst, L. Wacheul, M. Wey, A. Morillon, D. L. J. Lafontaine, P. Dedon and D. Hermand. Transcription-wide mapping of dihydrouridine (D) reveals that mRNA dihydrouridylation is essential for meiotic chromosome segregation. *Under revision*.
5. **L. K. Krüger** and P. T. Tran, The *S. pombe* spindle. *In preparation*.

# Talks & posters

- EMBO—EMBL Symposium - Microtubules: From Atoms to complex systems. Mai 2018, *EMBL Heidelberg, Germany* (awarded with a poster prize)
- JCS Worskhop - Reconstitution of the cell cytoskeleton *in vitro*. January 2019, *Wiston House, UK*, (Talk)
- DivIDE conference - From Pole to Pole. Mai 2019, *Barcelona, Spain* (Talk)
- EMBO workshop on fission yeast - 10th international meeting. June 2019, *Barcelona spain* (Poster)
- EMBO—EMBL Symposium - Microtubules: From Atoms to complex systems. Mai 2020, *virtual conference* (Talk)
- Mitotic spindle: From living and synthetic systems to theory. June 2021, *virtual conference* (Poster)

## RÉSUMÉ

Pendant la division cellulaire, une machine moléculaire hautement dynamique, le fuseau mitotique, sépare l'ADN précédemment dupliqué en deux ensembles identiques. Cette séparation est réalisée par le déplacement des chromatides soeurs vers les pôles opposés du fuseau (anaphase A) et par la séparation des pôles du fuseau entraînée par l'allongement du fuseau (anaphase B). Dans la plupart des organismes, l'allongement du fuseau en anaphase B est principalement entraîné par les forces de glissement des microtubules générées par les moteurs à kinésine au niveau de la zone médiane du fuseau, la région de microtubules se chevauchant de façon antiparallèle au centre du fuseau. En même temps, les microtubules du fuseau doivent croître afin de permettre l'allongement du fuseau. En fait, le glissement des microtubules et la croissance des microtubules doivent être coordonnés pour assurer une élongation sans faille du fuseau.

Ce travail démontre que, dans l'organisme modèle *Schizosaccharomyces pombe*, la kinésine-6 homotétramérique Klp9 est un régulateur crucial de l'allongement du fuseau en anaphase B. Une combinaison d'expériences in vivo et in vitro indique que le moteur possède une double fonction : il peut écarter les microtubules et réguler leur vitesse de croissance. Ainsi, le moteur peut coordonner de manière inhérente le glissement des microtubules et la croissance.
Par conséquent, la modification du nombre de moteurs présents dans la zone médiane du fuseau s'avère suffisante pour réguler la vitesse de l'élongation du fuseau en anaphase B. En fait, c'est utilisée par des cellules de tailles différentes pour ajuster la vitesse d'élongation du fuseau en anaphase B à la taille de la cellule. L'augmentation de la quantité de Klp9 permet aux cellules plus grandes, qui forment des fuseaux plus longs, d'allonger le fuseau à des vitesses plus élevées, par rapport aux cellules plus petites, qui forment des fuseaux plus courts. La mise à l'échelle de la vitesse d'élongation du fuseau permet finalement à des cellules de différentes tailles avec une longueur de fuseau différente de maintenir le processus de séparation des chromatides sœurs dans un temps constant, un avantage potentiel pour la viabilité des cellules.

## MOTS CLÉS

Mitose; fuseau mitotique; microtubules; moteurs moleculaires; protéine associée aux microtubules; kinésine

## ABSTRACT

During cell division, a highly dynamic molecular machine, the mitotic spindle, separates the previously duplicated DNA into two identical sets. This is achieved by movement of sister chromatids to opposite spindle poles (anaphase A) and separation of the spindle poles driven by elongation of the spindle (anaphase B). In most organisms, anaphase B spindle elongation is primarily driven by microtubule sliding forces generated by kinesin motors at the spindle midzone, the region of antiparallel overlapping microtubules at the spindle center. At the same time, the spindle microtubules have to grow in order to allow the spindle to elongate. In fact, microtubule sliding and microtubule growth have to be coordinated to ensure flawless spindle elongation.

This work demonstrates that, in the model organism *Schizosaccharomyces pombe*, the homotetrameric kinesin-6 Klp9 is a crucial regulator of anaphase B spindle elongation. A combination of in vivo and in vitro experiments indicates that the motor holds a dual function: it can slide microtubules apart and regulate their growth velocity. Thus, the motor may inherently coordinate microtubule sliding and growth during anaphase. Accordingly, altering the number of motors present at the spindle midzone was sufficient to alter the speed of anaphase B spindle elongation. In fact, this is utilized by cells of different sizes to adjust the spindle elongation velocity to cell size. Increasing the Klp9 amount allows bigger cells, which form longer spindles, to elongate the spindle with higher speeds, as compared to smaller cells, which form shorter spindles. Scaling of the spindle elongation velocity eventually allows cells of different sizes with different spindle length to keep the process of sister-chromatid separation in a constant time frame, a potential advantage for cell viability.

## KEYWORDS

Mitosis; mitotic spindle; microtubules; molecular motors; microtubule-associated proteins; kinesin; scaling